



Al-Mustansiriyah

ISSN 1814 - 635X

Journal of Science

Vol. 22, No. 2, 2011



Issued by College of Science - Mustansiriya University

Vol. 22
No. 2
2011

Al- Mustansiriyah Journal of Science

Issued by College of Science- Al- Mustansiriyah
University, Baghdad, Iraq

Head Editor

Prof. Dr. Redha I. AL-Bayati

General Editor

Dr. Salah Mahdi Al-Shukri

Editorial Board

Dr. Iman Tarik Al -Alawy	Member
Dr. Inaam Abdul-Rahman Hasan	Member
Dr. Awni Edwar Abdulahad	Member
Dr. Majid Mohammed Mahmood	Member
Dr. Ramzy Rasheed Al-Ani	Member
Dr. Hussain Kareem Al-Windawi	Member
Dr. Saad Najm Bashikh	Member

Consultant Committee

Dr. Yosif Kadhim Al-Haidari	Member
Dr. Tariq Salih Abdul-Razaq	Member
Dr. Mehdi Sadiq Abbas	Member
Dr. Abdulla Ahmad Rasheed	Member
Dr. Hussein Ismail Abdullah	Member
Dr. Muhaned Mohammed Nuri	Member
Dr. Monim Hakeem Kalaf	Member
Dr. Amir Sadiq Al-Malah	Member
Dr. Tariq Suhail Najim	Member

INSTRUCTIONS FOR AUTHORS

1. The journal accepts manuscripts in Arabic and English languages. Which had not been published before.
2. Author (s) has to introduce an application requesting publication of his manuscript in the journal. Four copies (one original) of the manuscript should be submitted. Manuscript should be printed by laser printer and reproduced on A4 white paper in three copies with CD should be also submitted.
3. The title of the manuscript together with the name and address of the author (s) should be typed on a separate sheet in both Arabic and English. Only manuscripts title to be typed again with the manuscript.
4. For manuscripts written in English, full name (s) of author (s) and only first letters of the words (except prepositions and auxiliaries) forming title of the manuscript should be written in capital letters. Author (s) address (es) to be written in small letters.
5. Both Arabic and English abstracts are required for each manuscript. They should be typed on two separate sheets (not more than 250 words each).
6. References should be denoted by a number between two bracket on the same level of the line and directly at the end of the sentence. A list of references should be given on a separate sheet of paper, following the interactional style for names and abbreviations of journals.
7. Whenever possible, research papers should follow this pattern: INTRODUCTION, EXPERIMENTAL (MATERIALS AND METHODS), RESULTS AND DISCUSSION, and REFERENCES. All written in capital letters at the middle of the page. Without numbers or underneath lines.
8. The following pattern should be followed upon writing the references on the reference sheet: Surname (s), initials of author (s), title of the paper, name or abbreviation of the journal, volume, number, pages and (Year). For books give the author(s) name(s), the title, edition, pages, publisher, place of publication and (Year).
9. A publication fees in the amount of ID. 25 thousand is charged upon a Receipt of the paper and 25 thousand upon the acceptance for publication for their ID. 50 thousand should be paid for the editorial board.

CONTENTS

ITEM	Page No.
Distribution of <i>Chlamydia trachomatis</i> in Falluja Women Jamal A. Rahman, Raghad W. Khleel, And Suad S. Shahatha	1-6
Effect of Gelatin Addition to Extender on Semen Quality of Rabbit Sabah A. H. A. Rahman	7-12
The Study of Antibacterial Activity of Acridone Derivatives Containing 1, 3, 4-Oxadiazole Fitua M. Aziz , Israa B. Raoof, Shiamaa I. Shuker, and Ayad K. Khan	13-26
Evaluation of The Process of Apoptosis through the Estimation of Fas and Fas Ligand Levels in Some Iraqi Hypertensive Pregnant Women Mohammed A. Saleh	27-34
Synthesis and Characterization of some New Heterocyclic Compounds Jumbad H. Tommal, Emad T. Ali, Ivan H. R. Tomi, Zahra A. M. Al-Witry ⁴ , Huda A. Hassan	35-44
Synthesis of New Phenobarbital Derivatives (Part I) Redha I. AL-bayati and Abdul Jabbar Kh. Atia	45-50
Synthesis of New Sugar Based Triazoles and Bis-Triazoles <i>via</i> Click Chemistry Adnan Ibrahim Mohammed	51-60
Spectrophotometric Determination of Copper in Steel Scrap Samples Thkra Ahmed Hassen	61-70
Synthesis of Some Heterocyclic Compounds Derived from 1,3-dihydro-2H-indol-2-one Nahida A. jinzeel	71-78
Synthesis of Dithiocarbamate Derivatives of ((nitrophenyl) diazenyl)-1, 3, 4 thiadiazole as Possible Anticancer Agent Azhar Mahdi Jasim, Tagreed N. A., and Mohammed Hassan Mohammed	79-88
Synthesis of New 3-(Pyrimidin-2-Yl Amino) Propane Hydrazide Derivatives Nisreen k. Abood	89-100
Synthesis and Characterization of Some Divalent Transition Metals Complexes of Schiff Bases Derived from Salicylaldehyde Diamine Derivatives. Tawfiq A. Al – Diwan	101-108
Synthesis of New 1,2,3-Triazole and 1,2,3-Triazoline Derived From Unsaturated D-Fructose Via 1,3-Dipolarcycloaddition Reaction Abdul Hussain K. Sharba ¹ , Yousif A. AL-Fattahi ² , and Firyal W. Askar	109-122

Simultaneous Determination of Chlorpromazine and Trifluoroperazine in Pharmaceutical Preparations Using High Performance Liquid Chromatography Jameel M. Dhabab	123-128
Study the Otoacoustic Emission in the Frequency Range Lower Than 1 Khz Adnan M. Ali AL-Maamury	129-140
Speckle Noise Reduction in SAR Images Using Non-Adaptive Mode-Filter Dunia F. Talab	141-150
Determination of the Energy Spectrum and Mass Composition Based on Cherenkov Light Lateral Distribution Function Sarah Hussein Ali and Al-Rubaiee Ahmed A.	151-158
Study the Effect of Thermal Annealing on Structural Properties of PbSe Thin Films Prepared by Thermal Evaporation in Vacuum Usama A. A. Dakhel, Hanan A. Naif, and Hala F. Dagher	159-166
A Study of the Deposition Angle Effect on the Structural Properties of (Cds) Thin Films Raad S. Al – Rawie and Hussein Ridha Ahmed	167-176
Empirical Models for Solar Radiation Estimation by Some Weather Data for Baghdad City Enas A. Habbib	177-184
Wind Power Potential and Characteristic Analysis of the "Bakrajo Region" Sulaimani /Iraq Salahaddin Abdul Qader Ahmed, Meeran Akram Omer, Awni Adwar Abdulahad	185-194

Distribution of *Chlamydia trachomatis* in Falluja Women

Jamal A. Rahman, Raghad W. Khleel, and Suad S. Shahatha

Department Of Biology, College Of Education And Pure Science - Al Anbar University,

Received 13/7/2010 – Accepted 2/3/2011

الخلاصة

أجريت الدراسة الحالية على (100) من النساء اللواتي يعانين من إفرازات مهبلية غير طبيعية راجع عن العيادة الخارجية في مستشفى ومركز رعاية الأسرة في مدينة الفلوجة، إذ تم جمع عينات الدم خلال المدة من شهر نيسان إلى شهر آب 2009 وممن تراوحت أعمارهن بين (20-40) سنة. أظهرت الدراسة الحالية وباستخدام تقنية الـ ELISA أعلى نسبة للأصباة ببكتريا الكلاميديا كانت 44% (25/11) من النساء اللواتي تراوحت أعمارهن بين (25-30) سنة، وأن أعلى نسبة كانت 28% (14/50) بين النساء الحوامل فيما يخص تشخيص الإصابة باستخدام مضادات الكلاميديا نوع (IgM) الخاصة بهذه البكتريا بينما كانت النسبة أوطأ 18% (9/50) للنوع (IgG). كما أظهرت هذه الدراسة بأن النساء القرويات سجلن أعلى نسبة 30% (15/50) فيما يخص مضادات بكتريا الكلاميديا النوع (IgM) بينما انخفضت النسبة إلى 20% (10/50) للنوع (IgG). من ناحية أخرى كانت نسبة الإصابة في النساء من سكنة المدينة 12% (6/50) و 6% (3/50) فيما يخص النوع (IgM) و (IgG) على التوالي.

ABSTRACT

The current study was carried out on one hundred women complaining from vaginal discharge. Who attended Gynecological Antenatal out patients and Family Planning Clinic at Falluja City. Blood samples collected during period from April to August 2009, age ranged from 20-40 years,

This study showed by using ELISA technique that higher percentage of infection was 44% (11/25) in the age group 25-30 years, as well as percentage of infection was higher 28% (14/50) in pregnant women for IgM antichlamydial antibodies, whereas it was 18% (9/50) for IgG.

Also the study showed that the rural infected women represented the higher percentage 30% (15/50) for IgM antichlamydial antibodies, while it was 20% (10/50) to IgG.

On the other hand the urban infected women were 12% (6/50) and 6% (3/50) for IgM and IgG antichlamydial antibodies respectively.

INTRODUCTION

Chlamydia infections are caused by the bacterium *Chlamydia trachomatis*. Clinically genital Chlamydia may present in males as a urethritis and in females as a mucopurulent cervicitis (1). In women 50-70% of Chlamydia infection are often clinically silent. Unrecognized and untreated infections can remain with the host for months and can be transmitted to sex partners (2). For females, complications resulting from untreated or under-treated Chlamydia can be severe: ectopic pregnancy (30%) pelvic inflammatory disease (25% - 65%) and infertility (3). Vertical transmission of Chlamydia is the primary pathogen responsible for infant infections conjunctivitis (40%) and infant pneumonia (37%) (4).

The morbidity of Chlamydia and its associated costs make Chlamydia infection an important public health issue. Genital

Chlamydia has been the most commonly reported sexually transmitted disease in England, Wales, Northern Ireland, United States and Canada since becoming a notifiable disease in 1999 (5). All sexually active women presenting with lower abdominal pain should be carefully evaluated for the presence of salpingitis and / or endometritis pelvic inflammatory disease (6).

Chlamydia is a symptomatic disease, but when it is symptomatic it causes any or all of dirty discharge, lower abdominal pain, pain on passing urine and sometimes high temperature (7).

Treatment consists of antibiotics usually doxy-Cycline, azithromycin or erythromycin for a period of up to seven days. Ideal practice dictates that a repeat the dosage be taken 2 weeks after completion of treatment to confirm effective eradication (8).

Aim of this study was to diagnose infection with Chlamydia within detection and measuring of anti-chlamydial antibodies (IgM) and (IgG) in patients serum by ELISA technique.

MATERIAL AND METHODS

Blood samples were collected from 100 women at the reproductive age of 20-40 years complaining of vaginal discharge during period from April to August 2009, who attended Gynecological Antenatal out Patients and Family planning Clinic at Falluja City. Kit for Immunological Test: *Chlamydia trachomatis* (IgM, IgG) Company: Lab. System. France. Patients were divided into four groups according to their ages, also divided into pregnant and non-pregnant women and then for two groups according to their places where they live (Rural and Urban). The test was done according to manufacturing instructions provided with the kit.

1. Blood centrifuged to obtain serums for test, 100µl serum from each sample put in wells found in the kit contained conjugated – enzyme (R1).
2. The kit incubated at 38°C for 30 min.
3. Then used shaker to get IgM antibodies plus serum.
4. Washing with distilled water (D.W) for 5 min.
5. Added 100µl of conjugated enzyme (R2) in each well.
6. Incubate the kit at 38°C for 30 min.
7. Washing with D.W then distilled with filter paper.
8. Adding 100µl of substrate solution (R3).
9. Incubated at 38°C for 15 min.
10. Adding of 100µ of stop solution (R4) to stop reaction. Finally absorbance degree detected by ELISA apparatus at wave length 450nm.

RESULT AND DISCUSSION

Results showed that higher percentage of infection with *chlamydia trachomatis* was 44% (11/25) at women of 25-30 year old(table-1) by detection of antichlamydial antibodies type IgM. While the lowest percentage of infection was 12% (3/25) at women of 20-25 and 35-40 year old.

Whereas infection percentage within detection of antichlamydial antibodies type IgG was 28% (7/25) at same age group(table-2), while the lowest percentage was 8% (2/25) at women of 35-40 year old.

Table (3) showed that the percentage of infection in pregnant women was 28% (14/50) for IgM antichlamydial antibodies, whereas 18% (9/50) for type IgG antichlamydial antibodies (table-4), while in non pregnant women was 14% (7/50) and 8% (4/50) for IgM and IgG respectively. The current study also showed that the rate of infection at rural women represented higher percentage 30% (15/50) for IgM and 20% (10/50) for IgG antichlamydial antibodies respectively(tables-5,6). While it was 12% (6/50) for IgM and 6% (3/50) for IgG in urban women (table -5,6).

Chlamydial infection does not make most people sick, those who have symptoms may have an abnormal discharge (mucus,pus)(9), and early symptoms may be very mild.Symptoms usually appear within one to three weeks after being infected(10),because the symptoms may be mild or not exist at all ,you might not seek care and get treated (11).The infection may move inside the body if it is not treated.therefor it can cause pelvic inflammatory disease (PID) in women(12).

In the current study we found one of the causes of vaginal discharge which is the *Chlamydia trachomatis* with total infection rate of IgM and IgG antibodies is valuable in diagnosing asymptomatic PID.

The rate of infection due to *Chlamydia trachomatis* IgM was high among infected women at all age group especially in(25-30)year (44%). At early period of marriage act to rise greater sexual activity in women,this lead to rise the level of oestrogen which make the vaginal walls suitable environment for the growth of bacteria.

The rate of infection due to *Chlamydia trachomatis* (IgG antibody) was high (28%) among women rang between (25-30) year also these may belong to the greater sexual activity at this period.

In pregnant women a high rate of infection (IgM and IgG antibodies) is show (28%) and (18%)respectively ,whereas in non-pregnant women the rate of infection (IgM and IgG antibodies) reaches (14%) and (8%) ,because pregnancy is state of hyper oestrogenism which provides high oestrogen and glycogen level in vagina mucosa and makes it good media for growth microorganism (1), under the influence of oestrogen affect the lactobacillus bacteria that found normally in vaginal epithelial

cell act to metabolize glycogen to glucose and finally to lactic acid that lower the pH and prevent growth pathogens(15). Infection with *Chlamydia trachomatis* in pregnant women high estrogen secretion proliferates and produces amino acid in the absence of acid formation lactobacillus.(13) These amino acids are split by other bacteria which also proliferate at this time and formed amines which are basic and cause an increase in the pH(4.5), make the cells in the vaginal mucosa sheet to produces the discharge and over growth of pathogenic bacteria like *Chlamydia trachomatis* (16). While in non-pregnant women it can also cause infection especially when women use intra uterine device (IUD) give risk factor for the development of PID. the explanation of the high percentage of infection among women with IUD could be attributed to the presence of IUD which may promote the growth of pathogenic bacterial vaginosis (12).

Higher rate(30%),(20%) of infection in rural women with *Chlamydia trachomatis* IgM and IgG antibodies than in urban women 12%, 6% may reflect the status of women living in the urban where they have higher socioeconomic and educational level than rural area (17).

The center for disease control and prevention (CDC) stated that all sexual active women under and over the age of 20 year have a risk factors for Chlamydia infection, on the other hand the infection with Chlamydia is easily treated with antibiotics and must be treated to prevent re-infection (18).

Table -1: Distribution of Infection according to age groups within IgM anti-chlamydial antibodies detection .

Age /Year	No. examined	No. infection	%
20-25	25	3	12 %
25-30	25	11	44 %
30-35	25	4	16 %
35-40	25	3	12 %
Total	100	21	21 %

Table -2 : Distribution of infection according to age group within IgG anti-chlamydial antibodies detection .

Age /Year	No. examined	No. infection	%
20-25	25	-	-
25-30	25	7	28%
30-35	25	4	16 %
35-40	25	2	8 %
Total	100	13	13 %

Table-3: Distribution of infection among pregnant and nonpregnant women according to IgM anti -chlamydial antibodies.

Status	Total	No. infection	%
Pregnant	50	14	28 %
Non Pregnant	50	7	14 %
Total	100	21	21 %

Table 4: Distribution of infection among pregnant and nonpregnant women according to IgG anti -chlamydial antibodies.

Status	Total	No. infection	%
Pregnant	50	9	18 %
Non Pregnant	50	4	8 %
Total	100	13	13 %

Table -5: Distribution of infection among urban and rural women according to IgM antichlamydial antibodies.

Status	No. Examined	No. Infection	%
Urban	50	6	12%
Rural	50	15	30%
Total	100	21	21%

Table -6: Distribution of infection among urban and rural women according to IgG antichlamydial antibodies..

Status	No. Examined	No. Infection	%
Urban	50	3	6%
Rural	50	10	20%
Total	100	13	13%

REFERENCES

- 1- PHLS, DHSS and PS and Scottish ISD(D) Collaborative Group. Sexually transmitted infections in the UK: new episodes seen at Genitourinary Medicine Clinics, 1995 to 2000, London: Public Health Laboratory Service, (2007).
- 2- Caul EO. "Laboratory diagnosis of Chlamydia trachomatis infections", PHLS Microbiology Digest(2008).
- 3- Gump DW, Gibson M, Ashikaga T., "Evidence of prior pelvic inflammatory disease and its relationship to Chlamydia trachomatis antibody and intrauterine contraceptive device use in infertile women". Am J Obstet Gynecol.,120:403-9, (2008).
- 4- Moore DE, Spadoni LR, Foy HM, et al., "Increased Frequency of serum antibodies to Chlamydia trachomatis in infertility due to distal tubal disease". Lancet, Infection Disease., J. 7(2):26-33, (2007).
- 5- Chernesky M, Luinstra K, Sellors J, et al., "can serology diagnose upper genital tract Chlamydia trachomatis infection? Studies on women with pelvic pain, with or without Chlamydia plasmid DNA in endometrial biopsy tissue. Sex Trans Dis., 23:145-150, (2008).
- 6- Wang SP, Grayston JT, Alexander ER, et al., "simplified microimmunofluorescence test with trachoma- lymphogranuloma venereum (Chlamydia trachomatis) antigens for use as a screening test for antibody", J. Clin Microbiol.,56:1203-1204, (2006).
- 7- Richmond SJ, Caul EO. "Fluorescent antibody studied in Chlamydia infections", J Microbiol.,31:1662-1664, (2002).

- 8- McKie A, Vyse A, Maple C., "Novel Methods for the detection of microbial antibodies in oral fluid", *Lancet Infectious Diseases*, J. 24:731-735, (2002).
- 9- Maple PAC, Jones CS, "Time – Resolved fluorometric immunoassay for rubella antibody-a useful method for serosurveillance studies Vaccine". (2003).
- 10- Wong YK, Sureur JM, Fall CHD, et al., "The species specificity microimmunofluorescence antibody test and comparisons with a time resolved fluoroscopic immunoassay for measuring (IgG) antibodies against *Chlamydia pneumonia*", *J. Clin. Pathol*, 95,: 335-344, (2006).
- 11- Black CM., "Current methods of laboratory diagnosis of *Chlamydia trachomatis* infections". *Clin Microbiol Rev.*, (2007).
- 12- Haralambieva I, Iankov I, Petrov D, et al., "Cross-reaction between the genus-specific lipopolysaccharide antigen of *Chlamydia* spp. And the lipopolysaccharide of *Porphyromonas gingivalis*, *Escherichia coli* 0119 and *Salmonella* Newington: implications for diagnosis", *Diagn Microbial Dis.*, 82:348-52, (2001).
- 13- Ortiz L, Angevine M, Kim S-Y, et al., "T-cell epitopes in variable segment of *Chlamydia trachomatis* major outer membrane protein elicit serovar – specific immune responses in infected humans", *Infected Immun.*, 59:599-605, (2000).
- 14- Mygind P, Christiansen G, Persson K, et al., "Detection of *Chlamydia trachomatis*-specific antibodies in human sera by recombinant major outer membrane protein polyantigens", *J. Med Microbiol.*, 232:559-60, (2000)..
- 15- Paukka M, Narvanen A, Puolakkainen M, et al., "Detection of *Chlamydia trachomatis* antibodies by 2 novel test: ELISA and peptide EIA", *Int J STD AIDS.*, 7:61-64, (2007).
- 16- Clad A, Kunze FM, Schnoeckel U, et al., "Detection of seroconversion and persistence of *Chlamydia trachomatis* antibodies in different serological tests", *Eur J Clin Microbiol infect Dis* ., 21:1402-1405, (2000).
- 17- Puolakkainen M, Vesterinen E, Purola, et al., "persistence of *Chlamydia trachomatis* after pelvic inflammatory disease. *J Clin microbial*, 163:515-520, (2009).
- 18- Conway D, Glazener CMA, Caul EO, et al., "persistence of *Chlamydial* serology in fertile and infertile women", *Lancet*, (2000).

Effect of Gelatin Addition to Extender On Semen Quality of Rabbit

Sabah A. H. A. Rahman

Department of Biology, College of Science, Al-Mustansiriyah University

Received 29/12/2010 – Accepted 2/3/2011

الخلاصة

تم إجراء هذه الدراسة لتقييم تأثير إضافة الجيلاتين إلى مخفف السائل المنوي للأرانب على حيوية الحيوانات المنوية وسلامة مقدم رأس الحيوانات المنوية بعد التخفيف – قسمت عينات السائل المنوي المجمعة في مخفف الترس إلى ثلاثة أجزاء - جزء لا يحتوي جيلاتين (للمقارنة) - جزء يحتوي 1 غرام جيلاتين/100 مل مخفف - جزء يحتوي 1.8 غرام جيلاتين/100 مل مخفف .
تم جمع السائل المنوي مرتين اسبوعياً ولمدة 12 أسبوع بواسطة المهبل الصناعي من ستة أرانب ذكور – كل تلقيحه مخففة تحتوي على $10^6 \times 100-80$ حيوان منوي نسبة التخفيف 1:3 سائل منوي مخفف على درجة 25°C .
تم تخزين السائل المنوي لمدة يومين على درجة 5°C ثم تم فحص عينة السائل المنوي على درجة 25°C وذلك بعد صفر 24-48 ساعة وقدرة الحركة التقدمية للحيوانات المنوية .
أدت إضافة الجيلاتين إلى المخفف إلى تحسين الحركة التقدمية وخفض نسبة الحيوانات المنوية الميتة والمشوهة والتالف من مقدم الرأس .
استخدام المخفف الذي يحتوي على الجيلاتين بمستوى 1 غرام/100 مل مخفف حسن الصفات التي درست بينما المخفف الذي يحتوي 1.8 غرام جيلاتين/100 مل مخفف أعطى نتائج أفضل بينما إطالة مدة التخزين أدت غالى انخفاض هذه القياسات .
أظهرت النتائج إن إضافة الجيلاتين أعطى معنوية ايجابية على صفات السائل المنوي المخزن .

ABSTRACT

The effect of gelatin addition to extender on the viability and acrosome integrity of rabbit spermatozoa was studied. Pooled semen samples were processed in a tris based extender with two different levels of gelatin that solidify semen at 5°C preventing sperm precipitation and unwanted energy expenditure movement. Semen was collected with an artificial vagina weekly from six rabbit bucks. Pooled semen was diluted in tris-based diluted which was provided with 1g or 1.8 gelatin (g/100ml extender). Dilution rate was 1 semen: 3 extender. The Final concentration rate was $80 - 100 \times 10^6$ spermatozoa /100 ml After storing semen up to 2 days at 5°C , semen samples were pre-warmed to 25°C then evaluated with light microscope to reveal the influence of gelatin addition and preservation time (0, 24 and 48 hrs) on sperm motility parameters.

Adding gelatin to the extender improved motility and reduced dead and abnormal spermatozoa and acrosomat damage. The low gelatin content extender improved these parameters, but the high gelatin content extender gave the best results. However, increasing storage time resulted in reducing these parameter Results showed that gelatin addition had a significant positive effect on the quality of the stored semen which would facilitate commercial distribution.

INTRODUCTION

Artificial insemination in rabbits is usually done with fresh diluted semen, yielding pregnancy rates similar or less than those would be achieved with natural mating [1]. However, attempts are underway to preserve fertility in semen stored for several days. Semen

cryopreservation is still a limiting factor for extensive commercial application program in sheep, horses and rabbits [2, 3]. Although frozen-thawed rabbit semen can result in reasonable kindling rates [4], commercial distribution is still of low significance due to semen precipitation and energy.

Expenditure movement during storing. Tris- buffer extenders were effective at preserving fertility for two days when spermatozoa were stored at 15°C [5] and the addition of gelatin (1g/100ml extender) increased viability and acrosomal integrity of spermatozoa stored for 72h [6].

The aim of this study was to investigate the effect of gelatin addition on the quality of rabbit semen after 0, 24 and 48 hrs preservation at 5°C.

MATERIAL AND METHODS

The experimental work of this study was carried out at Animal farm during the period from September to November 2010. Six sexually mature rabbit bucks (aged 1 year and 3kg body weight). Animals were housed in flat deck cages and fed a commercial concentrate pellet diet containing 16.3% crude protein, 13.3% crude fiber, 2.5% fat, 0.6% mineral mixture and 2600 kcal /kg digestible energy. Fresh water was made available all day through nipples drinker system. Before start, semen quality (color, volume, and progressive motility) was assessed and all bucks were selected to good semen quality and quantity.

2-Semen collection and evaluation:

Semen was collected twice weekly for twelve weeks from 6 buck rabbits with the aid of an artificial vagina. Gel plug was removed immediately after collection. Immediately after collection semen was evaluated and only ejaculates exhibiting active progressive motility percentages (over 65%) were used. Semen from different bucks was then pooled and divided to three equal portions. Each portion was diluted with one of three, one was without gelatin, second types of tris-fructose-yolk extender one was without gelatin, second types and third were containing 1 or 1.8g gelatin per 100ml extender, respectively. Addition to extender was at 30°C and 1:3 Semen extender. The basic extender consisted of 3.786gm Tris, 2.172gm citric acid anhydrous, 5gm fructose, 12% egg yolk 100000 IU

Penicillin procaine and 100000 µg streptomycin sulphates according to [7]. Extended semen samples were then cooled at 5°C in a refrigerator and stored for 0, 24 and 48 hrs sperm motility was recording to [8]. Acrosomal damage was estimated by fixing in a solution of 0.2 % glutaraldehyde and integral acrosome percentage was estimated according to [9]. Sperm motility (%) and acrosome damage (%) were estimated at each storage period.

3-Statistically analysis:

Data were statistically analyzed by analysis of variance according to [10] the difference between means were tested by using Duncan's new multiple range test [11] by using [12]

RESULTS AND DISCUSSION

The effect of gelatin addition and storage on buck Semen quality it's presented in Table 1. It could be observed that gelatin addition resulted in the highest sperm motility. The level of 1.8 gelatin gave the highest post cooling sperm motility ($P < 0.01$). Get extended semen samples stored at 5°C were solid (the spermatozoa were immotile). This solid state were clearly observable in all gelatin-stored samples throughout the study. Increasing storage time resulted in decreasing significantly sperm motility. However, adding gelatin reduced the adverse effect of storing time. These results partly agreed with those reported by [6].

The lowest sperm abnormality was recorded for 1.8 g gelatin / 100 ml extender (11%) as compared with 1 g gelatin / 100 ml extender (15%) adds without addition (22%). Abnormal spermatozoa increased with the increase of storage time. Increasing gelatin level improved sperm abnormality stat and reduced the adverse effect of storing time. These results are similar to those reported by [13].

Data presented in Table 1 showed that the gelatin addition in the extender affected significantly ($P < 0.01$) the percentage of acrosomal damage of the cooled rabbit spermatozoa.

The least acrosomal damage was noticed at highest gelatin level. Total acrosomal damage was increased with the increasing of the storage time. These results are in agreement with those found by [14].

Data presented in Table 1 showed that, the effect of gelatin addition to cooled extender on the percentage of dead spermatozoa was significantly ($P < 0.01$). The lowest beneficial over all mean of dead spermatozoa was at the highest gelatin level. Overall effect of storage time on total dead spermatozoa was 16, 20 and 24 for 0, 24 and 48 hrs, respectively. These results are similar to those reported by [15 and 16].

In conclusion, our results showed that there was a positive effect of adding gelatin on the viability and integrity of rabbit spermatozoa after the short-term storage. Our explanation of this finding is that, although buffers were added to the extenders to minimize PH- fluctuation due to the metabolic products of the spermatozoa [17], sedimentation of the sperm cells occur, during preservation. Therefore, PH may be lower at the region of sediment cells. Moreover, the concentration of some toxic metabolic products may be higher at this region. As gelatin prevents sedimentation, sperm cells are more uniformly distributed and buffers

can prevent Ph -changes more efficiently In addition, solidification by gelatin reduces sperm movement and lessens energy expenditure.

Table-1: Mean percentages of bucks semen characters at different levels of gelatin in Tris extender stored at 5°C

Semen characters (%)	Storage Time (hrs)	Gleatin level (g/100ml)			Overall Means
		0	1	1.8	
Motility (%)	0	68±1.67	75±2.31	85±1.64	76±1.11 ^A
	24	55±3.18	69±1.38	81±1.83	68±2.81 ^B
	48	39±1.27	66±1.55	77±1.38	61±1.89 ^C
	Overall means	54±7.11 ^c	70±6.38 ^b	81±6.15 ^a	
Abnormal Sperms (%)	0	16±1.15	12±1.22	8±1.16	12±1.15 ^C
	24	22±1.18	15±2.11	11±2.04	16±1.91 ^B
	48	28±2.05	18±1.33	14±1.51	20±1.12 ^A
	Overall Means	22±3.48 ^a	15±3.12 ^b	11±3.21 ^c	
Acrosomal Damage (%)	0	12±2.03	8±1.14	5±1.51	8±1.15 ^C
	24	16±1.35	11±1.56	7±1.12	11±1.55 ^B
	48	20±1.42	14±2.11	9±1.17	14±1.31 ^A
	Overall means	16±2.44 ^a	11±4.05 ^b	7±3.26 ^c	
Dead Spermatozoa %	0	21±1.28	16±1.88	12±1.21	16±1.15 ^C
	24	26±1.18	20±1.15	15±1.45	20±1.55 ^B
	48	31±1.81	24±1.28	18±1.77	24±1.31 ^A
	Overall means	26±3.18 ^a	20±2.91 ^b	15±3.41 ^c	

Means with different litters each item are significantly differ (P<0.01).

#

REFERENCES

1. Morrel, J. M.; Artificial insemination in rabbits. British Veterinary Journal , 151 :477-88 (1995)
2. Al-Jubouri , S. A. H. ; studies on preservation of ram semen by freezing and other Methods . Ph. D. University of zagazing , A.R.E. (1987)
3. Curry , M. R.; Cryopreservation of semen from domestic livestock . Review Reproduction , 5:46-52(2000)
4. Moce ,E. ; Vicente, J.S. ; lavara ;R. ;Effect of freezing –thawing protocols on the performance of semen from three rabbit lines after artificial insemination theriogenology ,60 :115-23(2003)
5. Roca, J ; Martinez , S.;Vaquez,J.M.;Lucas,X.; Prrilla ,I.and Martinez, E. A. ;Viability and fertility of rabbit spermatozoa

- diluted in tris –buffer extender and stored at 15⁰C. *Animal of Reproduction Sciene* , 64:103-112 (2000)
6. Nagy, S.Z. ;Sinkovics , G. Y. and Kovacs , A. ; Viability and acrosome integrity of rabbit spermatozoa proessed in a galatin – supplemented extender . *Animal of Reproduction Science* , 70:283-6 (2002)
 7. Zaghloul , A. A. ;Effect of sugar replacement to tris extender and level of egg yolk on rabbit sperm motility stored at 5⁰C , 4th scientific Conference on physiological Applications for Animal Wealth Development ,Cairo , Egypt 181-191(2006)
 8. Salisbury , G. W. ;van Demark , N. L. and lodge ,J.R. ; *Physiology of Reproduction and Artificial insemination of cattle* .W. H. freeman and company , san Francisco , USA(1978)
 9. Johanson , L.;W.F. Berndtson and B. W. Pickett ; An improved method for evaluating acrosomes of bovine spermatozoa. *Journal of Animal Science* , 24:951-954 (1976)
 - 10.Snedecor , G. W. and Cochran ,W. G. ; *Statistical methods* . 5th Edition Iowa state University Press , Ames , USA ; 1982
 - 11.Duncan ,D. B. ; *Multiple Ranges and Multiple F-tests* . *Biometciacs*, 11:1-42 (1955)
 - 12.Spss. *Spss Base 10 for for windows Users Guide*.Spss. Inc. , Editors , Cary , N. S. A. (1999)
 - 13.Cortell , C. and M. P. ,Viudes de castro ;Effect of gelatin addition to freezing extender on rabbit semen parameters and reproductive performance, *World Rabbit Congress* . June 10-13 , 2008-Italy (2008)
 - 14.Lopez – Gatiús , G. Sances , M. sancho , J. Yaniz , P. Santolaria , R. Gutierrez , M. Nunez , C. Soler : Effect of solid storage at

15°C on the subsequent motility , and fertility of rabbit semen
Theriogenology , 64 :252-260 (2005)

- 15.Issa ,H. H. nd S.A.H. Al-Juburi ; Effect of preservation methods on rabbit sperm motility and acrosome integrity . Third Science Conference On Technical Education Research , Establishment of Technical research – Baghdad –Iraq ; 14-16 April (1992)
- 16.Zeidan , A. E. B. , M. A. Abd El- Kareem ,M. M. Mohamed and L. B. Bahgat . Quality and fertility rate of the cooled rabbit spermatozoa in different extender . Third Science . Conference On Rubbit Production in Hot Climates , 8-11 Oct:pp:317 -328 (2002)
- 17.Levis , d. G. : Liquid Boar semen production current extender technology and where do we go from here .Boar semen Preservation , IV. : 121-128 (2000)

The Study of Antibacterial Activity of Acridone Derivatives Containing 1, 3, 4-Oxadiazole

Fitua M. Aziz , Israa B. Raoof, Shiamaa I. Shuker, and Ayad K. Khan
College of Pharmacy, AL-Mustansiryah University

Received 28/2/2011 – Accepted 2/3/2011

الخلاصة

لقد تضمن البحث ثلاثة أجزاء:
الجزء الأول: لقد تم خلال هذا الجزء تحضير مشتقات جديدة للأكريدون والحاوية على حلقات 1,3,4-أوكساديازول وهي:
ثنائي فنييل أمين-2، 4- ثنائي حامض كاربوكسيلي و 9-(H10)-أكريدون-2- حامض كاربوكسيلي و 2-[[5-(4-بنزين معوض)-4,3,1-أوكساديازول-2-إيل]-9-(H10)-أكريدون و 2-[[5-(4-بنزين معوض)-4,3,1-أوكساديازول-2-إيل]-9-(H10)-أكريدون (فنييل 4,3,1-أوكساديازول و 2-[[5-ثايول-4,3,1-أوكساديازول-2-إيل]-9-(H10)-أكريدون
الجزء الثاني: تشخيص تراكيب جميع المركبات المحضرة شُخصت باستخدام أطياف (UV ،F.T.IR) وكانت النتائج المستحصلة متوافقة مع التراكيب المقترحة ودونت في الجدول رقم (1).
الجزء الثالث: تم تقييم الفعالية البايولوجية لبعض المركبات المحضرة ضد سبعة سلاسل من البكتيريا. والنتائج المحصلة دونت في الجداول رقم (2) و(3).

ABSTRACT

The research involves three parts:

Part 1: In this part synthesis of Acridone derivatives containing 1, 3, 4-oxadiazole are:

Diphenylamine-2, 4'-dicarboxylic acid, 9(10H)-Acridone-2-carboxylic acid, 2-[[5-(4-Substituted benzene)-1,3,4-oxadiazol-2-yl]-9(10H)-acridone , 9(10H)-Acridone-yl]-5-[4(9(10H)-acridone-2-yl-carboxy) phenyl]-1, 3,4-oxadiazole , 2-[[5-Thiol-1, 3, 4-oxadiazol-2-yl]-9(10H)-acridone.

Part 2: Characterized the Structures of all these synthesized compounds by spectral (FTIR, UV) data. The results were discussed and found in agreement with the suggested structures are listed in Table (1).

Part 3: Antibacterial behavior of some of the synthesized compounds against seven strains of bacteria has been investigated; the results obtained are listed in Table (2), (3).

INTRODUCTION

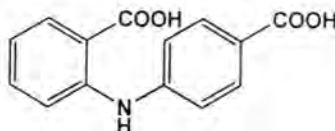
The synthesis of N-bridged Heterocycles have received much attention during recent years (1), oxadiazole ring having a five member ring containing one oxygen and two nitrogen (2). 1, 3, 4-oxadiazole derivatives lie in the field of liquid crystals and photosensitizer Substituted .1, 3, 4-oxadiazoles are considerable pharmaceutical importance, which is documented by several number of publications and patents a large number of drugs used clinically have oxadiazole (3). Also found to show a broad range of biological activities including anti-microbial, antitumoral, anti-inflammatory and analgesic activities(4), herbicidal effects(5), hypertensive activity(6).

Therapeutic importance of these rings prompted us to develop selective molecules in which a substituent could be arranged in a pharmacophoric pattern to display higher pharmacological activities (7). 1, 3, 4-oxadiazole and their synthetic analogs have also anti-cancer, anti-HIV agent, anti-parkinsonian and anti-proliferative agent (8).

Acridone are the oxidized product of acridines, Moreover the pharmacological activity of these intercalating drugs derives from their ability to inhibit the synthesis of nucleic acids by blocking the action of DNA metabolizing proteins(9), most of the compounds were active against the microorganism having significant activity against these bacteria comparable to standard drugs, ampicillin and chloramphenicol(10).

MATERIALS AND METHODS

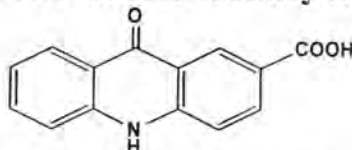
1- Synthesis of Diphenylamine-2, 4'-dicarboxylic acid [1], Ullmann condensation:



To a mixture of 2-chlorobenzoic acid (0.08mol), 4-aminobenzoic acid (0.08 mol) and copper oxide powder (0.002 mol) in (60 ml) of amyl alcohol, dry potassium carbonate (0.08 mol) was slowly added and the contents were allowed to reflux for (6h) at (100°C). The amyl alcohol was removed by evaporation and the mixture poured into (250 ml) of cold water, acidified with concentrated hydrochloric acid. The greenish black precipitate which formed was filtered, washed with cold water and collected.

The crude acid was dissolved in aqueous sodium hydroxide solution, boiled in the presence of activated charcoal and filtered, on acidification of the filtrate with concentrated of hydrochloric acid white precipitate of [1] was obtained which was washed with water and recrystallized from ethanol.

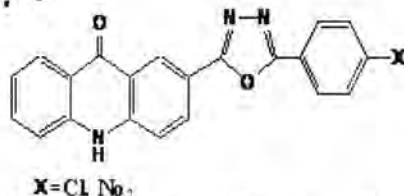
2- Synthesis of 9(10H)-Acridone-2-carboxylic acid [2]:



Compound [1] (0.04 mol) was placed in a round bottom flask which was added in (50 ml) of concentrated sulfuric acid, shaken well and heated on water bath for (3hrs). Appearance of yellow color indicated the completion of the reaction. Then, it was poured into (250 ml) of hot water. The yellow precipitate which formed was filtered, washed with

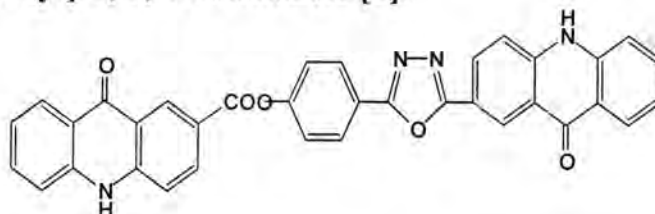
water and collected. The sample of 9(10H)-acridone-2-carboxylic acid [2] was recrystallized from methanol

3- Synthesis of 2-[5-(4-Substituted benzene)-1, 3, 4-oxadiazol-2-yl]-9(10H) - acridone [3, 4]:



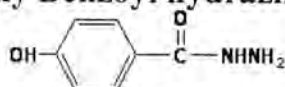
A mixture of 9(10H)-Acridone-2-carboxylic acid [2] (0.004 mol), 4-substituted benzoyl hydrazine (0.004 mol) and phosphorus oxychloride (5 ml) was refluxed overnight. The cold reaction mixture was poured on the crushed ice and made basic by adding sodium bicarbonate solution. The resulting solid was filtered, dried to give the desired product.

4- Synthesis of 2-[9(10H)-Acridone-yl]-5-[4(9(10H)-acridone-2-yl-carboxy) phenyl]-1, 3, 4-oxadiazole [5]:



Include:

A- Synthesis of 4-hydroxy Benzoyl hydrazines:

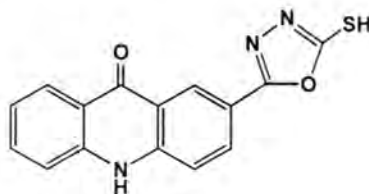


A mixture of 4-hydroxy ethyl benzoate (0.05 mol) and excess of hydrazine hydrate (10 ml) were refluxed for (2 hrs); ethanol (15 ml) was added and refluxed for (5-7 hrs). The 4-hydroxy Benzoyl hydrazines which separated on cooling was filtered and washed with cold water.

B- Synthesis of 2-[9(10H)-Acridone-yl]-5-[4(9(10H)-acridone-2-yl-carboxy) phenyl]-1, 3, 4-oxadiazole [5]:

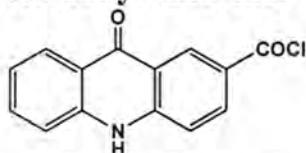
Mixture of compound [2] (0.004 mol), 4-hydroxybenzoyl hydrazine (0.002 mol) and phosphorus oxychloride (7.5ml) was refluxed overnight. The cold reaction mixture was poured on the crushed ice and made basic by adding sodium bicarbonate solution. The resulting solid was filtered, dried to give the desired product.

5- Synthesis of 2-[5-Thiol-1, 3, 4-oxadiazol-2-yl]-9(10H)-acridone [6]:



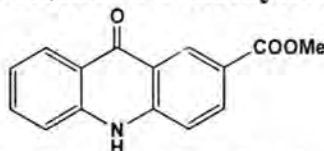
Include:

A- Synthesis of 9(10H)-Acridonyl chloride:



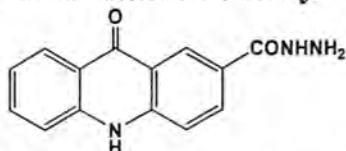
A mixture of (0.004 mol) 9(10H)-Acridone-2-carboxylic acid [2] and excess thionyl chloride (10 ml) was refluxed for (3 hrs), and then the excess of thionyl chloride was evaporated the precipitate of 9(10H)-Acridonyl chloride

B- Synthesis of 9(10H)-Acridone-2-methylcarboxylate:



To the compound 9(10H)-Acridonyl chloride (0.00194 mol), cold methanol (10 ml) was added almost readily and an instantaneous reaction occurred to give the title product. The crystals of ester were collected, filtered and washed with cold solution of 10% NaHCO_3 , and then with cold water to give the desired product.

C- Synthesis of 9(10H)-Acridone-2-carboxylic acid hydrazide:



A mixture of ester 9(10H)-Acridone-2-methylcarboxylate (0.00197 mol) and excess (85%) hydrazine hydrate (10ml) was refluxed for (3 hrs), DMSO (1ml) was added and the reflux continued for another (24 hrs). The crude product which was obtained after distilling off the excess DMSO. Cooling filtering then washing with a little cold water, this product was employed in the next step without further purification

D- Synthesis of 2-[5-Thiol-1, 3, 4-oxadiazol-2-yl]-9(10H)-acridone [6]:

Stirred solution of acid hydrazide 9(10H)-Acridone-2-carboxylic acid hydrazide (0.00169 mol) in ethanol (10mL) and potassium hydroxide (0.00169 mol), carbon disulfide (0.00338 mol) was added slowly at (0°C), and the mixture was refluxed for (6 hrs). The solvent

was evaporated and the residue dissolved in water and acidified with dilute hydrochloric acid. The precipitate was filtered and washed with little cold water. The crude product was recrystallized from ethanol to give the desired product.

Characterization:

F.T.IR spectrum and ultra-violet (UV) spectrophotometry technique with melting point (M.p) is used to characterize the synthesized compounds in dimethyl sulfoxide as a solvent.

1-Bacterial Strains:

Bacterial Strains used in the study are clinical strains, were obtained from medical city hospital at October –December 2009. They are *Klebsiella sp.*, *Enterococcus sp.*, *Streptococcus pneumoniae*, *Acinetobacter sp.*, *Salmonella typhi*, *Proteus sp.*, *Pseudomonas aeruginosa*.

2-Antibacterial activity:

The compounds were dissolved in dimethyl sulfoxide (DMSO) in order to obtain the concentrations (100, 50, 25) mg/ml. The agar well diffusion method was used to determine antibacterial activity (11). The culture medium was inoculated with one of tested bacteria suspended in nutrient broth. Six millimeter diameter wells punched into the agar and filled with 0.1 ml of each concentration. DMSO was used as control. The antibacterial activity was evaluated by measuring the inhibition zone diameter observed.

RESULTS AND DISCUSSION

F.T.IR spectrum and ultra-violet (UV) spectrophotometry technique with melting point (M.p) is used to characterize the synthesized compounds in dimethyl sulfoxide as a solvent found on Table 1. These λ_{max} could be assigned to $(\pi-\pi^*)$, $(n-\pi^*)$ [(acridone, oxadiazole, C=N (azomethine)] transitions. The spectra data found to be quite similar to other acridone derivatives reported in recent literature (12), (13).

Table -1: Physical properties and spectral data of synthesized compounds

Compd. No	M. p.	Mol Formula	Yield%	FTIR (cm-1)	UV-Visible (λ nm)
1	208-210	C ₁₄ H ₁₁ NO ₄	62	1. N-H stretch., 3315.4 2. O-H stretch., near 2500-3300 3. C=O stretch., of acid 1685 4. C=C stretch., 1596.9 5. Out-of-plane C-H bend., (p-disub. benzene) 842.8 6. Out-of-plane C-H bend., (o-disub. benzene) 754.1	399, 387, 330, 293, 272, 243
2	>330	C ₁₄ H ₉ NO ₃	72	1. N-H stretch., 3423.4 2. O-H stretch., 3267.2 3. Aromatic C-H stretch., 3103 4. C=O stretch., of acid 1685.7 5. C=O stretch., of ketone 1631.7 6. C=C stretch., 1587.3	538, 396, 378, 325, 286, 262, 239
3	>330	C ₂₁ H ₁₂ N ₃ O ₂ Cl	68	1. N-H stretch., 3398.3 2. Aromatic C-H stretch., 3087.8 3. C=N stretch., 1600.8 4. Asym. and sym. C-O-C stretch., 1260, 1035.5 5. Out-of-plane C-H bend., (p-disub. benzene) 833.2	402, 381, 364, 345, 288, 259, 232
4	302-304	C ₂₁ H ₁₂ N ₄ O ₄	74	1. N-H stretch., 3361.7 2. C=N stretch., 1614.3 3. Asym. and sym. C-O-C stretch., 1263.3, 1035.7 4. Asym. (Ar-NO ₂) N-O stretch., near 1500 5. Sym. (Ar-NO ₂) N-O stretch., 1311.5 6. Out-of-plane C-H bend., (p-disub. benzene) 835.1	411, 329, 258
5	324-326	C ₃₅ H ₂₀ N ₄ O ₅	60	1. N-H stretch. near 3400 2. Aromatic C-H stretch. Near 3050 3. C=O stretch. of ester 1732.0 and 1693.4 4. C=O stretch. of ketone, 1633.6 5. C=N stretch. 1595.0 6. Ring C=C stretch. 1485.1 7. Asym and sym. C-O-C stretch. near 1250, 1031.8	396, 378, 324, 287, 259
6	>340	C ₁₅ H ₉ N ₃ O ₂ S	69	1. N-H stretch., near 3400 2. S-H stretch., 2586.4 3. C=O stretch. of ketone, 1624 4. C=N stretch. near 1580 5. Ring C=C stretch., 1515.9 6. Asym. and sym. C-O-C stretch., 1278.7 and 1041.5 7. C=S stretch. 1332.	397, 379, 361, 327, 286, 267

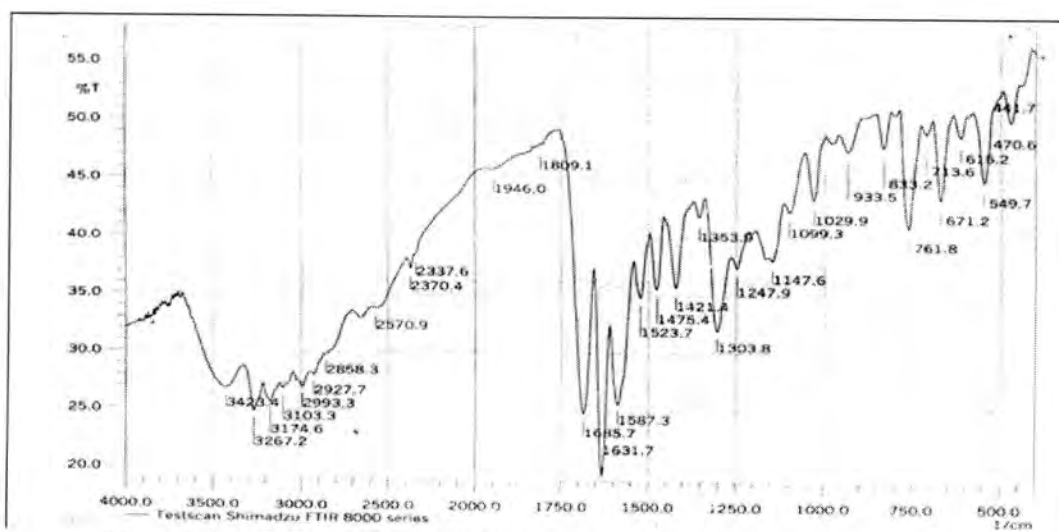


Figure -1: F.T.IR spectrum of 9(10H)-Acridone-2-Carboxylic acid [2].

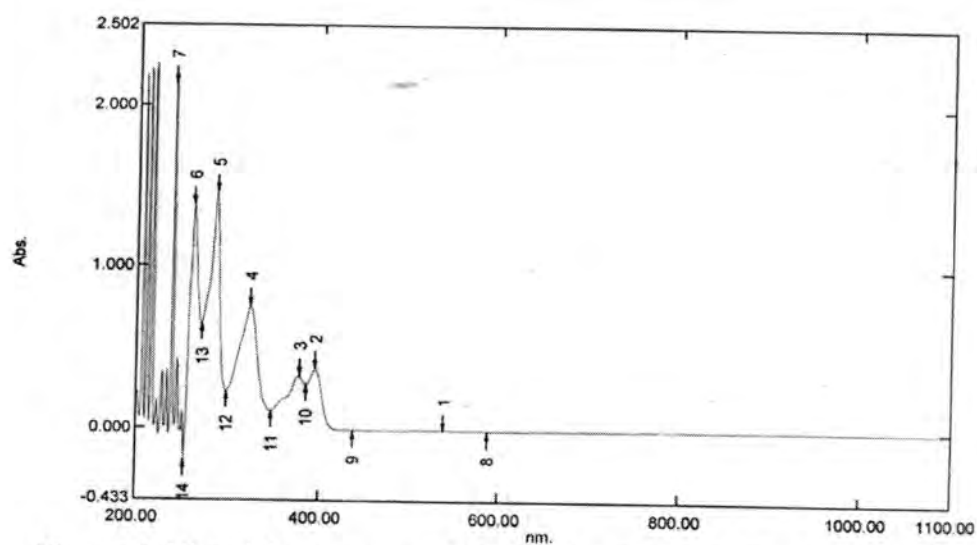


Figure -2: Ultraviolet spectrum of 9(10H)-Acridone-2-Carboxylic acid [2].

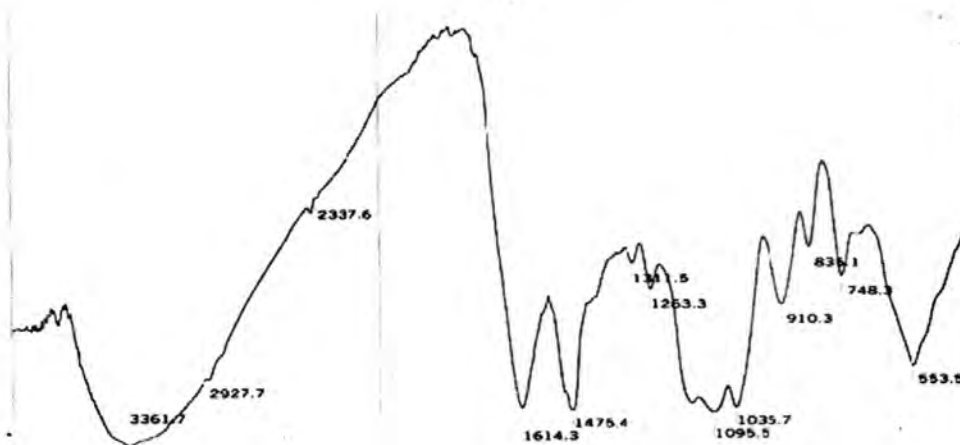


Figure -3: F.T.IR spectrum of 2-[5-(4-nitro benzene)-1, 3, 4-oxadiazol-2-yl]-9(10H)-acridone [4]

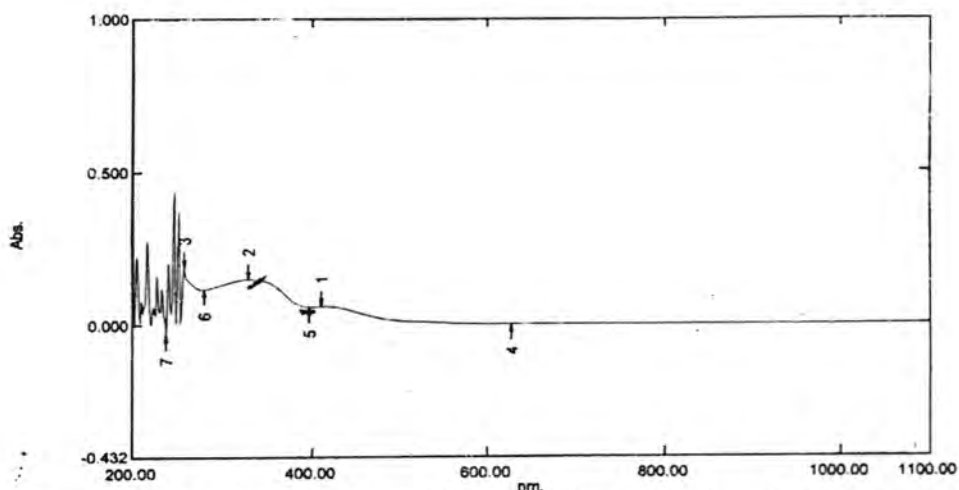


Figure -4: Ultraviolet spectrum of 2-[5-(4-nitro benzene)-1, 3, 4-oxadiazol-2-yl]-9(10H)-acridone [4]

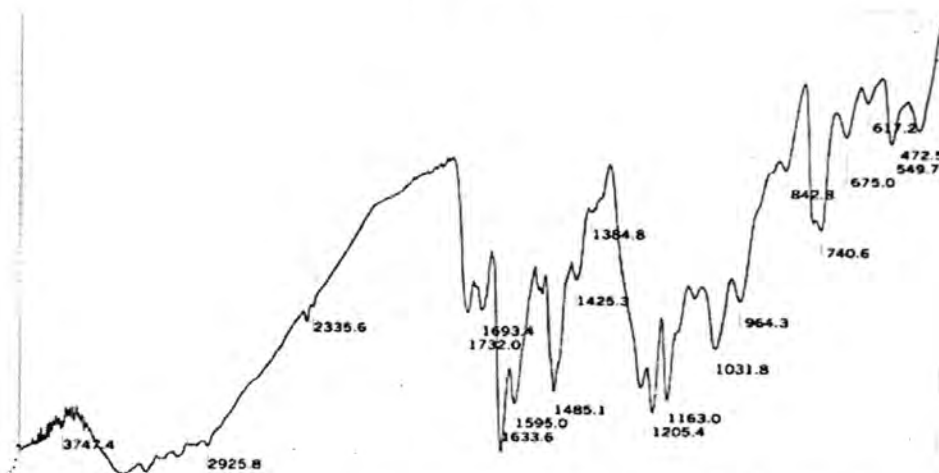


Figure -5: F.T.IR spectrum of 2-[9(10H)-Acridone-2-yl]-5-[4-(9(10H)-acridone-2-yl-carboxy) phenyl]-1, 3, 4-oxadiazole [5]

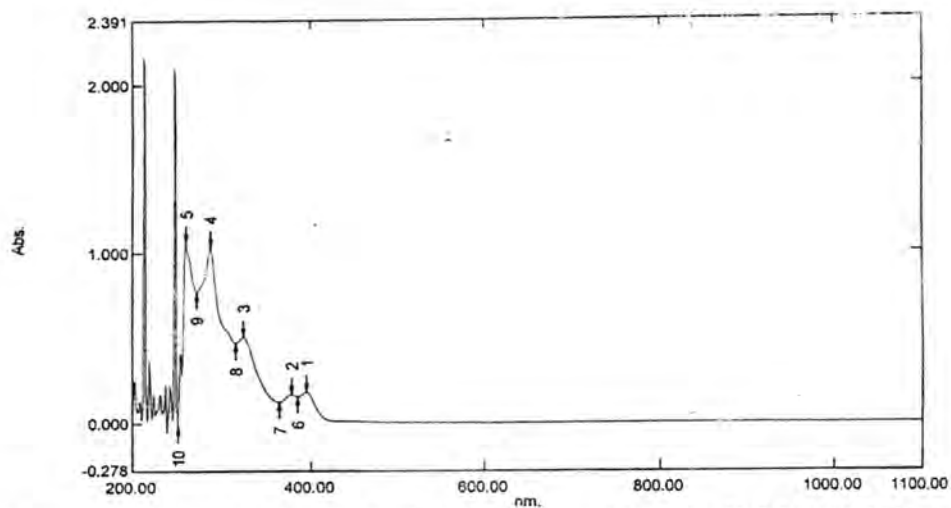


Figure -6: Ultraviolet spectrum of 2-[9(10H)-Acridone-2-yl]-5-[4-(9(10H)-acridone-2-yl-carboxy) phenyl]-1, 3, 4-oxadiazole [5]



Figure -7: F.T.IR spectrum of 2-[5-Thiol-1,3,4-oxadiazol-2-yl]-9(10H)-acridone [6].

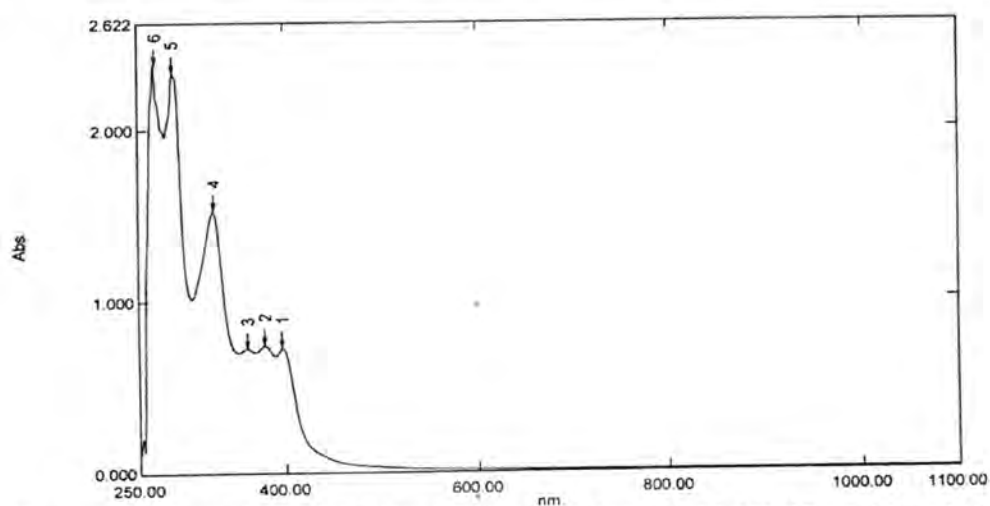


Figure -8: Ultraviolet of 2-[5-Thiol-1, 3, 4-oxadiazol-2-yl]-9(10H)-acridone [6].

Antibacterial activities:

The antibacterial activities of Acridone derivatives at concentrations of (100, 50, 25) mg/ml against pathogenic bacteria were investigated and results are present in table (2) and table (3)

All bacterial strains demonstrated degree of sensitivity to Acridone derivatives, table (2) showed that *Enterococcus*, *Salmonella typhi* were sensitive to compound 1 at concentrations of 100,50mg/ml., *Proteus sp.* was sensitive to compounds 1at concentration of 100,25mg/ml while *Streptococcus pneumonia* was sensitive to compounds 2at concentration of 50 mg/ml all Bacterial Strains resist to compound 3. *Pseudomonas aeruginosa*, *Klebsiella sp.*, were not appear inhibition zone to 1, 2, 3 compounds

Table -2: antibacterial activity of compounds 1, 2, 3

	Inhibition zone diameter (mm) concentrations(mg/ml)									Control
	1			2			3			
	100	50	25	100	50	25	100	50	25	
Tested bacteria										
<i>Klebsiella sp.</i>		-	-	-	-	-	-	-	-	-
<i>Enterococcus</i>	30	30	-	-	-	-	-	-	-	-
<i>Streptococcus pneumonia</i>	-	-	-	-	15	-	-	-	-	-
<i>Acinetobacte sp.</i>	-	-	-	-	-	-	-	-	-	-
<i>Salmonella typhi</i>	32	20	-	-	-	-	-	-	-	-
<i>Proteus sp.</i>	15	-	20	-	-	-	-	-	-	-
<i>Pseudomonas aeruginosa</i>	-	-	-	-	-	-	-	-	-	-

(-): no inhibition zone

(Control): Dimethyl sulfoxide (DMSO) *Pseudomonas aeruginosa* was

Table (3) showed the antibacterial activity of 4,5,6 compounds *Pseudomonas aeruginosa* was sensitive to three compounds 1at different concentrations *Salmonella typhi* sensitive to compound 4 at concentration of 50 mg/ml and compound 5 at all concentrations . *Klebsiella sp.*, *Enterococcus* sensitive to compound 6 at different concentrations. There was no inhibition zone for *Streptococcus pneumonia*, *Acinetobacte sp.*, *Proteus sp.*to all compounds at concentrations were uses.

Table -3: antibacterial activity of compounds 4, 5, 6

Tested bacteria	Inhibition zone diameter (mm) concentrations(mg/ml)									Control
	4			5			6			
	100	50	25	100	50	25	100	50	25	
<i>Klebsiella sp.</i>		-	-	20	15	-	22	-	-	-
<i>Enterococcus</i>	-	-	-	18	-	-	-	5	10	-
<i>Streptococcus pneumonia</i>	-	-	-	-	-	-	-	-	-	-
<i>Acinetobacte sp.</i>	-	-	-	-	-	-	-	-	-	-
<i>Salmonella typhi</i>	-	30	-	22	15	7	-	-	-	-
<i>Proteus sp.</i>	-	-	-	-	-	-	-	-	-	-
<i>Pseudomonas aeruginosa</i>	-	-	20	-	20	25	-	7	7	-

(-): no inhibition zone

(Control): Dimethyl sulfoxide (DMSO)

We found compounds [1] melting point (208-210°C) and by F.T.IR spectrum which showed the disappearance of absorption bands due to NH_2 stretching of amino group in *p*-amino benzoic acid and the appearance of a band at 3315.4 cm^{-1} for (N-H).

The presence of a carboxyl group (-COOH) is recognizable by the presence of O-H stretching absorption band at ($2500\text{-}3500 \text{ cm}^{-1}$), as well as the C=O absorption at 1685 cm^{-1} . Evidence of the presence of aromatic ring was the presence of (C=C) aromatic stretching band at (1596.9 cm^{-1}) and also a sharp bands at (754.1 cm^{-1}) and (842.8 cm^{-1}) that were assigned to the out of plane bending of *o*- and *p*-Disubstituted benzene ring, respectively.

Compound [2] found very high melting point ($>330^\circ\text{C}$). Also by F.T.IR spectrum, which displays a broad (O-H) stretching absorption band in the region of (3267.2 cm^{-1}) as well as the carboxylic acid (C=O) absorption band at (1685.7 cm^{-1}), also ketone (C=O) aromatic, (C=C) and amine (N-H) absorption band at (1631.7 cm^{-1}), (1587.3 cm^{-1}) and (3423.4 cm^{-1}) respectively.

The F.T.IR spectra of compounds [3, 4] were devoid of the amide bands present in the spectrum of the aryl hydrazines in regions between ($3427.3\text{--}3184.3\text{ cm}^{-1}$) of asymmetric and symmetric N-H stretching of (NH_2), as well as the disappearance of O-H band at (3267.2 cm^{-1}) of compound [2]. The appearance of bands near (1600 cm^{-1}) assigned to (C=N) band of oxadiazole moiety and bands near ($1260, 1035\text{ cm}^{-1}$).

The structure of compound [5] was established on the melting point ($324\text{--}326\text{ }^\circ\text{C}$), F.T.IR absorption bands show disappearance of the broad band at ($3300\text{--}3170\text{ cm}^{-1}$) assigned to O-H stretching and appearance of the carbonyl stretching at (1732 cm^{-1}) are good evidence to the success of the esterification step.

The structure of compound [6] was elucidated on the basis of its melting point and F.T.IR spectral data. The F.T.IR spectrum of this compound revealed a sulfhydryl absorption band (S-H) at (2586.4 cm^{-1}) and absorption of (C=S) band at (1332.5 cm^{-1}). Also F.T.IR show a typical absorptions of oxadiazole ring endo cyclic C-O-C asymmetrical and symmetrical at (1278.7 and 1041.5 cm^{-1}) and absorption band of (C=N) near (1580 cm^{-1}).

The UV-Visible absorption maxima ($\lambda\text{ nm}$) of diphenylamine-2, 4'-dicarboxylic acid derivatives is present different value of each compounds.

1, 3, 4-oxadiazole derivatives have been found to exhibit diverse biological activities (14) most of our bacterial strains were susceptible to compounds at different levels. The susceptibility due to the activity of these compounds which may make impairment of variety of enzyme systems including those involved in energy production and structural compounds synthesis (15).

REFERENCES

1. X.Hui, L.Zhang and F.Wang, Synthesis and Antibacterial activity of s-Triazoles, s-Triazole (3,4-b)-1,3,4-thiadiazolines and s-Triazolo(3,4-b)-1,3,4-thiadiazoles of 5-Methylisoxazole, J.Chinese Chem.Soc, 47:535, (2000).
2. Sharma S., Sharma P. K., Kumar N, Dudhe, Oxadiazole Their Chemistry and Pharmacological Potentials, J.Der Pharma Chemica, 2(4): 253-263(2010).

3. Mudasir R.Bandaya , Rayees H Mattoob and Abdul Rauf , Synthesis, characterization and anti-bacterial activity of 5-(alkenyl)-2-Amino- and 2-(alkenyl)-5-phenyl-1, 3, 4-oxadiazoles, J. Chem. Sci, 122:2:177-182,(2010).
4. Kok Wai Lam a, Ahmad Syahida b, Zaheer Ul-Haq c, Mohd. Basyaruddin Abdul Rahman d, Nordin H. Lajis a, d, Synthesis and biological activity of oxadiazole and triazolothiadiazole derivatives as tyrosinase inhibitors, Bioorganic & Medicinal Chemistry Letters 20: 3755-3759(2010).
5. 5.Zao-Zao Qiu , Chao-Feng Dai , Shu-Jun Chao ,Peng-Fei Xu and Zi-Yi Zhang , A New Route to Synthesis of 3,6-Diaryl-1,2,4-triazolo[3,4-b]1,3,4-oxadiazolesJournal of the Chinese Chemical Society, 51:1343-1346(2004).
6. Sanjeev Kumar, Synthesis and biological activity of 5-substituted-2-amino-1, 3, 4-oxadiazole derivatives, Turk J. Chem, 34:1-10(2010).
7. Mohammd Shahar Yar and Mohammd Wasim Akhter, Synthesis and anticonvulsant activity of substituted oxadiazole and thiadiazole activity, Journal of Acta Poloniae Pharmaceutica Drug Research, 66: 4: 393-397(2009).
8. Dhansay Dewangan¹, Alok Pandey¹, T.Sivakumar¹, R.Rajavell¹, Ravindra Dhar Dubey², Synthesis of some Novel 2, 5-Disubstituted1, 3, 4-Oxadiazole and its Analgesic, Anti-Inflammatory, Anti-Bacterial and Anti-Tubercular Activity, J..ChemTech Research Coden (USA), 2:.3:1397-1412(2010).
9. V. Sourdan, S. Mazoyer, V. Pique and J. Gally, Synthesis of new Bis- and Tetra-Acridone, J.Molecules, 6:673(2001).
- 10.Mojahidul Islam ¹ ,Anees A Siddiouil,Ramadoss Rajeshi,Afroz Bakhtl and Sunil Goyal², Synthesis of antibacterial activity of some novel oxadiazole derivatives, J.Acta Poloniae Pharmaceutica Drug Research, 65 : 4 : 441-447(2008).
- 11.Anesini, C.andPerez, C. Screening of plants used in argentine folk medicine for antibacterial activity .J.Ethnopharmacol.3:25:47(1993).
- 12.M.Mitsui and Y.Ohashima, S.Svibronic spectra of benzene clusters revisited.II. The trimer, J.Phys.Chem. A: 104:8638(2000).

- 13.T.S.Wu and C.M.Chen, Acridone Alkaloids from the Root Bark of *Severinia buxifolia* in Hainan, J.Chem. Pharm.Bull. 48(1):85-90(2000).
- 14.Sanjeev Kumar, J.Chil, Anodic synthesis, Spectral characterization ; and antimicrobial activity of novel 2-amino-5-substituted-1, 3, 4-oxadiazole, J.Chem. Soc, 1:55(2010).
- 15.Conner, D.E, Beuchat, L. ,Sensitivity of heat stressed yeast to essential oils of plants J.Applied Environ. Microbial. 4:65(1984).

Evaluation of The Process of Apoptosis Through the Estimation of Fas and Fas Ligand Levels in Some Iraqi Hypertensive Pregnant Women

Mohammed A. Saleh

Biology Department, College of Science , Diyala University.

Received 19/01/2011 – Accepted 2/3/2011

الخلاصة

ارتفاع ضغط الدم من أكثر المشاكل الطبية شيوعاً أثناء الحمل وأشير في بعض التقارير بأن بعض النساء الحوامل المصابات بارتفاع ضغط الدم يعانين من تغييرات مناعية مثل ارتفاع مستوى Fas و Fas ligand. لذا فإن هذه الدراسة تهدف إلى تقييم وقياس مستوى Fas و Fas ligand (موت الخلايا المبرمج) لدى بعض العراقيات الحوامل المصابات بارتفاع ضغط الدم. شملت الدراسة مأمجوعه 70 امرأة حامل والتي منهم 36 امرأة حامل مصابة بارتفاع ضغط الدم وأعمارهم تتراوح من 19-39 سنة كمجموعة مرضى و 34 امرأة حامل ضغط الدم لديهم طبيعي وبأعمار تتراوح من 20-38 سنة كمجموعة سيطرة. جميع النساء الحوامل كانوا من المراجعات للعيادة الطبية الخارجية في مستشفى العلوية للولادة. أظهرت نتائج هذه الدراسة بأن هناك ارتفاع معنوي في مستوى Fas و Fas ligand في النساء الحوامل المصابات بارتفاع ضغط الدم بالمقارنة مع النساء الحوامل ذوات ضغط الدم الطبيعي، وكذلك سجلت نتائج هذه الدراسة بأن متوسط العمر بالنسبة لمجموعة المرضى كان 27.89 ± 6.43 سنة بينما كان 29.09 ± 5.72 سنة لمجموعة السيطرة مع عدم وجود أي فرق معنوي. إضافة إلى ذلك أظهرت نتائج هذه الدراسة وجود زيادة معنوية في ضغط الدم الانقباضي والانساطي في مجموعة المرضى بالمقارنة مع مجموعة السيطرة. من جانب آخر أوضحت الدراسة وجود زيادة معنوية في مستوى سنثياز الحامض الدهني Fas و Fas ligand خلال الثلث الأول والثاني من الحمل لدى النساء الحوامل المصابات بارتفاع ضغط الدم بالمقارنة مع مجموعة السيطرة. في النهاية فإن نتائج الدراسة أثبتت تأثير عوامل موت الخلايا المبرمج (Fas و Fas ligand) في ارتفاع ضغط الدم أثناء الحمل.

ABSTRACT

Hypertension is the most common medical problem encountered during pregnancy. Certain pregnant women with high blood pressure have been reported to exhibit immunological abnormalities such as elevated level of soluble Fas and Fas ligand, therefore the aim of this study was to estimate the role of Fas and Fas L (apoptosis) in some Iraqi hypertensive pregnant women. A totality of 70 pregnant women consist of 36 hypertensive pregnant women their age range between 19-39 year and 34 normotensive pregnant women with age range of 20-38 year they served as control group. All pregnant women included in this study were attending the outpatient clinic in the Al-ulwea Hospital for delivery. The results of this study clarified that a level of Fas and Fas ligand were significantly elevated ($p < 0.001$) in hypertensive pregnant women as compared to normotensive group. Beside, the results revealed that the mean of age was 27.89 ± 6.43 year among patients group whereas 29.09 ± 5.72 year among second group with no significant difference observed between them. Furthermore, hypertensive pregnant women group also showed a significant increment ($p < 0.001$) in systolic and diastolic blood pressure in comparison to normotensive group. Additionally, the level of Fas and Fas ligand increased significantly during first and second trimester in gestational hypertensive women as compared to control group. Finally our findings prove the influence of apoptotic factors (Fas and FasL) on hypertension in pregnancy.

Key words: apoptosis, Fas, Fas ligand, hypertension

INTRODUCTION

Fas (CD95/APO-1) is a cell-surface membrane member of the tumor necrosis factor (TNF) receptor super family and mediate programmed cell death, or 'apoptosis', upon engagement by its ligand, FasL. Fas is widely expressed in numerous different cell types throughout the body, whereas FasL expression appears to be more restricted (1, 2).

Following activation, different cell types within the immune system express FasL, including T and B cells. FasL is also expressed in cells within areas of 'immune privilege', including the eye and reproductive organs. FasL-induced apoptosis plays both regulatory and effector functions in the immune system and appears to contribute to inflammatory process (3).

Hypertension is the most common medical problem encountered during pregnancy, complicating 2-3% of pregnancies. Blood pressure is the amount of force exerted by the blood against the walls of the arteries. A person's blood pressure is considered high when the readings are greater than 140 mm Hg systolic (the top number in the blood pressure reading) or 90 mm Hg diastolic (the bottom number). In general, high blood pressure, or hypertension, contributes to the development of coronary heart disease, stroke, heart failure and kidney disease (4). Although many pregnant women with high blood pressure have healthy babies without serious problems, high blood pressure can be dangerous for both the mother and the fetus. Women with pre-existing, or chronic, high blood pressure are more likely to have certain complications during pregnancy than those with normal blood pressure. However, some women develop high blood pressure while they are pregnant (often called gestational hypertension) (5). The effects of high blood pressure range from mild to severe. High blood pressure can harm the mother's kidneys and other organs, and it can cause low birth weight and early delivery. In the most serious cases, the mother develops preeclampsia--or "toxemia of pregnancy"--which can threaten the lives of both the mother and the fetus (6).

Soluble Fas and soluble FasL is derived by specific proteolytic cleavage of the extracellular domain of membranous Fas and FasL by matrix metalloproteinases (MMPs), some studies suggested that FasL is able to act as neutrophils chemoattractant, by stimulation of the neutrophils migration in vitro assays, and is not responsible for neutrophils recruitment in vivo, and may even opposite this Fas-mediated inflammatory effect (7). The contribution of Fas to some disorders is suggested by the finding of elevated Fas levels in serum of patients with conditions such as myocarditis, alcoholic liver disease, hypertension and rheumatoid arthritis these findings suggested that Fas have a pro-inflammatory role which may be inhibited by inhibition of

lymphocyte apoptosis(8). The Fas/Fas ligand system could reportedly help to identify a mechanism for increase blood pressure in pregnant women during pregnancy. However, there are few reports on soluble Fas and Fas ligand as an inhibitor of apoptosis during pregnancy. Abnormalities in apoptosis, particularly affecting the soluble Fas / Fas ligand are implicated in the pathogenesis of hypertensive in pregnancy. Apoptosis can be trigger in hypertensive pregnant women by expression of proteins (apoptosis inducing factor) coupled to MHC class 1 on the surface of the placental cell, allowing recognition by cells of the immune system (such as natural killer and cytotoxic T cells) that then induce to produce Fas and Fas ligand (19) . The aim of this study was undertaken to evaluate the process of apoptosis by measurement of Fas and FasL levels in some Iraqi hypertensive pregnant women compared to normotensive pregnant women's .

MATERIALS AND METHODS

A total sum of 70 pregnant women comprising as 36 hypertensive pregnant women their age range between 19-39 year and 34 normotensive pregnant women with age range between 20-38 year served as control group .All pregnant attended the outpatient clinic in the Al-ulwea hospital for delivery . A questionnaire was used to record a special notes regarding hypertensive pregnant women as follow : Name, age, time of onset of disease, level of blood pressure which includes systolic and diastolic pressure, address, and gestational trimester . Moreover , samples were collected from control group (normotensive pregnant) who were not receiving any medication and did not have a history of a chronic or acute illness

Specimens collection

From each individual included in this study, 5 ml of blood was drawn by vein puncture using disposable syringes. The blood was placed in plastic disposable tubes, it was left to stand at room temperature (20-25°C) to allow it to clot, then the sera was separated by centrifugation for 5 minutes, and divided into aliquots (250 µl) and stored at -20°C till examination. Each aliquot of the serum was used once to avoid thawing and freezing. All sera and reagents were allowed to stand at room temperature before use in the test.

Determination of human Fas and FasL :

Serum levels of Fas and FasL were measured quantitatively in sera of studied groups by enzyme linked immunosorbent assay method using ELISA kits (Bender MedSystems, Austria), measurement as recommended by the manufacturer(9).

I. Principle

An anti-Fas or anti-FasL monoclonal antibody is adsorbed onto micro wells . Fas or FasL present in sample or standard binds to antibodies adsorbed to the micro wells ; a biotin-conjugate monoclonal anti-Fas or

anti-FasL antibody is added and binds to the Fas or FasL captured by the first antibody.

Following incubation unbound biotin-conjugate anti-Fas or anti-FasL is removed during a wash step. Streptavidin-HRP is added and binds to the biotin-conjugated anti-Fas or anti-FasL. After incubation unbound streptavidin-HRP is removed during the wash step. And substrate solution reactive with HRP is added to the wells . A colored product is formed in proportion to the amount of the Fas or FasL present in the sample. The reaction is terminated by addition of sulfuric acid and absorbance is measured at 450 nm. A standard curve is prepared by using several dilutions of Fas or FasL and sample concentration determined(10) .

II. Assay procedure :

Estimation of Fas and FasL according to the manufacture:

The detailed procedure was carried out as has been suggested in the leaflet supplied with the test kit

Statistical analysis

The usual statistical methods were used in order to assess and analyze our results and included:

Descriptive statistics: including Mean and Standard deviation (SD).

Inferential statistics: Data have been analyzed statistically using SPSS program version 10. Analysis of quantitative data was done using t-test and ANOVA (analysis of variance). Acceptable level of significance was considered to be below 0.05 (11).

RESULTS AND DISCUSSION

Certain pregnant women with high blood pressure have been reported to exhibit immunological abnormalities such as elevated level of soluble Fas and Fas ligand (12) . We were investigating the mechanisms involved in immunological disturbances found in gestational hypertension , with focus on the Fas-mediated apoptotic pathway. In sera of hypertensive pregnant women the levels of Fas and Fas ligand were significantly elevated ($p < 0.001$) as compared to normotensive group. Fas levels (mean \pm SD) was 3.22 ± 1.55 ng/ml and Fas ligand level (mean \pm SD) was 2.48 ± 1.4 ng/ml in comparison to normotensive group 1.58 ± 0.7 ng/ml and 1.61 ± 0.63 ng/ml respectively as shown in table (1,2). This study showed a remarkable increment in the serum concentrations of Fas and FasL in hypertensive pregnant women group as compared to other group ,these results are similar to the results obtained by Vellore *et al.* (16) reported that the serum concentrations of Fas and FasL in hypertensive pregnant women were significantly elevated . Fas is a cell surface receptor protein which

belongs to the tumor necrosis factor receptor family and the abnormalities in Fas and other related molecules have been reported in hypertensive condition in pregnant women and human idiopathic autoimmune diseases such as systemic lupus erythematosus and rheumatoid arthritis. In addition, it has also been suggested that Fas-mediated apoptosis plays a crucial role in the acquisition of hypertension because mutations of the Fas and Fas ligand genes (Mutations of these genes, which lead to defects in programmed cell death) have been identified in some individuals have malignant hypertension(13,14, 15) , therefore the results of this study suggesting the important role of apoptosis (Fas and Fas ligand) in gestational hypertension.

Besides, the distribution of patients and control groups according to the age are shown in table 1, the results according to the table recorded that the patients group age ranged 19-39 y with mean of 27.89 ± 6.43 whereas the control group age ranged 20-38 y mean of 29.09 ± 5.72 , no significant difference was noticed between them as presented in table 2. The optimum age for women fertility begins at the age of 18, until about the age of 25, women will be at their most fertile and most likely to get pregnant. Beginning around 25 or 26, a woman's fertility starts to decline. This decline is relatively gradual for the next ten years, however, from the age of 35 the process of losing fertility begins to speed up more rapidly. By the time a woman reaches the age of 40, she is exponentially more likely to have problems getting pregnant. In fact, around 2/3 of women who are over the age of 40 will have issues with infertility for some reason or another (17).

Furthermore, hypertensive pregnant women group also showed a significant increment ($p < 0.001$) in systolic and diastolic blood pressure in comparison to normotensive group , a level of systolic blood pressure in patients group was 152.25 ± 10.66 mm Hg in comparison to control group 123.23 ± 9.83 mm Hg ,whereas a level of diastolic blood pressure in patients group was 94.17 ± 8.32 mm Hg in comparison to control group 77.94 ± 6.29 mm Hg as pointed out in table 1,2. These results in agreement with the previous study done by poon *etal.* (17) who established that the systolic and diastolic pressure among hypertensive pregnant women was 150 mm Hg and 95 mm Hg respectively. Blood pressure is usually classified based on the systolic and diastolic blood pressures. Systolic blood pressure is the blood pressure in vessels during a heartbeat. Diastolic blood pressure is the pressure between heartbeats. A systolic or the diastolic blood pressure measurement higher than the accepted normal values for the age of the individual is classified as pre-hypertension or hypertension, moreover normal blood pressure is below 120/80; blood pressure between 120/80

and 139/89 is called "pre-hypertension", and a blood pressure of 140/90 or above is considered high (18).

Table -1: Descriptive Statistics for hypertensive and normotensive pregnant women

parameter	Hypertensive pregnant women			Normotensive pregnant women		
	No.	Mean	Std.Dv	No.	Mean	Std.Dv
Age	36	27.89 year (19-39y)	6.431	34	29.09 year (20-38y)	5.723
Fas	36	3.22 ng/ml	1.550	34	1.58 ng/ml	0.701
Fas ligand	36	2.84 ng/ml	1.400	34	1.61 ng/ml	0.613
Systolic blood pressure	36	152.25 mm Hg	10.662	34	123.23 mm Hg	9.838
Diastolic blood pressure	36	94.17 mm Hg	8.324	34	77.94 mm Hg	6.290

Table- 2: t-test and p-value for hypertensive and normotensive pregnant women

Hypertensive pregnant women	Normotensive pregnant women	t-test	p-value	C.S
Age	Age	1.089	P>0.05	NS
Fas	Fas	5.386	P<0.001	HS
Fas ligand	Fas ligand	4.467	P<0.001	HS
Systolic blood pressure	Systolic blood pressure	11.171	P<0.001	HS
Diastolic blood pressure	Diastolic blood pressure	9.143	P<0.001	HS

Additionally ,the level of Fas and Fas ligand were increase significantly during first and second trimester in gestational hypertensive women as compared to normotensive group , Fas levels in first and second trimester (mean \pm SD) was 3.26 ± 1.26 ng/ml and 3.82 ± 1.76 ng/ml respectively in comparison to normotensive group 1.46 ± 0.68 ng/ml and 1.83 ± 0.81 ng/ml respectively whereas the level of Fas ligand in first and second trimester (mean \pm SD) was 2.82 ± 0.96 ng/ml and 3.24 ± 1.79 ng/ml respectively in comparison to normotensive group 1.84 ± 0.51 ng/ml and 1.52 ± 0.78 ng/ml respectively as shown in table (3,4). These results agreed with Vellore *etal.* (16) who reported that a level of Fas and Fas ligand increase during first and second trimester in hypertensive pregnant women's , therefore, we propose that increase secretion of Fas and FasL may be one mechanism is responsible for increase blood pressure during pregnancy and therefore high blood pressure can be dangerous for both the mother and the fetus. Women with pre-existing, or chronic, high blood pressure are more likely to have certain complications during pregnancy than those with normal blood pressure. Conclusion our findings confirm the influence of apoptotic factors (Fas and FasL) on hypertension in pregnancy.

Table- 3: Mean serum level of Fas in hypertensive and normotensive pregnant women according to gestational trimester

Gestational trimester	Hypertensive pregnant women		normotensive pregnant women		
	Fas		Fas		C.S
	Mean	Std.Dev	Mean	Std.Dev	
First	3.269	1.268	1.464	0.680	S
Second	3.826	1.764	1.830	0.816	S
Third	1.987	0.714	1.510	0.610	NS

Table- 4: Mean serum level of Fas Ligand in hypertensive and normotensive pregnant women according to gestational trimester

Gestational trimester	Hypertensive pregnant women		normotensive pregnant women		
	Fas Ligand		Fas Ligand		C.S
	Mean	Std.Dev	Mean	Std.Dev	
First	2.823	0.966	1.842	0.519	S
Second	3.240	1.791	1.520	0.789	S
Third	2.100	0.907	1.380	0.865	NS

REFERENCES

- 1- Connell, J. O. Role of Fas-FasL in inflammatory diseases. *Exp. Rev. Mol. Med.*, 1 (9): 1-18 (2001).
- 2- Nagata, S. Apoptosis by death factor. *J. Cell*; 88 :355-365 (1997).
- 3- Bantel, H. and Osthoff, K.S. Apoptosis in hepatitis C infection. *J. Cell Dea. and Differen.*; 10 : 48-58 (2003).
- 4- Magee , L.A.; Helewa, M. and Moutquin ,J.M . Diagnosis, Evaluation, and Management of the Hypertensive Disorders of Pregnancy. *J. of Obst. and Gynaecol.*;30:S1-S48 (2008).
- 5- Hedderson, M.M. and Ferrara, A. High blood pressure before and during early pregnancy is associated with an increased risk of gestational diabetes mellitus. *Diabet Care.*;31(12):2362-2367 (2008).
- 6- Facchinetti ,F.; Allais, G.; Nappi, R.E.; D'Amico, R. ; Marozio ,L. and, Bertozzi, L. Migraine is a risk factor for hypertensive disorders in pregnancy: a prospective cohort study. *Cephalal.* ;29(3):286-292 (2009).
- 7- Nozawa, K.; Dinarello, C.A. and Chen, P. Soluble Fas (APO-1,CD95) and soluble Fas ligand in rheumatic disease. *J. Arthri. Rheum.* ; 40: 1126-1129 (1997).
- 8- Hohlbaum, A.M.; Moe,S. and Rothstein, R.A. Opposing effects of trans-membrane and soluble Fas ligand expression on inflammation and tumor cell survival. *J.Exp.Med.*;191:1209-1220 (2000).
- 9- Rose, N.R.; Hamilton,R.G. ; and Detrick,B . Manual of Clinical Laboratory Immunology .6th ed. ASM. Press.USA (2002).

- 10- Hasegawa, D. and Kojima, S. Elevation of the serum FasL in patients with emophagocytic syndrome and Diamond-Blackfan anemia. *J. Blood*, 8: 2793-2799 (1998).
- 11- Sorlie , D.E. Medical biostatistics and Epidemiology : Examination and board review. 1st ed. Appleton and Lange, Norwalk, Connecticut. P : 47-88 (1995) .
- 12- Zhang, J.; Klebanoff, M.A., Levine R.J. The puzzling association between smoking and hypertension during pregnancy. *Am J Obstet Gynecol.* ;181(6):1407-1413(1999).
- 13- Nagata ,S. and Golstein, P. The Fas death factor. *Science* ;267:1449–1456 (1995) .
- 14- Nagata, S. Apoptosis by death factor. *Cell* ;88:355–365 (1997).
- 15- Aali, B.S. and Nejad, S.S. Nifedipine or hydralazine as a first-line agent to control hypertension in severe preeclampsia. *Acta. Obstet. Gynecol. Scand.* ;81(1):25-30(2002).
- 16- Vellore ,J.; Shahirose, J.; Balu, B. and Deirdre, A. Serum soluble Fas and soluble Fas ligand in hypertension in pregnancy . *J. Am. Coll. Cardiol.* ;55; 60-66 (2010).
- 17- Poon ,L.C.; Kametas, N.A.; Maiz, N. ; Akolekar, R. and Nicolaides, K.H. First-trimester prediction of hypertensive disorders in pregnancy. *Hyperten.* ;53(5):812-818(2009).
- 18- Luma, G.B. and Spiotta, R.T. Hypertension in children and adolescents. *Am Fam Physician* ;73 (9): 1558–1568(2006).
- 19- Okura, T.; Watanabe, S.; Jiang, Y. Nakamura, M.; Takata, Y. Soluble Fas ligand and atherosclerosis in hypertensive patients. *J. Hypert.*; 20(5):895-898(2002).

Synthesis and Characterization of New Heterocyclic Compounds

Jumbad H. Tomma¹, Emad T. Ali², Ivan H. R. Tomi³, Zahra A. M. Al-Witry⁴, and Huda A. Hassan⁵
^{1,2,4,5}Department of Chemistry, College of Education Ibn Al- Haitham, University of Baghdad,
³Department of Chemistry, College of Science, University of Al-Mustansiriya

Received 27/10/2011 – Accepted 2/3/2011

الخلاصة

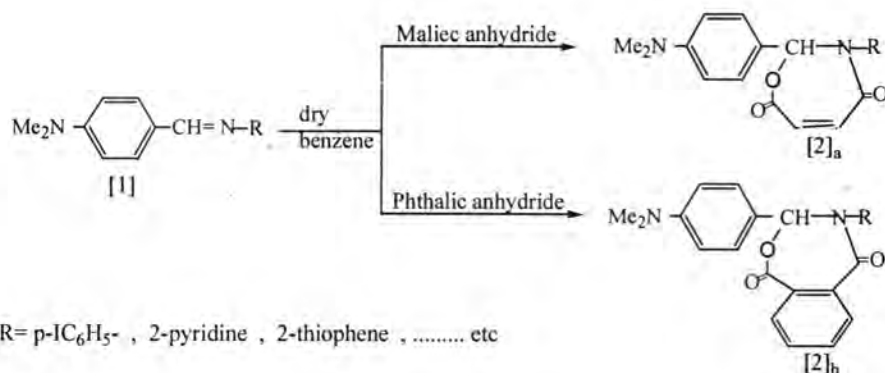
تناول هذا البحث تحضير مركب جديد لمشتق 2-امينو-4,3,1- ثياديازول عن طريق تفاعل الغلق الحلقي لحمض ثنائي الكربوكسيل مع ثايوسيمكاربازيد بوجود POCl_3 . وتم الحصول على قواعد شف جديدة بواسطة تكثيف مشتق 2-امينو-4,3,1- ثياديازول المحضر مع الديهايدات اروماتية متنوعة. كما شمل البحث على تحضير مشتقات 1,3-او كسازيبين نادرة عن طريق تفاعل الاضافة لقواعد شف مع انهيدرات الحوامض المناسبة في البنزين الجاف. شخّصت جميع المركبات المحضرة باستعمال القياسات الفيزيائية والطيفية.

ABSTRACT

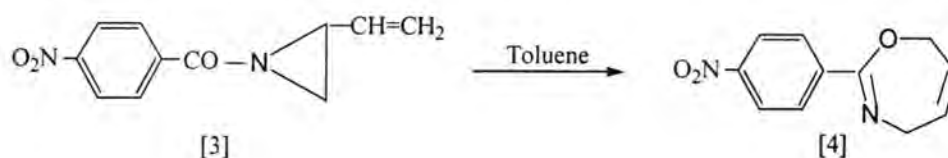
A new bis-2-amino-1,3,4-thiadiazoles were synthesized by the ring closure reaction of di carboxylic acid with thiosemicarbazide in POCl_3 . New Schiff bases were obtained by condensation of the synthesized 2-amino-1,3,4-thiadiazoles with different aromatic aldehydes. New 1,3-oxazepines derivatives were also synthesized by addition reaction of Schiff bases with appropriate acid anhydride in dry benzene. All synthesized compounds were characterized by physical and some spectral data.

INTRODUCTION

1,3,4-Thiadiazoles have occupied an important place in the drug industry. Some 2-amino-5-substituted-1,3,4-thiadiazoles and their derivatives are used as: anticonvulsive agent (1), antibacterial agent (2), antidiabetic, anti-inflammatory (3), antimicrobial and antifungal agents (4). Furthermore, some of these compounds are of interest in photography and as potential anticancer agents (5). Schiff bases are used as substrates in the preparation of a large of bioactive and industrial compounds via ring closure, cyclo addition and replacement reactions (6). In addition, Schiff bases are well known to have biological activities (7-10). Recently, J. Salimon et al. synthesis a new antimicrobial Schiff bases derived from 2-hydrazino-1,3,4-thiadiazoles (11). 1,3-Oxazepine is non-homologous seven member ring, that contains two heteroatoms oxygen and nitrogen. Oxazepines is used as antibiotics, enzyme inhibitors pharmacological interest; it has been much chemical and biological studied (12). Al-Jamali synthesis a new oxazepines $[2]_{a,b}$ from reaction of Schiff bases $[1]$ with maliec anhydride and phthalic anhydride, respectively in dry benzene (13).



Another method to synthesis oxazepines include thermal rearrangement of 1-p-nitrobenzoyl-2-vinylaziridine [3] in toluene with reflux to yielded 2-p-nitrophenyl-4,7-dihydro-1,3-oxazepine [4] (14).



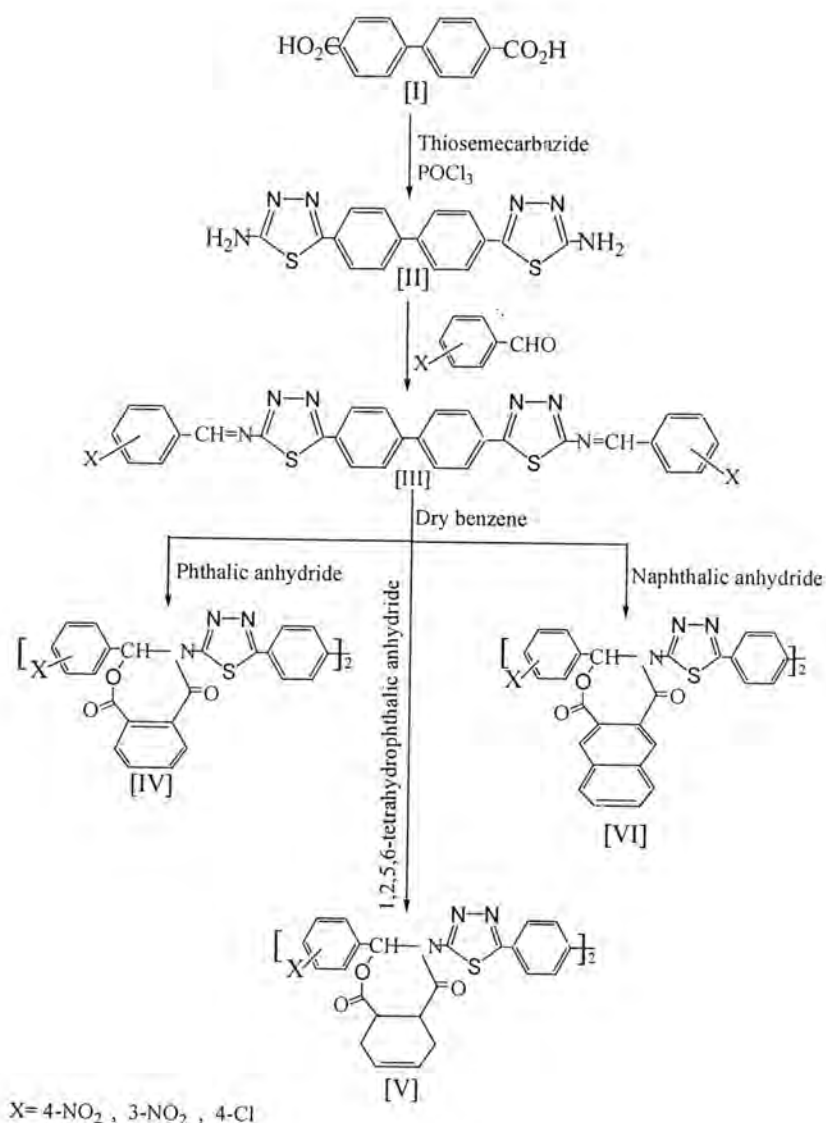
According to above facts, we decided to synthesize a new Schiff bases derived from 2-amino-1,3,4-thiadiazoles then converted to a novel oxazepine derivatives.

MATERIALS AND METHODS

Chemicals: All chemicals were supplied by Merck and Aldrich Chemicals Co. and used as received.

Apparatus: Uncorrected melting points were determined by using Hot-Stage, Gallen Kamp melting point apparatus. The FTIR spectra were recorded using potassium bromide discs on a 8400S Shimadzu Spectrophotometer, UV spectra of solutions were performed on CECL 7200 Inland Spectrophotometer using CHCl₃ as a solvent, ¹HNMR spectra was carried out by: Bruker, model: ultra shield 300 MHz, origin: switzerland and are reported in ppm (δ), DMSO was used as a solvent with TMS as an internal standard. Measurements were made in Al-albyat University, Jordon.

General procedures: The new compounds were synthesized according to scheme 1.



Scheme 1

Biphenylene-4,4'-bis-[2-amino-1,3,4-thiadiazol-5-yl] [II]

A mixture of biphenylene-4,4'-dicarboxylic acid (compound I) (2.42 gm, 0.01mol), thiosemicarbazide (1.82 gm, 0.02mol), phosphorus oxychloride (10 mL) was refluxed gently for 48 hrs. After cooling, ice water (50 mL) was added in portions with stirring. The yellow precipitate was filtered, washed with hot water (15), recrystallized from DMF-water and dried, yield 68%, m.p 108 °C. FTIR (KBr disc, cm⁻¹) ν : two peaks at 3277 and 3138 (NH₂, asym. and sym.); 3056 (CH arom.); peak at 1634 (C=N, thiadiazole rings); and 833 of bending para substituted benzene ring. ¹HNMR (DMSO, ppm) δ : 7.3-7.9 (m, 8H, aromatic proton, and 4H, 2NH₂ group).

Schiff Bases [III]_{a-c}

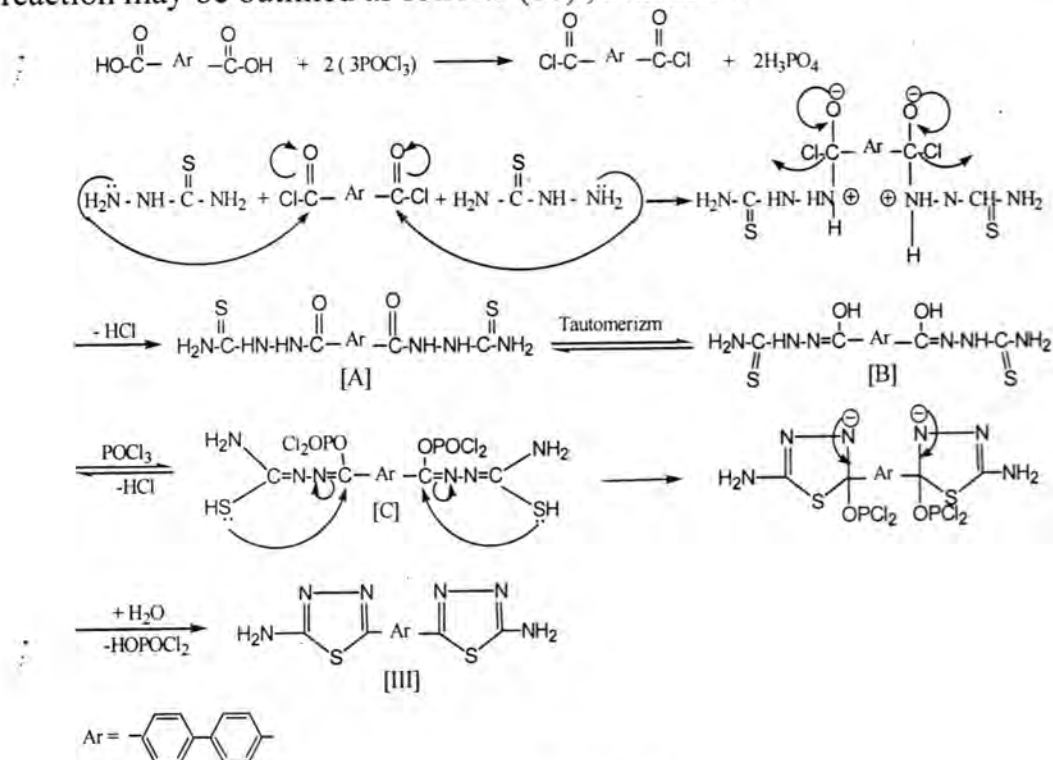
A mixture of compound [II] (3.52 gm, 0.01 mol), and a suitable aldehyde (0.022 mol), in absolute ethanol (15 mL) and three drops of glacial acetic acid was refluxed for 6 hours. After cooling the separated solid was filtered and recrystallized from chloroform. The physical properties of the synthesized compounds are listed in Table 1. ¹HNMR (DMSO, ppm) [III]_a δ: 9.9 (s, 2H, 2CH=N); 7.5-8.05 (m, 16H, aromatic proton).

Oxazepine Derivatives [IV]_{a-c}, [V]_{a-c} and [VI]_{a-c}

A mixture of compound [III]_a (6.15 gm, 0.01mol), and appropriate acid anhydride (0.02 mol) in (30 mL) dry benzene was refluxed for 6 hours. The solvent was removed and the resulting colored solid was recrystallized from ethanol. The physical properties of the synthesized compounds are given in Table 1, and the spectral data (FTIR) are listed in Table 2. ¹HNMR (DMSO, ppm) [VI]_a δ: 2.1 (s, 2H, 2CH=N); 8.50-8.65 (t, 2H, aromatic proton); 7.4-8.0 (m, 12H, aromatic proton).

RESULTS AND DISCUSSIONS

Bis-2-aminothiadiazole derivative [II] was synthesized from the reaction of di carboxylic acid compound [I] and thiosemicarbazide with phosphorous oxychloride (POCl₃). The suggestion mechanism of this reaction may be outlined as follows (16), scheme 2.

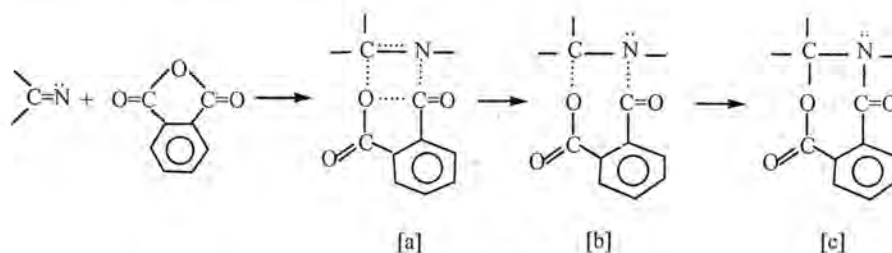
**Scheme 2**

The reaction is initiated by conversion of acid to the acid chloride, followed by nucleophilic attack of the most nucleophilic nitrogen of thiosemicarbazide on the carbonyl carbon of the acid chloride in a nucleophilic substitution reaction to form intermediate (A) which tautomerises to (B). The enol form (B) is stabilized by converting the (OH) group to ester by (POCl₃) to form intermediate (C). The latter compound suffers from internal nucleophilic attack by the sulfur atom of the thiol to form the thiadiazole ring [II].

The structural assignments of the compound [II] were based on melting point and their spectral (FTIR and ¹HNMR) spectroscopy. The FTIR spectrum of this compound exhibited significant two bands at 3277cm⁻¹ and 3138cm⁻¹ which could be attributed to asymmetric and symmetric stretching vibrations of NH₂ group, a weak peak at 3056 due to C-H aromatic stretching. Besides these, a band about 1634cm⁻¹ is due to cyclic C=N stretching for 1,3,4-thiadiazole moiety. The ¹HNMR spectrum of compound [II] was exhibited a broad multiplet signals in the region δ 7.3-8.2 ppm that could be attributed to the eight aromatic protons and the protons of NH₂ groups. 2-Amino-1,3,4-thiadiazoles reacted with different substituted aldehyde to yielded a new Schiff bases [III]_{a-c}. These imines compounds characterized by their melting points, FTIR and ¹HNMR spectroscopy.

FTIR absorption-spectra showed the disappearance of absorption bands due to NH₂ and C=O groups of the starting materials (amine and aldehyde) together with appearance of new absorption band in the region (1690-1705) cm⁻¹ which is assigned to endocyclic azomethine CH=N stretching. The ¹HNMR spectrum of compound [III]_a is show a singlet signal at δ 9.9 ppm that could be attributed to the protons of CH=N group, multiplet signals in the region δ 7.5-8.05 ppm that could be attributed to the sixteen aromatic protons.

The 1,3-oxazepine derivatives were obtained by addition reaction of Schiff bases with acid anhydride in dry benzene, the mechanism of this reaction may be outline in scheme 3.

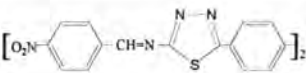
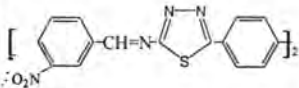
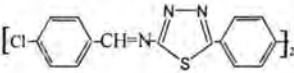
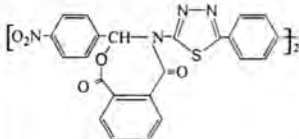
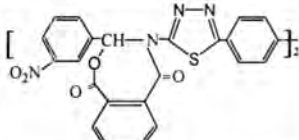


Scheme 3

The mechanism involves the addition of one σ -carbonyl to π -bond of C=N to give 4-membered cyclic and five membered ring of anhydride in the same transition state [T.S a], which opens to give 7-membered cyclic ring 1,3-oxazepine [b]. These new compounds were identified by their melting points, FTIR, and ^1H NMR spectra (some of theme).

FTIR spectra showed the disappearance of absorption bands due to C=N of Schiff bases together with appearance of two new absorption bands in the region $(1730-1769) \text{ cm}^{-1}$ which is assigned to C=O stretching of lactam and lactone, a good peak in the region $(1232-1250) \text{ cm}^{-1}$ due to ether cyclic C-O-C. The other data of functional groups which are characteristic of these compounds are given in Table (2). ^1H NMR spectrum of compound [VI]_a were exhibited: triplet signal at δ 8.5-8.65 ppm which is assigned to two aromatic protons of naphthalic rings, many signals in the region δ 7.4-8.0 ppm that could be attributed to the other aromatic protons. The ^1H NMR spectrum also showed a sharp signal at 2.0 ppm which could be to the protons of 2 CH=N group.

Table-1: physical properties of new synthesized compounds [III]_{a-c} , [IV]_{a-c} , [V]_{a-c} and [VI]_{a-c} .

Comp No.	Structural formula	Nomenclature	M.P $^{\circ}\text{C}$	Yield %	Color
[III] _a		4,4'- bis[2-(p-nitro-amino-benzylidene)-1,3,4-thiadiazol-5-yl]-biphenylene	180	75	Pale yellow
[III] _b		4,4'- bis[2-(m-nitro-amino-benzylidene)-1,3,4-thiadiazol-5-yl]-biphenylene	184	70	yellow
[III] _c		4,4'- bis[2-(p-chloro-amino-benzylidene)-1,3,4-thiadiazol-5-yl]-biphenylene	146	85	Pale yellow
[IV] _a		bis[2-(p-nitrophenyl)-3-(5-phenyl-1,3,4-thiadiazol-2-yl)-2,3-dihydro benz[1,2-e] oxazepine-4,7-diones]	168-170	60	yellow
[IV] _b		bis[2-(m-nitrophenyl)-3-(5-phenyl-1,3,4-thiadiazol-2-yl)-2,3-dihydro- benz[1,2-e] oxazepine-4,7-diones]	138-140	75	Pale yellow

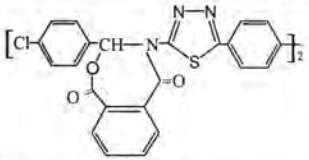
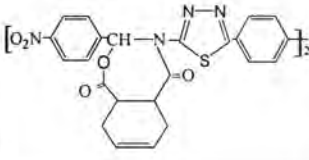
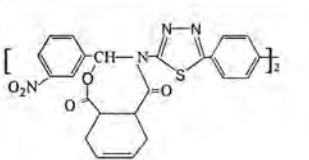
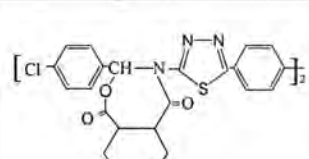
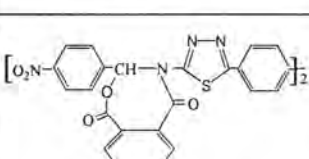
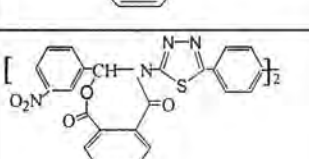
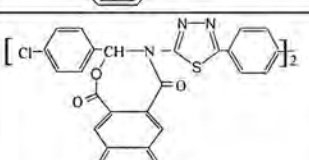
[IV] _c		bis[2-(p-chlorophenyl)-3-(5-phenyl-1,3,4-thiadiazol-2-yl)-2,3-dihydro- benz[1,2-e] oxazepine-4,7-diones]	150	70	Pale yellow
[V] _a		bis[2-(p-nitrophenyl) -3-(5-phenyl-1,3,4-thiadiazol-2-yl)-2,3-dihydro-4,5-cyclohexene[1,2-e] oxazepine-4,7-diones]	>280	72	Off white
[V] _b		bis[2-(m-nitrophenyl) -3-(5-phenyl- 1,3, 4-thiadiazol-2-yl)-2,3-dihydro-4,5-cyclohexene[1,2-e] oxazepine-4,7-diones]	182	78	yellow
[V] _c		bis[2-(p-chlorophenyl)-3-(5-phenyl-1,3,4 -thiadiazol-2-yl)-2,3-dihydro-4,5-cyclohexene[1,2-e] oxazepine-4,7-diones]	205	70	yellow
[VI] _a		bis[2-(p-nitrophenyl) -3-(5-phenyl-1,3,4-thiadiazol-2-yl)-2,3-dihydro-naphth[2,3-e] oxazepine-4,7-diones]	245	90	Off white
[VI] _b		bis[2-(m-nitrophenyl) -3-(5-phenyl-1,3,4-thiadiazol-2-yl)-2,3-dihydro-naphth[2,3-e] oxazepine-4,7-diones]	>280	92	pale yellow
[VI] _c		bis[2-(p-chlorophenyl)-3-(5-phenyl-1,3,4-thiadiazol-2-yl)-2,3-dihydro-naphth[2,3-e] oxazepine-4,7-diones]	254	95	pale yellow

Table- 2: FTIR and data of oxazepines [IV]-[VI].

Comp. No.	λ_{max} (nm)	FTIR spectra (KBr disc. , $\nu \text{ cm}^{-1}$)						
		νCH arom.	$\nu\text{C=O}$ lactam	$\nu\text{C=O}$ lactone	$\nu\text{C=N}$ endo cyclic	$\nu\text{C=C}$ arom.	$\nu\text{C-O-C}$ ether cyclic	other
[IV] _a	278.0	3045	1760	1730	1638	1595	1078	p-NO ₂ (str.):1345
[IV] _b	288.5	3045	1760	1732	1635	1600	1075	-
[IV] _c	286.0	3050	1755	1730	1638	1595	1078	p-Cl (str.):1085
[V] _a	278.0	3048	1750	1735	1635	1595	1085	p-NO ₂ (str.):1340
[V] _b	276.0	3042	1755	1732	1635	1590	1082	-
[V] _c	263.0	3045	1758	1730	1630	1600	1075	p-Cl (str.):1089
[VI] _a	330.5	3066	1769	1738	1636	1590	1080	p-NO ₂ (str.):1340
[VI] _b	294.0	3060	1765	1735	1635	1595	1080	-
[VI] _c	331.0	3062	1765	1735	1632	1600	1082	p-Cl (str.):1086

REFERENCES

- 1- Yar, M. Sh. and Akhter, M. W., "Synthesis and Anticonvulsant Activity of Substituted Oxadiazole and Thiadiazole Derivatives", Polish Pharmaceutical Society, 66(4), 393-397 (2009).
- 2- Salimon, J., Salih, N., Hameed, A., Ibraheem, H. and Yousif, E., "Synthesis and Antibacterial Activity of Some New 1,3,4-Oxadiazole and 1,3,4-Thiadiazole Derivatives" J. of Applied Sciences Research, 6(7), 866-870 (2010).
- 3- Pattan, Sh. R., Kekare, P., Dighe, N. S., Nirmal S. A., Musmade, D. S., Parjane, S. K. and Daithankar, A. V., "Synthesis and Biological Evaluation of Some 1,3,4-Thiadiazoles", J. of Chemical and Pharmaceutical Research , 1(1), 191-198 (2009).
- 4- Ashutosh, B., Ankur, Kumar, J. N., Sonia, R., Niharika, G. S., Vivek, D. and Pramod, S., "Synthesis, Characterization and

- Antimicrobial Activity of Azol Substituted Derivatives”, IJPSSDR , 1(3), 207-210 (2009).
- 5- Siddiqui, N., Ahujaa, P. , Ahsan, W., Pandeya, S. N., Shamsher Alam, M., Musmade, D. S., Parjane, S. K and Daithankar, A. V., “Thiadiazoles: Progress Report on Biological Activities”, J. of Chemical and Pharmaceutical Research, 1(1), 191-198 (2009).
 - 6- Wasserman, A., “Diels-Alder Reactions”, Elsevier, New York, 133 (1965).
 - 7- Vicini, P., Geronikaki, A., Incerti, M., Busonera, B., Ooni, G., Kabras, C. A. and Colla, P. L., “Synthesis and Biological Evaluation of Benzo[d]isothiazole, Benzothiazole and Thiazole Schiff bases ” , Bio.org. Med. Chem. 11, 4785-4789 (2003).
 - 8- Shiradkar, M. R. and Nikalje, A. G., ARKIVOC, (xiv), 58-74 (2007).
 - 9- Kahveci, B., Bekircan, O. and Karaoglu, S.A., “Synthesis and Antimicrobial Activity of Some 3-Alkyl-4-(arylmethyleneamino)-4,5-dihydro-1H-1,2,4-triazol-5-ones”, Indian J. Chem. ,44B , 2614-2617 (2005) .
 - 10- Betircan, O., Kahveei, B. and Kucuk, M., “Synthesis and Anticancer Evaluation of Some New Unsymmetrical 3,5-diaryl-4H-1,2,4-triazole Derivatives”, Tur. J. Chem., 30 , 29-40 (2006) .
 - 11- Salimon, J., Salih, N., Yousif, E., Hameed, A. and Ibraheem, H., “Synthesis, Characterization and Biological Activity of Schiff Bases of 2,5-Dimercapto-1,3,4-Thiadiazole”, Australian Journal of Basic and Applied Sciences, 4(7) , 2016-2021(2010).
 - 12- Bilgiç, S., Bilgiç, O., Bilgiç, M., Gündüz, M. and Karakoç, N., “Synthesis of 2-Aryl-1,2- dihydronaphtho[1,2-f][1,4]oxazepin-3(4H)-ones . Part I”, ARKIVOC, xiii 185-192 (2009).
 - 13- Al-Jamali, N. M., “Synthesis, Characterization of New 1,3-Oxazepine, Diazepine, Thiazepine derivatives and Open Ring of Thio Compounds”, Ph.D. Thesis, College of Education Ibn –Al Haitham , University of Baghdad (2008) .
 - 14- Tawfiq, M. T., “Synthesis of Substituted 1,3-Oxazepines and 1,3-Diazepines Via Schiff Bases ”, Ph.D. Thesis, College of Education Ibn –Al Haitham, University of Baghdad (2004).

- 15- Tomma, J. H., Rou'il, I. H. and Al-Dujaili, A. H., "Synthesis and Mesomorphic Behavior of Some Novel Compounds Containing 1,3,4-Thiadiazole and 1,2,4-Triazole Rings", *Mol. Cryst. Liq. Cryst.* , 501, 3-19 (2009).
- 16- Rou'il, I. H., "Synthesis and Characterization of Novel Heterocyclic Liquid Crystalline Compounds and Polymers", Ph.D. Thesis, College of Education Ibn –Al Haitham, University of Baghdad (2007).

Synthesis of New Phenobarbital Derivatives (Part I)

Redha I. AL-bayati and Abdul Jabbar Kh. Atia

Department of Chemistry, College of science, AL- Mustansiriya university, Baghdad, Iraq.

Received 1/02/2011 – Accepted 2/3/2011

الخلاصة

يتناول هذا البحث تفاعل 2-Bromoacetic acid مع 5-Ethyl-5-phenyl barbituric acid في الميثانول بوجود كربونات الصوديوم للحصول على 5-Ethyl-5-phenyl barbituryl -1-acetic acid ثم تحويل مجموعة الكربوكسيل الى كلوريد الحامض بمعاملته مع الثايونيل كلورايد بعدها تم الحصول على مشتق الهيدرازيد عن طريق تفاعل كلوريد الحامض مع الهيدرازين المائي (99%) ، قواعد شيف حضرت بتفاعل مشتق الهيدرازيد مع الديهايدات او كيتونات مختلفة ثم اجراء الغلق الحلقي مع مركبتو حامض الخليك . تم تشخيص المركبات بالطرائق الطيفية (IR, UV and C.H.N.) .

ABSTRACT

5-Ethyl-5-phenyl barbituric acid has been refluxed with 2-Bromoacetic acid in methanol in presence of sodium carbonate to give 5-Ethyl-5-phenyl barbituryl -1-acetic acid, which has been converted to 5-Ethyl-5-phenyl barbituryl-1-acetyl chloride by treatment with thionyl chloride, then converted to acid hydrazide by refluxing with hydrazine hydrate (99%). Schiff's bases have been synthesized by treatment of acid hydrazide with different aldehyde and ketone, then cyclization of Schiff's bases have been achieved by mercapto acetic acid.

All compounds were characterized by IR, UV spectra and C.H.N. analysis.

INTRODUCTION

Barbituric acid system is a structural element of many drugs that have anticancer activity such as raltitrexed and thymitag and their activity as thymidylate enzyme inhibitors(1,2). Heterocyclic of barbituric acid represent as a new class of antitumor drugs, it was found to inhibit the epidermal growth factor receptor (EGFR)(3,4). Further more, barbituric acid exert their antitumor activity through inhibition of DNA repair enzyme system, enzyme – mediated repair of strand lesion in DNA is an established mechanism for resistance toward antitumor DNA damaging drugs and radiotherapy(5-7). Schiff's bases can be considered as useful tools to prepare many compounds, the azomethine group is ready made nucleophilic center for synthesis of condensed heterocyclic ring (8-10). In the present study we report on the synthesis of compounds derived from azomethine group comprising various moieties on azomethine group with the purpose of further investigation of their possible antibacterial and antifungal activities

MATERIALS AND METHODS

All chemicals are of analar grade (Merk, Fluka) and used without further purification. Melting point was determined in open capillary tubes on a Galten Kamp melting point apparatus and are uncorrected.

FT-IR spectra (KBr discs) were recorded with 8300 Shimadzu in the range $(4000 - 600) \text{ cm}^{-1}$.

The (C.H.N) elemental analysis were done using (C.H.N) Carlo Erba 1106 elemental analyzer. UV. Spectra were recorded on Hitachi 2000 spectrophotometer using absolute methanol as solvent

Synthesis of 5-Ethyl-5-phenyl barbituric acid (1)

To a mixture of sodium carbonate (0.02 mole, 2 gm) in (20 ml) methanol and 5-Ethyl-5-phenyl barbituric acid (0.02 mole, 4.64 gm), bromo acetic acid was added, the mixture was refluxed for 3hrs. After cooling the mixture was filtered, the filtrate was acidified with Conc. HCl then the precipitate was recrystallized from ethanol. (yield 65 %), (m.p, $^{\circ}\text{C}$) (102-104), IR.(KBr) (ν , Cm^{-1}) 3450-2500 (OH), 3360 (NH) 3080 (C-H Ar.), 2980-2890 (CH Aliph.) 1700, 1680 (C=O), 1590-1460 (C=Car).

Synthesis of 5-Ethyl-5-phenyl barbituric acid (2)

A mixture of compound (1) (0.01mole, 2.9 gm) and thionyl chloride (10 ml) was refluxed gently for 2hrs. after cooling the excess of thionyl chloride was removed under vacuum. The product collected without recrystallized (yield 90 %), (m.p, $^{\circ}\text{C}$) (110), IR.(KBr) (ν , Cm^{-1}) 3066 (C-H Ar.), 1800 (C=O, acid chloride) 700 (C-Cl).

Synthesis of 5-Ethyl-5-phenyl barbituric acid (3)

To a stirring mixture of compound (2) (0.005 mole, 1.5 gm) in dry benzene (15 ml), a mixture of hydrazine hydrate (99%) (0.01 mole, 0.35 gm) and benzene (10ml) was added drop wise. After that, the mixture was refluxed for 1h. After cooling the excess of benzene was removed under vacuum. The product was recrystallized from ethanol. (yield 57 %), (m.p, $^{\circ}\text{C}$) (165-167), IR.(KBr) (ν , Cm^{-1}) 3400-3300 (NH₂) 3100 (C-H Ar.), 2960-2850 (CH Aliph.) 1710, 1650 (C=O), 1600-1500 (C=Car), 770 (C-Cl). C.H.N. analysis C₁₄H₁₆N₄O₄ (Cal., Foun.) C% H% N% (55.26, 54.96), (5.26, 6.16), (18.42, 18.23)

Synthesis of 1-acetyl (N-arylidene hydrazinyl) -5-ethyl-5-phenyl barbituric acid (4a - h)

To a stirred solution of compound (3) (0.003 mole, 0.9 gm) in absolute ethanol (20ml) was added aldehyde or ketone (0.003 mole). The mixture was refluxed for 3hrs. and cooled, the precipitate was filtered and recrystallized from appropriate solvent.

4a. (yield 83 %), (m.p, C°) (260-262), IR.(KBr) (ν , Cm^{-1}) 3190 (NH) 3050 (C-H Ar.), 2985-2890 (CH Aliph.) 1700, 1680 (C=O), 1590-1460(C=Car), 770 (C-Cl). C.H.N. analysis $\text{C}_{21}\text{H}_{19}\text{N}_2\text{O}_4\text{Cl}$ (Cal. Foun.) C% H% N% (59.57 , 59.27), (4.49, 4.28), (13.23, 13.08)

4b.(yield 85 %), (m.p, C°) (276-278), IR.(KBr) (ν , Cm^{-1}) 3210 (NH) 3090 (C-H Ar.), 2970-2830 (CH Aliph.) 1705, 1690 (C=O), 1610-1500(C=Car), 830 (C-Br)C.H.N. analysis $\text{C}_{21}\text{H}_{19}\text{N}_2\text{O}_4\text{Br}$ (Cal. Foun.) C% H% N% (57.79 , 57.32), (4.35, 4.13), (12.48, 11.95)

4c.(yield 70 %), (m.p, C°) (287-289), IR.(KBr) (ν , Cm^{-1}) 3200 (NH) 3100 (C-H Ar.), 2985-2880 (CH Aliph.) 1700, 1690 (C=O), 1600-1510(C=Car), C.H.N. analysis $\text{C}_{21}\text{H}_{20}\text{N}_4\text{O}_5$ (Cal. Foun.) C% H% N% (61.76 , 61.35), (4.90, 4.55), (13.72, 13.34)

4d.(yield 90 %), (m.p, C°) (303d), IR.(KBr) (ν , Cm^{-1}) 3230 (NH) 3080 (C=Car), 2960-2900 (CH Aliph.) 1710, 1680 (C=O), 1590-1450(CH Ar), C.H.N. analysis $\text{C}_{21}\text{H}_{20}\text{N}_5\text{O}_6$ (Cal., Foun.) C% H% N% (57.53 , 57.21), (4.56, 64.1625), (15.98, 15.75).

4e.(yield 74 %), (m.p, C°) (295-297), IR.(KBr) (ν , Cm^{-1}) 3210 (NH) 3080 (C-H Ar.), 2965-2890 (CH Aliph.) 1700, 1680 (C=O), 1590-1480(C=Car), C.H.N. analysis $\text{C}_{21}\text{H}_{23}\text{N}_5\text{O}_4$ (Cal. , Foun.) C% H% N% (62.70 , 61.90), (5.46, 4.56), (16.62, 16.12)

4f.(yield 63 %), (m.p, C°) (310d), IR.(KBr) (ν , Cm^{-1}) 3200 (NH) 3056 (C-H Ar.), 2985-2880 (CH Aliph.) 1710, 1700 (C=O), 1610-1500(C=Car), C.H.N. analysis $\text{C}_{21}\text{H}_{23}\text{N}_4\text{O}_5$ (Cal. , Foun.) C% H% N% (62.55 , 62.18), (5.21, 5.09), (13.79, 13.11)

4g.(yield 65 %), (m.p, C°) (213-215), IR.(KBr) (ν , Cm^{-1}) 3225 (NH) 3080 (C-H Ar.), 2935-2810 (CH Aliph.) 1710, 1685 (C=O), 1550-1490(C=Car), C.H.N. analysis $\text{C}_{22}\text{H}_{22}\text{N}_4\text{O}_4$ (Cal., Foun.) C% H% N% (65.02 , 64.79), (5.41, 4.95), (13.79, 12.22)

4h.(yield 65 %), (m.p, C°) (219-221), IR.(KBr) (ν , Cm^{-1}) 3230 (NH) 3080 (C-H Ar.), 2975-2890 (CH Aliph.) 1700, 1650 (C=O), 1550-1490(C=Car), C.H.N. analysis $\text{C}_{22}\text{H}_{21}\text{N}_4\text{O}_4\text{Cl}$ (Cal., Foun.) C% H% N% (59.93 , 59.60), (4.77, 4.13), (12.72, 12.02)

4i.(yield 43 %), (m.p, C°) (315d), IR.(KBr) (ν , Cm^{-1}) 3200 (NH) 3090 (C-H Ar.), 2987-2856 (CH Aliph.) 1700, 1690 (C=O), 1600-1495(C=Car), C.H.N. analysis $\text{C}_{22}\text{H}_{23}\text{N}_5\text{O}_6$ (Cal., Foun.) C% H% N% (58.27 , 57.95), (5.07, 4.78), (15.45, 15.11)

Synthesis of 2-aryl-3-(5-ethyl-5-phenyl barbiturnoyl-1-acetamido) thiazolin-4-one (5a – d)

To a stirring mixture of compound (4a, 4b, 4c, 4d) (0.005 mole) in dry benzene (5 ml), a mixture of mercapto acetic acid (0.005 mole, 0.46 gm) in dry benzene (15ml) was added drop wise. After that, the mixture was refluxed for 1h. after cooling the excess of benzene was removed

under vacuum. The residue was treated with sodium carbonate (5%) (20ml) product was recrystallized from appropriate solvent.

5a. (yield 52 %), (m.p, C°) (201-203), IR.(KBr) (ν , Cm^{-1}) 3390 (NH) 3100 (C-H Ar.), 2980-2880 (CH Aliph.) 1700, 1680 (C=O), 1610-1520(C=Car), 780 (C-Cl). C.H.N. analysis $\text{C}_{23}\text{H}_{21}\text{N}_4\text{O}_5\text{SCl}$ (Cal., Foun.) C% H% N% (55.20, 55.01), (4.20, 4.11), (11.20, 11.08)

5b. (yield 57 %), (m.p, C°) (208-210), IR.(KBr) (ν , Cm^{-1}) 3310 (NH) 3050 (C-H Ar.), 2990-2850 (CH Aliph.) 1710, 1690 (C=O), 1600-1520(C=Car), 640 (C-Br). C.H.N. analysis $\text{C}_{23}\text{H}_{22}\text{N}_4\text{O}_5\text{SBr}$ (Cal., Foun.) C% H% N% (54.10, 53.85), (4.11, 4.08), (10.98, 10.79)

5c. (yield 43 %), (m.p, C°) (227-229), IR.(KBr) (ν , Cm^{-1}) 3350-3170 (OH) 3050 (C-H Ar.), 2910-2850 (CH Aliph.) 1695, 1660 (C=O), 1590-1500(C=Car), C.H.N. analysis $\text{C}_{23}\text{H}_{22}\text{N}_4\text{O}_6\text{S}$ (Cal., Foun.) C% H% N% (57.26, 58.22), (4.54, 5.11), (11.61, 12.32)

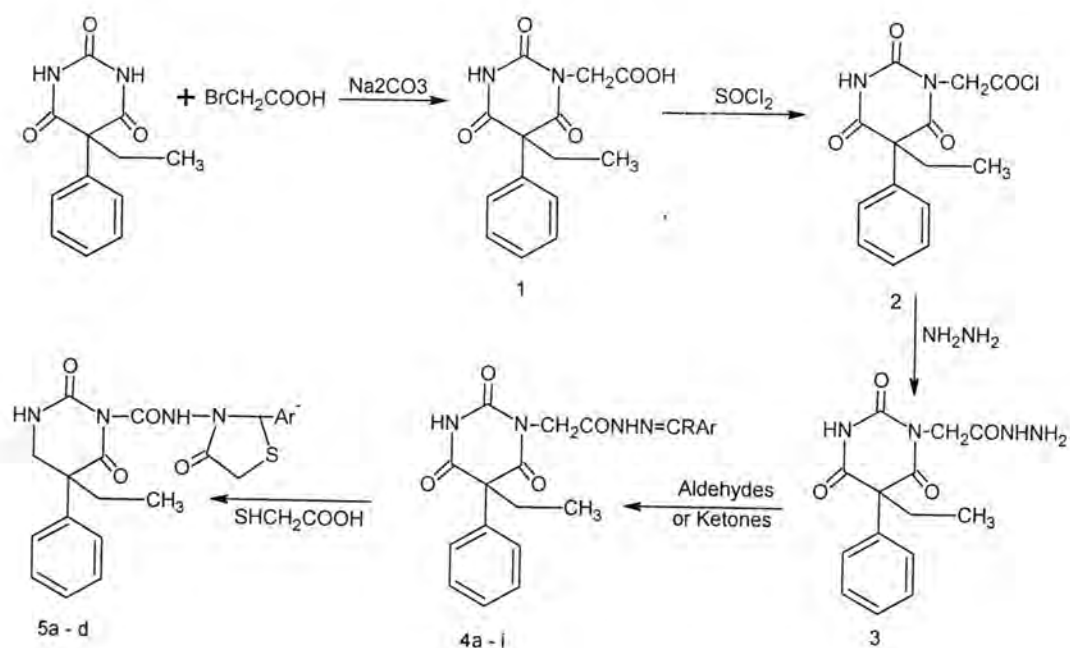
5d. (yield 43 %), (m.p, C°) (215-217), IR.(KBr) (ν , Cm^{-1}) 3230 (NH) 3090 (C=Car), 2910-2850 (CH Aliph.) 1710, 1690 (C=O), 1590-1460(CH Ar), C.H.N. analysis $\text{C}_{23}\text{H}_{21}\text{N}_5\text{O}_7\text{S}$ (Cal. Foun.) C% H% N% (54.01, 53.00), (4.10, 3.83), (13.269, 12.95)

RESULTS AND DISCUSSION

Scheme 1 summarizes all the performed reaction in this work. Physical properties and spectra data are given in experimental part.

The structure of compound (1) was confirmed by melting point and appearance of hydroxyl group of carboxylic acid at $3350\text{-}2500\text{ Cm}^{-1}$. The UV spectrum shows band at 237nm due to $\pi \rightarrow \pi^*$ and at 363 nm for $n \rightarrow \pi^*$. The data of (C.H.N.)analysis show the found data was so close from calculated data for above compound

The structure of compound (2) acid chloride, was confirmed by the change in melting point compared with the corresponding acid and the IR spectrum shows the disappearance of the strong and broad band at $3350\text{-}2500\text{ Cm}^{-1}$ and appearance strong band at 1800 Cm^{-1} due to carbonyl of acid chloride. The UV spectrum shows two bands the first at 204nm for $\pi \rightarrow \pi^*$ and at 226nm due to $n \rightarrow \pi^*$.



Comp. No.	Ar	R
5a	4a	p-Cl-ph
5b	4b	p-Br-ph
5c	4c	p-OH-ph
5d	4d	o-NO ₂ -ph
4e	p-NH ₂ -ph	CH ₃ -
4f	p-OH-ph	CH ₃ -
4g	ph	CH ₃ -
4h	o-Cl-ph	CH ₃ -
4i	2-OH-3-CH ₃ -6-CH ₂ OH	-C ₅ H ₅ N

Scheme 1

Acid hydrazide (3) was confirmed by observing two bands at 3400-3300 cm^{-1} in its IR spectrum. Also, it showed two carbonyl absorptions appeared at 1650 cm^{-1} . The data of (C.H.N.)analysis show the found data was so close from calculated data for above compounds

The IR spectra of compounds (4a – h) show disappearance of the two bands of NH₂ and the large change in melting point.

The structure of compounds (5a – d) were confirmed by absorption bands at 700-750 cm^{-1} which corresponded to C-S-C and at 850 cm^{-1} corresponded to para substituted for the aromatic thiazolidine-4-one. UV spectra data show the two bands at 229-250nm due to $\pi \rightarrow \pi^*$ and at 307-387nm for $n \rightarrow \pi^*$. The data of (C.H.N.)analysis show the found data was so close from calculated data for above compounds.

REFERENCES

1. J. Michel, L.Cedric, V.Alexandra and T.Besson, "Synthesis of novel pyrimidine containing pyrazolinone, pyrazole and pyridinone moieties", *Eur.J.Mid.Chem.*, 43:1469-1477 (2008) .
2. A.Kalil, S.Hamide and H.I.El-Sabbagh, "Synthesis of some novel oxadiazole and barbituric acid analogues for their biological activity", *Arch. Pharm. Chem.*, 2: 95-103 (2003) .
3. J.B.Smaill, G.W.Rewcastle and J.A.Loo, "Synthesis and in-vitro anticancer evaluation of new 2-substituted mercapto- pyrimidine analogs", *J.Med.Chem.*, 43:1380-1926 (2000) .
4. W.Wissner, D.M.Berger, D.H.Boshelli and N.Zhang, "Synthesis and antitumer evalution of 4(3N)-Quinazolinone derivatives", *J.Med.Chem.*, 43:3244-3256 (2000) .
5. J.D.Hayes, C.R.Walf, *Biochem.*, "6-Bromo purine nucleosides as reagents for nucleoside analogue synthesis", *J.*, 272,281-295 (1999) .
6. A.L.Griffin, S.Srivivasan and N.J.Gurtin, "RNA cleavage by a DNA enzyme with extended chemical functionality", *J. Med. Chem.*, 41:5247-5256 (2004) .
7. S.G.Abdel Hamid, H.A.El-Obid and A.K.Rashood, "Synthesis antitumor activity of Quinazolin-4-one derivatives", *Sci. Pharm.*, 69:351-366 (2001) .
8. S.Shawli, F.I.Zeid and A.Al-Talbawy, "Synthesis and antibacterial activity of 3-amino-2-methyl-4(3H) Quinazolinone derivatives", *J.Chinese. Chem.. Soc.*, 48:68 (2001).
9. S.B.Vashi and V.H.Shah, "Synthesis and antimicrobial activities of some new phenyl methyl (2-methyl-4-oxaquinazoline derivatives", *Indian J. Chem.*, Vol. 35 B:111-115 (1996).
10. M.H.R and P.V.S, "Synthesis, Anticonvulsant and Muscle relaxant activities of substituted Quinazoline-4(3H)-one", *J.Serb. Chem.. Soc.*, 66(2): 87-93 (2001) .
11. C.Parkanyi and D.S.Schmidt, "Synthesis of 5-chloro-2-methyl-3-(5-methyl thiazole-2-yl)-4(3H)-quinazolinone and related compounds with potential biological activity", *J.Hetero.Chem.*, 37: 725-729 (2000) .

Synthesis of New Sugar Based Triazoles and Bis-Triazoles *via* Click Chemistry

Adnan Ibrahim Mohammed

Department of Chemistry, College of Science, University of Kerbala

adnanimchem@yahoo.com

Received 4/8/2010 – Accepted 4/11/2010

الخلاصة

تم تحضير نوعين جديدين من مركبات الترايازولات ابتداءً من سكرين أساسيين: د-كلوكوز و د-مانيتول. مفاعلة د-مانيتول مع الأسيتون في وسط حامضي (كلوريد الخارصين) أعطى المركب 1,2:5,6-ثنائي أيزوبروبيلدين-د-مانيتول (1). أخضاع المركب (1) لتفاعل وليامسون مع بروميد البروباجيل وبوجود هيدروكسيد الصوديوم أنتج المركب (2). الأضافة الحلقية [3+2] للمركب (2) إلى الأزيد السكري (5) وباستخدام ظروف (click) أعطى مركبات الترايازول 4,1-ثنائية التعويض (6) و (7).

ABSTRACT

Two types of new triazoles have been synthesized from two essential sugars D-glucose and D-mannitol. The reaction of D-mannitol with acetone in acidic media gave 1,2:5,6-di-*O*-isopropylidene-D-mannitol (1). Williamson etherification of (1) with propargyl bromide catalyzed by NaOH yielded (2). The [2+3] cycloaddition of compound (2) with glycosyl azide (5) using click conditions gave the targeted 1,4-disubstituted triazoles (6) and (7).

INTRODUCTION

The reaction of a terminal alkyne with a substituted azide was discovered by Arthur Michael 116 years ago (Figure 1). Later, R. Huisgen carried out systematic studies of this particular reaction and other 1,3-dipolar cycloadditions.(1) However, it was only after the publication of the copper(I)-catalyzed variant that the potential of the transformation could be fully exploited. The chemistry was subsequently further developed in parallel by the groups of Meldal(2) and Sharpless(3) and became synonymous with the broader concept of 'Click chemistry', also known as copper(I) catalyzed cycloaddition of an alkyne and azide (Figure 2).

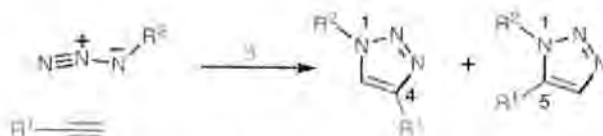


Figure - 1: Traditional triazole formation 1,4 and 1,5 regioisomers

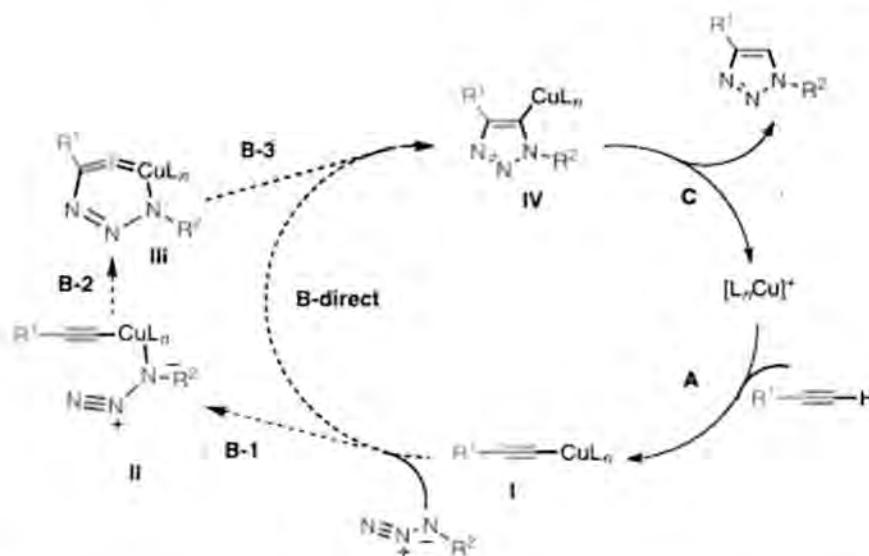


Figure - 2: Formation of triazoles via click conditions only 1,4 regioisomer (4)

The 1,2,3-triazole system has widespread uses, and it has been considered as an interesting component in terms of biological activity (5,6). Although the use of heterocyclic moieties in peptidomimetics has been widely reported, the application of 1,2,3-triazoles in the field of conformational studies has occurred only recently (7). The generation of N-glycosyl-triazoles from simple acetylenes, sugar, amino acid and steroid-derived terminal acetylenes (C-linked alkynes, O-propargyl ethers, ynamides) has been reported (8,9). Recently, new methods technologies have been used for the synthesis of triazoles like; ultrasound (10) and microwave (11). In this work we prepared two new triazoles starting from D-glucose using click conditions.

MATERIALS AND METHODS

Materials

Chemical reagents and starting materials were obtained from Ajax and Sigma-Aldrich Chemical.

Instrumentations

Infrared spectra were recorded using AVATAR 320 FT-IR. ^1H and ^{13}C NMR spectra were recorded using 300 MHz Bruker DPX spectrometers. Microelemental analysis was performed with Elemental Analyzer EA-300 Eurovector. Mass spectra were recorded using Waters 996 Micromass. Silica TLC plates were used with an aluminum backing (0.2 mm, 60 F₂₅₄). The reactions were monitored by TLC and visualized by development of the TLC plates with an alkaline potassium permanganate dip.

Synthesis of 1,2:5,6-di-O-isopropylidene-D-mannitol[1] ⁽¹²⁾

To a suspension of zinc chloride (60 g) in (300 mL) of anhydrous acetone, finely powdered D-mannitol (10 g, 55 mmol) was added. The mixture was stirred vigorously at room temperature until the D-mannitol dissolved (3 hr) then allowed to stand for (16 hr). the reaction mixture was poured into a solution of K_2CO_3 (50g in 100 mL water) and stirred for (30 min) then extracted with ether (3x100 mL), dried and evaporated under reduced pressure to give a solid residue. Recrystallization of the solid from light petroleum (40-60 °C) gave the product as a white solid (9.0 g, 63%), mp 122-124° C. Microelemental analysis for $C_{12}H_{22}O_6$ calculated: C, 54.95; H, 8.45, found: C, 54.90; H, 8.43.

Synthesis 3,4-O-Dipropargyl-1,2:5,6-di-O-isopropylidene-D-mannitol [2]

1,2:5,6-Di-O-isopropylidene-D-mannitol (**1**) (1.018 g, 3.00 mmol) was dissolved in DMF (30 mL), to this was added crushed NaOH (0.48 g, 12 mmol) and the mixture was stirred for 10 minutes. Propargyl bromide (1.77 mL, 8.54 mmol) was added and the mixture was stirred for a further 24 hours. The reaction was quenched with water (30 mL) and and extracted with ether (3 x 30 mL). The combined organic layers were washed sat. NH_4Cl (3 x 20 mL), water, dried over Na_2SO_4 , filtered and the solvent was evaporated under reduced pressure to yield a pale yellow oil. Purification by column chromatography (Alumina, 3:1 light petroleum: ether) yielded 3,4-O-propargyl-1,2:5,6-di-O-isopropylidene-D-mannitol as needle crystals (1.15 g, 83 %) mp 95-97° C. Microelemental analysis for $C_{18}H_{26}O_6$ calculated: C, 63.89; H, 7.74, found: C, 63.85; H, 7.70.

Synthesis of Glucopyranose pentaacetate [3]

A solution of pyridine (75 ml)/acetic anhydride (50 ml) 3:2 (v/v) was cooled in an ice bath under nitrogen. D-glucose (10 g, 45 mmol) was added, the suspension was stirred until the sugar dissolved then allowed to warm to room temperature and stirred for a further 16 h under nitrogen. After this time, the solution was poured into ice water (200 mL); α -D-glucopyranose pentaacetate was crystallized out rapidly, filtered, washed with cooled water and dried under vacuum (19.4 g, 90%); mp 113-114°C; later crops yielded β -D-glucopyranose pentaacetate.; $[\alpha]_D +105$ (c 1.0, $CHCl_3$). Microelemental analysis for $C_{16}H_{22}O_{11}$ calculated: C, 49.23; H, 5.68, found: C, C, 49.27; H, 5.65.

Synthesis of 2,3,4,6-Tetra-O-acetyl- α -D-glucopyranosyl bromide [4]

1,2,3,4,6-penta-O-acetyl- α -D-glucopyranose (10 g, 25.40 mmol) portion wise (0.5 g at a time) to a stirred solution of HBr (33%) in glacial acetic

acid (25 mL) at 0 °C. After all the sugar has been added, the reaction mixture was allowed to warm to room temperature. After 45 min, TLC analysis (hexane:ethyl acetate, 1:1) indicated formation of product (R_f 0.5). The reaction was quenched with ice water (50 mL), extracted with DCM (2 x 60 mL), the combined organic extracts were washed with a solution of NaHCO_3 (aq., sat., 2 x 50 mL), dried with Na_2SO_4 , filtered and then concentrated in vacuo. The residue was crystallizes from ether/petrol to afford 2,3,4,6-tetra-O-acetyl- α -D-glucopyranosyl bromide (8.80 g, 83%) as a white crystalline solid, mp 87–89° C; $[\alpha]_D^{+20}$ (c 0.5 in CHCl_3). Microelemental analysis for $\text{C}_{14}\text{H}_{19}\text{BrO}_9$ calculated: C, 40.89; H, 4.66; Br, 19.43, found: C, 40.91; H, 4.70; Br, 19.47.

Synthesis of 2,3,4,6-Tetra-O-acetyl- β -D-glucopyranosyl azide [5]

Sodium azide (1.95 g, 30 mmol) was added to the stirred solution of glycosyl bromide (**5**) (4.10 g, 10 mmol) in DMF (50 mL), the mixture was heated to 70 °C for (3hrs), the reaction was quenched with water (50 mL) and extracted with ether (3 x 50 mL), the combined organic layers was washed with brine (50 mL), water (50 mL), dried over Na_2SO_4 and evaporated under reduced pressure to give the titled compound (1.73 g, 98%) as a white crystalline solid, mp 102-104 ; $[\alpha]_D^{-18}$ (c 0.5 in CHCl_3). Microelemental analysis for $\text{C}_{14}\text{H}_{19}\text{N}_3\text{O}_9$ calculated: C, 45.04; H, 5.13; N, 11.26, found: C, 45.08; H, 5.15; N, 11.30.

Synthesis of Triazoles [6] and [7]

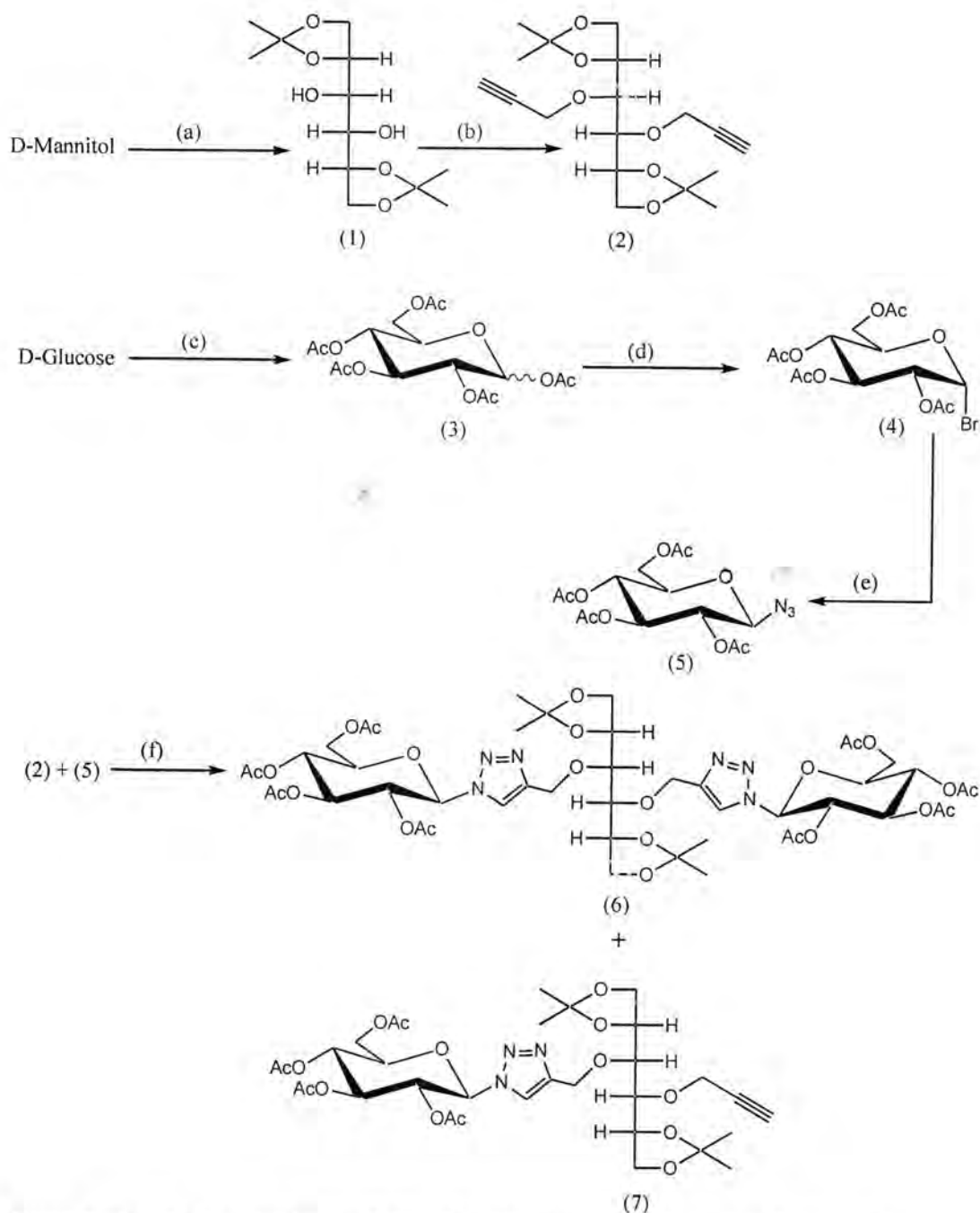
A solution of compound (**2**) (2.05 mmol) in DMF (2 mL) was added to the suspension of CuI (3.1 mmol) and diethylisopropylamine (DEIPA) (3.15 mmol) in DMF (5 mL). Glycosyl azide (3.00 mmol) was added and the mixture was heated at 70 °C for (24 h). The solution was diluted with water (20 mL) and extracted with EtOAc (3x25 mL), the combined organic layers dried over Na_2SO_4 and evaporated under reduced pressure. Flash chromatography of the residue (Silica, 3:1 ether, light petroleum) produced the titled compounds.

Compound (**6**), white solid (0.50 g, 46%), mp 141-143. Microelemental analysis for $\text{C}_{46}\text{H}_{64}\text{N}_6\text{O}_{24}$ calculated: C, 50.92; H, 5.95; N, 7.75, found: C, 50.91; H, 5.97; N, 7.78, MS (FAB) m/z : 1107 ($[\text{M} + \text{Na}^+]$).

Compound (**7**), white solid (0.26 g, 37%), mp 127-129. Microelemental analysis for $\text{C}_{32}\text{H}_{45}\text{N}_3\text{O}_{15}$ calculated: C, 54.00; H, 6.37; N, 5.90, found: C, 54.05; H, 6.41; N, 5.93. MS (FAB) m/z : 734 ($[\text{M} + \text{Na}^+]$).

RESULTS AND DISCUSSION

The triazoles (6) and (7) were prepared according to the following scheme:



Reagents and conditions: (a) Acetone, ZnCl_2 rt 3hrs; (b) propargyl bromide, NaOH, DMF rt 24 h; (c) Ac_2O , pyridine rt 16 h; (d) 33% HBr/AcOH 0-rt 1 h; (e) NaN_3 , DMF 70°C 3 hrs; (f) CuI, DEIPA, DMSO, 24 h 70°C .

The work commenced by the reaction of D-mannitol with anhydrous acetone in the presence of zinc chloride as an acidic catalyst to give the diacetone-mannitol (**1**), FT-IR bands in cm^{-1} (nujol): 3461 and 3311 (O-

H) stretching at C3 and C4, 2923 and 2854 (**C-H**) stretching of nujol⁽¹³⁾, 1456 and 1376 (**C-H**) bending nujol, the (**C-H**) stretching and bending bands of the sugar overlap with mineral oil bands. ¹H NMR (300 MHz (CD₃)₂SO) δ ppm: 4.68 (d, $J=7.7$ Hz, 2H, O-H), 3.95 (m, 4H, CH₂(C1and6)-O), 3.83 (dd, $J=4.6$ Hz, 2H, CH(C2 and C5)-O), 3.45 (t, $J=7.7$ Hz, 2H, CH(C2 and C3)-O), 1.27 and 1.23 (s, 12H, CH₃-C), 3.33(s, O-H) water and 2.49(m, DMSO)⁽¹⁴⁾. ¹³C NMR (300 MHz (CD₃)₂SO) δ ppm: 108.4 (2C, C_{isopropylidene}), 75.1 (2C, CH₂, 1 and 6), 70.2 (2 C, CH, 2 and 5), 67.0 (2C, CH, 3 and 4), 27.0 and 25.7 (4C, CH₃ isopropylidene).

Williamson etherification of compound (**1**) using propargyl bromide and crushed sodium hydroxide in DMF at room temperature yielded compound (**2**).

FT-IR spectrum of (**2**) showed the following bands in cm⁻¹(nujol): 3251 (\equiv **C-H**) stretching, 2986 (**C-H**_{propargyl}) stretching, 2935 and 2884 (**C-H**) stretching which overlapped with mineral oil bands, 2114 (**C \equiv C**) stretching, (**C-H**) bending at 1458, 1376 and 1347, and different (**C-O**) stretching 1266-1057. ¹H NMR (300 MHz (CDCl₃) δ ppm: 4.36 (dd, $J=2.3, 1.9$ Hz, 4H, CH₂C \equiv C), 2.45(t, $J=1.7$ Hz, 2H, C \equiv CH), the same coupling constant of the mentioned signals shows there is a long range coupling between the acetylenic proton and the other two protons, the other signals due to the rest of the sugar molecule. ¹³C NMR (300 MHz (CDCl₃) δ ppm: 79.7(2C, CH₂-C \equiv CH), 74.6 (2C, CH₂-C \equiv CH), 59.4 (2C, CH₂-C \equiv CH). The two dimensional NMR spectrum HC Heteronuclear Single Quantum Coherence (HSQC) shown below supports the above signals assignment. The other signals are belong to the rest of the sugar molecule.

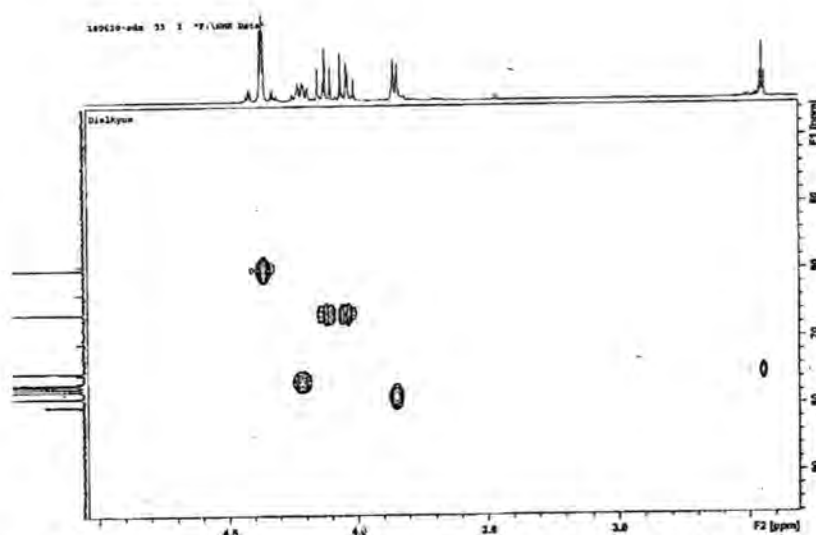


Figure – 3: Two dimensional NMR HSQC expansion of compound (**2**)

Keeping the D-glucose in the acetylation mixture acetic anhydride/pyridine for 16 h gave the glucose pentaacetate (**3**). FT-IR spectrum of (**3**) showed the following bands in cm^{-1} (nujol): 1745 (**C=O**) stretching and 1229-1044 (**C-O**) stretching. ^1H NMR (300 MHz (CDCl_3)) δ ppm: 5.72 (d, $J=7.9$ Hz, 1H, **H-1**), 5.25 (t, $J=9.3$ Hz, 1H, **H-4**), 5.16 (t, $J=9.0$ Hz, 1H, **H-3**), 5.13 (t, $J=9.0$ Hz, 1H, **H-2**), 4.30 (dd, $J=8.0$ Hz, $J=4.5$ Hz 2H, **H-6_a** and **b**), 3.84 (ddd, $J=9.9$ Hz, $J=4.9$ Hz, $J=2.3$ Hz, 1H, **H-5**), 2.12, 2.09, 2.03 and 2.01 (s, 15H, **CH₃** acetate). The signal at 1.56 ppm attributed to water in CDCl_3 ⁽¹⁴⁾. ^{13}C NMR (300 MHz (CDCl_3)) δ ppm: 170.5, 170.0, 169.3, 169.1 and 168.8 (5C, **C=O** acetate), 91.6 (1C-**C1**), 72.67 (1C-**C5**), 72.60 (1C-**C4**), 70.1 (1C-**C2**), 67.6 (1C-**C3**), 61.3 (1C-**C6**) and the signals around 20 (5C-**CH₃** acetate).

The treatment of compound (**3**) with HBr/HOAc in dry conditions for 45 min produced acetobromoglucose (**4**) in very good yield. FT-IR spectrum of (**4**) showed the following bands in cm^{-1} (nujol): 1743 (**C=O** acetate) stretching and 1165 (**CH-Br**) bending (wagging). The (**C-Br**) stretching band should be out of spectrum because it appears around 550 cm^{-1} ⁽¹³⁾.

^1H NMR (300 MHz (CDCl_3)) δ ppm: 6.60 (d, $J=4.1$ Hz, 1H, **H-1**), 5.55 (t, $J=9.7$ Hz, 1H, **H-4**), 5.15 (t, $J=10.1$ Hz, 1H, **H-3**), 4.83 (dd, $J=10.0$ Hz, $J=4.0$ Hz, 1H, **H-2**), 4.30 (m, 2H, **H-5** and **H-6_a**), 4.12 (dt, $J=9.2$ Hz, $J=4.1$ Hz, $J=2.0$ Hz, 1H, **H-6_b**), 2.10, 2.09, 2.05 and 2.03 (s, 14H, **CH₃** acetate). The ^1H NMR data gave an excellent confirmation for glycosyl bromide due to the shift of the anomeric proton signal downfield from 5.75 ppm to 6.60 ppm, also the change of integration of (**CH₃**) signals. The coupling constant value of the anomeric proton 4.1 Hz indicates that the bromide formed in α -conformation only.

^{13}C NMR (300 MHz (CDCl_3)) δ ppm: 170.4, 169.7 and 169.4 (4C, **C=O** acetate), 86.4 (1C-**C1**), 72.0 (1C-**C4**), 70.4 (1C-**C3**), 70.0 (1C-**C2**), 69.9 (1C-**C6**), 60.8 (1C-**C5**) and 20.5 (4C-**CH₃** acetate).

The S_N^2 reaction between glycosyl bromide (**4**) and sodium azide in DMF for 3 hrs gave glycosyl azide (**5**) in quantitative yield due to the nucleophile strength (N_3^-) and the neighboring group participation of acetate in position 2 of the sugar. FT-IR spectrum of (**5**) showed the following important bands in cm^{-1} (nujol): 2118 ($-\text{N}_3$) stretching, 1754 and 1732 (**C=O** acetate) stretching. ^1H NMR (300 MHz (CDCl_3)) δ ppm: 5.20 (t, $J=9.4$ Hz, 1H, **H-4**), 5.09 (t, $J=9.3$ Hz, 1H, **H-3**), 4.94 (t, $J=8.9$ Hz, 1H, **H-2**), 4.64 (d, $J=8.8$ Hz, 1H, **H-1**), 4.20 (ddd, $J=13.5$ Hz, $J=9.0$ Hz, 3.1 2H, **H-6_a** and **b**), 3.84 (ddd, $J=9.2$ Hz, $J=4.1$ Hz, $J=2.9$ Hz, 1H, **H-5**), 2.08, 2.06, 2.01 and 1.99 (s, 15H, **CH₃** acetate). ^{13}C NMR (300 MHz (CDCl_3)) δ ppm: 170.5, 170.0, 169.2 and 169.1 (4C, **C=O** acetate),

87.8 (1C-C1), 73.9 (1C-C4), 72.4 (1C-C3), 70.51 (1C-C2), 67.7 (1C-C6), 61.5 (1C-C5), 20.5 and 20.4 (4C-CH₃ acetate).

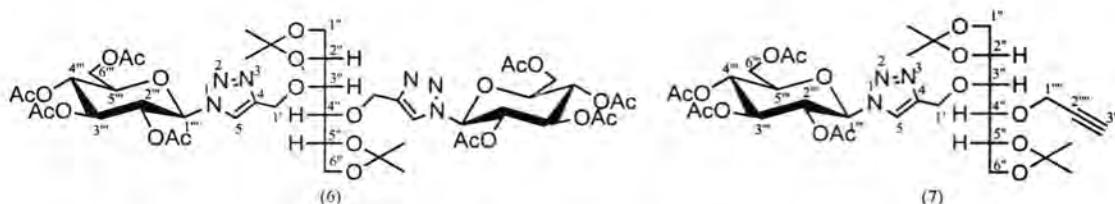


Figure – 4: Numbering the final compounds

The cycloaddition of glycosyl azide (**5**) to the diacetylene (**2**) using click conditions in DMF at 70°C for 24 h afforded the two targeted triazoles (**6**) and (**7**). FT-IR spectrum of (**6**) showed the following important bands in cm⁻¹(nujol): 3069 (C-H_{triazole}) stretching, 1754 and 1737 (C=O) stretching. To explain the NMR data we numbered the final compounds as follows:

¹H NMR (300 MHz (CD₃)₂SO) δ ppm: 8.40 (s, 2H, H-5), 6.32 (d, *J*=8.8 Hz, 2H, H-1^{'''}), 5.67 (t, *J*=8.9 Hz, 2H, H-4^{'''}), 5.53 (t, *J*=8.9 Hz, 2H, H-3^{'''}), 5.16 (t, *J*=8.8 Hz, 2H, H-2^{'''}), 4.67 (q, *J*=7.9 Hz, 4H, H-6^{'''}), 4.34 (ddd, *J*=7.8 Hz, *J*=4.1 Hz, *J*=2.0 Hz, 2H, H-5^{'''}), 4.07 (m, 6H, H-1['], H-3^{''} and H-4^{''}), 3.90 (t, *J*=6.4 Hz, 2H, H-2^{''} and H-5^{''}), 3.74 (dd, *J*=6.1 Hz, *J*=4.2 Hz, 4H, H-1^{''} and H-6^{''}), 3.33 (water), 2.49 (m, DMSO)⁽¹⁴⁾, 2.07, 2.01, 1.97, 1.94, 1.26 and 1.24 (s, 36H, CH₃ acetate and isopropylidene). The ¹³C NMR (300 MHz (CD₃)₂SO) spectrum showed the following new signals δ ppm: 145.4 (2C-C4) and 121.3 (2C-C5) which due to the aromatic triazoles rings, also increasing in signals of the (C=O acetate) around 169.

The other compound produced from the above cycloaddition is compound (**7**), we will explain the major differences in spectra between the two compounds (**6**) and (**7**). FT-IR spectrum of (**7**) showed the following new band cm⁻¹(nujol): 3278 (≡C-H) stretching, 3072 (C-H_{triazole}) stretching, very weak band at 2116 (C≡C) stretching and 1750 (C=O) stretching.

¹H NMR (300 MHz (CD₃)₂SO) δ ppm: 4.25 (t, *J*=2.5 Hz, 2H, H-1^{'''}), 3.46 (t, *J*=2.4 Hz, 1H, H-3^{'''}) in addition to the same signals of compound (**6**) but with half integration. Also the ¹³C NMR (300 MHz (CD₃)₂SO) spectrum of (**7**) showed almost the same signals of (**6**) with the following changes δ ppm: (4C, C=O acetate) around 170.0, 76.4 (1C, C-3^{'''}), 107.8 (1C, C-1^{'''}). The two dimensional NMR (HSQC) spectrum figure (5) gives an excellent the above signals assignment.

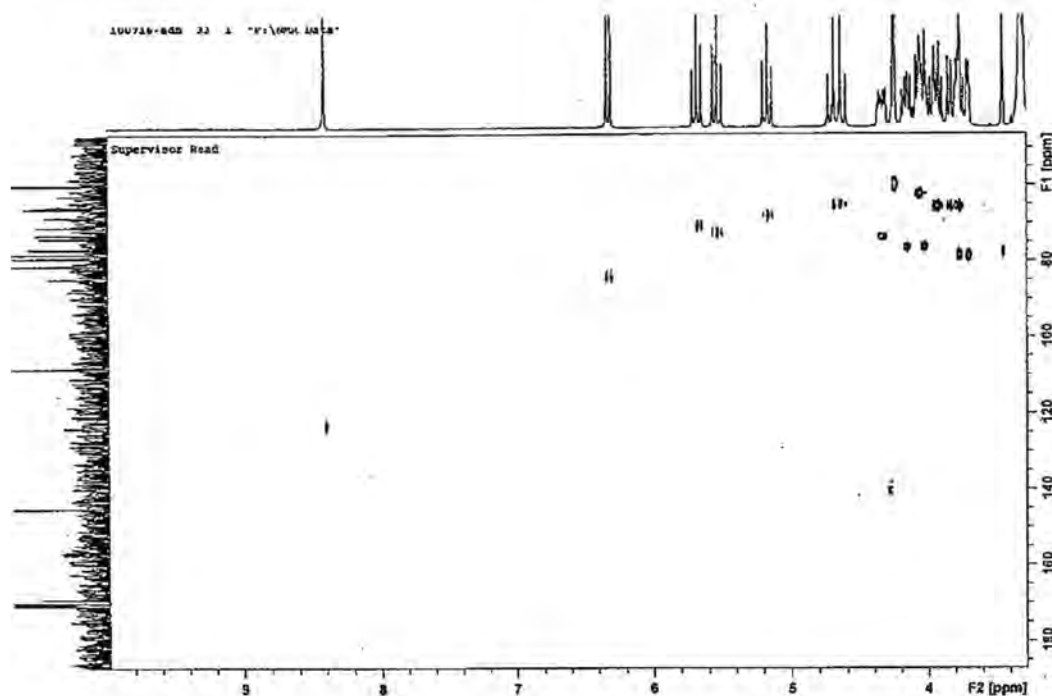


Figure – 5: Two dimensional NMR HSQC expansion of compound (7)

ACKNOWLEDGEMENT

Thanks for Austraining International, Department of Education, Employment and Workplace Relations (DEEWR) Australia for the postdoctoral research fellowship also to the School of Chemistry, The University of New South Wales (UNSW) Sydney especially to Associate Professor Dr. Roger Read for his support.

REFEREFCS

- 1- R. Huisgen, 1,3-Dipolar Cycloaddition Chemistry; Padwa, A., Ed.; Wiley: New York, 1-176 (1984).
- 2- C. W. Tornøe, C. Christensen and M. Meldal, Peptidotriazoles on Solid Phase: [1,2,3]-Triazoles by Regiospecific Copper(I)-Catalyzed 1,3-Dipolar Cycloadditions of Terminal Alkynes to Azides, , J. Org. Chem. 67, 3057 (2002).
- 3- H. C. Kolb and K.B. Sharpless, Drug Discovery Today, The growing impact of click chemistry on drug discovery, 8, 1128 (2003).
- 4- V. Rostovtsev, L. Green, V. Fokin and K.B. Sharpless, A Stepwise Huisgen Cycloaddition Process: Copper(I)-Catalyzed Regioselective Ligation of Azides and Terminal Alkynes, Angew. Chem., Int. Ed. 41, 2596 ,(2002).
- 5- D. Giguère, R. Patnam, M. Bellefleur, C. St-Pierre, S. Sato and R. Roy, , Carbohydrate triazoles and isoxazoles as inhibitors of galectins-1 and -3, Chem. Commun.,2379 (2006).

- 6- B. Holla, M. Mahalinga, M. Karthikeyan, B. Poojary, P. Akberali and N. Kumari, Synthesis of a polyprenyl-type library containing 1,4-disubstituted-1,2,3-triazoles with anti-biofilm activities against *Pseudoalteromonas* sp., *Eur. J. Med. Chem.*, 40, 1173 ,(2005).
- 7- M. Martinelli, T. Milcent, S. Ongerì and B. Crousse ,Synthesis of new triazole-based trifluoromethyl scaffolds, *Beilstein Journal of Organic Chemistry* 4, 1 (2008).
- 8- S. Dedola, S. Nepogodieva and R. Field, Recent applications of the Cu(I) catalysed Huisgen azide-alkyne 1,3-dipolar cycloaddition reaction in carbohydrate chemistry, *Org. Biomol. Chem.* 5, 1006 (2007).
- 9- T. Ziegler and C. Hermann, Synthesis of novel multidentate carbohydrate-triazole ligands, , *Tetrahedron Lett.*,49, 2166 ,(2008).
- 10- G. Cravotto, V. Fokin, D. Garella, A. Binello, L. Boffa and A. Barge, , Ultrasound-Promoted Copper-Catalyzed Azide-Alkyne Cycloaddition, *J. Comb. Chem.*,12, 13 (2010).
- 11- C. Kappe, D. Dallinger and S. Murphree, Practical Microwave Synthesis for Organic Chemists. Strategies, Instruments and Protocols; Wiley-VCH: Weinheim, Germany, 124(2009).
- 12- B. Furniss, A. Hannaford, P. Smith and Tatchell Vogel's Text Book of Practical Organic Chemistry, 5th ed., Longman Ltd., Harlow, UK, 654 ,(1989).
- 13- D. Pavia, G. Lampman and G. Kriz, Introduction to Spectroscopy, Thomson Learning, NY, USA, 30 ,(2001).
- 14- G. Fulmer, A. Miller, N. Sherden, H. Gottlieb, A. Nudelman, B. Stoltz, J. Bercaw and K. Goldberg, , NMR Chemical Shifts of Trace Impurities: Common Laboratory Solvents, Organics, and Gases in Deuterated Solvents Relevant to the Organometallic Chemist, *Organometallics*, 29, 2176 ,(2010).

Spectrophotometric Determination of Copper in Steel Scrap Samples

Thkra Ahmed Hassen

Dept. of Basic Science, College of Dentistry, University of Al Mustansiriya

Received 1/9/2010 – Accepted 2/3/2011

الخلاصة

أكثر السبائك شيوعاً هي سبائك البراص و البرونز ، البراص مصطلح يطلق على سبائك النحاس والزنك في الحالة الصلبة ، كمية النحاس في سبائك البراص تتراوح بين 5% و 45% حسب نوع السبيكة ، البرونز تتكون بصورة رئيسية من النحاس والقصدير ، النسبة المثالية للنحاس في سبيكة القصدير تتراوح من 40 الى 60 % . تم في البحث تعيين واستخراج النحاس من نماذج مختلفة مصنوعة من سبائك النحاس المشهورة (البراص والبرونز) والتي تم الحصول عليها من خردة الحديد من السوق المحلية والنماذج التي جمعت هي { مفصلات الابواب المعدنية ، الثريات المعدنية ، عاكسات الضوء ، النوابض (البرنكات) ، الصنج (صفائح معدنية للموسيقى) ، اطارات الشبابيك الحديدية وجهاز تبريد السيارات (الرادياترات) } ، وقد تم تحليلها طيفياً لاستخراج نسبة النحاس وتم قياس الامتصاص باستخدام تقنية UV عند الطول الموجي 620 نانومتر ، كانت نسبة النحاس هي (56% ، 89% ، 52% ، 55% ، 92% ، 56% و 65%) وعلى التوالي ، ان السبب في اختلاف نسب النحاس بين هذه النماذج يعتمد على النوع والغرض الذي صنعت لاجله ، هذه الطريقة في التحليل مفضلة كونها دقيقة وحساسة ورخيصة التكاليف ، نستنتج من النتائج اعلاه انه يمكن الحصول على كميات جيدة من النحاس بطريقة سريعة ، بسيطة ورخيصة وكذلك من الضروري استغلال الكم الهائل من خردة الحديد الموجودة حالياً في البلد للحصول على النحاس .

ABSTRACT

A simple and rapid spectrophotometric method used for determination of copper in some alloy samples of steel scrap. Different alloy samples which were obtained from steel scrap in local market were analyzed for copper content (Hings, Chandelier, Light reflectors, Spring, Cymbal, Window frame and Car radiator), which determined spectrophotometrically, the copper amount percent were (56% , 89% , 52% , 55% , 92% , 56% and 65%) respectively., this method is simple, sensitive, and unexpensive methods for the determination of copper in their alloys (brass and bronze). All absorption measurement were carried out at (620)nm .

The result showed the amount of copper which got from their alloy samples of steel scrap in this work was good and satisfied . The amount of copper in brass and bronze alloys which were used in this work varies between 52% and 92% by weight depending on the type of brass and its intended use .

. The recommendation is to utilize the huge amount of steel scrap which is available in local market to obtaining copper and other elements.

Keywords: Spectrophotometry; steel scrap, copper alloys and bronze alloys.

INTRODUCTION

. Copper is one of the most widely recycled of all metals; approximately one-third of all copper consumed worldwide is recycled. Recycled copper and its alloys can be remelted and used directly or further reprocessed to refined copper without losing any of the metal's chemical or physical properties.[1]

combination of metal with other chemical elements (metallic or nonmetallic), forming a solution An **alloy** is the or chemical compound that retains metallic properties. Generally, a number of properties of the alloy are significantly different from those of its components. An alloy

with two components is called a binary alloy; one with three is a ternary alloy; one with four is a quaternary alloy.[2]

Among commonly known alloys are brass and bronze,

Brass is the term used for alloys of copper and zinc in a solid solution. It has a yellow color, somewhat similar to gold. It was produced in prehistoric times, long before zinc was discovered, by melting copper with calamine, a zinc ore.

Brass is relatively resistant to tarnishing and is often used for decorative purposes. Its malleability and acoustic properties have made it the metal of choice for musical instruments ."[3,4]

Aluminum makes brass stronger and more corrosion-resistant. It forms a transparent, self-healing, protective layer of aluminum oxide (Al_2O_3) on the surface. Tin has a similar effect and finds its use especially in seawater applications (naval brasses). Combinations of iron, aluminum, silicon, and manganese make brass resistant to wear and tear.[5]

Bronze refers to a broad range of copper alloys, usually with tin as the main additive, but sometimes with other elements such as phosphorus, manganese, aluminum, or silicon. Typically, bronze is about 60 percent copper and 40 percent tin .

The use of bronze was particularly significant for early civilizations, leading to the name "Bronze Age." Tools, weapons, armor, and building materials such as decorative tiles were made of bronze, as they were found to be harder and more durable than their stone and copper predecessors. In early use, the natural impurity arsenic sometimes created a superior natural alloy, called "arsenical bronze." [6,7]

Though not as strong as steel, bronze is superior to iron in nearly every application. Bronze develops a patina (a green coating on the exposed surface), but it does not oxidize beyond the surface. It is considerably less brittle than iron and has a lower casting temperature. Several bronze alloys resist corrosion (especially by seawater) and metal fatigue better than steel; they also conduct heat and electricity better than most steels.[8]

Bronze has myriad uses in industry. It is widely used today for springs, bearings, bushings, and similar fittings, and is particularly common in the bearings of small electric motors. It is also widely used for cast metal sculpture and is the most popular metal for top-quality bells and cymbals.[9]

Commercial bronze, otherwise known as brass, is 90 percent copper and 10 percent zinc.[10]

The purpose of this work is to determine the mass percent of copper in a samples of

Brass and bronze alloys using spectrophotometric analysis by utilizing the huge amount of steel scrap in the local market .

MATERIAL AND METHODS

All the experimental work has been done under the standard conditions.

Determination of copper in alloys :-

A 0.1g amount of an alloy (brass and bronze) samples were accurately weighed and placed in a 250-mL beaker. To it, (in fume hood), slowly pour the 10-mL of concentrated HNO_3 (Analytical reagent, Grainland chemical company, UK) to react with alloy sample, 50-mL of deionized water were carefully added and then the resulting solution were poured into a 100 ml volumetric flask, small amount of deionized water were added to the reaction beaker , swirl, this rinse water was added to the solution in the 100 ml .volumetric flask (repeating two more times), then making this 100 ml. of solution

0.72g amount of the copper(II) sulfate pentahydrate (Analytical reagent, Grainland chemical company, UK) was accurately weighed and placed in a 100-ml beaker , then making it 100 ml solution with deionized water, then three other solution were prepared by dilution of stock solution to construct the calibration graph.

The absorbances of the calibration and sample solutions were measured at wavelength 620nm (spectrophotometer , Otima SP -300).

the absorbance to zero was setted with blank deionized water.

The copper content in an unknown sample was determined using a concurrently prepared calibration figher2.[11]

Statistical Analysis:-

Statistical analysis was conducted to describe different variables and parameters in current study and to describe relationships as well.

RESULTS AND DISCUSSION

Table (1) and graph (1) show that the amount percent of copper in some famous alloys products (Hings, Chandelier, Light reflectors, Spring , Cymbal , Window frame , Car radiator), the percent of copper amount of above alloys products were (56% , 89% , 52% , 55% , 92% , 56% and 65%) respectively. which determined spectrophotometrically this method is simple, sensitive, selective and unexpensive methods for the determination of copper in their alloys (brass and bronze).

The absorption spectrum of copper II showed an absorption maximum at (620) nm, so all absorption measurments were carried out at (620)

In this work some samples which collected from the steel scrap from local market had been used to determine the copper amount in these samples .

Table (1) and graph (1) show that there are a good and satisfied amount percent of copper in the most of copper alloy samples in steel scrap, The amount of copper in brass and bronze alloys which were used in this

work varies between 52% and 92% by weight depending on the type of brass and its intended use .

Joseph R D [12] reported in his book that :-

Springs made of from alpha bronze which consists of the alpha solid solution of tin in copper. Alpha bronze alloys is 55 - 54% copper and 45-44% tin are used also to make coins, turbines and blades, Light reflectors made of from bismuth bronze which is a bronze alloy with a composition of 52 parts copper, 30 parts nickel, 12 parts zinc, 5 parts lead, and 1 part bismuth. It is able to hold a good polish and so is used in light reflectors and mirror , Window frames and hinges made of from Silicon alloys which are alloys of 56% copper ,44% tin with 3% silicon and 1% manganese. Silicon bronzes strength and ductility, good corrosion resistance and easy weldability. They are used in architectural applications , Cymbals made of from bronze alloy which is 90% copper and 10% tin ,Chandelier made of from brasses containing a high percentage of copper are made from electrically refined copper that is at least 99.3% pure to minimize the amount of other materials, It is able to hold a good polish, and Car radiators made out of 65% copper and 35% Zinc brass alloy.

According to these standard results ,the amount percent of copper in their alloys are approximately coincide with the results of the copper amount percent which were obtained from copper alloys samples of steel scrap in this work. Also many works have been achieved about copper and copper alloys (13 ,14)

Finally it can be concluded the following

1. The analytical method which is used in this work is simple ,sensitive and cheap
2. It found that the copper amount percent of the alloys which used in this work varies from 52% to 92% depending on the type of brass and its intended use
3. The amount of copper which obtained from the copper alloys of steel scrap is satisfied and a good amount
4. It is very necessary to utilize the huge amount of steel scrap which is available in local market to obtaining copper .

Table -1: shows the relationship between alloy samples and copper amount percent

Alloys samples products	Copper percent
1-Hings	56%
2-Chandelier(Luster)	89%
3-light reflectors	52%
4-Springs	55%
5-Cymbal	92%
6-Window frames	56%
7-Car radiator	65%

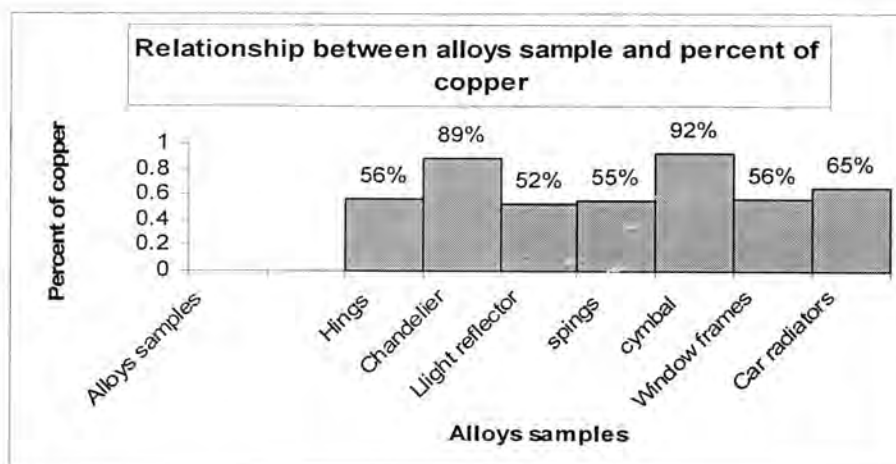


Fig -1: shows the relationship between alloys samples and percent of copper

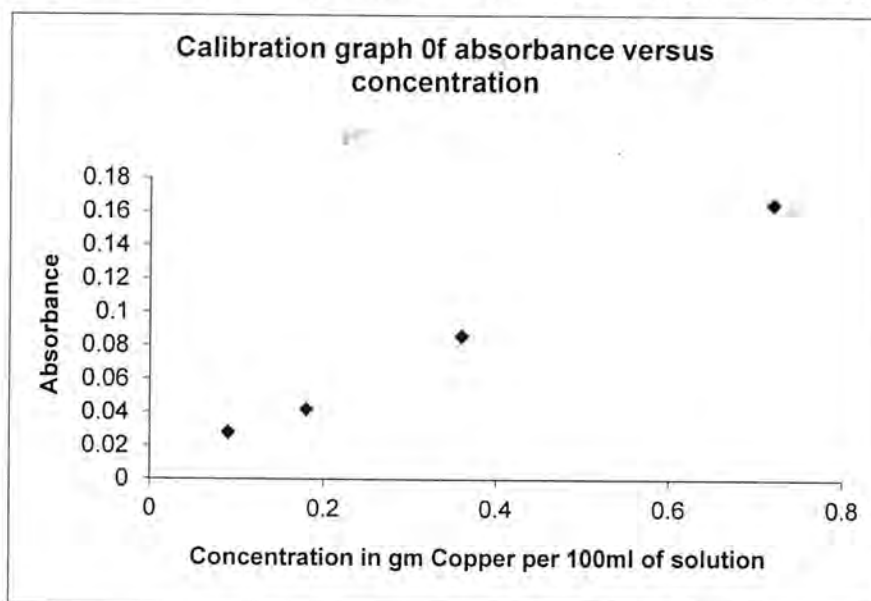


Fig-2: Calibration graph of absorbance versus concentration of copper

Statistical Analysis:-

To calculate the weight of copper in some types of scrap we chose 7 alloys as samples of products as follows :-

- 1.hings
- 2.chandelier(luster)
- 3.light reflectors
- 4.springs
- 5.cymbal
- 6.window frames
- 7car radiator

We take from each type 0.1 gram as samples and separate copper from it then we have the following results as shown in table 1

Table-2: Weight of alloys ,copper and other material in alloys (in gram) weight of . Alloy sample products alloy copper other material

hings	0.1	0.056	0.044
Chandelier (luster)	0.1	0.089	0.011
light reflectors	0.1	0.052	0.048
springs	0.1	0.055	0.045
cymbal	0.1	0.092	0.008
window frames	0.1	0.056	0.044
car radiator	0.1	0.065	0.035

Weight of copper as shown in table (1) in is higher then Weight of other material in alloy in each type in figure as shown . then we calculate the percentage of copper in alloy and the percentage of other materials we have the same results as shown in table (2)

Table -3: Percentage of copper and other material in alloys Percentage of Alloys sample product copper other materia

hings	65%	44%
Chandelier (luster)	89%	11%
light reflectors	52%	48%
springs	55%	45%
cymbal	29%	8%
window frames	56%	44%
car radiator	65%	35%

As we see in table (1) percentage of copper higher than percentage of other materials and the highest percentage is in cymbal which equal to(92%) as shown in figure (2) than the second percentage is in chandelier (luster) and equal to 89% see figure the third percentage we see is in car radiator and equal to 65%see figure (4) the forth percentage is in hings and window frames and equal to 56%see figure (5) and(6) then the fifth percentage is in springs and equal to 55% see figure (7) and the last percentage is in light reflectors and equal to 52%see figure (8) as shown in table (4)

Table -4: Percentage of copper in alloys

Alloys sample	Copper percentage
symbal	92%
Chandelier(luster)	89%
Car radiator	65%
hings	56%
Window frames	56%
Springs	55%
Light reflectors	52%

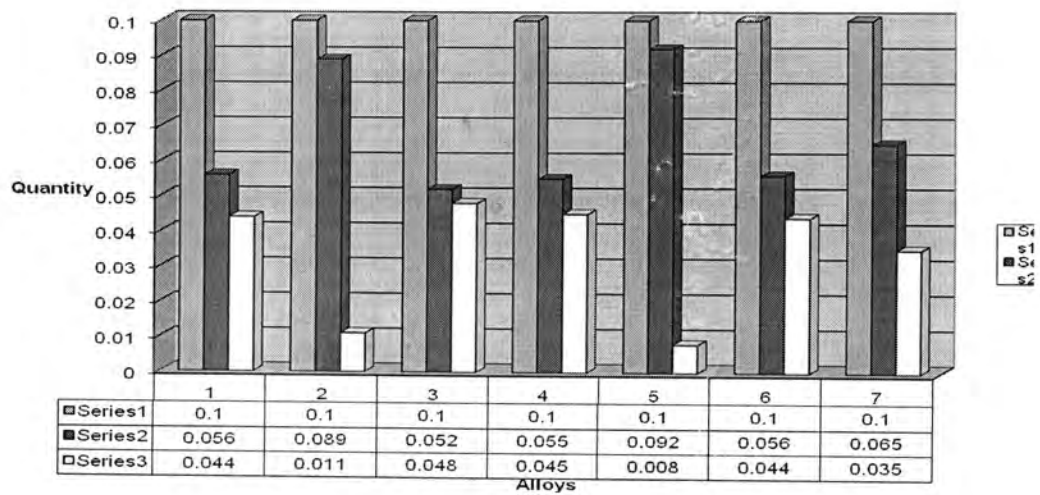


Fig-3: shows the quantity of alloy,copper & other materials



Fig-4: shows the percentage of copper & others in cymbal



Fig-5:percentage of copper & other in chandelier

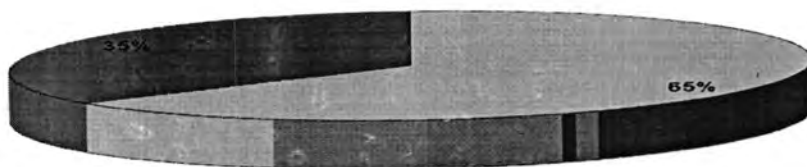


Fig-6: percentage of copper & other in car radiator



Fig-7: percentage of copper & other in hinges



Fig-8: : percentage of copper & other in window frames



Fig-9: : percentage of copper & other in springs



Fig-10: : percentage of copper & other in light reflectors

REFERENCES

1. Recknagel, S. J. Analysis of copper alloys. Federal institute for material and testing ,Berlin ,Germany,Metrologia Journal ,V46. (2009).
2. Los Alamos National Laboratory-Copper. <http://en.Wikipedia.org/wiki/Copper>.
3. Singh, k. A, Extraction spectrophotometric determination of trace amounts of copper in alloys and biological samples,*Journal of Analytical Chemistry*, 63:232-38.(2008).
4. Kochatekar AR, spectrophotometric method for the determination of copper and its application in alloys, *Bull. Chem. Soc. Ethiop.*, 21(1): 129-134. (2007).
5. Shpigun, L., Shushenachev, Ya. and Kamilova, P. Spectrophotometric determination of copprr (II) and zinc (II) based on their kinetic separation in flow-injection systems. *Journal of Analytical Chemistry*, 62 (7): 623-31 . (2007).
6. Fu, D. and Yuan, D. Spectrophotometric determination of copper in arsenical bronze samples , *Spectrochim. Acta. A. Mol. Biomol. Spectrosc.* (July 19).(2006).
7. Ghazy, S. E., El-Shazly R. M., El-Shahawi, M. S., Al-Hazmi, G. A. A. and El-Asmy, A. A. Spectrophotometric Determination of Copper (II) in Natural Waters, Vitamins and Certified Steel Scrap Samples Using Acetophenone-*p*-chlorophenylthiosemicarbazone, *Journal of the Iranian Chemical Society*, 3(2):140-50. (2006).
8. Massoud and Nejati- Yazdnejad. Spectrophotometric determination of trace Cu (II) ion based on complexation with Anthraquinine derivative, *Anal Sci.*, 22: 617-19. (2006).
9. Shishehbore, M. R., Nasirizadeh, N., Haji Shabni, A. M., Tabatabaee, M. Spectrophotometric determination of trace copper after Precocentration with 1,5-Diphenylcarbazone on Microcrystalline 11.

- Naphthalene, *Canadian Journal of Analytical Science and Spectroscopy*, 50: 130-34.(2005).
10. Rekhai, D. Suvardhani, K Kumar, K.S. Reddyprasad, P. Jayaraj B. and Chiranjeevi, P. Extractive spectrophotometric determination of copper (II) in alloy samples , *J. Serb. Chem. Soc*, 72(3):3299.(2007).
 11. Ahmed M,J, Saifuddin M.T, and Tasnima J.K. 2010. A rapid Spectrophotometric Method for the Determination of Copper(II) in all0ys samples , *Bangladesh council of scientific and industrial research (BCSIR)*, Chittagong, Bangldesh .(2010).
 12. Joseph,R.D. Copper and copper alloys .International Handbook committee,Lndon, UK.(2001).
 13. Zhang,X.C Shenglong, Y.H. Zhimin, S. N Lianpeng, J.X.and Feng, W. M.Aging Characteristics of the Alloys Cu-Zn-Cr[J];Rare Metal Materials and Engineering;2003-02.(Central South University, Changsha , China.(2003).
 14. WANG Y-N, LIU P, L Jing-, KANG B-X,andTIAN B-H.Influence of Heat Treatment on Characteristic of Cu-Ag-Cr Alloy (School of Materials Science and Engineering, Henan University of Science and Technology, Luoyang , China .(2005).

Synthesis of Some Heterocyclic Compounds Derived from 1,3-dihydro-2H-indol-2-one

Nahida A. jinzeel

Department of Chemistry ,College of Science , University of AL-Mustansiriyah.

Received 14/11/2010 – Accepted 2/3/2011

الخلاصة

في هذا العمل حضر (2-اوكسو- 2,3-ثنائي هيدرو- H 1-اندول -1-ايل) حامض الخليك (1) من 3,1-ثنائي هيدرو-2- H اندول -2-اون مع 2-كلورو حامض الخليك وبمعاملة المركب (1) مع أورثو فنييلين ثنائي الامين اعطى المشتق (2) وبمعاملة المركب (1) مع كلوريد الثايونيل اعطى المشتق (3) حضر المركب (4) من المشتق (3) مع الهيدرازين المائي. تفاعل المركب (4) مع انهدريد السكسينيك يعطى المركب (6) 1- (2-اوكسو- 2,3-ثنائي هيدرو- H 1-اندول -1-ايل) اسيتايل [تتراهيدرو 1-بيردiazين-6,3 - ثنائي اون.تفاعل المركب (4) مع نترت الصوديوم في حامض الخليك اعطى المركب (5) (2-اوكسو- 3,2-ثنائي هايدرو- H 1-اندول -1-ايل) اسيتايل ازايذ. تفاعل المركب (4) مع فنييل ايزوثايوسيانات وهيدروكسيد الصوديوم اعطى المركب (8) 1- (5- مركبتو-4-فنييل -4,5-ثنائي هايدرو- H 1-اندول -1-ايل) اسيتايل [تتراهيدرو 1-بيردiazين-6,3 - ثنائي هايدرو- H 2-اون.مركبات ازوميثين (9-11) حضرت من تكاثف (4) مع الالدهايدات الاروماتية ثم المركبات (9-11) ثم تحويلها الى عدد من مشتقات اوكسودايازول (12-14) شخصت هذه المركبات من خلال درجة الانصهار وتقنية (FTIR) وتحليل العناصر وتقنية (NMR).

ABSTRACT

In this work (2-oxo-2,3-dihydro-1H-indol-1-yl)Acetic acid was prepared from (1,3-dihydro-2H-indol-2-one) with chloro acetic acid(1). Treatment of (1) with o-Phenylenediamine gave 1-(4,5-dihydro-1H-imidazole-2-yl-methyl)-1,3-dihydro-2H-indol-2-one(2). Treatment of (1) with thionyl chloride gave(3) compound(4) was prepared from (3) with hydrazine hydrate.Reaction of(4)with sccinic anhydride gave 1-[(2-oxo-2,3-dihydro -1H-indol-1-yl) acetyl]tetrahydro pyridazine-3,6-dione(6). Reaction of (4) with sodium nitrate in acetic acid gave (2-oxo-2,3-dihydro-1H-indol-1-yl)acetyl azide(5).Reaction of (4) with phenyl iso thyo cyanate and NaOH offorded 1-[(5-mercapto-4-phenyl-4,5-dihydro-1H-1,2,4-triazole -3-yl)methyl]1,3-dihydro-2H-indol-2-one(8).Azomethene(9-11) were prepared through condensation of (4) with aromatic aldehydes then compounds (9-11) are converted into a number of oxadiazol derivatives(12-14).The structures of these compounds were characterized from their melting point, FTIR,UV-visible spectroscopy, elemental analysis, and NMR.

INTRODUCTION

Benzimidazole and its derivatives have attracted researcher's interest in the fields of bioorganic and medical chemistry to their significant antifungal , antibacterial and insecticidal properties(1).

Synthetic pyridazinone derivatives as important scaffolds in drug discovery with many of their analog being used in the treatment of various human pathological states(2).

The therapeutic effects of Schiff bases and 1,2,4-triazole derivatives have been studied for a number of pathological conditions with include antifungal(3) antiviral(4),antibacterial(5) and anti – inflammatory(6).

Derivatives of 1,3,4-oxadiazole and 1,3,4-thiodiazole have been

found to possess a wide spectrum of pharmacological, Medical and biological activities(7).

We now report on the synthesis of compounds derived from (1,3-dihydro-2H-indol-2-one) containing benzimidazole, pyridazinone, triazole, oxadiazole mixtures with the purpose of investigation in the future their possible anti bacterial and anti-fungal activities.

MATERIALS AND METHODS

Instruments

Melting points were determined by open capillary tubes on Gallen K&mp melting point apparatus and are uncorrected. The IR spectra discs (KBr) were recorded with a Shimadzu FTIR-8400, UV spectra were recorded on a Shimadzu 160A UV/vis spectrophotometer using absolute ethanol as solvent. Element analysis was done on EUROEA instrument. ^1H NMR spectra were recorded on BRUKER model Ultra shield 300MHz spectrophotometer. Starting chemical compounds were obtained from Fluka or BDH.

Preparation of (2-oxo-2,3-dihydro-1H-indol-1-yl) acetic acid [1].

To (0.01mole, 1.33gm) (1,3-dihydro-2H-indol-2-one) in (20ml) of ethanol, (0.01mol, 0.56gm) KOH was added followed by (0.01mole, 0.95gm) mono chloro acetic acid. The reaction mixture was heated under reflux for (8hr.). The hot solution was evaporated under reduced pressure. The reaction mixture was cooled, acidified with 10% HCl to precipitate the acid [1], the obtained compound was filtered, washed with cold distilled water and dried. table(1)

Preparation of 1-(4,5-dihydro-1H-imidazo)-2-yl-methyl)1,3-dihydro-2H-indol-2-one[2]:

Compound[1] (0.01 mole, 1.91gm) was refluxed for (12hrs.) with o-phenylene diamine (0.01mole, 1.08gm) in 4N HCl (20ml). The reaction mixture was cooled and then neutralized ammonia to precipitate benzimidazol. Table(1).

Preparation of (2-oxo-2,3-dihydro-1H-indol-1-yl)acetyl chloride [3].

To compound[1] (0.01mol, 1.9gm) was added thionyl chloride (15ml). The mixture was held at reflux for (7hrs). The excess of thionyl chloride removed under reduced pressure to get compound [3]. table(1).

Preparation of (2-oxo-2,3-dihydro-1H-indol-1-yl) acetohydrzide [4].

A mixture of compound [3] (0.0mole, 2.09gm) and hydrazine hydrate (10ml) was refluxed for (3hrs.), ethanol (15ml) was added and refluxed for (4hrs.). The separated precipitate was filtered and washed with cold water and recrystallized from ethanol to get compound[4] table(1).

$\text{C}_{10}\text{H}_{11}\text{N}_3\text{O}_2$ calc. for (C.H.N)%

C, 58.47, H5.35, N, 20.46

Found % C 58.57, H.5.15, N, 20.86.

Preparation of (2-oxo-2,3-dihydro-1H-indol-1-yl) acetyl azide[5].

To a cold suspension of compound[4] (0.01mol,2.05gm) in acetic acid(30.ml), a cold solution of sodium nitrate (0.03mole,2gm) in water (10ml) was added drop wise with stirring . Stirring was continued for (1hrs.) at room temperature. The solid product thus formed was filtered , washed with water , dried and recrystallized from ethanol.table(1).

Preparation of 1-[(2-oxo-2,3-dihydro-1H-indol-1-yl) acetyl] tetrahydro pyridazine(-3,6-dione[6]

Succinic anhydride(0.01mole,1.5gm) dissolved in(30ml) acetic acid was added to carbohydrazide[4](0.01mole,2.05gm) and the reaction mixture was refluxed for (7hrs.). Then the mixture was poured on crushed ice. The formed solid product was filtered off and recrystallized from pet. Ether.table(1).

Preparation of 2[(2-oxo-2,3-dihydro-1H-indol-1-yl)acetyl]-N-Phenyl hydrazine carbothiamide [7].

A mixture of compound [4] (0.01mole,2.05gm) and phenyl isothiocyanate(0.01mole,1.31gm) in absolute ethanol(20ml) was refluxed for (3hrs) and cooled. The solid product was filtered and recrystallized from ethanol.table(1).

Compound[7]($C_{17}H_{16}N_4O_2S$) calc. for (C.H.N.)%

C,59.92,H,4.70,N,16.45,S,9.40.

Found% C,59.80,H,4.60,N,16.26,S,9.30.

Preparation of 1-[(5-mercapto-4-phenyl-4,5-dihydro-1H-1,2,4-triazole-3-yl)methyl]-1,3-dihydro-2H-indol-2-one[8].

Compound[7] (0.01mole,3.4gm) were refluxed in NaOH solution (2N,30ml) for (3hrs). Cooled , then neutralized to pH 6 using dilute hydro chloric acid to give the crude product which was filtered , washed with water and recrystallized from ethanol.table(1).

Compound [8] ($C_{17}H_{16}N_4OS$) Calc. for (C.H.N)% C,62.88, H,4.73, N,17.26 , S,9.86.

Found% : C,62.86,H,4.71,N,17.05,S,9.60.

Preparation of compounds (9-11)

A mixture of compound(4) (0.002mole,0.41gm) and the corresponding aryl aldehyde (0.002mole) in absolute ethanol (20ml) was refluxed for (3hrs.) and cooled. The solid product was filtered and recrystallized from ethanol.table(1).

Preparation of compounds (12-14) [5-substituted -1,3,4-oxadiazole -2- yl] methyl]-1,3-dihydro-2H-indol-2-one.

A mixture of compounds[9-11] (0.01mole) , anhydrous Sodium acetate (0.02mole) and glacial acetic acid was placed in a round bottomed flask equipped with a separating funnel for the addition of bromine (0.8ml in

5ml of glacial acid) was added slowly to it while stirring magnetically. After (1.5hrs) of stirring the solution was poured on crushed ice, and the recrystallized from aldehyde free ethanol.

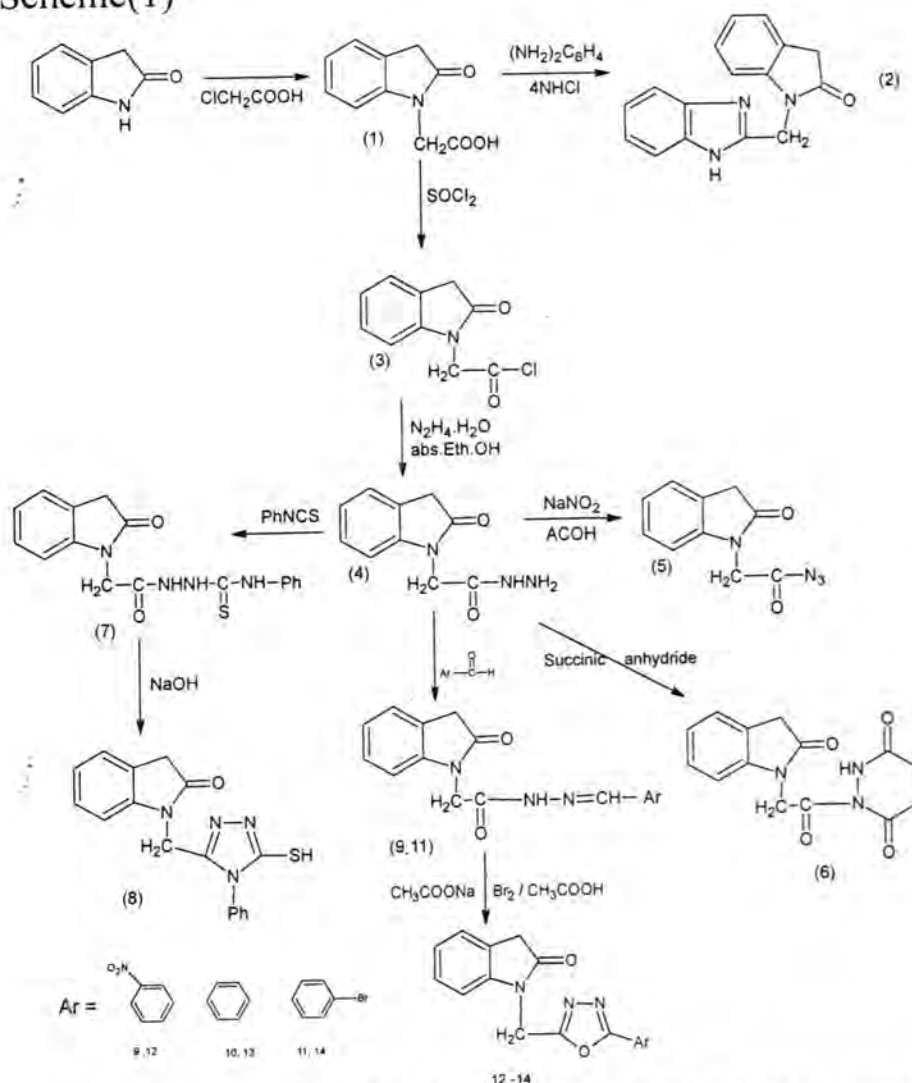
Compound [12](C₁₄H₁₃N₄O₄)% Calc. for (C.H.N.) %
C,60.65,H,3.56,N,16.65.

Found% : C,60.85,H,3.45,N,16.70.

All physical constant for these compounds were reported in table (1).

RESULTS AND DISCUSSION

The reaction sequence for titled compounds is out lined in Scheme(1)



The starting material for the synthesis of targeted compounds is (1,3-dihydro-2H-indol-2-one)

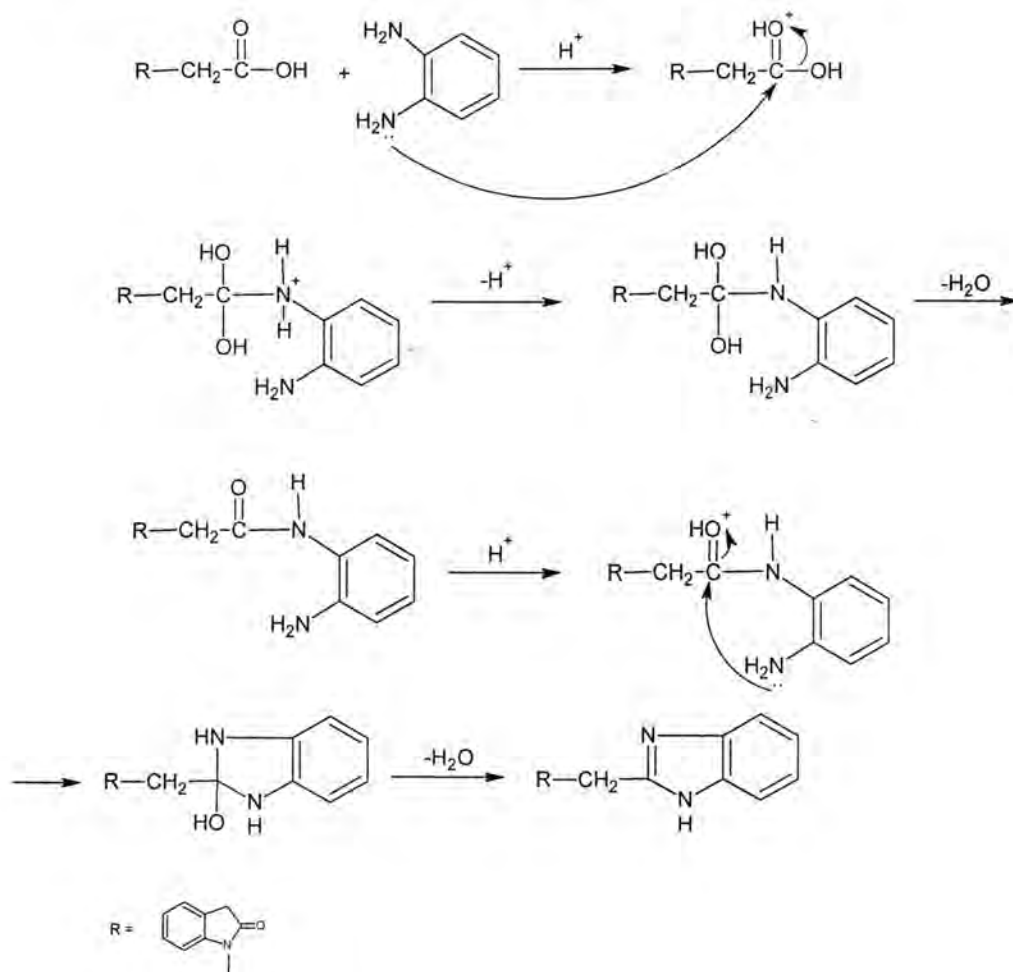
Treatment of the starting materials with chloro acetic acid produced compound(1).

The structure of(1) was confirmed by their FTIR and UV. Spectra

through the appearance of bond at 3419cm^{-1} for (-OH) and 1700cm^{-1} for (C=O) carboxylic acid.

Condensation of compounds(1) with O-Phenylene diamine yielded the benzimidazole derivative(2). Structure of compound(2) was confirmed by FTIR spectra data which showed the disappearance of bonds at 3419cm^{-1} and 1700cm^{-1} attributed to (-OH) and (C=O) of carboxylic acid in compound(1).

The mechanism of reaction is shown in schem(2).



Treatment of (1) with SOCl_2 produced compound(3) (2-oxo-2,3-dihydro-1H-indol-1-yl) acetylchloride compound(4) was prepared by the reaction of (3) with hydrazine hydrate. The FTIR spectrum of the hydrazide(4) show two stretching bands at $(3300-3200)\text{cm}^{-1}$ which were assigned to the NH_2 stretching frequency compound (4) shows band at 1635 for (C=O).

Treatment of (4) with sodium nitrate in acetic acid yielded compound(5).

FTIR spectrum of(5) shows band at $(2200)\text{cm}^{-1}$ for(N_3) with the

disappearance of (NH_2) at $(3300-3200)\text{cm}^{-1}$.

Treatment of (4) with succinic anhydride gave compound (6). FTIR spectrum of (6) shows bands at 3460cm^{-1} and 3210cm^{-1} which were assignable for (NH) stretching vibration and at 1720cm^{-1} was due to (C=O) moiety of pyridazine ring while the (C=O) stretching of amide $(1624)\text{cm}^{-1}$ compound (6):H-NMR:(t,2H) in $(1.87-2.03)$ two equivalent

methylene groups of pyridazine ring (S,2H) in 2.78 due to $(\text{CH}_2 - \overset{\text{O}}{\parallel}{\text{C}})$ (m,4H,Ar-H) 7.7-8, Pyridazine (N-H) absorption at $(9.45-9.67)$.

Reaction between (4) and phenyl isothiocyanate afforded the corresponding thiosemicarbazide (7) in moderate yield. The FTIR spectra of (7) display (C=S) stretching band at 1250cm^{-1} and (NH) stretching band at 3226cm^{-1} .

Reflexing of compound (7) with NaOH solution for three hours afforded triazole derivative (8) which exists in tautomeric thiol – thione equilibrium as indicated by the (C=S) stretching band at 1180cm^{-1} and S-H stretch at 2550cm^{-1} (9).

Compound (8): HNMR ppm : 2.78(S,2H)(-N-CH₂),

3.8(S,1H,N-H thione),

8.3-8.9(m,9H,Ar-H).

Condensation of (4) with aryl aldehydes in ethanol gave the Schiff's bases (9-11). The formation of these Schiff's bases was indicated by the presence in their FTIR spectra of azomethine (C=N) stretching band at $(1600-1640)\text{cm}^{-1}$, combined with the disappearance of (NH_2) stretching band. Moreover, treatment of Schiff's bases (9-11) with $(\text{Br}_2/\text{CH}_3\text{COOH})$ produced oxadiazole derivatives (10) [12-14]. Structures of these compounds which displayed two bands at 1245cm^{-1} and 1080cm^{-1} for the (C-O-C) asymmetric and symmetric stretching, in addition to the band at 1620 for the (C=N) stretch.

Table -I: Physical constant and spectroscopic data for compounds.

Infra red data (vcm^{-1}), KBr disc	UV- λ_{max} (EtOH)	Yield %	M.P $^{\circ}\text{C}$	Formula	Comp. No.
3419(OH), 1700(C=O) (3030(C-H _{or}), 2930(C-H _{alfa} .)	225 340	70	188-190	C ₁₀ H ₉ NO ₃	1
3130(N-H), 1640(C=N), 3040(C-H _{aro} .), 2980(C-H _{alfa} .)	210 390	75	165-167	C ₁₆ H ₁₉ N ₃ O	2
1730(C=O), 3037(C-H _{ar} .) 2928(C-H _{alfa} .)	219 350	65	210-212	C ₁₀ H ₈ NO ₂ Cl	3
3300, 3200, (NH, NH ₂), 1635(C=O), 3030(C-H _{ar}), 2920(C-H _{alfa} .)	250 339	75	218-220	C ₁₀ H ₁₁ N ₃ O ₂	4
200(N ₃), 1640(C=O)	260 370	80	186-187	C ₁₀ H ₈ N ₄ O ₂	5
(3460, 3210)(OH, NH ₂), 1720(C=O)	204 245	65	75-77	C ₁₄ H ₁₃ N ₃ O ₄	6
(3226, 3186)(NH, 1250)(C=S)	204 260 367	72	250-252	C ₁₇ H ₁₆ N ₄ OS	7
(3160)(NH), 2550(S-H), 1180(C=S).	202 250 360	60	260-262	C ₁₇ H ₁₆ N ₄ OS	8
3270(NH), 1640(C=N), 1336(NO _{2sym}) 1510 (NO _{2asym} .)	206 270 388	80	215-217	C ₁₇ H ₁₄ N ₄ O ₄	9
3211(N-H), 3090(C-H _{ar} .) 1645(C=N)	208 287 302	83	230-232	C ₁₇ H ₁₅ N ₃ O ₂	10
3105(NH), 3020(C-H _{or} .) 1630(C=N), 910(C-Br)	204 260 290	82	256-258	C ₁₇ H ₁₄ N ₃ O ₂ Br	11
1245, 1080(C-O-C), 1620(C=N), 1330(NO _{2sym}) 1520(NO _{2asym} .)	206 240 310	60	234-236	C ₁₇ H ₁₂ N ₄ O ₄	12
1240, 1090(C-O-C) 1630(C=N)	202 255	65	200-202	C ₁₇ H ₁₃ N ₃ O ₂	13
1246, 1082(C-O-C) 1640(C=N), 910(C-Br)	204 249 396	58	228-229	C ₁₇ H ₁₂ N ₃ O ₂ Br	14

REFERENCES

1. J. D. Rawan, "Biochemistry", Neil Patterson publishers International Edition, North Carolina, p 1105 (1989).
2. Vanadma, S.A. and Sharma, K.V. "Synthesis and Biological some 3,5-Diaryl-1-benzothiazolopyrazoline Derivatives", Ejournal of chemistry. 6(2):356-384(2006)
3. Mndasir Rashid Banday and Abdul Rauf "Substituted 1,2,4-triazoles and thiazolidinones from fatty acids", J. Ind. Chem. Vol 48B:97-102

- (2009).
4. Nadia Adil Salih "Synthesis and characterization of Novel Azol Hetrocycles Based on 2,5 Di substituted Thiadazole" Turk.J.chem. Vol.132:229-235(2008)
 5. Abd yl Jabar ,Kh. "Synthesis and Autibacterial Activities of New Metronidazole and Imidazole Derivatives" Molecules.14:2431-2446(2009).
 6. Pradip,D and Berad , B.N. "Synthesis characterization and antimicrobial study of substituted bis -[1,3,4]-oxadiazole,bis-[1,3,4]thiadiezol and bis-[1,2,4]-triazol derivatives" J.Indin chem. Soc.85:1153-1158(2008)
 7. A.Hussain,K.Sharba,R.H.Al-Bayati,M.Aouad and N.Rezki, "Synthesis of Oxadiazoles, Thiadiazoles and Triazoles Dervied from Benzo[b] thiophene" Molecules , 10:116-1168(2005).
 8. Maymona M.Kandeel,Mohaded S.Abbady "Some Reactions of 3-Methyl-5-oxo-1-phenylpyrazoline-4-thio-carbohydrazid" Bull.Korean chem.Soc 23(1):41-47(2002).
 9. phillip Crews,J.R. and Jaspars, organic structure Analysis 2nd ed oxford ,University press , Inc . New york p.552(1998)
 10. Harish RAJAK,MurliDhar KHARUA, and Pradeep MISHRA, The Pharmaceutical Society of Japan . 127(10):1757-1767(2007).

Synthesis of Dithiocarbamate Derivatives of ((nitrophenyl) diazenyl)-1, 3, 4 thiadiazole as Possible Anticancer Agent

Azhar Mahdi Jasim, Tagreed N. A., and Mohammed Hassan Mohammed
Department of Pharmaceutical Chemistry, College of Pharmacy - University of Baghdad
e-mail: dr.mhassan 666666 @Yahoo. Com.

Received 5/9/2010 – Accepted 14/11/2010

الخلاصة

إن الخاصية الفسلجية للانسجة والخلايا السرطانية هي الميل لتجميع تراكيز عالية لمواد معينة مثل النحاس. أن الدور الاساسي للنحاس في الخلايا السرطانية غير واضح ولكن المثبت علميا ان النحاس ضروري لتكوين الأوردة الدموية الجديدة. تشير التقارير الحديثة الى ان المركبات اعضوية الحاوية على النحاس تشكل نوع جديد من مثبطات البروتيسوم وتؤدي الى الموت المبرمج للخلايا السرطانية. تم في هذه الدراسة تصميم ونخليق ثلاث مركبات جديدة هي المركبات 4، 6 و 7 لأستهداف الخلايا السرطانية التي تتميز بمحتوى عالي من النحاس ولقد تم تخليق هذه المركبات باتباع طريقة التفاعل متعدد الخطوات و تم متابعة جميع التفاعلات والتأكد من نقاوتها بواسطة كروماتوغرافيا الطبقة الرقيقة، كذلك تم متابعة المركبات الوسيطة والنهائية والتأكد من تخليقها من خلال قياس درجات الانصهار والتحليل الطيفي للأشعة تحت الحمراء.

ABSTRACT

A physiological feature of many tumor tissues and cells is the tendency to accumulate high concentrations of certain substances, such as copper . While the precise role of copper in tumors is cryptic, copper is required for angiogenesis. Recently reported that organic copper-containing compounds comprise a novel class of proteasome inhibitors and tumor cell apoptosis inducers. In the current study three compounds (IV),(VI) and(VII) designed and synthesized to selectively targeted the cancer cell characterized by elevated level of copper. The generation of the target compounds(IV),(VI) and(VII) were accomplished following multi step reaction procedures. The reaction and purity of the products were checked by TLC, the structure of the final compounds and their intermediates were confirmed by their melting points (uncorrected), infra red spectroscopy.

Key words: Dithiocarbamate, 1,3,4-Thiadiazole, Anticancer

INTRODUCTION

Copper is an essential trace metal for animals. The amount of copper in an organism is tightly regulated (1). Copper plays an important role in conserved processes, such as respiration, and highly specialized processes such as angiogenesis, a process critical for tumor growth, required copper as an essential cofactor (2,3). High level of copper have been found in many types of cancers, including prostate, breast, lung and brain(4). The ubiquitin-proteasome pathway is essential for many process, including the cell cycle, apoptosis, angiogenesis and differentiation (5,6). Pyrrolidine dithiocarbamate and other dithiocarbamate derivatives (Fig. 1) are a class of metal chelating compounds and it's have ability to induce apoptosis in conjunction with copper in different types of cancer cells by inhibiting proteasomal

chymotrypsin-like activity (7,8,9). Recently it was reported that 1,3,4-thiadiazoles possess variety biological activities like antibacterial, antifungal, antiviral and anticancer(10). 1,3,4-thiadiazoles exhibit wide spectrum of biological activities, possibly due to presence of toxophoric N-C-S moiety(11). Additionally 1,3,4-thiadiazoles moiety act as "hydrogen binding domain" and two-electron donor system(12). New series of 1,3,4-thiadiazoles derivatives(Fig.1), were synthesized and showed good anticancer activities against Hella cell lines(13). These finding present a strategy for design and synthesis three derivatives to targeted the cancer cell characterized by elevated level of copper.

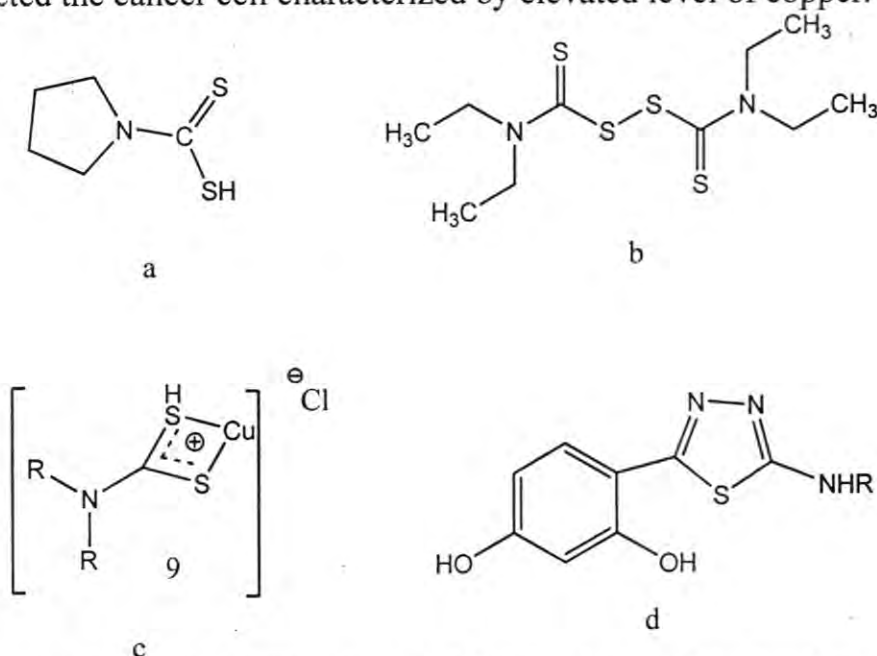


Figure-1: a-Pyrrolidine dithiocarbamate, b-dithiocarbamate derivative (disulferam), c-dithiocarbamate-copper complex, d-1,3,4-thiadiazoles derivatives.

MATERIALS AND METHODS

Thiosemicabazide, cysteine and sodium nitrite were purchased from Fluka (Germany); p-Nitro aniline was purchased from Fisons(England); carbene disulfide was purchased from Riedel-Dehen (Germany); 1-bromo butane and triethylamine were purchased from Hopkins and Williams (England); N-bromosuccinamide was purchased from Aldrich (Germany). All chemicals and reagents grade and obtained from standard commercial sources.

Melting points were measured on Thomas Hoover Electronic melting point apparatus; and were uncorrected; Infra red spectra were recorded as KBr disc on FT-IR Spectrophotometer.

Synthesis of 2-amino-5-mercapto-1,3,4-thiadiazole. Compound (I):

Thiosemicabazide(4g, 0.043 mol) was suspended in absolute ethanol(30ml), anhydrous sodium carbonate (2.23g, 0.021 mol) and

carbon disulfide(9.5g,0.0125 mol) were then added with stirring and the reaction mixture was refluxed for 5h. The reaction mixture was then allowed to cool to room temperature and filter. The filtrate was evaporated under vacuum then distilled water (90 ml) was added acidifying with concentrated hydrochloric acid gave greenish- yellow precipitate ,filtering and washing with distilled water and recrystallization from hot water gave(2-amino-5-mercapto-1,3,4-thiadiazole) (14). The physical properties ,melting point and percent yield were summarized in table(1) while IR Spectra were summarized in table(2).

Synthesis of 2-amino-5-(butylthio)-1,3,4-thiadiazole. Compound(II):

Dissolve compound (I) (0.76g, 0.0053mol) in (20ml) ethanol. Solution of sodium hydroxide (0.21g, 0.0053 mol) in a little volume of distilled water was added. The reaction mixture was refluxed for 15 min. 1- Bromobutane (0.73g,0.0053mol)was added gradually and the reaction mixture was refluxed for additional 4h. The solvent was evaporated to dryness under vacuum and the precipitate was extracted by a mixture of distilled water(50ml) and ethyl acetate(100ml),filtering and evaporating the solvent and recrystallized from methanol then wash the product with dichloromethane gave (2-amino-5-(butylthio)-1,3,4-thiadiazole) (15) .The physical properties, melting point and percent yield were summarized in table(1) while IR Spectra were summarized in table(2).

Synthesis of 2-(((5-(butylthio)-1,3,4-thiadiazol-2-yl) diazenyl)-4-nitroaniline. Compound (III):

Compound (II)(2.84g,0.015mol) was dissolved in a solution of concentrated hydrochloric acid (30ml) and distilled water (30ml) ,and the mixture cooled to 0°C. Cold sodium nitrite solution 20% (6ml) was added drop by drop with continuous stirring and cooling .P-nitro aniline (2.07g,0.015 mol)was dissolved in hydrochloric acid 30%(30ml), and the mixture cooled to 0°C,then was added to first solution drop by drop with continuous stirring and cooling. Set aside at same temperature for 2h ,filter, wash the precipitate with cold distilled water and recrystallized from ethanol to give compound (III) (16) .The physical properties, melting point and percent yield were summarized in table(1) while IR Spectra were summarized in table(2).

Synthesis of S-(2-(((5-(butylthio)-1,3,4-thiadiazol-2-yl) diazenyl) -4-nitrophenyl carbamothioyl)-N,N,N-triethylthiohydroxyl ammonium .Compound (IV):

A mixture of compound (III) (1.125g,0.0037 mol) ,triethylamine (0.374g,0.0037 mol)and carbon disulfide(0.281g, 0.0037 mol) in ethyl

acetate was refluxed at 60°C for 3h. The resulted solution was evaporated to dryness under vacuum, diluted with absolute ethanol and then filtered over anhydrous magnesium sulfate. A precipitate was formed by addition of cold diethylether. The precipitate was filtered, washed with cold diethylether and recrystallized from ethanol- diethylether to give compound (IV) (17). The physical properties, melting point and percent yield were summarized in table (1) while IR Spectra were summarized in table (2).

Synthesis of potassium- 2-amino-3-(2,5-dioxopyrrolidine-thio) propanoate. Compound (V):

A solution of potassium hydroxide (2.25g, 0.04 mol) in absolute ethanol (10ml) was added to a solution of cysteine (2.44g, 0.02 mol) in absolute ethanol (50 ml). The result precipitate was filtered, dried and suspended in dichloromethane (40ml), cooled to 0°C. Then similarly cooled suspension of N-bromosuccinimide (3.58g, 0.02 mol) in dichloromethane (20ml) was added. After stirring at 0°C for 10min, the suspension was stirred for additional 2h at room temperature. The insoluble material was then filtered to give potassium bromide, and the filtrate was evaporated to dryness under vacuum, the residue was recrystallized from ethanol-distilled water to give light brown powder of compound (V) (18). The physical properties, melting point and percent yield were summarized in table (1) while IR Spectra were summarized in table (2).

Synthesis of 2-amino-3 -((2-((5-(butylthio)-1,3,4-thiadiazol-2-yl) diazenyl) -4-nitrophenyl carbamothioyl) disulfanyl) propanoic acid. Compound (VI):

A solution of compound(IV) (1.15g, 0.0022 mol) and compound(V) (0.45g, 0.0022 mol) in N,N-dimethylformamide DMF (20 ml) was refluxed for 3h. A precipitate was obtained by acidification and addition of distilled water which is filtered and washed with diethylether to give compound (VI) (18). The physical properties, melting point and percent yield were summarized in table (1) while IR Spectra were summarized in table (2).

Synthesis of butyl-2-((5-(butylthio)-1,3,4-thiadiazol-2-yl) diazenyl) -4-nitrophenyl carbamodithioate. Compound (VII):

To a solution of compound(IV) (1.12g, 0.0022 mol) in absolute ethanol (20 ml), 1-bromobutane (0.298g, 0.0021 mol) was added gradually and the reaction mixture was refluxed for 4h. The solution was evaporated to dryness under vacuum and the precipitate was

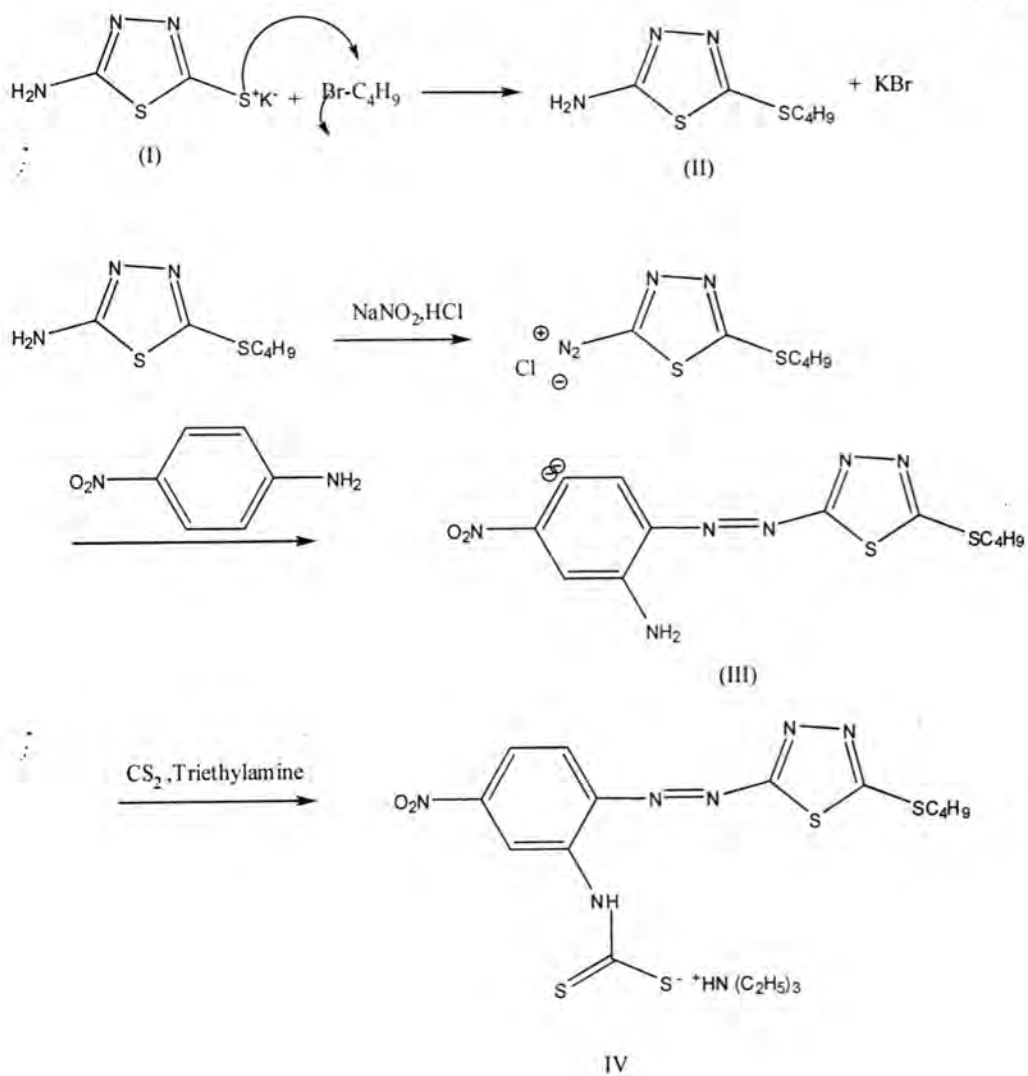
extracted by mixture of distilled water (50ml) and ethyl acetate (100ml), filter and evaporate the solvent and recrystallized from ethanol - dichloromethane, wash the product with dichloromethane to give compound (VII) (19). The physical properties, melting point and percent yield were summarized in table (1) while IR Spectra were summarized in table(2).

RESULTS AND DISCUSSION

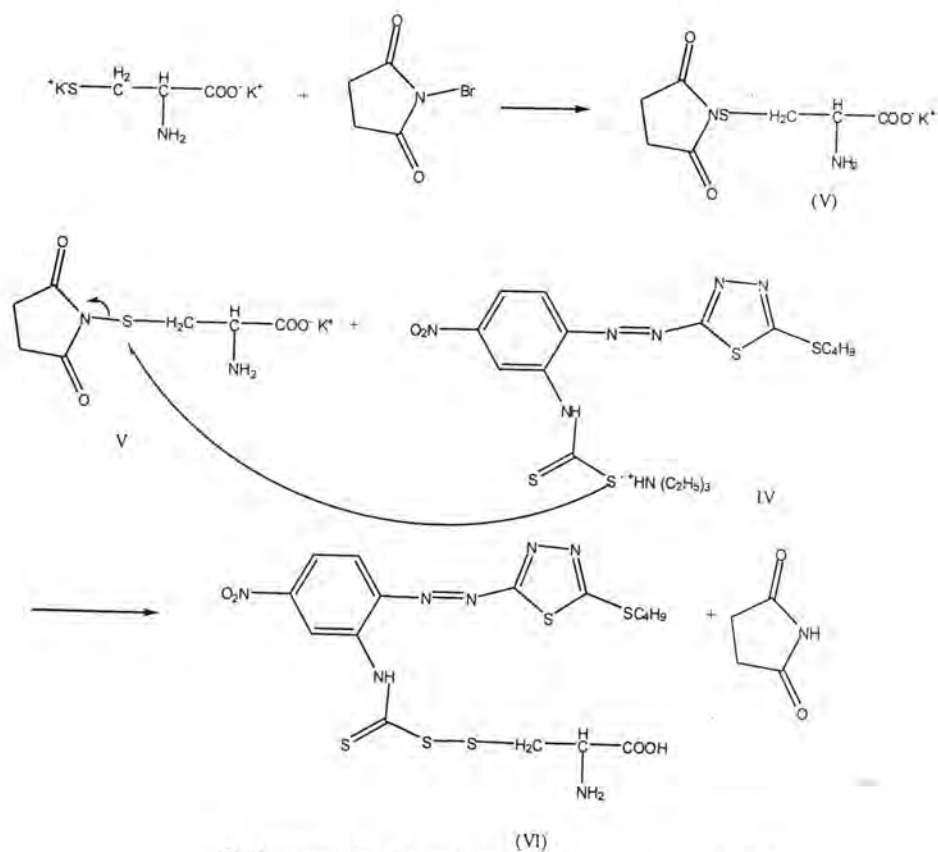
The synthetic procedures for the designed target compounds IV, VI and VII are illustrated in schemes (1),(2)and(3) respectively . Target compound (IV), was obtained from the reaction of compound (III) and carbon disulfide in the presence of triethylamine. The reaction is nucleophilic addition reaction in which the nucleophile amino group attach the electrophile carbon disulfide(17). Compound (III) obtained from the reaction of diazonium salt of compound (II) and P-nitro aniline by diazotization⁽¹⁵⁾ . The compound (VI) was synthesized from reaction of compound (IV) and compound (V). Compound (V) is a sulfenimide derivative synthesized from the reaction of potassium salt of cysteine amino acid with N-bromosuccinimide. The thiolate anion of the cysteine attacked the nitrogen of N-bromosuccinimide leading to the formation of sulfenimide with the liberation of potassium bromide. Then compound (VI) was obtained from the reaction of thiol containing compound, (compound IV) and sulfenimide derivative, (compound V). The reaction followed a nucleophilic substitution mechanism in which the thiol moiety attacked the sulfur of the sulfenimide generating the disulfide and succinimide(18,20). Compound (VII) obtain by alkylation of compound (IV) by thiol alkylation method (19). The IR spectra of the synthesized compounds and their intermediates, tables (2) showed a characteristic bands of absorption which were in consistence with the proposed structures of the compounds(21,22).

Synthesis of Dithiocarbamate Derivatives of ((nitrophenyl) diazenyl)-1, 3, 4 thiadiazole as Possible Anticancer Agent

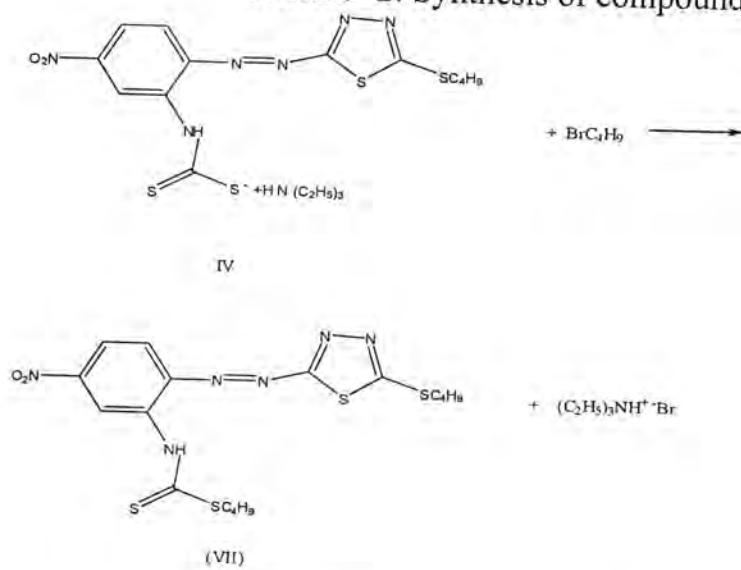
Azhar



Scheme -1: Synthesis of compound (IV).



Scheme -2: Synthesis of compound (VI).



Scheme-3: Synthesis of compound (VII).

Table-1: The physical properties ,melting point and percent yield of the synthesized compounds.

compou nd	molecular formula	molecular weight	recrystilliztion solvent	percent yield	color	melting point
(I)	C ₂ H ₃ N ₃ S ₂	133	Hot D.W.	85	Greenish-yellow	227
(II)	C ₆ H ₁₁ N ₃ S ₂	282	Ethanol	55	orange	120-122
(III)	C ₁₂ H ₁₄ N ₆ O 2S ₂	338	Methanol- dichlromethane		Orange-yellow	178-180
(IV)	C ₁₉ H ₂₉ N ₇ O 2S ₄	514	Ethanol-diethyl ether	60	Light brown	190-192
(V)	C ₇ H ₉ N ₂ O ₄ S	204	Ethanol-D.W.	60	Light brown	122-126
(VI)	C ₁₆ H ₁₉ N ₇ O 4S ₅	533	diethyl ether	75	Red brown	70-72
(VII)	C ₁₇ H ₂₂ N ₆ O 2S ₄	470	Ethanol- dichlromethane	75	Light brown	206-208

Table-2: The IR absorption bands of compounds (I, II, III, IV, V, VI and VII).

compound	Bands (cm ⁻¹)	characterization
Compound (I)	3394 and 3274 2550 and 670 1630	asym. and sym. st.vib. of NH ₂ st.vib. of SH and C-S st.vib. of C=N
Compound (II)	3390 and 3275 670 2995 , 2925 and 2875	asym. and sym. st.vib. of NH ₂ st.vib. of C-S st.vib. of CH ₂ and CH ₃
Compound (III)	3255 and 3248 1579 1545 and 1340	asym. and sym. st.vib. of NH ₂ st.vib. of N=N st.vib. of nitro
Compound (IV)	1570 1540 and 1330 1470, 1300 and 1170	st.vib. of N=N asym. and sym st.vib. of nitro st.vib. of C=S of dithiocarbamate
Compound (V)	3490 and 3360 1771 and 1693 1550 and 1411	asym. and sym. st.vib. of NH ₂ str.vib. of C=O of five member cyclic imide asym. and sym st.vib. of carboxylate ion.
Compound (VI)	3450 and 3410 3000-2500 1703 1570 1500 and 1360 1470, 1300 and 1170	asym. and sym. st.vib. of NH ₂ st.vib. of carboxyl str.vib. of C=O st.vib. of N=N asym. and sym st.vib. of nitro st.vib. of C=S of dithiocarbamate
Compound (VII)	1570 1540 and 1330 1470, 1300 and 1170	st.vib. of N=N asym. and sym st.vib. of nitro st.vib. of C=S of dithiocarbamate

REFERENCES

1. Labbe S, Thiele DJ: Pipes and wiring: the regulation of copper uptake and distribution in yeast. *Trends Microbiol*, 7:500-505 (1999).
2. Eatok M.M., Schatzlein A., Kaye S. B., Tumor vasculature as a target for anticancer therapy. *Cancer. Oncology*, 46:230-234 (2000)
3. Fox, S. B. Gasparini G., Harris A. L. Angiogenesis: pathological, prognostic, and growth-factor pathways and their link to trial design and anticancer drugs. *Lancet Oncol.*, 2:278-289 (2001),.
4. Chen, D., Peng F., Cui, Q. C., Daniel K. G., Orlu S., Liu J., and Dou Q.P. Inhibition of prostate cancer cellular proteasome activity by a pyrrolidine dithiocarbamate copper complex is associated with suppression of proliferation and induction of apoptosis *Front Biosci*, 10:2932-2939 (2005).
5. Landis-Piwowar K. R., Milacic V., Chen D., Yang H., Zhao Y., Chan T.H., Yan B., Dou Q. P. The proteasome as a potential target for novel anticancer drugs and chemosensitizer *Drug Resist Updates*, 9:263-273 (2006).
6. Milacic V., Chen D., Giovagnini L., Diez D., Fregona D., Dou Q.P., Pyrrolidine dithiocarbamate - zinc(II) and copper (II) complexes induce apoptosis in tumor cells by inhibiting the proteasomal activity. *Toxicology and Applied Pharmacology*, 231:24-33 (2008)
7. Cen D, Brayton D, Shahandeh B, Meyskens FL Jr, and Farmer PJ: Disulfiram facilitates intracellular Cu uptake and induces apoptosis in human melanoma cells. *J Med Chem*, 47:6914-6920 (2004).
8. Daniel K.G., Chen D., Orlu S., Cui Q. C., Miller F.R., Dou Q.P., Clioquinol and Pyrrolidine dithiocarbamate complex with copper to form proteasome inhibitors and apoptosis inducer in human breast cancer cells. *Breast Cancer Res.*, 7:R897-R908 (2005).
9. Kim I., Kim C.H., Kim J.H., Lee J., Chen Z. A., Lee M. G., Chung K. C., Hsu C. Y., Ahn Y. S., Pyrrolidine dithiocarbamate and zinc inhibit proteasome-dependent proteolysis. *Exp. Cell Res.*, 298:229-238 (2004).
10. Sunil D., Isloor A. M., Shetty P., Synthesis, characterization and anticancer activity of 1,2,4-Triazolo[3,4-b]-1,3,4-thiadiazole on Hep G2 cell lines. *Der Pharma Chemica*, 1:19-26 (2009).
11. Kamotra P., Gupta A.K., Gupta R., Somal P., Singh S.: Microwave-assisted synthesis and biological activity of 3-alkyl/aryl-6-(1-chloro-3,4-dihydronaphth-2-yl)-5,6-dihydro-s-triazolo[3,4-b][1,3,4]thiadiazoles, *Indian J. Chem*, 46B: 980 (2007).

12. Siddiqui N., Ahuja P., Ahsan W., Pandeya S. N., Alam M. S., Tiadiazoles: Progress Report on Biological Activities. J.Chemical and Pharmaceutical Research, 1:19-30(2009).
13. Wei M. X., Feng L., Li X. Q., Zhou X. Z., Shao Z. H.: Synthesis of New Chiral 2,5-Disubstituted 1,3,4-Thiadiazoles Possessing γ -Butenolide Moiety and Preliminary Evaluation of in vitro Anticancer Activity, Eur. J. Med. Chem., 44:2776-2781(2009).
14. Petrow V., Stephenson O., Thomas A. J., Wild A. M.: Preparation and hydrolysis of some derivatives of 1 : 3 : 4-thiadiazole , J.Chem. Soc.1508(1958).
15. Hiba M.A.Al-Bader:Study and synthesis of new 2-amino-5-thiol-1,3,4-thiadiazole derivatives, MSc, Thesis, Baghdad University /college of science for women(2007).
16. Vogel A.: Text book of practical organic chemistry (5th Ed.). Langman, New York. (1989); pp. 946.
17. Pedro Ortega-Luoni, Leonel Vera, Claudio Astudillo, Miguel Guzman and Pedro Ortega-Lopez: Synthesis of metallic azoderivatives of 2-amino-5-mercapto-1,3,4-thiadiazole, J. Chil. Chem. Soc., 52(1):1120-1122 (2007).
18. Boustany, K.A. and Sulliran, A.B.: Sulfinimides. A useful sulfur-transfer agent. *Tetrah. Lett.*; 3547(1970).
19. Rajesh Sharma, Jitendra Sainy and Subhash Chandra Chaturvedi: 2-Amino-5-sulfanyl-1,3,4-thiadiazoles: A new series of selective cyclooxygenase-2 inhibitors, *Acta Pharm.* 58:317-326(2008).
20. Harpp, D.N. and back, T.G.: Disulfide from mercaptan and sulfenimides. *J. Org. Chem.*; 36: 3828(1971).
21. Silverstin, R.M.; Bassler, G.C. and Morrill, T.C.: Spectrometric identification of organic compounds (4th ed.). John Wiley and Sons, New York, (1981)
22. Nakanishi K., Solomon P. H., Infrared Absorption Spectroscopy (2nd ed). Holden-Day, INC., San Francisco, (1977).

Synthesis of New 3-(Pyrimidin-2-Yl Amino) Propane Hydrazide Derivatives

Nisreen K. Abood

Department of Chemistry, College of Science, Al-Mustansiriyah University

Received 13/2/2011 – Accepted 2/3/2011

الخلاصة

أن تكاتف 2-امينو بريميدين مع مثيل اكريليت بوجود حامض الخليك اعطى المركب مثيل 3-(بريميدين -2-يل امينو) بروبانويت. تفاعل المركب (1) مع الهيدرازين المائي ينتج مشتق بروبان هيدرازيد (2). معاملة المشتق (2) مع ماللك انهايدير، فثالك انهايدير، سكسنيك انهايدير اعطى مشتقات جديدة من البيردايزين (3-5) ومعاملة المشتق (2) مع استايل اسيتون، اثيل اسيتو استيت واثيل سيانو استيت يعطي مشتقات جديدة من البيرازول (6-8). معاملة المشتق (2) مع الالديهيدات والكيونوات الاروماتية المختلفة يعطي مشتقات جديدة من قواعد شف (9-13) وان معاملة قواعد شف مع ماللك انهايدير بوجود البنزين الجاف سوف يعطي مشتقات جديدة من الاوكسازيبين (14-18) وشخصت هذه النواتج بالاعتماد على بعض الخواص الطيفية ¹HNMR, IR, UV

ABSTRACT

Condensation of 2-aminopyrimidin with methyl acrylate in acetic acid gave methyl 3-(pyrimidin -2-yl amino) propanoate compound (1). Reaction of compound (1) with hydrazine hydrate resulted propanoyl hydrazide derivatives (2). Treatment of (2) with malic anhydride, phthalic anhydride, succinic anhydride afforded pyridazine derivatives (3-5) and then with acetylacetone, ethylacetoacetate, ethylcyanoacetate afforded a new derivatives pyrazole compound (6-8). Compound (2) react with different aldehydes or ketones gave new Schiff's bases derivatives (9-13). Schiff's bases converted into heterocyclic compound by react with malic anhydride in dry benzene to gave oxazepine (14-18). The identification of isolated and purified compounds were elucidated by ¹HNMR, IR, UV.

INTRODUCTION

Hydrazide derivatives have been frequently found in heterocyclic chemistry as key intermediates for synthesis of hetero cyclic compound and they have been reported to exhibit biological activity [1]. Pyridazine derivatives have been reported to possess antimicrobial and potent analgesic [2], pyrazole derivatives are associated with antibacterial antiviral [3], ant diabetic and bactericidal [4] activities. Oxazepine derivatives have some important biological and anti-inflammatory effect [5] such as on the central nervous system as enzyme inhibitors [6], analgesic [5] and antidepressant [7,8].

MATERIALS AND METHODS

Melting point were determined in open capillary tubes on Gallen kamp melting point apparatus are uncorrected. The IR spectra KBr disc were recorded with Shimadzu -2N, FTIR-8400 S. UV spectra were recorded on Varian. UV-Vis spectrophotometer using absolute ethanol as solvent, ¹HNMR spectra were determined at Bruker 300 MHZ spectrometer using DMSO as solvent.

Synthesis of methyl 3-(pyrimidin-2-yl amino)propanoate [9](1).

2- amino pyrimidin (0.05 mole, 4.75 g) with (0.05 mole, 4.3 g) from methyl acrylate in 10 ml of acetic acid was refluxed on steam bath for 15 hrs., then it poured with stirring into crushed ice . The solid precipitate was filtrated washed with cold water dried and recrystallized from ethanol table (1) .

Synthesis of 3-(pyrimidin-2-ylamino)propanehydrazide[3,10](2).

To a solution of methyl 3-(pyrimidin -2-yl amino) propanoate[1] (0.01 mole, 1.8 g) in absolute ethanol 50 ml, hydrazine hydrate (0.01mole) was added and the reaction mixture was refluxed 6 hrs. On cooling, the precipitate formed was filtered off and recrystallized from ethanol table (1) .

Synthesis of 1-[3- (pyrimidin-2-ylamino)propanoyl]-Aryl hydropyridazine -3,6-dione[11](3,4).

A mixture from different anhydride compounds (0.001 mole) (malic anhydride ,succinic anhydride) respectively dissolve in 30 ml of acetic acid with (0.001 mole, 0.18 g) from compound [2] the mixture was refluxed for 7 hrs., then poured into ice water filtered the precipitate and recrystallized from petroleum ether and acetic acid (1:1) table (1) .

Synthesis of 2-[3-(pyrimidin-2-ylamino)propanoyl]-2dihydro phthalazine -1,4-dion[11] (5).

A mixture from phthalic anhydride (0.001 mole, 0.15 g) with 30 ml of acetic acid, (0.001 mole, 0.18 g) from hydrazide [2] the mixture was refluxed for 7 hrs. Then proud into ice water filtered and recrystallized from petroleum ether and acetic acid(1:1) table (1) .

Synthesis of pyrazole derivatives(General procedure) [2,12] (6,7,8).

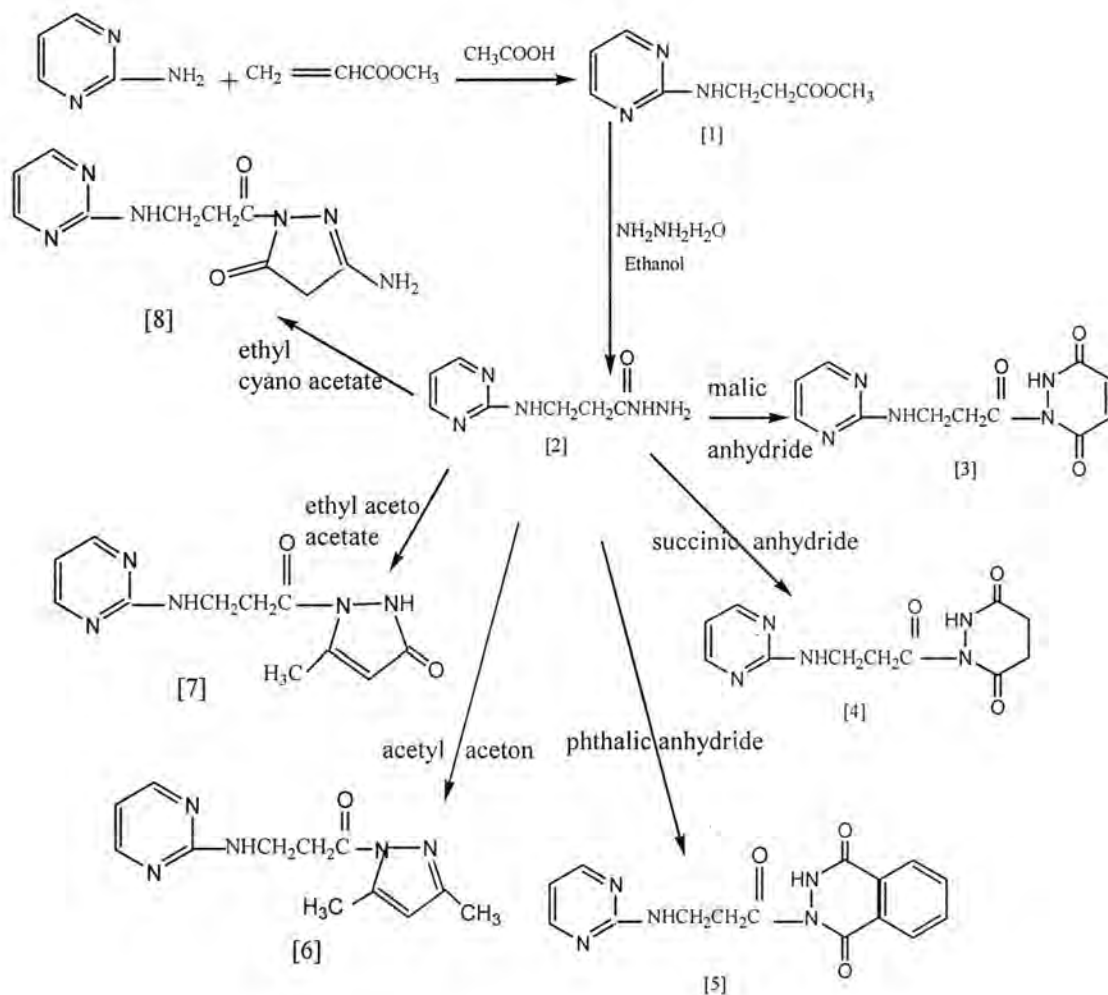
To a mixture of (0.001 mole, 0.181 g) from hydrazide compound[2] with (0.001 mole) acetyl acetone, ethylaceto acetate and ethyl cyano acetate with 0.1ml acetic acid in 30 ml absoulut ethanol ,the mixture was refluxed 7 hrs. Then cooled the precipitate and filtered off ,recrystallized by ethanol table (1) .

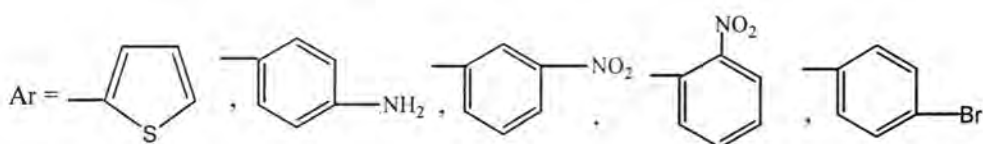
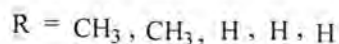
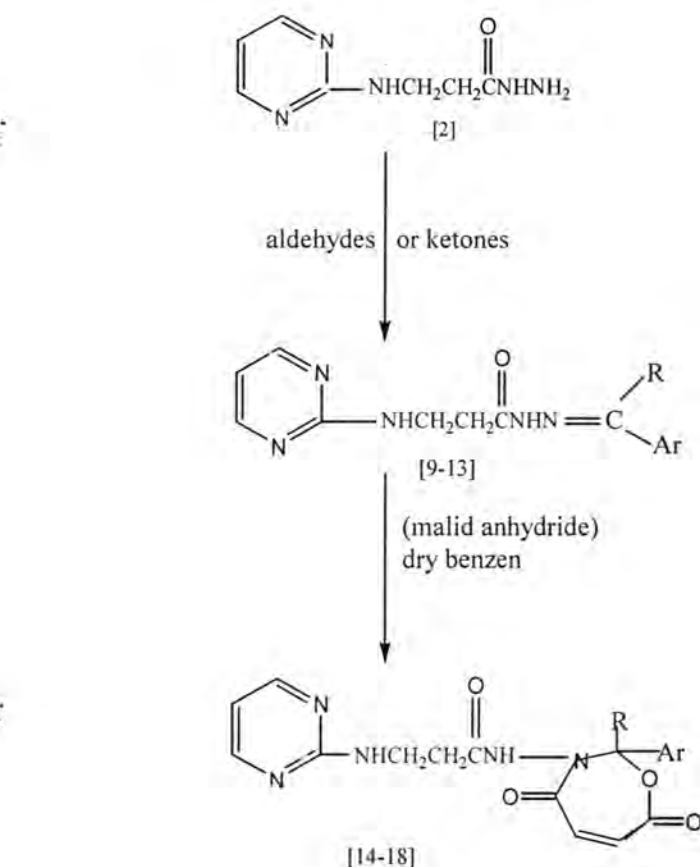
Synthesis of Schiff bases (General procedure) [13,14] (9-13).

To a stirring solution of compound [2] (0.01 mole, 1.8 g) in absolute ethanol (15 ml) , appropriate aldehydes or ketones (0.01 mole) was added , the mixture was refluxed for 6 hrs. and cooled to room temperature. precipitate was filtered and recrystallized from ethanol table (1) .

Synthesis of oxazepin (General procedure) [15](14-18).

To a mixture of (0.01 mole) Schiff bases with (0.01 mole, 0.98 g) malic anhydride in 20 ml dry benzene, the mixture was refluxed in steam bath at 70 C⁰(2 hrs.), removed the excess of solvent then cooled the precipitated and filtrated off ,recrystallized by different solvent table (1) .

**Scheme 1**



Scheme 2

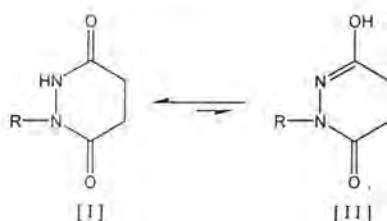
RESULTS AND DISCUSSION

The new derivatives of pyridazin, pyrazole, Schiff's bases and oxazipine were prepared following the reaction sequences outlined in scheme I and scheme II.

Compound [1] prepared by the reaction of 2-amino pyrimidine with methyl acrylate in acetic acid to give the methyl 3-(pyrimidin -2-yl amino) propanoate. The IR spectra have been studied and were in agreement with the required structure. IR. (cm⁻¹) of compound [1] show of several bands (3352 cm⁻¹), (1737 cm⁻¹) stretching band of (NH) and

C=O of ester respectively ,UV. Spectra of mostly showed intense maxima at (248,210 nm) , (394,305 nm) which belonged to $\pi \rightarrow \pi^*$ and $n \rightarrow \pi^*$ transition respectively (table 2). Treatment of compound [1] with hydrazine hydrate in absolute ethanol gave the key intermediate hydrazide compound [2].The IR. Spectra show decrease frequency of carbonyl group at (1737 cm^{-1}) to (1645 cm^{-1}) and appearance band at (3369 cm^{-1}) stretching band of NH. UV. Spectra of mostly showed intense maxima at (241,209 nm), (338 nm) due to $\pi \rightarrow \pi^*$ and $n \rightarrow \pi^*$ transition respectively (table 2). The ^1H NMR ($\text{DMSO-}d_6$) of compound [2] : 6.5(d, 3H , CH aromatic), 8.5 (s , 1H,NH) , 3.4 , 2.5 (2t , 2(2H), CH_2CH_2) , 5.3 (s ,2H,NH₂).

Pyridazine derivatives have been synthesis by treatment of propane hydrazide[2] with (malic anhydride, succinic anhydride and phthalic anhydride) in acetic acid giving the derivatives of pyridazine compounds [3,4,5].The IR. Spectra presence appearance the band of (O-H), at ($3504\text{-}3464\text{ cm}^{-1}$) and (NH) stretching vibrations bands appearance at ($3369\text{-}3213\text{ cm}^{-1}$). Pyridazine ring appearance at band ($1745\text{-}1707\text{ cm}^{-1}$) , and the band ($1674\text{-}1640\text{ cm}^{-1}$) was due to the $\text{V}(\text{C}=\text{O})$ of amide this value appear to be lower than expected due to the hydrogen bond between it and (N-H) group of pyridazine ring. From the above mentioned results we can say that the compound [3,4and 5] can be exist in two tautomeric forms; keto [I] and enol [II] forms



UV. Spectra of mostly showed intense maxima at (244-209 nm) , (348-338 nm) which belonged to $\pi \rightarrow \pi^*$ and $n \rightarrow \pi^*$ transition respectively show the table 2. The ^1H NMR($\text{DMSO-}d_6$) of compound [3]: 6.2 (d , 3H, aromatic proton), 8.2(s,1H,NH), 3.4, 2.6 (2t, 2(2H), CH_2CH_2), 10.1(s,1H, NH pyridazin), 6.8,7.2 (2d,2(1H), $\text{CH}=\text{CH}$).

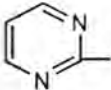
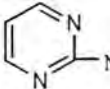
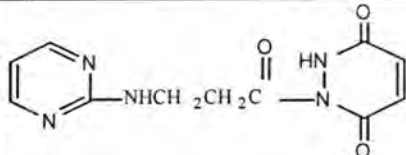
Condensation of compound [2] with (acetyl acetone, ethyl aceto acetate and ethyl cyano acetate) in absolute ethanol in catalytic amount acetic acid gave the derivatives of pyrazoles compounds [6,7,8]. The IR. Spectra presence the band at ($1763\text{-}1701\text{ cm}^{-1}$) and ($1660\text{-}1626\text{ cm}^{-1}$) ($\text{C}=\text{O}$) moiety of pyrazole ring . UV. Spectra of mostly showed intense maxima at (276-209nm),(338nm) which belonged to $\pi \rightarrow \pi^*$ and $n \rightarrow \pi^*$ transition respectively (table 2). ^1H NMR ($\text{DMSO-}d_6$) of compound [6] :

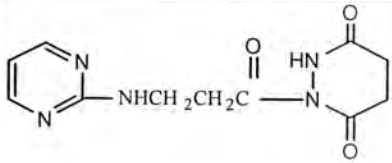
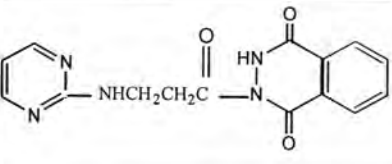
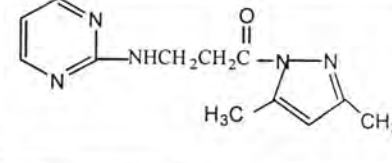
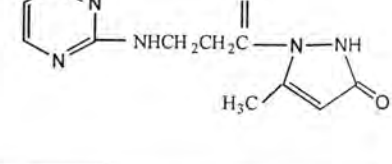
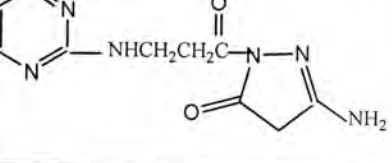
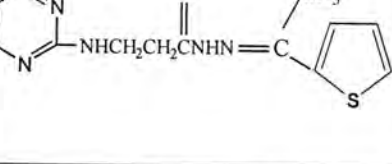
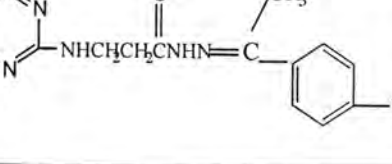
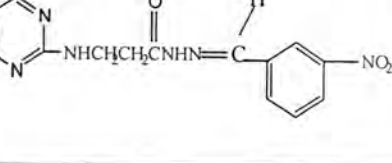
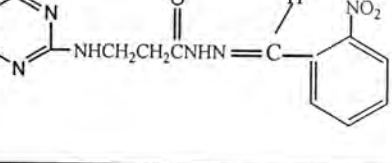
3.9 (d,3H, aromatic proton), 9.1(s,1H,NH), 3.6,4.2 (2t,2(2H), CH₂CH₂), 2.7,2.5 (2s, 2(3H), CH₃).

Condensation of compound [2] with aryl aldehydes and ketones in absolute ethanol gave the Schiff's bases compounds [9,10,11,12,13] the formation of these compound indicated by the presence in their IR. Spectra of azomethine (CH=N) stretching bands at (1624-1604 cm⁻¹). UV. Spectra of mostly showed intense maxima at (243-206 nm), (473,390-316nm) which belonged to $\pi \rightarrow \pi^*$ and $n \rightarrow \pi^*$ transition respectively (table 2). ¹H NMR (DMSO-d₆) of compound [13] : 6.5 (m, 7H, aromatic proton), 8.4(s, 1H,NH), 3.4,2.4 (2t,2(2H),CH₂CH₂) , 6.7 (s, 1H,HC=N).

Treatment of Schiff's bases with malic anhydride in dry benzene gave the derivatives compounds [14,15,16,17,18]. The IR. Spectra show the disappearance of absorption band of (CH=N) in the region (1624 cm⁻¹), combined with the appearance of absorption band at (1759-1707 cm⁻¹) of moiety of oxazepin ring and (1699-1641 cm⁻¹) carbonyl group of amide . UV. Spectra of mostly showed intense maxima at (296-204 nm) , (339-325nm) which belonged to $\pi \rightarrow \pi^*$ and $n \rightarrow \pi^*$ transition (table 2). ¹H NMR (DMSO-d₆) of compound [18] : 7.5(m, 7H, aromatic proton), 8.2(s,1H, NH), 3.8,2.6(2t,2(2H), CH₂CH₂), 6.2(s, 1H, HC=CH).

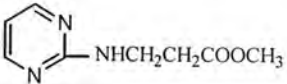
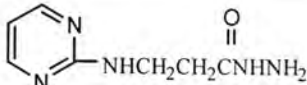
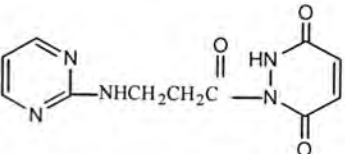
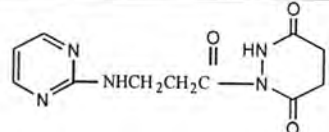
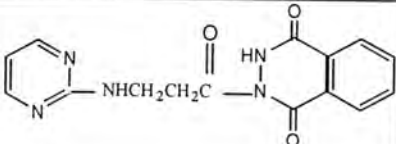
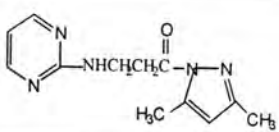
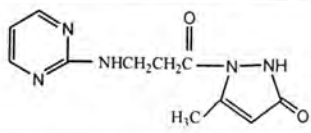
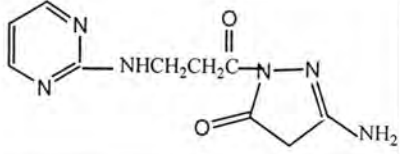
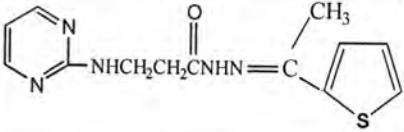
Table -1: physical properties

NO.	Compound	Yield %	Mp. C ⁰	Recrystallization	Molecular formula	M.Wt g mole ⁻¹
1.		70 %	120-122	Ethanol	C ₈ H ₁₁ N ₃ O ₂	181
2.		70%	138-140	Ethanol	C ₇ H ₁₁ N ₅ O	181
3.		65%	182-184	Petroleum ether	C ₁₁ H ₁₁ N ₅ O ₃	261

4.		65%	190-192	Petroleum ether	$C_{11}H_{13}N_5O$ ₃	263
5.		70%	198-200	Acetic acid	$C_{11}H_{13}N_5O$ ₃	311
6.		70%	204-206	Ethanol	$C_{12}H_{15}N_5O$	245
7.		65%	155-157	Ethanol	$C_{11}H_{13}N_5O$ ₂	247
8.		65%	199-201	Ethanol	$C_{10}H_{12}N_6O$ ₂	248
9.		75%	190-192	1:1 Ethanol +H ₂ O	$C_{13}H_{15}N_5O$ _S	289
10.		70%	156-158	1:1 Ethanol +H ₂ O	$C_{15}H_{18}N_6O$	298
11.		75%	167-169	1:1 Ethanol +H ₂ O	$C_{14}H_{14}N_6O$ ₃	348
12.		65%	162-164	1:1 Ethanol +H ₂ O	$C_{14}H_{14}N_6O$ ₃	348

13.		60%	171-173	Ethanol	$C_{14}H_{14}N_5BrO$	303
14.		65%	188-190	Benzene	$C_{17}H_{17}N_5O_4S$	387
15.		60%	230-232	Benzene	$C_{19}H_{20}N_6O_4$	396
16.		65%	266-286	Benzene	$C_{18}H_{16}N_6O_6$	412
17.		65%	255-257	chloroform	$C_{18}H_{16}N_6O_6$	412
18.		65%	228-230	Chloroform	$C_{18}H_{16}N_5O_4Br$	366

Table-2: Spectral data

NO	Compound	UV λ_{\max} nm	I.R (KBr) cm^{-1}						Others cm^{-1}
			$\text{V}(\text{CH})$ cm^{-1} aromatic	$\text{V}(\text{CH})$ cm^{-1} aliphatic	$\text{V}(\text{C}=\text{O})$ cm^{-1}	$\text{V}(\text{C}=\text{N})$ cm^{-1}	NH cm^{-1}	C=C cm^{-1}	
1.		394 305 248 210	3061	2985 2935	1737 ester	1602	3352	1473	----- --
2.		338 241 209	3178	2999 2972	1645	1620	3369 3265	1531	----- --
3.		348 339 244 209	3101	2993 2933	1730 1720 1674	1597	3360 3302	1521	V(OH) 3504
4.		338 241 209	3030	2978 2920	1705 1660	1593	3225	1512	V (OH) 3506
5.		338 242 209	3234	2999	1745 1653	1595	3350	1521	V(OH) 3464
6.		338 241 209	3107	2920 2850	1763 1716	1608	3124	1433	----- --
7.		276 211	3107	2941 2852	1701 1626	1608	3213	1525	V(OH) 3481
8.		338 241 209	3093	2980 2920	1707 1660	1595	3225	1512	V (NH ₂) 3468
9.		338 240 204	3186	2999	1658 1647	1604	3381 3288	1529	----- --

10.		337 226 206	3030	2924 2850	1680	1624	3281	1523	V(NH ₂) 3460
11.		390 242 204	3101	2941 2883	1656	1599	3342 3257	1508	NO ₂ 1300
12.		473 316 206	3084	2910 2858	1668	1602	3335	1519	NO ₂ 1305
13.		390 348 243 204	3018	2875	1654	1618	3298	1560	C-Br 750
14.		296 224	3165	2998	1734 1678	1597	3360	1518	C-O 1178 C- N 1234
15.		338 240 204	3093	2997 2935	1759 1716 1699	1589	3381	1489	NH ₂ 3491 C- N 1224 C-O 1172
16.		339 241 204	3000	2939	1757 1691	1612	3452	1529	C-N 1224 C- O 1172 NO ₂ 1396
17.		325 205	3093	2978 2920	1707 1660	1595	3225	1512	C-N 1219 C- O 1114 NO ₂ 1396
18.		338 240 205	3101	2991 2895	1735 1676 1641	1597	3362 3304	1521	C-N 1269 C- O 1141 C-Br 750

Table -3: Chemical shifts HNMR spectra

Compound No.	Chemical shift(S) ppm.	Type of signal	No. of proton	Remarks
2	6.5	d	3H	Due to aromatic proton.
	8.5	S	1H	Due to NH proton.
	3.4,2.5	t,t	2H,2H	Due to CH ₂ CH ₂ proton
	5.3	S	2H	Due to NH ₂ proton.
3	6.2	d	3H	Due to aromatic proton.
	8.2	S	1H	Due to NH proton.
	3.4,2.6	t,t	2H,2H	Due to CH ₂ CH ₂ proton
	10.1	S	1H	Due to NH pyridazin.
	6.8,7.2	d,d	1H,1H	Due to CH=CH proton
6	6.4	d	3H	Due to aromatic proton.
	9.1	S	1H	Due to NH proton
	3.6,3.2	t,t	2H,2H	Due to CH ₂ CH ₂ proton
	2.7,2.5	S,S	3H,3H	Due to CH ₃ proton
13	6.9	m	7H	Due to aromatic proton
	8.4	S	1H	Due to NH proton
	3.4,2.4	t,t	2H,2H	Due to CH ₂ CH ₂ proton
	6.7	S	1H	Due to HC=N proton
18	7.5	m	7H	Due to aromatic proton
	8.2	S	1H	Due to NH proton
	3.8,2.6	t,t	2H,2H	Due to CH ₂ CH ₂ proton
	6.2	S	1H	Due to HC=CH proton

REFERENCES

1. Chernkh, V.P., Kabehnyi, V.J., Shapova, V.A., Poroknyah, L.A., Beletsk aka, O.V. and Savchenko, V.N., Biologically active hydrazide derivatives of succinic acid heteroamides, *khim.farm* 828(1989), C.A, 112, 55726C (1990).
2. Mohammad Asif and Anita Singh "Exploring potential synthetic methods pyridazinone". 2.(2), 1112-1128 (2010).
3. R. Kalirajan, Leela Rathore, S. Jubie, B. Cowramma, S. Gomathy, S. Sankar and K. Elango "Micro wave Assisted synthesis and Biological Evaluation of pyrazole derivatives of Benzimidazoles. *Indian J. Pharm. Educ. Res* 4 (44) (2010).
4. Nada M. Abunada, Hamdi M Hassaneen, Nadia G. Kandile and Omar A. Miqdad "Synthesis and Antimicrobial Activity of some new pyrazole , fused pyrazole [3,4-d]-pyrimidine and pyrazolo[3,4-c][1,2,4]-triazolo[1,5-c]pyrimidine derivatives .*J Molecules* 13:1501-1517 (2008).
5. Hikmet Agirbas .Sedo Sagdinc ,Fatma Kandemirli, Berat Kemal " Synthesis , infrared spectral studies and theoretical calculations of

- 4-phenyl-4-5,dihydro benzo[f][1,4].oxazipin 3(H)-one thion .Journal of Molecular structure ,892 :132-139 (2008).
6. Standridge ,R.T.U.S.Patent 4 125 538, 1978:Chem Abstr. 90, 722461(1979).
 7. VWilson L .Gaulfield,Samuel Gibson and Dqncan R. Rae "synthesis of 1-amino -1,2,3-14b tetrahydro-4H-Pyrido[1,2-d]-dibenzo [b-f] [1,4] oxazpine and related compounds . J. Chem. Soc., Pevkin trans 1:545-553 (1996).
 8. t2921, (b) cohen,V. I. ; Jin, B.; Cohem, E. I.; Zeebeg, B. R. J. Hetrocycl Chem., 35:675(1998).
 9. Manisha Vs, K. R. Alagwadi, Reyee N, M. D. Bahanushali "synthesis and antimicrobial activity of some substituted azomethine derivative India International Journal of pharma.Ressearh and Development ISSN :0774-9446 (2010).
 - 10.K. Narasimha Sarma, M. C. S Subha and K. Chowdojirao Afacial "Synthesis and antimicrobial activity of some pyrazole derivatives carrying Indole .E-Journal of chemistry, 7(3),745-750 (2010).
 - 11.B H M Mruthyunjaya sawmy and S M Basvarajaiah " synthesis and antimicrobial activity of novel ethyl -5- (ethoxy carbonyl)-4-methylthiazol-2-yl-carbamate compounds .Indian Journal of chemistry ,.48B, 1274-1278 (2009).
 - 12.M.A.EL-EL-Fellah."organic reaction ,Mechanisum,"1sted.,Benkazy ,(1997).
 - 13.Roui I.H., "synthesis and biological activity of some new Twin compounds containing heterocyclic unit, "Al-Mustansiriya .J.Sci.,19.(4) :41-52(2008).
 - 14.F. A. Hussein et. al "Synthesis of N-substituted saccharins via schiff bases " Iraq Journal of chemistry , vol.26, No. (1) :42-50 (2000).
 - 15.F.A. Hussein and Obaid H. Abid "Synthesis and characterization of 2-Aryl -3- (p-methoxy phenyl)-2,3-dihydro-1,3-oxazpine -4-7 diones via schiff bases , 27, (2) : 381-392 (2001).

Synthesis and Characterization of Some Divalent Transition Metals Complexes of Schiff Bases Derived from Salicylaldehyde Diamine Derivatives.

Tawfiq A. Al – Diwan

Department of Chemistry, College of Science, Al- Mustansiriyah University

Received 9/12/2009 – Accepted 5/10/2010

الخلاصة

تم في هذا البحث تحضير الليكاند $[N,N'$ -bis(4-بنزين آزو) سلسلديهايد] أثيلين داي أمين (H_2L) من قواعد شف رباعية التناسق والمحضر من تفاعل السلسلديهايد مع الأثيلين داي أمين، هذا الليكاند موضوع لدراسات عديدة (1). لقد تمت مفاعلة الليكاند مع الأيونات الفلززية الثنائية التكافؤ (النيكل والكوبلت والكادميوم) وقد أعطى معقدات وتم تشخيص الليكاند والمعدقات عن طريق قياس التوصيلية والإمتصاص الذري اللهيبي والتحليل الطيفية. وتم مقارنة النتائج مع نتائج معقدات نفس الأيونات الفلززية مع ليكاند آخر هو $[N,N'$ -أثيلين بس (سلسلدامين)] H_2L' ، وفي هذه الدراسة تبين طريقة التناسق الرباعي لهذا الليكاند مع الأيونات الفلززية كذلك تبين تأثير الأصرة الهيدروجينية في البنية التناسقية لهذه المعقدات.

ABSTRACT

The synthesis and characterization of tetra-dentate Schiff bases derived from salicylaldehyde and ethylenediamine have been subject for many studies (1). The present study includes synthesis Schiff bases $[N,N'$ -bis(4-benzeneazo)salicylaldehyde] ethylenediamine (H_2L) together with its complexes with Ni (II), Co (II) and Cd(II). The results has been compared with other similar ligand $[N,N'$ -ethylene bis(salicyldemimine)] H_2L' ; Which has been also prepared with similar complexes and subjected to the same study.

The study discuss the coordination mode of the ligands under investigation, where the ligands expect to behave as tetra-dentate complexes. Intra and inter-hydrogen bonding would expect to affect the coordination course.

Characterization of ligands and complexes were done by elemental analysis, molar conductivity measurements, infra-red, electronic spectra, and atomic adsorption.

INTRODUCTION

The present study aim to investigate the synthesis and reaction of H_2L and H_2L' ligands derived from the condensation of ethylenediamine with salicylaldehyde derivatives with metal (II) ions. The study revels and throws light on the coordination path of the above mentioned ligands, towards some metal ions.

Schiff bases offer many flexible series of ligands capable to bind with various metal ions to give complexes with suitable properties for theoretical and practical applications [2]. These various classes of Schiff base can be prepared by condensation of different type of amine and carbonyl compounds [3]. A large number of Schiff bases and their complexes have studied and considered due to their importance in

industry and their activity as antifungal , antibacterial , anticancer and herbicidal [4,5] .

It is well known that Nitrogen and Oxygen atoms play a role in the coordination with metals at active site of the ligands [6,7] . So this required that H_2L and H_2L' act as tetra - dentate chelating ligands, which gives complexes fairly rigid structure [8]. The presence of two nitrogen atoms and two oxygen atoms , cause the coordination to take place with one metal ion through the four coordination sites [9] , this leads to the formation of three chalets rings . The double bond attached to the nitrogen atoms contributes in enhancing the basicity of both nitrogen atoms, which leads to increase the stability of the complex formed [10,11] .

MATERIALS AND METHODS

All chemicals used are of analytical grade and have been used without further purification. Elemental analysis was carried out by (Euro-vector 3000) elemental analyzer . IR spectra were recorded on Shimadzu (FIR-8400s) and Shimadzu (FTIR-8000) spectrophotometers . UV-Visible was taken on (Cary 100) spectrometer. Atomic absorption measurements were taken by (Phoneix-986).

Preparation of H_2L :

0.05 mole of aniline was dissolved in 12 ml of concentrated hydrochloric acid and cooled with ice. Solution of sodium nitrite (prepared by dissolving 4 gm. of $NaNO_2$ in 20 ml of water) was added drop wise to the above solution with continuous stirring ; the resulting mixture was kept for one hour at $0^\circ C$ (solution No. 1).

A solution of salicylaldehyde (0.05 mole) and anhydrous sodium carbonate (18 gm.) dissolved with water (150 ml.) the solution was added drop wise to (solution No.1) , the mixture was left for 2 hours at $0^\circ C$. The resulted mixture was acidified with hydrochloric acid to precipitate 4- (Benzeneazo) salicylaldehyde as a light orange solid . The product filtered and recrystallized with ethanol.

A solution of 0.06 mole of 4- (Benzeneazo) salicylaldehyde in 30 ml ethanol added slowly to 0.03 mole ethylenediamine (98%) ; the mixture was refluxed for one hour , the precipitate washed several time using cold ethanol, then crystallized with ethanol and dry at $50^\circ C$ overnight. The yield is 70% .

Elemental Anal. Calc. for $C_{28}H_{24}N_6O_2$: C, 70.5 ; H, 5.0 ; N, 17.6 % .
Found: C, 70.7; H, 5.4; N, 17.2 % .

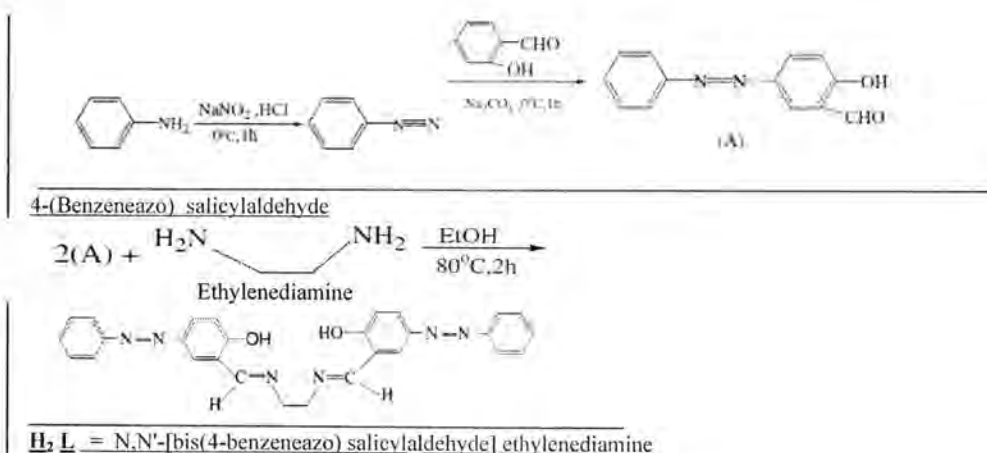


Figure-1:

Preparation of H_2L Complexes :

Ni (II) , Cd (II) and Co (II) complexes were prepared as follows :

1.0 mmole of metal (II) Chloride was dissolved in 25 ml of hot ethanol, and added to a ligand solution (1.0 mmole dissolved in 25 ml of hot ethanol) . The mixture was then refluxed for a period of one hour. The solid product was then filtered and re-crystallized with ethanol followed by drying at 50°C for overnight.

Preparation of $\text{H}_2\text{L}'$ Ligand :

The ligand $\text{H}_2\text{L}'$ was synthesized using method mentioned in literature [12] as follows:-

A solution of 2.8 mmole of salicylaldehyde in 25 ml hot ethanol (95%) added to 1.4 mmole of ethylenediamine (98%) ; the mixture solution was cooled after stirring for a few minutes . The yellow precipitate formed was filter off, re- crystallized with ethanol and dried.

Melting point is 128°C .

Elemental Ana. Calc. for $\text{C}_{16}\text{H}_{16}\text{N}_2\text{O}_2$: C, 70.8 ; H, 6.4 ; N, 11.9 % .

Found: C, 71.0 ; H, 5.9 ; N, 10.4 % .

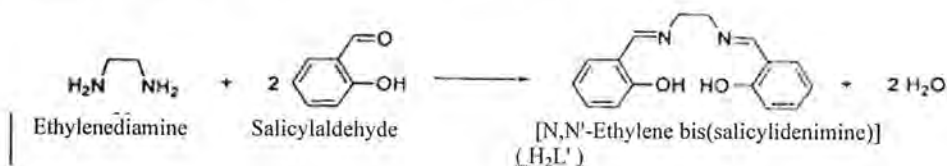


Figure-2:

Preparation of $\text{H}_2\text{L}'$ Complexes :

Ni (II) , Cd (II) and Co (II) complexes were prepared as follows :

A solution of metal (II) chloride (0.01 mole) in hot ethanol (25 ml.) was added to a solution of H_2L' (0.01 mole) dissolved in 25 ml of hot ethanol . The resulting mixture was refluxed for a period of 1 hr. the solid product was filtered and washed several times with distilled water and then re-crystallized with ethanol.

RESULTS AND DISCUSSION

The complexes are air – stable, colored, insoluble in water, and soluble in DMF. Decomposition occurs with conc. nitric acid, and con. hydrochloric acid. Measurements of molar conductivity were taken and tabulated in table - 1 - , as all measurements indicate that all complexes solution for both ligands are none electrolytes. The atomic absorption analysis for complexes of H_2L and H_2L' showed that the ratio of $L : M$ is (1 : 1) .

The infra-red spectra data for ligand H_2L and its complexes are given in table -1- . The table also includes infra-red data for the H_2L' ligand and its complexes for the sake of comparison. The spectra in the region $(3051 - 3059) \text{ cm}^{-1}$ for both of the ligands, showed the presence of hydroxyl group - OH , which suggest existing of hydrogen bonding [13] . Intra – hydrogen bonding is expected to occur in case of H_2L as in case of H_2L' due to the structural similarity of the two ligands [14]. The relative small difference in absorbance between the two ligands can be explain in term of more acidic hydrogen in case of H_2L due to the withdrawal properties of the azo group attached .

The azo group is expected not to influence the coordination through structural factor as this group is quite far away from the coordination sites ; formation of intra – hydrogen bonding in fact supports planar pattern of the ligand (Figure -3-) , inter – hydrogen bonding would also formed in both ligands .



Figure-3: Structural representation of hydrogen bonding.

The Phenolic - C – O spectra appeared at 1286 cm^{-1} and 1294 cm^{-1} for H_2L and H_2L' respectively , this reflects the higher acidity of OH group in H_2L' , which in turn affects the strength of the C- O bond . Values will be shifted towards lower frequency on coordination with metal ions, due to participation of oxygen in formation of the C - O - M bond[15].

The band appear at 1635 cm^{-1} for both H_2L and H_2L' ligands is

assigned to the C = N stretching vibration [16,17], again shifting occur on coordination as a result of Nitrogen engagement in this coordination. The ring skeletal vibration (C = C) were constant in all derivatives and unaffected by complexation as shown in table -1-.

In the low frequency region, observed in the complexes in the region (415 – 453) cm^{-1} was attributed to ν (M - O), and the region (534 -535) cm^{-1} was attributed to ν (M - N) [18], this showed that the coordination occur through phenolic Oxygen, and imino Nitrogen [19].

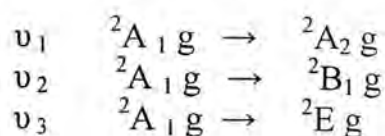
Table- 1 - IR Spectral Data of the Schiff bases and Their Complexes

Compound	ν (C=N)	ν (Phenolic C-O)	ν (M-N)	ν (M-O)	ν (C=C)	Conductivity ($\mu\text{S/cm}$)	Color
$\text{H}_2\text{L} = \text{C}_{28}\text{H}_{24}\text{N}_6\text{O}_2$	1635	1286	-----	-----	1486	-----	Orange
$\text{L} \cdot \text{Ni} = \text{C}_{28}\text{H}_{22}\text{N}_6\text{O}_2\text{Ni}$	1624	1226	535	420	1469	21.2	Reddish - Brown
$\text{L} \cdot \text{Cd} = \text{C}_{28}\text{H}_{24}\text{N}_6\text{O}_2\text{Cd}$	1606	1226	489	453	1489	16.0	Yellowish- Brown
$\text{L} \cdot \text{Co} = \text{C}_{28}\text{H}_{24}\text{N}_6\text{O}_2\text{Co}$	1610	1230	534	415	1471	21.1	Dark Brown
$\text{H}_2\text{L}' = \text{C}_{16}\text{H}_{16}\text{N}_2\text{O}_2$	1635	1294	---	-----	1498	-----	Yellow
$\text{L}' \cdot \text{Ni} = \text{C}_{16}\text{H}_{14}\text{N}_2\text{O}_2\text{Ni}$	1626	1290	540	415	1450	26.1	Reddish Brown
$\text{L}' \cdot \text{Cd} = \text{C}_{16}\text{H}_{14}\text{N}_2\text{O}_2\text{Cd}$	1633	1284	478	430	1458	23.4	Yellowish- brown
$\text{L}' \cdot \text{Co} = \text{C}_{16}\text{H}_{14}\text{N}_2\text{O}_2\text{Co}$	1600	1282	475	418	1450	22.1	Brownish Green

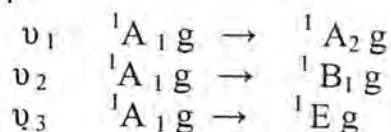
The electronic absorption spectra data is very helpful in the explanation of ligands and the metal complexes. The electronic spectra of H_2L and $\text{H}_2\text{L}'$ ligands showed strong allowed absorption originated from $\pi \rightarrow \pi^*$ and aromatic system of the benzene ring. -OH phenolic group shows $n \rightarrow \pi^*$ absorption and this absorption interferes with $\pi \rightarrow \pi^*$ absorption resulting in Batho - Chromic Shift towards the lower wave length. All the above mentioned absorption within the UV-region.

The electronic spectra of the Cadmium ion complexes showed no electronic transfer within the $d \rightarrow d$ orbital as the 3d has 10 electrons. The color for the Cd (II) complexes resulted from charge transfer, which is located between the Visible and Ultra - Violet region.

For the Co (II), it is noticed that the multicibility of the complexes is (2) due to the unpaired electrons in $3d^7$ for Co^{+2} ion. The band transitions for this complex related to the following transition:



The electronic $d - d$ transition for the Ni(II) complexes located at the visible area of the spectrum and this due to the following absorption :



Also , noted that the meltisibility for the Ni(II) complexes is (1) , which is related to the electronic configuration $3d^8$ for Ni^{+2} ion .from the above consideration can be concluded that the Ni(II) complexes is square planer[20].

The spectral and physical data for the ligands H_2L and H_2L' and their complexes , assumed that the metal ions are bonded to the ligands via phenolic oxygen and the imino nitrogen as illustrated in figure -4-. The coordination process forced the structure of the complexes to be shaped in style where to accommodate the metal ion complexes in order to satisfy the required coordination number. Producing a square planer structure [20]. This has been attributed to $d -$ orbital participation for the Co(II) and Ni(II) ions which bonded to nitrogen and oxygen atoms of the ligands to give stable complexes . In case of Cd(II) complexes show tetrahedral geometry to give stable coordination bonds with nitrogen and oxygen atoms of H_2L and H_2L' ligands.

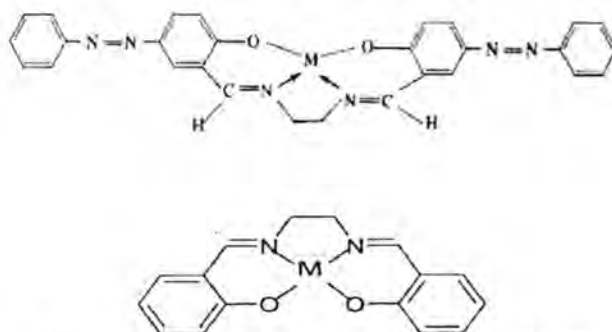


Figure -4:Structural of the Schiff base complexes

REFERENCES

1. a- Calvin M. Bailes R. H. and Wilmoth W. K. The Oxygen - Carrying Synthetic Chelate Compounds; J. Am. Chem. Soc. 68, 2254, (1946).
b- Martell A.E. and Calvin M. Chemistry of the Metal Chelate Compounds. Page 336-357, Prentice - Hall , New York . (1952).
2. A. E. Martell and M. Calvin "Chemistry of Metal Chelate Compounds " Prentice - Hall, New York, N.Y.,. Chapter 7 and 8,(1952).

3. Coleman W. M. , Gochring R. R. , Taylor L. T. , Mason J. G. Bogger R. K . Am. Chem. Soc., 101, 2311, (1979).
4. Sheldon R. A., Kochi J. K. Metal – Catalyzed Oxidation of Organic Chemistry ;, Page 184. Academic, New York (1981).
5. Chandra S, Sangeetika J. and Idian J. , EPR and electronic spectra studies on copper (II)complexes of some N-O doner ligands , Chem. Soc. 81. 203-206. (2004).
6. Pampa Mukherjee , Chaitali Biswas, Michael G.B. Drew B ,Ashutosh Ghosh . Structural Variations in Ni(II) complexes of salen type di-Schiff base ligands . Polyhydron ,26. 3121-3128, (2007).
7. Cozzi P.G. Metal – Salen Schiff Base Complexes in Catalysis : Practical Spectra. Chem. Soc. Rev. 33, 410-421, (2004).
8. Reedijk , J. Hetrocyclic Nitrogen – Donor Ligands . In Comprehensive Coordination Chemistry : The Synthesis , Reactions, properties and Application of Coordination Compounds, Eds.; Pergamon Press; Oxford , Vol. 2, Chapter 13.2. (1987)
9. Calligaris, M., Randaccio , L. In Comprehensive Coordination Chemistry. Eds.; Pergamon Press; Oxford , Vol. 2, Chapter 20, (1987)
10. Peter Sykes . Mechanism In Organic Chemistry , 6th Edition . Page; 53. (1987).
11. Carboraro, L.Isola, M. Lapagna, P. Senatore, L. Marchetti, F. Spectrophotometric study of the equilibrium between Nickel (II) Schiff- Base complexes and alkaline earth or Nickel(II) cations in acetonitrile solution. Inorganic Chemistry, 38, 5519 ,(1999).
12. Valko M. clement R. and Pilikan . Copper (II) and Cobalt (II) Complexse with Derivatives of Salen and Tetrahydrosalen : An Electronic spin Resonance , Magnetic , Susceptibility, and Quantum Chemical Study . J.Phys. Chem., 98, 137-143, (1995).
13. Kazuo Nakamoto, Infrared and Spectra of Inorganic and coordination Compounds. Fourth Edition. Page 133 . Jone Wiley & Son . (1986).
14. Desiraju, G. R. , Steiner, T. The week Hydrogen bonding (IUCR Monograph on Crystallography 9) ; Oxford Science Pub. (1999).
15. Toyssie P. and Charette. 3,3' –(alkanediyl)bis-(2,2,2-triary-1-oxa-2-stiba-3-azabenzodicyclohex-5-enes). Spectrochem. Acta. 19. 1407 – 1423. (1963).
16. Lopez-Garriga, J.j.; Babcock, G.T.; Harrison, J. F.; Factors influencing the C:N stretching frequency in natural ad protonated Schiff's Bases. J. Amer. Chem. Soc. 108, (1986).
17. S. Sarawat G. , Srivastava S. and. Mehrotra. C. Schiff base complexes of organotin (IV) .Reactions of trialkyltin(IV) chlorides

- and alkoxides with *N*-substituted salicylideneimines J. Organo. Met. Chem. 129, 155-161 (1977).
18. R. S. Downing and F. L. Urbach, An anomalous sign reversal in the circular dichroism spectra of tetradentate Schiff base complexes of nickel(II) and copper(II). J. Amer. Chem. Soc., 90, 5344, (1968).
 19. B. Bosnich, An interoperation of the Circular Dichroism and Electronic Spectra of Salicylaldehyde Complexes of Square – Coplanar Diamagnetic Nickel (II). J. Amer. Chem. Soc. 90, 627, (1968).
 20. Aguiari, A., Bullita, E., Casellato, U. Guerriero, P. Tamburini, S. Vigato, P. A. Preparation, properties and coordination behavior of planar or tridimensional compartmental Schiff bases. Inorg. Chem. Acta, 219, 135-146. (1994).

Synthesis Of New 1,2,3-Triazole And 1,2,3-Triazoline Derived From Unsaturated D-Fructose Via 1,3-Dipolarcyclo addition Reaction

Abdul Hussain K. Sharba¹, Yousif A. AL-Fattahi², Firyal W. Askar³

^{1,3}Department of Chemistry, College of Science, Al-Mustansiriya University

²Department of Chemistry, College of Science, Baghdad University

e-mail: hussainirk@yahoo.com

Received 4/1/2011 – Accepted 2/3/2011

الخلاصة

يتضمن هذا العمل تحضير مشتقات كربوهيدراتية جديدة تحتوي حلقة 3,2,1-تريازولين و 3,2,1-تريازولين مشتقة من سكر الفركتوز غير المشبع بطريقة تفاعل الإضافة ثنائية القطب 3,1 الحلقي. للحصول على هذه المشتقات، حضر 6,4,3,1-رباعي-O-بنزويل-β-D-فركتوفورانوز (1) الذي يحتوي على مجموعة هيدروكسيل حرة في الموقع 2- كمادة أولية لهذا الهدف. تم الحصول على مشتقات السكر غير المتجانسة ثنائية الحلقة (5-7) من تفاعل السكر غير المشبع (4) مع أزيد أريل سلفونيل. استخدم تفاعل الإضافة الحلقي للحصول على مشتقات التريازولات (9-11) ومشتقات التريازولين (13-15) من مفاعلة مشتقات السكر الحاوية على أواصر غير مشبعة خارجية (8) و (12) مع أزيد أريل سلفونيل. بينما بمفاعلة أزيد السكر (3) مع (8) بوجود $(\text{ph}_3\text{P})_3\text{CuI}$ كعامل مساعد تم الحصول على التريازول (16) الحاوي على جزيئين من السكر. المركبات المحضرة تم تشخيصها باستخدام الطرائق الطيفية مثل IR, FT-IR, UV, $^1\text{H-NMR}$, $^{13}\text{C-NMR}$. تم تقويم الفعالية المضادة للبكتيريا لبعض المركبات المحضرة وأختبر نوعان من البكتيريا هما *Staph. aureus* و *E. coli* لهذا الغرض ومقارنتها مع نوعين من المضادات (Gentamycin, Ampicillin). وتم إجراء التقويم الحيوي لبعض المركبات المحضرة على نوعين من الفطريات المرضية *Panic. Spp.* و *Asp. Flaveus* وكذلك *Candida*. وقد أظهرت نتائج التقويم زيادة كبيرة في فعالية المركبات كما موضح في الجدول (1). وتم دراسة أقل تركيز يحدث عند التثبيط (MIC) لبعض المركبات المحضرة، جدول (2).

ABSTRACT

This work describes synthesis of new fructofuranosyl derivatives containing 1,2,3-triazole ring, 1,2,3-triazoline ring or tetrazole ring derived from unsaturated D-fructose via 1,3-dipolar cycloaddition reaction. 1,3,4,6-tetra-O-benzoyl-β-D-fructofuranose (1) was prepared as starting material, to synthesize sugar derivatives (2-4). The 1,3-dipolar cycloaddition reaction of vinylic sugar (4) and aryl sulfonyl azides gave sugar based spiro heterocyclic derivatives (5-7). Cycloaddition reaction was also carried out with two sugar derivatives with an exo unsaturated bond (8 and 12) and aryl sulfonyl azides. The triazole derivatives (9-11) and triazoline derivatives (13-15) successfully obtained. Moreover, the reaction of the azidosugar (3) with (8) in presence of $(\text{ph}_3\text{P})_3\text{CuI}$ as catalyst afforded a triazole with two substituted sugar residues (16). The prepared compounds were identified by spectroscopic methods; IR, FT-IR, UV, $^1\text{H-NMR}$ AND $^{13}\text{C-NMR}$. Antibacterial and antifungal activities of some of the synthesized compounds were studied and compared with that of two antibiotics (Ampicillin and Gentamycin). The activities were determined *in vitro* using disc diffusion method against *Staph. aureus*, *Escherichia coli* and three pathogenic strains of yeast (*Candida*) and fungus (*Aspergillus flaveus* and *Penicillium spp.*). The results revealed that some of the studied compounds showed measurable activity. The minimal inhibitory concentration (MIC) have been also studied to determine the low concentration for inhibition.

INTRODUCTION

Most of the known triazole compounds possess low solubility in water, therefore the new researches include preparation of new carbohydrate derivatives containing 1,2,4-triazole and 1,2,3-triazole^[1-5], these derivatives have high solubility in water and possessing possible biological activity.

Some 1,2,3-triazole derivatives have antibacterial^[6], antifungal^[7], antiviral^[8], and antitumor activities^[9]. Other 1,2,3-triazoles can be used as corrosion inhibitors, while some are used as charge-donating materials for electrostatographic development⁽¹⁰⁾. 1,2,3-Triazole links have emerged as a popular bridging units in carbohydrate chemistry because of the facile efficient method of their introduction, which referred to as "click chemistry". The later method is based on Cu(I)-catalyzed version of Huisgen's 1,3-dipolarcycloaddition of azido sugar to terminal alkynes and it has been successfully applied for the synthesis of various glycoconjugates including multivalent glycosides^[11].

Hydrolysis of the benzoate groups of some novel compounds afforded a new carbohydrate derivatives containing 1,2,3-triazoline and 1,2,3-triazole, and such derivatives are expected to have high solubility in water and may possess biological activity.

The presence of carbohydrate moiety in drug may also overcome the frequently observed water insolubility problem.

The present work was directed toward the synthesis of new carbohydrate derivatives containing 1,2,3-triazole, 1,2,3-triazoline and tetrazole ring starting from unsaturated D-fructose via 1,3-dipolar cycloaddition reaction. Such derivatives are expected to have high solubility in water and may possess biological activity.

MATERIALS AND METHODS

Melting points were recorded using Electrothermal 9100 melting point apparatus and are uncorrected. The IR spectra (KBr discs or thin films) were recorded on Perkin-Elmer 1310 infrared spectrophotometer, or Shimadzu FTIR-800.

UV spectra were recorded on UV-Visible Varian UV-Cary-100 spectrophotometers. ¹H-NMR and ¹³C-NMR spectra were recorded on Varian Gemini 200BB spectrometer (200MHz) in Lodz University, Poland, on a Bruker-300 at 300 MHz for proton nucleus and 75 MHz for carbon nucleus in Al-Albait University, Jordan and on a 400 MHz in Hanover University, Germany. Tetramethylsilane was used as an internal reference and CDCl₃ as solvent. (TLC) was performed on aluminum plates precoated with silica-gel f₂₅₄, supplied by Merck. Column chromatography was carried out with silica-gel 60 (Fluka). Spots were detected with iodine vapor.

Synthesis of Compounds

Compounds (1) and (2) were prepared according to the literatures⁽¹²⁾

1,3,4,6-Tetra-O-benzoyl-2-azido-2-deoxy- β -D-fructo-furanose (3)

Compound (2) (1g, 1.48 mmol) and excess of sodium azide were added to DMF (20 mL). The mixture was heated with stirring at (50-60 °C) for 20 h. The reaction was monitored by TLC [Benzene:MeOH; 8:2]. The reaction mixture was poured on a cold water and extracted with chloroform (3×15 mL), then dried with anhydrous sodium sulphate. The solvent was evaporated to give a syrup (0.8 g, 86% yield), $R_f = 0.6$ [CHCl₃:MeOH; 8:2], FTIR (film) 2137 cm⁻¹ (N₃), 1720 cm⁻¹ (C=O).

1,3,4,6-Tetra-O-benzoyl-1-deoxy-D-1,2-fructene (4)

Compound (2) (1g, 1.48 mmol) was dissolved in dry benzene (20 mL), then diethyl amine (1.48 mmol) and tetrabutylammonium iodide (0.1 g) were added. The reaction was stirred at reflux temperature for 24 hrs. Reaction was monitored by TLC [benzene:MeOH; 8:2]. The mixture was diluted with diethyl ether, then the diethyl amine hydrobromide was filtered. The organic layer was washed with water and dried with anhydrous sodium sulphate, then the solvent was evaporated to dryness to give a syrup (0.6 g, 70% yield), $R_f = 0.4$ [benzene:MeOH; 8:2], IR (film) 1625 cm⁻¹ (C=C), 3100 cm⁻¹ (=C-H).

General procedure for cycloaddition of vinylsugar (4) with arylsulfonyl azides:

Preparation of compounds (5-7):

The vinylic sugar (4) (0.1g, 0.131 mmol) and (0.131 mmol) aryl-sulfonyl azide were heated with stirring in toluene (20 mL) at (60-70 °C) on an oil-bath for 80 hrs. The mixture was poured onto ice-cold water to give a brown precipitate. Recrystallization of residue from ethanol gave the triazole derivative.

Spiro[1-benzenesulfonyl)-5-benzoyloxy-1H-1,2,3-triazolin-4,2'-(3',4'-dibenzoyloxy-6'-benzoyloxymethyl) tetrahydrofuran] (5)


M.p. (193-195 °C); 54% yield; $R_f = 0.3, 0.25$ [Benzene:MeOH; 8:2]; IR (KBr disc) 3075 cm⁻¹ (C-H_{arom.}), (C-H_{ali}) 2920 cm⁻¹, 1720 cm⁻¹ (C=O), 1380, 1165 cm⁻¹ (SO₂), UV(CHCl₃) (λ_{max} , nm): 248.

Spiro[1-(p-toluenesulfonyl)-5-benzoyloxy-1H-1,2,3-triazolin-4,2'-(3',4'-dibenzoyloxy-6'-benzoyloxymethyl) tetrahydrofuran] (6)

M.p. (210-212 °C); 45% yield; $R_f = 0.23, 0.26$ [Benzene:MeOH; 8:2]; IR (KBr disc) 3085 cm^{-1} (C-H_{arom.}), 1720 cm^{-1} (C=O), $1372, 1165\text{ cm}^{-1}$ (SO₂), UV(CHCl₃) (λ_{max} , nm): 245.

Spiro[1-(m-nitrobenzenesulfonyl)-5-benzoyloxy-1H-1,2,3-triazolin-4,2'-(3',4'-dibenzoyloxy-6'-benzoyloxy methyl) tetrahydrofuran] (7)

M.p. (230-232 °C); 44% yield; $R_f = 0.19, 0.21$ [Benzene:MeOH; 8:2]; IR (KBr disc) 3090 cm^{-1} (C-H_{arom.}), 1730 cm^{-1} (C=O), $1380, 1160\text{ cm}^{-1}$ (SO₂), $1535, 1330\text{ cm}^{-1}$ (NO₂).

¹H-NMR (CDCl₃) δ (ppm): 4.58 (2H, m, H-6', 6'), 4.8 (2H, m, H-3', H-5'), 5.61 (1H, m, H-4'), 5.88 (1H, m, H-5), 7.48-8.14 (24H, m, 4BzO, Ar); ¹³C-NMR (CDCl₃) δ (ppm): 63.6, 66.2, 69.2, 69.9, 90.2 and 95 (C_{6'}, C_{5'}, C_{4'}, C_{3'}, C_{2'} and C₅), 129-133.7 (C-aromatic), 139 (C-SO₂), 141.7 (C-NO₂), 164.3-166.5 (C-Bz).


(Propyn-2-yl)-1,3,4,6-tetra-O-benzoyl-2-deoxy-D-Fructofuranoside (8)

Benzolyted sugar (1) (2g, 3.36 mmol) was dissolved in benzene (30 mL), then (20%) sodium hydroxide solution (10 mL) and tetrabutylammonium iodide (0.1 g, 0.56 mmol) were added with stirring followed by addition of propargyl chloride (1.18 g, 10 mmol). The mixture was refluxed with continuous stirring for 16 hrs. TLC [benzene:MeOH; 9:1] indicated completion of the reaction and the mixture was extracted with benzene (3×15 mL). The organic phase was dried over anhydrous Na₂CO₃ and evaporated to dryness to give a syrup, which was purified on a silica-gel column, which was eluted with benzene. The fructoside (8) (1.8 g, 80% yield) was obtained as syrup, FTIR (film) 3300 cm^{-1} (C≡C-H), 2240 cm^{-1} (C≡C), 1724 cm^{-1} (C=O).

2-(Propen-2-yl)-1,3,4,6-tetra-O-benzoyl-2-deoxy-D-fructofuranoside (12)

Using the same method for preparation of compound (8), but allyl chloride (1.16 mmol) was used instead of propargyl bromide. TLC [benzene:MeOH; 8:2] indicated completion of the reaction. The product was purified on a silica-gel column. The fructoside (12) was obtained as

a syrup, IR (film) 1620 cm^{-1} (C=C), 3075 cm^{-1} (=C-H), 1725 cm^{-1} (C=O).

General procedure for cycloaddition of propynyl fructofuranoside (8) with arylsulfonyl azides:

Preparation of compounds (9-11)

Compound (8) (0.1g, 0.9 mmol) was dissolved in toluene (20 mL) and aryl sulfonyl azide. The mixture was heated with stirring at (60- 70 °C) for 80 h. The mixture was poured on an ice water, then extracted with chloroform (3×15 mL) and the chloroform extracts were dried with anhydrous Na_2SO_4 . The extract was evaporated to give a syrup, which was decolorized with charcoal. Column chromatography [CH_2Cl_2 :Diethyl ether; 8:2] gave pure syrup of triazole derivative.

1-Benzenesulfonyl-4-(1',3',4',6'-tetra-O-benzoyl-β-D-fructofuranos-2'-yl)oxymethyl-1H-1,2,3-triazole (9)

60% yield; $R_f = 0.2, 0.18$ [CH_2Cl_2 :Diethyl ether; 8:2]; IR (film) 1720 cm^{-1} (C=O), $1372, 1175\text{ cm}^{-1}$ (SO_2).

1-(p-Toluenesulfonyl)-4-(1',3',4',6'-tetra-O-benzoyl-β-D-fructofuranos-2'-yl)oxymethyl-1H-1,2,3-triazole (10)

57% yield; $R_f = 0.15, 0.12$ [CH_2Cl_2 :Diethyl ether; 8:2]; IR (film) 1715 cm^{-1} (C=O), $1368, 1170\text{ cm}^{-1}$ (SO_2).

1-(m-Nitrobenzenesulfonyl)-4-(1',3',4',6'-tetra-O-benzoyl-β-D-fructofuranos-2'-yl)oxymethyl-1H-1,2,3-triazole (11)

65% yield; $R_f = 0.13, 0.10$ [CH_2Cl_2 :Ethyl acetate; 8:2]; FTIR (film) 1764 cm^{-1} (C=O), $1350, 1170\text{ cm}^{-1}$ (SO_2).

$^1\text{H-NMR}$ (CDCl_3) δ (ppm): 4.42 (3H, dd, H-6', 6', H-5'), 4.96 (2H, d, H-1', 1'), 5.12 (1H, d, H-4'), 5.40 (1H, s, H-3'), 7.40-8.18 (27H, m, O- CH_2 , H-5, 4BzO, Ar).

General procedure for cycloaddition reaction of allyl ether sugar (12) with arylsulfonyl azides : Preparation of compounds (13-15)

Compound [12] (0.1g, 0.9 mmol) and arylsulfonyl azide (0.9 mmol) was heated with stirring in toluene (20 mL) at (60-70 °C) for 82 hrs. The mixture was poured on an ice water and extracted with chloroform (3×15 mL). The organic layer was dried with anhydrous Na_2SO_4 , then evaporated to give a syrup, which was decolorized with charcoal and concentrated, then was purified on a silica-gel column. The column was eluted with chloroform.

1-Benzenesulfonyl-4-(1',3',4',6'-tetra-O-benzoyl-β-D-

fructofuranos-2'-yl)oxymethyl-1H-1,2,3-triazoline (13)

70% yield; $R_f = 0.2, 0.16$ [$\text{CHCl}_3:\text{MeOH}$; 9:1]; IR (film) 1725 cm^{-1} (C=O), $1380, 1165\text{ cm}^{-1}$ (SO_2).

1-(p-Toluenesulfonyl)-4-(1',3',4',6'-tetra-O-benzoyl- β -D-fructofuranos-2'-yl)oxymethyl-1H-1,2,3-triazoline (14)

65% yield; $R_f = 0.15, 0.11$ [$\text{CHCl}_3:\text{MeOH}$; 9:1]; IR (film) 1715 cm^{-1} (C=O), $1380, 1173\text{ cm}^{-1}$ (SO_2).

1-(m-Nitrobenzenesulfonyl)-4-(1',3',4',6'-tetra-O-benzoyl- β -D-fructofuranos-2'-yl)oxymethyl-1H-1,2,3-triazoline (15)

55% yield; $R_f = 0.12, 0.09$ [$\text{CHCl}_3:\text{MeOH}$; 8:2]; FTIR (film) 1720 cm^{-1} (C=O), $1530, 1350\text{ cm}^{-1}$ (NO_2), $1370, 1170\text{ cm}^{-1}$ (SO_2).

1-(1',3',4',6'-tetra-O-benzoyl- β -D-fructofuranos-2'-yl)-4-(1'',3'',4'',6''-tetra-O-benzoyl- β -D-fructofuranos-2''-yl)oxymethyl-1H-1,2,3-triazole (16)

The azidosugar (3) (0.1 g, 0.165 mmol) was added to a solution of compound [8] (0.1g, 0.9 mmol) in a mixture of (t-BuOH:H₂O; 1:2) (20 mL), $(\text{ph}_3\text{P})_3\text{CuI}$ (0.1 g) was added as a catalyst. The reaction mixture was refluxed for 18 hrs. TLC [$\text{CHCl}_3:\text{MeOH}$; 9:1] indicated the completion of the reaction. The mixture was diluted with water and extracted with chloroform (3 \times 15 mL). The combined chloroform extracts dried with anhydrous Na_2SO_4 and evaporated to give a syrup, which was purified on silica-gel column. A syrup material of (16) was obtained (0.06 g, 30% yield); $R_f = 0.08$ [CHCl_3 :Ethyl acetate; 9:1]; IR (film) 3050 cm^{-1} (C=CH), 1625 cm^{-1} (C=C), 1730 cm^{-1} (C=O).

Biological screening, antimicrobial activity test

The biological activity of some prepared compounds was tested against one strain of Gram +ve bacteria (*Staphylococcus aureus*), Gram -ve bacteria (*Escherichia coli*), yeast (*Candida*) and fungi (*Aspergillus flavus*).

Two *in vitro* techniques were proceeded for studying antibacterial activity against the two strains, DMSO was used as a solvent and as a control, for both techniques the concentration of the compound in this solvent was 10^{-3} M .

The first technique was the Disc Sensitivity test ⁽¹³⁾, this method involves the exposure of the zone of inhibition toward the diffusion of microorganism on agar plate. The plates were incubated for 24 hrs. at 37°C , the zone of inhibition of bacterial growth around the disc was measured.

The second was to get the sensitivity of each microorganism toward some new compounds by determining the minimal inhibitory concentration (MIC), which was achieved by using Tube Dilution Method. The (MIC) of the new compounds for each microorganism was measured at the lowest concentration required to inhibit the growth of this microorganism. The tubes containing different concentrations of the new compounds were incubated at 37 °C for 45 hrs. Furthermore, two of the known antibiotics (Ampicillin and Gentamycin) were taken as standard to compare their activity with those of the new compounds. In order to complete this study, some of the new compounds were tested for their *in vitro* growth inhibitory activity against yeast (*Candidas*) and a pathogenic fungi i.e. *Aspergillus flavus*, *Penicillium spp* on potato dextrose agar medium, then incubated at 30 °C for 72 hrs. DMSO was used as a solvent and as control.

Table -1: Antimicrobial activities of the compounds (10-3 mg. mL⁻¹)

Compound	<i>Staph. aureus</i>	<i>E. Coli</i>	<i>Candidas</i>	<i>Asp. flavus</i>	<i>Penici. spp</i>
Control (DMSO)	-	-	-	-	-
Ampicillin	17	24	20	10	22
Gentamycin	20	22	22	17	24
7	10	15	20	20	25
10	8	15	15	20	22
11	10	20	15	15	20

Where:

6-8: (+)

10-20: (+++)

8-10: (++)

20-30: (++++)

Table -2: Minimal inhibitory concentration (MIC) for some new compounds (µg. mL⁻¹)

Compound	<i>Staphylococcus aureus</i>						<i>Escherichia coli</i>					
	0.05	0.1	0.25	0.5	1.0	2.5	0.05	0.1	0.25	0.5	1.0	2.5
Ampicillin	+	MIC	-	-	-	-	+	MIC	-	-	-	-
Genatmycin	+	MIC	-	-	-	-	+	+	+	MIC	-	-
7	+	+	+	+	+	+	+	+	+	+	+	+
10	+	MIC	-	-	-	-	+	+	MIC	-	-	-
11	+	+	MIC	-	-	-	+	MIC	-	-	-	-

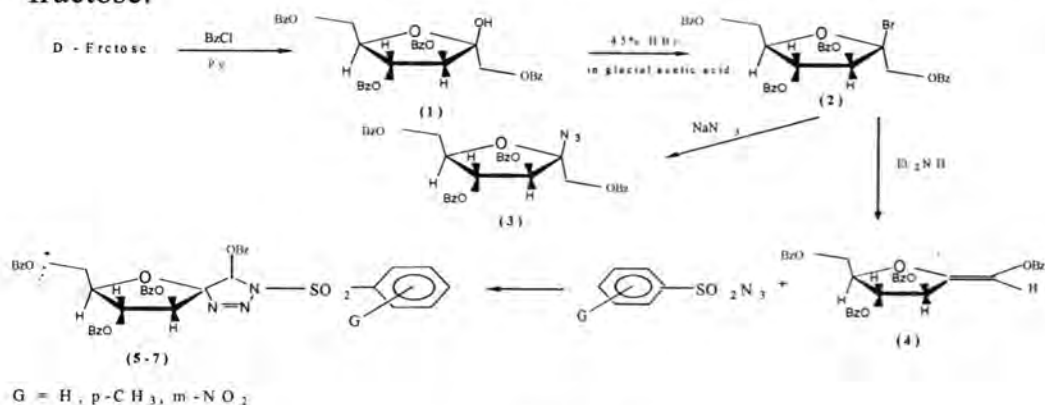
Where:

(+: Growth, (-): No growth, MIC: 99%

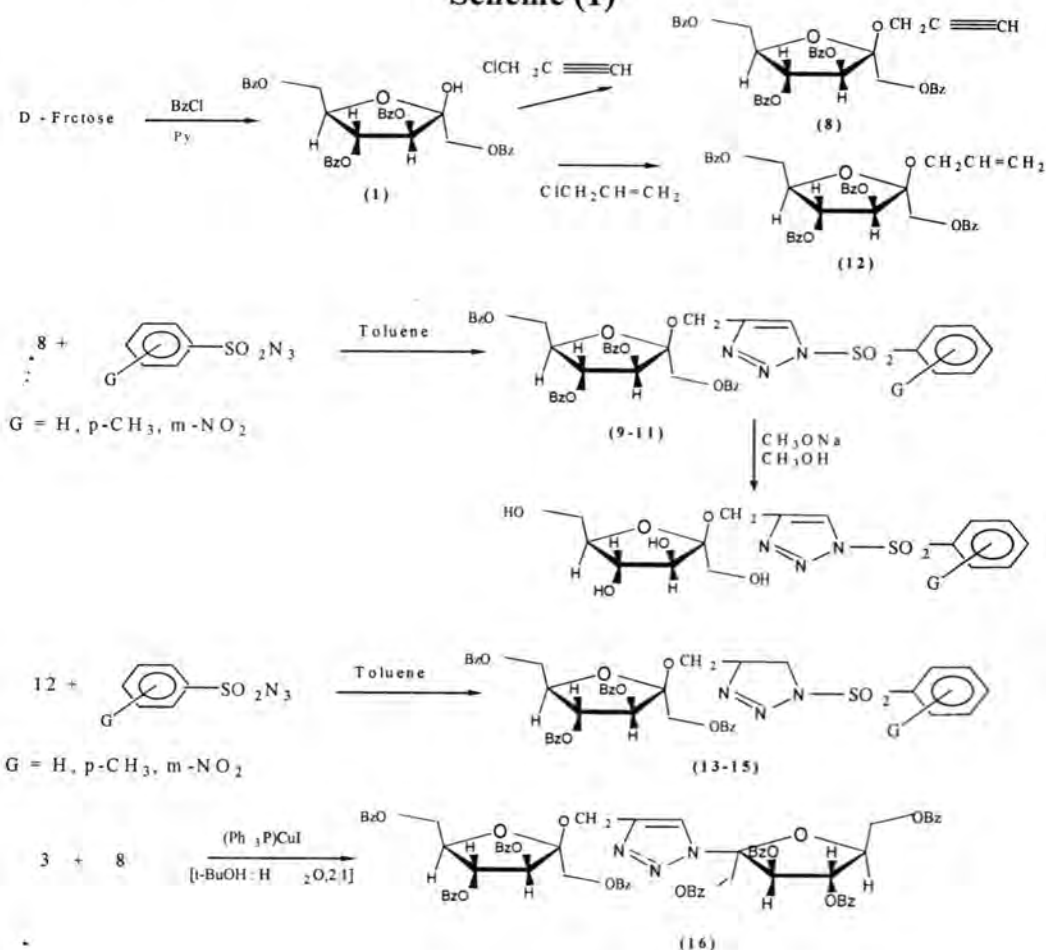
RESULTS AND DISCUSSIONS

Three types of new sugar-based monocyclic triazole and triazoline derivatives of D-fructose have been synthesized and characterized. These compounds have been synthesized using [3+2] cycloaddition

reaction. The reaction sequences are outlined in schemes (1 and 2) from fructose:



Scheme (1)

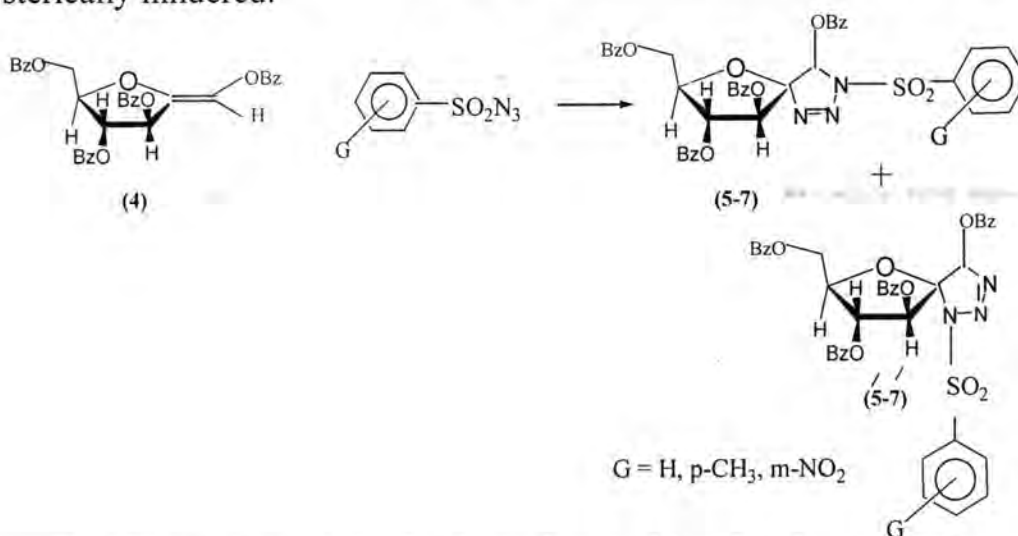


Scheme (2)

For the preparation of the titled compounds (5-7), -Fructose was first converted to 1,3,4,6-tetra-*O*-benzoyl- β -D-fructofuranose (1). When compound (1) was treated with 45% HBr solution in glacial acetic acid it gave 1,3,4,6-tetra-*O*-benzoyl- β -D-fructofuranosyl bromide (2). Treatment of the benzoylated bromide derivative (2) with sodium azide in DMF gave the azide (3) in 86% yield.

The 1,3-dipolar cycloaddition reaction was carried between the vinylic sugar (4) and aryl sulfonyl azides, which gave the expected spiroheterocyclic triazoline sugar derivatives (5-7). TLC showed that the product was a mixture of two isomers, which were characterized by IR and UV spectral data.

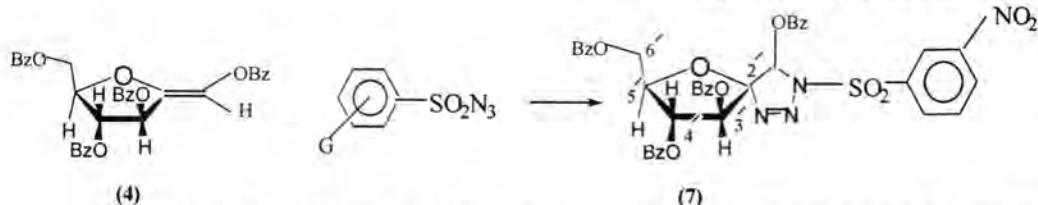
Attempts to isolate the two isomers were unsuccessful. The isomers (5-7) are expected to be the main products because it is less sterically hindered.



The IR spectrum of (5) showed stretching bands at 3075 cm^{-1} ($\text{C-H}_{\text{arom.}}$), 2950 cm^{-1} ($\text{C-H}_{\text{aliph.}}$), 1720 cm^{-1} (C=O), 1380 cm^{-1} , 1165 cm^{-1} (SO_2), 750 cm^{-1} and 690 cm^{-1} due to the out of plane bending for mono substituted benzene ring and the disappearance of the azide band at 2300 cm^{-1} .

The IR spectrum of (7) showed stretching bands at 3090 cm^{-1} ($\text{C-H}_{\text{arom.}}$), 2960 cm^{-1} ($\text{C-H}_{\text{aliph.}}$), 1730 cm^{-1} (C=O), 1535 cm^{-1} , 1330 cm^{-1} (NO_2), 1380 cm^{-1} , 1130 cm^{-1} (SO_2) and disappearance of the azide band.

The $^1\text{H-NMR}$ spectrum of (7), showed a signal at δ 5.88 ppm assigned for H-5 proton (integrated for 1H), a signal at δ 5.61 ppm was assigned for H-4' proton (integrated for 1H), a signal at δ 4.8 ppm was assigned to H-3' and H-5' protons (integrated for 2H), a signal at δ 4.58 ppm was assigned to H-6', 6' protons (integrated for 2H). Aromatic protons appeared as multiplet at δ 7.48-7.67 ppm and δ 7.98-8.14 ppm.



^{13}C -NMR spectrum of (7), showed signals at 63.6, 66.2, 69.2, 69.9, 90.2 and 95 ppm are attributed to (C_6' , C_5' , C_4' , C_3' , C_2' and C_5) respectively. The aromatic carbons appeared at 129-133.7 ppm and at 139, 141 ppm, which were attributed to phenyl carbon attached to the sulfonyl group and nitro group. The four carbonyl of benzoate group appeared at 16.3-166.5 ppm. The triazoline carbon atom appeared at 95.0 and the quaternary carbon atom at 90.2, respectively.

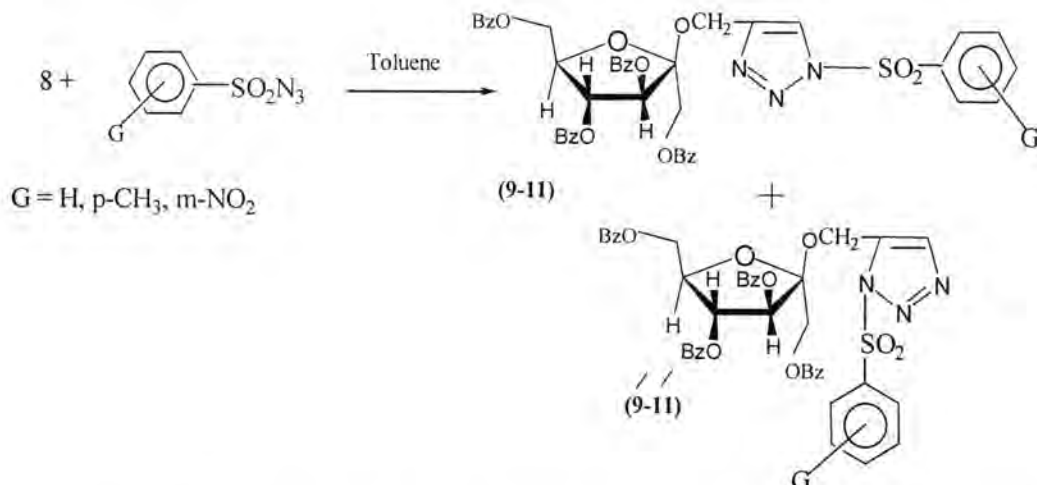
The ^1H -NMR and ^{13}C -NMR values obtained for (7) are in accord with that theoretically calculated using chem-office program

It was decided that the cycloaddition reaction to be tested with fructo derivative having an exo-unsaturated bond part of the glycosidic triazole. For the synthesis of compounds (9-11), the first step in this proposed reaction, scheme (2), was to react the tetrabenzoate sugar (1) with propargyl chloride to give a glycoside with an exo-triple bond that may inter cycloaddition reaction with aryl sulfonyl azides. Glycosidation of the tetrabenzoate derivative (1) with propargyl chloride afforded the fructoside (8). This glycoside was successfully obtained using phase transfer catalysis. Treatment of (1) in benzene with propargyl chloride using tetrabutyl ammonium bromide as phase transfer catalyst and 20% sodium hydroxide solution for 12 hrs. gave 2(propyn-2-yl)-1,3,4,6-tetra-*O*-benzoyl- β -D-fructofuranoside (8).

The propargyl ether derivative (8) showed, in the FT-IR spectrum, the characteristic bands for the ($\text{C}\equiv\text{CH}$) at 3300 cm^{-1} , and ($\text{C}\equiv\text{C}$) at 2240 cm^{-1} and the disappearance of the hydroxyl stretching band at 3400 cm^{-1} .

The fructoside (8) was then entered with aryl sulfonyl azides in a [3+2] cycloaddition reaction, which gave after work-up a mixture of two triazole isomers expected to be.

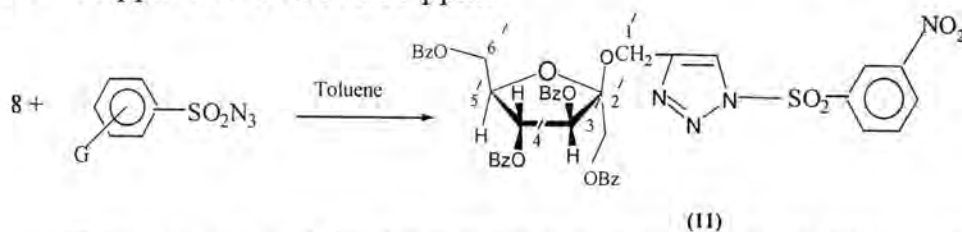
Considering steric and electronic factors, the isomers (9-11) are expected to be the major isomers.



The FT-IR spectrum of the triazole (9), showed strong stretching bands at 1372 cm^{-1} , 1175 cm^{-1} assigned for the SO_2 group with disappearance of the bands for the (N_3), ($\text{C}\equiv\text{C}$) and ($\text{C}\equiv\text{CH}$) functions.

Similarly, (10) showed stretching bands at 1368 cm^{-1} , 1170 cm^{-1} for (SO_2 group) and again the (N_3), ($\text{C}\equiv\text{C}$) and ($\text{C}\equiv\text{CH}$) bands have disappeared.

The $^1\text{H-NMR}$ spectrum of (11), showed signals at δ 4.42 ppm assigned for (3H); δ 4.96 ppm (2H), δ 5.12 ppm (1H), δ 5.40 ppm (1H) were assigned for H-6', 6', H-5', H-1', 1', H-4' and H-3' respectively. The triazole ring proton appeared as multiplet with aromatic protons at δ 7.40-7.66 ppm and δ 7.95-8.18 ppm.



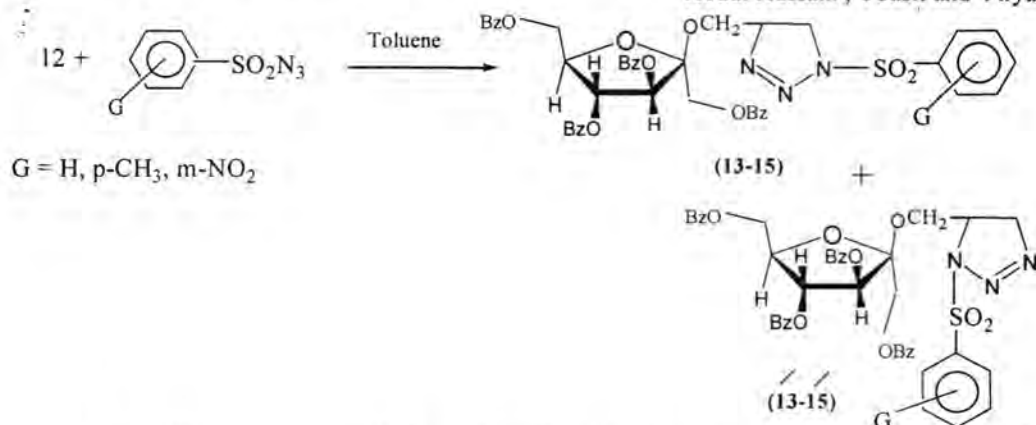
The strategy used for the synthesis of triazolines (13-15) was first reacting the benzoylated sugar (1) with allyl chloride to give propen-2-yl-1,3,4,6-tetra-*O*-benzoyl-2-deoxy-D-furanoside (12), then (12) was allowed to enter cycloaddition reaction with arylsulfonyl azides.

The IR spectrum of (12) showed stretching bands at 3075 cm^{-1} ($\text{C-H}_{\text{arom.}}$), 2900 cm^{-1} ($\text{C-H}_{\text{aliph.}}$), 1725 cm^{-1} for ($\text{C}=\text{O}$) and 1650 cm^{-1} ($\text{C}=\text{C}$).

Treatment of allyl ether derivative (12) with aryl sulfonyl azide gave two isomers, the major is expected to be the isomers (13-15) with the less sterically hindered isomers.

Synthesis Of New 1,2,3-Triazole And 1,2,3-Triazoline Derived From Unsaturated D-Fructose Via 1,3-Dipolarcycloaddition Reaction

Abdul Hussain , Yousif and Firyal



The IR spectrum of the triazoline (13) showed absorption bands at 3100 cm⁻¹ (C-H_{arom.}), 2980 cm⁻¹ (C-H_{aliph.}) and 1380 cm⁻¹, 1165cm⁻¹ (SO₂) and disappearance of (N₃) stretching band.

Copper(I)-catalyzed 1,3-dipolar cycloaddition reaction was applied to prepare compound (16).

Treatment of compound (8) with azido sugar (3) in [t-BuOH: H₂O; 2:1] mixture and (ph₃P)₃CuI as catalyst under reflux, afforded the desired triazole with two substituted sugar residues.

TLC showed that one product was formed which was separated on silica-gel column as a syrup in 60% yield.

The IR spectrum of (16) showed stretching band at 3050 cm⁻¹ for (C=CH_{arom.}), 1730 cm⁻¹ (C=O), 1625 cm⁻¹ (C=C) and devoid bands at 2137 cm⁻¹, 2240 cm⁻¹ and 3300 cm⁻¹ attributed to stretching frequencies of (N₃), (C≡C) and (C≡C-H).

Biological activity tests^[14]

From the data presented in table (1 and 2), the following points were concluded:

1. The new compounds were found to have high activity against *E. coli* because they contain a fructose moiety, which competitively inhibited the absorption of pathogenic *E. coli* to urinary tract epithelial cells, acting as an analogous for mannose as found by researchers in the early 1990s.
2. All compounds prepared are expected to exhibit a large number of biological activities, the reason for that may be due to the presence of sulfonyl group in these compounds that may behave like sulfa drugs and also due to toxophoric properties of C-N-S group.
3. The results of (MIC) study for compounds are shown in table (2), which indicate that some of the new compounds exhibited antibacterial activity against (*Stapholcoccus citrus*) and (*Escherichia coli*) at low concentrations, while they did not show such activity at higher concentrations. On comparison of these values with those of

two studied antibiotics (Ampicillin and Gentamycin), it was shown that the new compounds were more active.

REFERENCES

1. S.A.Nepogodiev, S.Dedola, L.Marmuse, M.T.de Oliveira and R.A.Field, "Synthesis of triazole-linked pseudo-starch fragments", *Carbohydr. Res.*, 342, 529-540 (2007).
2. I.Leban, M.Jeselnik, J.Sieler and J.Kobe, "Conformational flexibility in a triazole nucleoside", *Nucleosides, Nucleotides & Nucleic Acids*, 23(1) 521-530 (2004).
3. B.H.M.Kuijpers, S.Groothuys, A.R.Keereweer, P.J.L.M. Quaedflieg, R.H.Blaauw, F.L.Van Delft and F.P.J.T.Rutjes, "Expedient synthesis of triazole-linked glycosyl amino acids and peptides", *Organic Letters*, 6(18)3123-3126 (2004).
4. A. Hussain K. Sharba, Yousif A. AL-Fattahi and Firyal W. Askar, "Synthesis of New Carbohydrate Derivatives Via 1,3-Dipolarcycloaddition Reaction", *Al-Nahrain Journal of Science* (under press).
5. H. Wamhoff and H. Warnecke, "Synthesis and cycloaddition reaction {2-deoxy - 3,5 -bis (O - (P-toluoyl) - α - D - ribofuranosyl} ethyne", *ARKIVOC*, Vol. II, 95-100 (2001).
6. F.Palacios, A.M.Ochoa De Retena, J.Pagalday and J.M.Sanchez, "Organic preparation and procedures INT", 27 (6) 603-612(1995).
7. M.M Pearson, P.D. Rogers J.D.Cleary and S.W. Chapman, "Voriconazole : A new triazole antifungal agent", *Ann - Pharmacother*, 73 (3)420-432(2003).
8. Himanshu, Tyagi - Rahul, Olsen - Carl - E, Errington -willian, Parmarvirinder, Prasad and Psho K., "Synthesis and antiviral activity evaluation of novel 2-phenyl - 4- (D-arabino -4' - cycloaminobutyl : triazoles , acyclonucleosides containing un natural bases", *Bioorg. Med. Chem.*, 10 (4),963 - 968(2002).
9. N.A. Al-Masoudi and Y.A. Al - Soud, "Nucleosides - Nucleotides - Nucleic acids", 21 (4-5) 361 -375 (2002).
10. S.T. Abu-Orabi, "Review 1,3 - dipolar cycloaddition reaction of substituted benzyl azide with acetylenic compounds", *Molecules*, 7 302-314(2002).
11. Sergey A. Nepogodiev, Simone Dedola, Laurence Marmuse, Marcelo T. de Oliveira and Robert A Field, "synthesis of triazole - linked pseudo - starch fragments", *Carbohydr. Res.* 342, 529-540(2007).
12. R.K. Ness and H.G. Fleteher, "Crystalline tetrabenzoyl - β -D - fructopyranosyl bromide and its reduction by lithium aluminum

hydride to 1,5 – anhydro – D – mannitol and 1,5 – anhydro – L – gulitol", J. Am. Chem. Soc., 75, 2619-2623(1953).

13. M.R. Atlas, E. Alfres, Brown and C. Lawrence Parks, "Laboratory Manual Experimental Microbiology", Mosby-Year Book Inc. (1995).
14. A.Hussain K. Sharba, Yousif A. AL-Fattahi and Firyal W. Askar, " Synthesis of new carbohydrate derivatives via 1,3-dipolar cycloaddition reaction", Ph.D. Thesis, Al-Mustansirya University, Baghdad, (2006) .

Simultaneous Determination of Chlorpromazine and Trifluoperazine in Pharmaceutical Preparations Using High Performance Liquid Chromatography

Jameel M. Dhabab

Department of Chemistry, College of Science, Al-Mustansiriya University

Received 10/6/2010 – Accepted 2/3/2011

الخلاصة

تم استخدام تقنية كروماتوغرافيا السائل عالي الاداء الطور المعكوس لفصل وتعيين كميات من الكلوربرومازين وتراي فلوپيرازين في مزيج وفي بعض مستحضراتهما الصيدلانية وذلك باستخدام طور متحرك يحتوي على حجوم بنسبة 5:1:1 من سايلوهكسان:ميثانول: ثنائي ميثيل امين مع معدل جريان 1.5 مل/دقيقة. وقد امكن فصل هذين المركبين ثم القياس وعند طول موجي مقداره 254 نانو متر وازمان احتجاز قدرها 7.18 و 9.62 دقيقة لكل من المركبين على التوالي. وتم الحصول على خطية من التركيز ضمن مدى يتراوح 20-0.02 مايكروغرام/مل للكلوربرومازين و 20-0.05 مايكروغرام/مل للتراي فلوپيرازين. وكانت النتائج للطريقة المقترحة ذات مصداقية جيدة (Rec., 98.6%-98.8%) ودقة عالية (RSD, 1.19%) مما يسمح باستخدامها لتقدير الكلوربرومازين وتراي فلوپيرازين في بعض المستحضرات الصيدلانية.

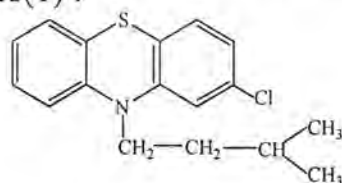
ABSTRACT

Reversed phase high performance liquid chromatography (RP- HPLC) was used for the simultaneous determination of chlorpromazine and trifluoperazine in pharmaceutical preparations, with a mobile phase of cyclohexane: methanol: dimethylamine (5:1:1) volume ratio at 1.5 mL.min⁻¹ flow rate to separate both compounds by detection at 254 nm. This method gave the best resolution of chlorpromazine and trifluoperazine at retention times of 7.18 and 9.62 minutes, respectively. Linearity was obtained in the concentration range of 0.02-20 µg mL⁻¹ for chlorpromazine and 0.05-20 µg mL⁻¹ for trifluoperazine. The obtained results were highly accurate (Rec., 98.6%-98.8%) and good precise (RSD, 1.19%-1.95%). The described method showed to be appropriate for simultaneous determination of chlorpromazine and trifluoperazine in pharmaceutical dosage forms.

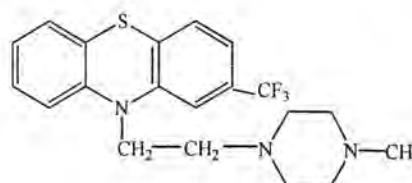
Keywords: Iralzine, RP- HPLC, chlorpromazine, trifluoperazine, Largapromatetil.

INTRODUCTION

Chlorpromazine and trifluoperazine are two important derivatives of phenothiazine which are widely used against antipsychotic diseases(1).



Chlorpromazine



Trifluoperazine

The wide applications of these two drugs prompted the development of various analytical methods for their determination. These methods include voltammetry(2), capillary zone electrophoresis(3), fluorimetry(4), turbidimetry(5), titrimetry, potentiometric titrations(6,7), spectrophotometric(8-11), extraction-liquid chromatography(12) and chromatographic methods(13-16). High performance liquid chromatography methods have been established and

are thoroughly validated(17). The purpose of the present study is to investigate the utility of HPLC in the assay of combination of chlorpromazine and trifluoperazine in the pharmaceutical preparations without the necessity of sample pretreatment. The method has sufficiently good accuracy and precision. .

MATERIALS AND METHODS

Apparatus

Shimadzu liquid chromatography system consisted of a gradient liquid delivery pump model LC-AVP, connected with UV-VIS detector (SPD-10AVP) operating at 254 nm rheodyn manual 3298 (USA) injection valve, with a 20 μ l loop the HPLC system has been interfaced with computer (Shimadzu VP5).The chromatographic data were supplied by Epson LQ-300 printer (p852A Japan).

The column type Polaris 5u C18-A (50x2mm) was used.

The mobile phase was obtained by mixing cyclohexane: methanol: dimethylamine (5:1:1, v/v/v). The flow rate was 1.5 ml.min⁻¹ 20- μ l of each solution was injected and the chromatograms were recorded.

Materials

All chemicals and solvents are of analytical reagent grade. Trifluoperazine hydrochloride and chlorpromazine hydrochloride were provided by SDI, Iraq Pharmaceutical samples were obtained from the same company. Cyclohexane, methanol, dimethylamine were obtained from different companies. Standard solutions of each of chlorpromazine and trifluoperazine were prepared separately by dissolving 0.1 g of each drug in methanol and made up to 100 ml.

Stock Solutions

The standard solutions of each drug were prepared individually by diluting aliquots of the stock solutions to prepare a concentrations in a range of 0.01-30 μ g. ml⁻¹ for each drug. Triplicate 20 μ l were injected for each solution and peak area was plotted against the corresponding concentration to obtain the calibration curve. The amounts of chlorpromazine and trifluoperazine were calculated from the corresponding regression equation.

Preparation of pharmaceutical formulation

Tablets analyses: 5 tablets of 100 mg of trifluoperazine hydrochloride and 200 mg of chlorpromazine hydrochloride were crushed and mixed in a mortar and weighed accurately. It was found that the weight average was equal to 100 mg and 200 mg for trifluoperazine hydrochloride and chlorpromazine hydrochloride, respectively. An accurate weight(10g) of the prepared powder was transferred into 100 mL flask and dissolved with methanol using ultrasonicator for 5min. Then filtrated and washed. The filtrate was collected in a clean flask.

Solutions were prepared by taking suitable aliquot of a clean filtrate and diluted with methanol. The amounts of trifluoperazine hydrochloride and chlorpromazine hydrochloride were calculated from the corresponding regression equation.

Syrup analysis: 10ml of drug syrup was transferred to 100 ml flask and diluted with methanol and the assay was carried out as described earlier.

RESULTS AND DISCUSSION

A reliable, simple, and validated analytical method requires studying the optimum conditions such as resolution, composition of mobile phase, flow rate, retention time, tailing and capacity factors. The mixture of cyclohexane: methanol: dimethylamine (5:1:1) at 1.5 ml. min⁻¹ flow rate, was proved to be better than other mixtures and flow rates since the chromatograms peaks in this case have better resolution as shown in Fig 1. The suitable wavelength for the detection was 254 nm with sample loop of 10 μ L. The retention times were 7.18 and 9.62 min for chlorpromazine hydrochloride and trifluoperazine hydrochloride, respectively as shown in Table 1. Linear regression parameters of the peak area versus concentration at ranges of 0.05-20 and 0.02-20 μ g. ml⁻¹ for trifluoperazine and chlorpromazine, respectively are presented in Table 2.

The statistical data such as determination coefficient (R^2), RSD, slope, were also shown in Table 2.

Sample analysis

Chlorpromazine hydrochloride was determined in 10g of largapromactil tablets and 10g of largapromactil syrup while trifluoperazine hydrochloride determined in 10 μ g.ml⁻¹ of iralzin tablets. The results of the analysis of the tablets and syrup are listed in table 3.

The retention times were 7.18 and 9.62 min for chlorpromazine hydrochloride and trifluoperazine hydrochloride respectively, indicating that the times of analyses were short, with system chromatogram of preparation of standard solutions which suitable for USP requirements(18). According to value of detection limit, analytical method was sensitive. In order to prove the validity and applicability of the proposed HPLC method, the recovery testes carried out by analyzing in the binary mixture of chlorpromazine and trifluoperazine in tablet samples. In this work were compared with reference method 19 as shown in table 4.

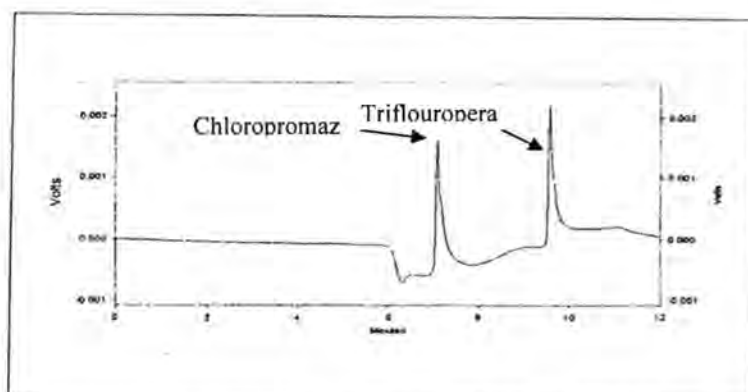


Fig-1: HPLC Chromatogram of chlorpromazine hydrochloride and trifluoperazine hydrochloride in a mixture at 254 nm (10 $\mu\text{g.mL}^{-1}$) each.

Based on the results, These drugs were well separated. Under the described optimized chromatographic conditions, they all eluted within 9.62 min. The limit of quantification is the lowest concentration on the standard curve that can be measured with acceptable accuracy, precision and variability. The lower practical limit of quantification of chlorpromazine hydrochloride and trifluoperazine hydrochloride were 0.02 and 0.05 $\mu\text{g. mL}^{-1}$ respectively.

This method was found to be very effective and sensitive for analysis of samples containing trifluoperazine hydrochloride and chlorpromazine hydrochloride.

Table-1: Chromatographic parameters for the separation of trifluoperazine and chlorpromazine

Drug name	Retention time (min)	Resolution factor	Capacity factor
Chlorpromazine	7.18	-	1.64
Trifluoperazine	9.62	1.200	0.95

Table-2: Statistical data of the calibration curve for trifluoperazine and chlorpromazine

Statistical data	Trifluoperazine	Chlorpromazine
Slope	0.28	0.17
Intercept	0.042	0.054
Correlation coefficient	0.9998	0.9996
Detection limit ($\mu\text{g.mL}^{-1}$)	0.02	0.008
Reproducibility (RSD %)	1.54	1.60
Repeatability (RSD %)	1.78	1.82

Table-3: Results of determination of trifluoperazine and chlorpromazine in pharmaceutical preparation (at N=5)

Drugs	Iralzin (tablet)	Largapromaetil (tablet)	Largapromaetil (syrup)
Retention time (min)	9.63	7.21	7.18
Drug taken ($\mu\text{g.mL}^{-1}$)	10	10	10
Drug found ($\mu\text{g.mL}^{-1}$)	9.86	9.78	9.88
Relative Error %	-1.4	-1.8	-0.12
Recovery %	98.6	98.8	98.8
RSD %	1.95	1.15	1.85

Table-4: Results of determination of trifluoperazine and chlorpromazine in pharmaceutical preparation using proposed RP- HPLC and spectrophotometric methods

Drugs	Revered-phase method	HPLC	Spectrophotometric method(ref.)
Irlazin (tablet)	Recovery %	98.6	98.2
	Error %	-1.4	-1.8
Largapromaetil (tablet)	Recovery %	98.8	98.2
	Error %	-1.2	-1.6

The suitability of the HPLC method for the determination of two drugs has been studied. The reported spectrophotometric method by nabil et al.(19) involve a spectral derivatives but this method is simple. the analytical method offered higher precision (RSD) and better recovery% range of 1.14-1.95 and 98.6-98.8 respectably. Both low and high doses of the two drugs can be measured simultaneously , with detection limits (0.008-0.02 $\mu\text{g. mL}^{-1}$) and satisfactory validation characteristics. The analytical results were obtained for the determination of two pharmaceutical compounds good agreement with the given-labeled quantity.

Finally, this HPLC method has sensitivity, precision and accuracy may be useful for the determination of pharmaceutical preparations.

REFERENCES

- Bertram, G. K. "Basic and clinical pharmacology " McGraw-Hill, London, pp 265- 269(2001).
- Huang Fei, Yan Quan-Ding and Zeng Bai-Zhao "Electrochemical behavior and determination of trifluoperazine at decanethiol self-assembled monolayer modified gold electrodes" j. natural science,10, 2, 435-440,(2006)
- Muijselaar, P.G; Claessens, H. A.; Cramers, " sensitiv detection of trifluoperazine using apoly-ABSA/SWNTs film C. A. " J., Chromatogr , A735, 395-402(1996).
- Kaul PN,Whitfield LR,Clarc ML, " chlorpromazine metabolism VII:new quantitation fluorometric determination of chlorpromazin and its sulfoxide" J pharm sci. 65 :689-694(1978).
- Amir, K. S.; Mirali, F.; Ramin, M. " a comparative study of the interaction of chlorpromazine, Trifluoperazine, and promethazine with mouse brain tubulin " Anal. Lett., 36, 2183-2198(2003).
- Ahemd K. Hassan and Suhaam T. Ameen, " potentiometric sensor for the determination of trifluoperazine HCl pharmaceutical prepration " J. Analytical science, 25, 11, 1295, (2009).
- Krishnamurthy, G.; Basavaiah, K.; " titrimetric micro determination of some phenothiazine neuroleptics with potassium hexacyanoferrate(III) " Talanta, 47,1, 59-66(1998).

8. El-Gindy, B. El Zany, T. Awad and M. M. Shabanch "spectrophotometric determination of trifluoperazine HCl and isopropamide iodide in binary mixture using second derivative and second derivative of the ratio spectramethods" *J. pharm biomed Anal.*, 26(2), 203 - 210, (2001)
9. RB Saudagar, Swarnlata Saraf, S Saraf, "spectrophotometric determination of chlodiazepoxide and trifluoperazine HCl from combine dosage form" *J. pharmaceutical Sciences*, 69, 1, 149-152, (2007).
10. Jayarama, M. V.; Ythirajan, H. S. Rangaswamy D. "analytical applications of reactions of Iron(III) and hexacyanoferrate(III) with 2,10-disubstituted Phenothiazines" *Talanta*, 33, 352-354 (1986).
11. Basavaiah, K. "Spectrophotometric determination of trifluoperazine in pharmaceutical preparations using potassium iodate" *Farmaco*, 59, 315-321 (2004).
12. Shaghayegh B., Zahra T., Noushin A., Hassan Y. Aboul- Enein; a simple and reliable stir bar sorptive extraction-liquid chromatography procedure for the determination of chlorpromazine and trifluoperazine in human serum using experimental design methodology" *J. of Separation Science*, 34, 1, 90-97, (2011)
13. Shree S. K. "simultaneous quantitation of plasma doxorubicin and prochlorperazine content by HPLC" *J. Chromatographia* 69, 393-396 (2009).
14. Temerdashev, Z. A., Kiseleva N. V.; Klishchenko R. A., Udalov A. V. "Stability indicating RP-HPLC Method for the estimation of Trifluoperazine HCl as API and estimation in Tablet dosage form" *Atlanta s*, 43, 8, 1291-1296 (2006).
15. Shettip p, Venkatachalama A. "stability indicating HPLC method for simultaneous Quantification of trihexyphenidyl HCl, trifluoperazine HCl and chlorpromazine HCl from tablet formulation" *E j. of Chemistry*, 7, 1, 299-S313, (2010).
16. Anna M. "Comparison of methods for calculation of the partition coefficients of selected tocopherols" *J. planar chromatography*, 20, 6, (2007).
17. Magdalena, W. K.; Agnieszka, S. Anna M. "HPLC with electrochemical detection to measure chlorpromazine, thioridazine and metabolites in human brain" *Russ.; J. Anal. Chem* 61, 1, 1061-9348 (2006).
18. Easton, R.; Mc Nally Taunton M.A, "The US pharmacopia", 24th Edn., (2000).
19. Nabil, S.; Jameel, M.; Ahemed, R. "using of spectrophotometric derivatives for determination of phenothiazines in pharmaceutical formulations" *J. Thykar* 2, 27-31, (2007).

Study the Otoacoustic Emission in the Frequency Range Lower Than 1 Khz

Adnan M. Ali AL-Maamury

Department of physics, college of science, AL-Mustansiriya university

Received 9/6/2010 – Accepted 14/11/2010

الخلاصة

تم في هذا البحث دراسة الترددات الأقل من واحد كيلو هيرتز للانبعاث السمعي العابر لمجموعة من الأشخاص؛ حيث ان الفسحة الزمنية القصيرة (20 ملي ثانية) للانبعاث السمعي تسبب تقدير غير جيد لمعدل الفترة الزمنية للعملية السمعية؛ لذلك نريد ان نقدم القيم الغير اعتيادية للفترة الزمنية و تردداتها وهذه القيم غير متفقة مع القيم الاخرى للمدى من 1 كيلو هيرتز الى 4 كيلو هيرتز وهذا بسبب النافذة بين 2.5 ملي ثانية و 5 ملي ثانية.

ABSTRACT

This study illustrates the behaviour of the frequencies lower than 1 kHz for the TEOAE latency at different persons, the short acquisition interval (20 ms) may causes underestimate of the average latency, we would like to show the abnormal values of the latency of the frequencies and the values of this range are not in agreement with the another frequencies specially the frequencies from 1kHz to 4 kHz, due to the window onset between 2.5 and 5 ms.

INTRODUCTION

Otoacoustic emissions (discovered by Kemp 1978) are narrow-band acoustic signals generated by the inner ear of normal hearing individuals, either in the absence of acoustic stimulation (spontaneous emissions) or in response to acoustic stimulation (evoked emissions).

One of the most exciting advances in our understanding of hearing processes during recent years concerned the discovery of the otoacoustic emissions (OAEs)(1).

Otoacoustic emissions describe the responses that the cochlea emits in the form of acoustic energy. The recognition that the cochlea not only receives sound, but also produces acoustic energy has been a major factor in modifying recent thinking concerning cochlea function.

The OAE findings in combination with those from a number of other recent experiments demonstrating voltage-dependent contractions and elongations in isolated hair cells (2), suggest that the outer hair cells (OHCs) of the cochlea furnish an active source of mechanical energy that influences basilar-membrane motion (3).

Gold (4) proposed the hypothesis that the sharp frequency selectivity exhibited by the cochlea resulted from a feedback system consisting of mechanical-to-electrical transduction process coupled to an electrical-to-mechanical transduction process.

Gold's postulate of a reverse-transduction process in the form of an electromechanical conversion mechanism suggested the possibility of detecting this process in the form of sound in the ear canal.

However, Gold's hypothesis was never taken seriously until Kemp (1978)(5) demonstrated that energy was indeed emitted by the cochlea and that it was recordable as acoustic vibration in the ear canal using specialized method and equipment.

The discovery of OAEs was important for both theoretical and practical reasons. The presence of evoked sound pressure oscillations in the ear canal provided direct evidence of the existence of active mechanical mechanisms within the cochlea. This possibility made it essential for physical modelers of the cochlea to accommodate the newly proposed active processes within their theories. Moreover, anatomical structures capable of effecting active and rapid oscillations had to be designated or discovered. This necessity led to new interpretations of many of the well established finding from ultrastructural examinations of the cochlea including the subsurface cisternae of the OHC (6), demonstration of action in the stereocilia and the cuticular plate (7), and the attachment of the stereocilia to the inferior aspects of the tectorial membrane (8). Knowledge of OAEs also resulted in the reexamination or clarification of certain baffling physiological findings that were either newly discovered or had been puzzling for many years. For example, the discovery of OAEs led to a better understanding of how the medial olivocochlear efferent system influences the receptor potentials of the inner hair cells (9). Awareness of OAEs also suggested a role for the OHCs in the stimulus-transduction process given the knowledge the these receptors do not possess a prominent afferent-nerve fiber innervation (10). Finally, the discovery of OAEs permitted the proposition of testable hypotheses account for several psychoacoustical phenomena including the microstructures of behavioral sensitivity and loudness enhancement which were incomprehensible in terms of conventional models of the auditory system (11).

Another significance of OAEs was the potential they promised to provide by allowing the details mechanical aspects of cochlear function to be studied in a noninvasive and objective manner (12), from the distinctive "viewpoint" of the OHCs.

The kinds of otoacoustic emissions are, (TEOAEs, SOAEs, DPOAEs, SFOAEs).

The noninvasive attribute of the OAE-recording method permits repeated measures over lengthy periods of time, without interfering with the cochlea's normal mode of operation and promises to make such procedures an important research tool in the auditory science.

Otoacoustic emissions OAEs are acoustic signals generated in the cochlea and detected in the ear canal, either spontaneously SOAEs or following acoustical stimulation (13).

The evoked OAE classification is based on the evoking technique: transient evoked OAEs TEOAEs are evoked by a broadband transient stimulus, whereas stimulus frequency OAEs SFOAEs are evoked by a pure tone. DPOAEs (Distortion product of otoacoustic emissions) are nonlinearly generated at the frequency $2f_1-f_2$ apical DPOAE by the interaction of two primary tones f_1 and f_2 , with frequencies in a particular ratio usually $f_2/f_1=1.22$.

The latency of TEOAEs is measurable quantity that provides important information about cochlear mechanisms and in principle could also be useful for clinical diagnostic purpose. Indeed, the latency of a given frequency component is sensitive to the position of corresponding OAE source along the cochlear partition and to the speed of the corresponding spectral component of the traveling wave along its round-trip path. The position of the OAE source is given by the tonotopic Greenwood map (14).

The speed is a model-dependent function of frequency and cochlear position, which in transmission-line cochlear models, involves the bandwidth of the cochlear filter associated with each frequency (15). Increased bandwidth of the auditory filters is generally observed in hearing impaired subjects, associated with damage of outer hair cells.

TEOAE latency estimates have been obtained in several studies, either using time-domain analysis of the TEOAE wave form to identify the onset time of each frequency component or based on measurements of the TEOAE phase gradient delay.

Time-domain analyses include the analysis of the OAE response to tone bursts (16,17). A narrow-band filtering technique was recently applied to the estimate of SFOAE and DPOAE latencies in order to improve the accuracy of time-domain estimates of the OAE latency as a function of the stimulus level in normal-hearing and hearing-impaired subjects. Similar information had also been obtained from studies of the DPOAE onset time (18,19), directly measured in the time domain, using an ad hoc acquisition technique to cancel the primary contribution without filtering.

MATERIALS AND METHODS

The matching pursuit algorithm was introduced by Mallat and Zhang (20).

The method relies on adaptive decomposition of the signal into waveforms (also called atoms) from a large and redundant dictionary of functions.

These waveforms are selected in order to best match the signal structures. Although a matching pursuit is non-linear, like an orthogonal expansion, it maintains an energy conservation which guarantees its convergence. It is closely related to projection pursuit strategies, (21).

A matching pursuit decomposition provides an interpretation of the signal structure. If a structure does not correlate well with any particular dictionary element, it is sub-decomposed into several elements and its information is diluted.

A matching pursuit is a greedy algorithm that chooses at each iteration a waveform that is best adapted to approximate part of the signal (20, 22), in this work the new version of MP (23), is used to calculate the values of latencies and the frequencies.

RESULTS AND DISCUSSION

This work illustrates the effect of the range of frequency less than 1 kHz, the aim of this work shows the behavior of the part of otoacoustic emissions less than 1 kHz and in the same time study the behavior of this part, the distribution of the latency is logical or not with respect to another parts of the expectation TEOAEs. So the latency is calculated for four persons by using the matching pursuit method (23).

The results and the discussion includes three steps, the first step is to study the distribution of the frequencies and there latencies , this step includes two cases, the frequencies with the range less than 1 kHz and without this range, the second step to find the fitting of the first step and the third step to study the frequencies less than 1 kHz, as following :

The first step (TEOAE latency, as a function of frequency)

This step includes two cases, as following :

1-The first case, the frequency includes the range less than 1 kHz.

Table (1) shows the values of the latency and the frequency for all values of the range (include the values less than 1 kHz), whereas the latency is a function of the frequency.

Table -1: The frequencies (include the range less than 1 kHz) and there latencies

First person		Second person		Third person		Fourth person	
Freq.(kHz)	Latency(ms)	Freq.(kHz)	Latency(ms)	Freq.(kHz)	Latency(ms)	Freq.(kHz)	Latency(ms)
0.49	3.94	0.54	6.58	0.49	10.00	0.54	15.46
0.54	14.68	0.73	14.02	0.68	15.10	0.73	12.10
0.63	12.52	0.88	9.28	0.88	11.32	0.83	6.64
0.78	5.08	0.93	13.78	1.17	11.62	1.12	16.18
1.03	14.68	1.22	16.60	1.22	5.14	1.22	13.24
1.07	7	1.32	11.38	1.42	8.08	1.66	12.52
1.27	12.58	1.32	7.36	1.81	12.34	1.86	4.78
1.37	14.98	1.56	9.40	1.81	12.28	1.95	9.40
1.46	11.68	1.71	10.72	1.86	9.52	1.95	16.96
1.61	7.18	1.81	16.66	1.86	4.36	2.54	12.40
1.61	15.64	1.95	13.36	2.05	12.16	3.22	10.48
1.95	7.3	2.10	8.08	2.15	5.98	3.71	5.38
2.20	5.02	2.10	5.80	2.88	8.44	3.86	6.82
2.29	10.24	2.98	4.90	3.08	6.40		
2.93	8.56	2.98	11.86	3.42	5.08		
3.42	5.92	3.17	6.22				
4.39	5.74	3.91	5.14				
		4.44	5.86				

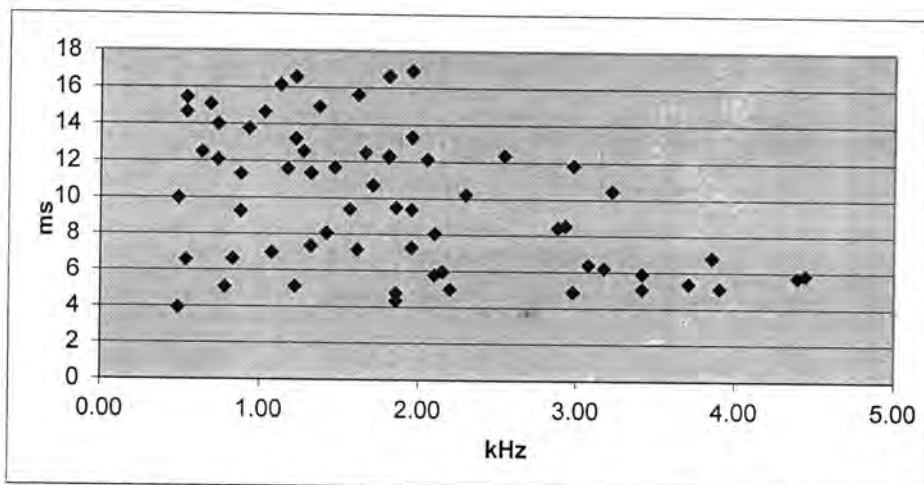


Figure-1: TEOAE latency, as a function of frequency (include the range less than 1 kHz)

Fig. 1 shows the relation between the latency and the frequency for the data which is shown in the table no. 1 that includes the range of frequency less than 1 kHz.

2-The second case, the frequency without the range less than 1 kHz.

Table (2) shows the values of the latency and the frequency (without the range less than 1 kHz), whereas the latency is a function of the frequency .

Table -2: The frequencies (without the range less than 1 kHz) and there latencies

First person		Second person		Third person		Fourth peron	
Freq.(kHz)	Latency(ms)	Freq.(kHz)	Latency(ms)	Freq.(kHz)	Latency(ms)	Freq.(kHz)	Latency(ms)
1.03	14.68	1.22	16.60	1.17	11.62	1.12	16.18
1.07	7	1.32	11.38	1.22	5.14	1.22	13.24
1.27	12.58	1.32	7.36	1.42	8.08	1.66	12.52
1.37	14.98	1.56	9.40	1.81	12.34	1.86	4.78
1.46	11.68	1.71	10.72	1.81	12.28	1.95	9.40
1.61	7.18	1.81	16.66	1.86	9.52	1.95	16.96
1.61	15.64	1.95	13.36	1.86	4.36	2.54	12.40
1.95	7.3	2.10	8.08	2.05	12.16	3.22	10.48
2.20	5.02	2.10	5.80	2.15	5.98	3.71	5.38
2.29	10.24	2.98	4.90	2.88	8.44	3.86	6.82
2.93	8.56	2.98	11.86	3.08	6.40		
3.42	5.92	3.17	6.22	3.42	5.08		
4.39	5.74	3.91	5.14				
		4.44	5.86				

Fig. 2 shows the relation between the latency and the frequency (without the range less than 1 kHz) for the data which is shown in the table no. 2 .

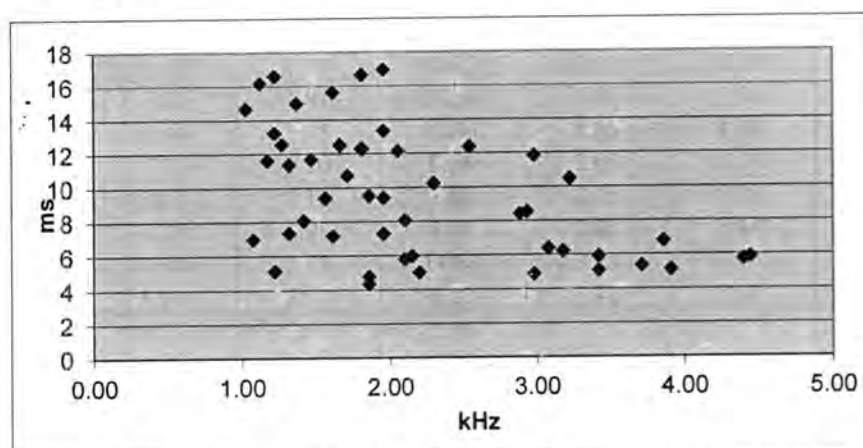


Figure-2: TEOAE latency, as a function of frequency (without the range less than 1 kHz)

In the first case the work show the distribution of frequency-latency for the frequency include the range of frequency less than 1 kHz, figure no. 1 shows this case, and in the second case the frequency without the range less than 1 kHz, figure no.2 shows this case.

The second step (the fitting of the first step)

The experimental latency-frequency relation can be fitted to a power law: (23,24) :

$$\tau(f) = a f^b \dots\dots\dots (A)$$

Where (τ) is the latency, with (f) in kHz, $a \approx 10$ ms, $b \approx -0.4$ (24).

By using equation (A), the fitting is found and the parameter (b) is calculated, the fitting for the figure no.1 and figure no.2 is found, in the same time the values of (b) is calculated, figure no.3 shows the fitting of the frequency which includes the range 1 kHz and, the value in this case is ($b = -0.245$), figure no.4 shows the fitting without the range less than 1 kHz, the value in this case is ($b = -0.5183$).

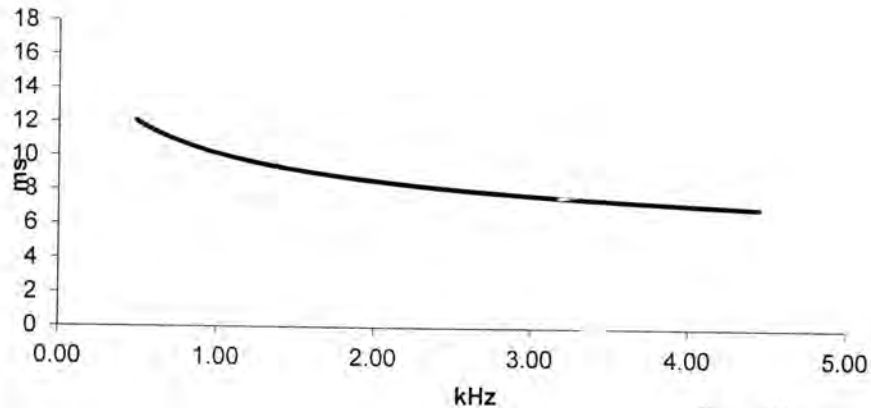


Figure-3: The fitting of the first case

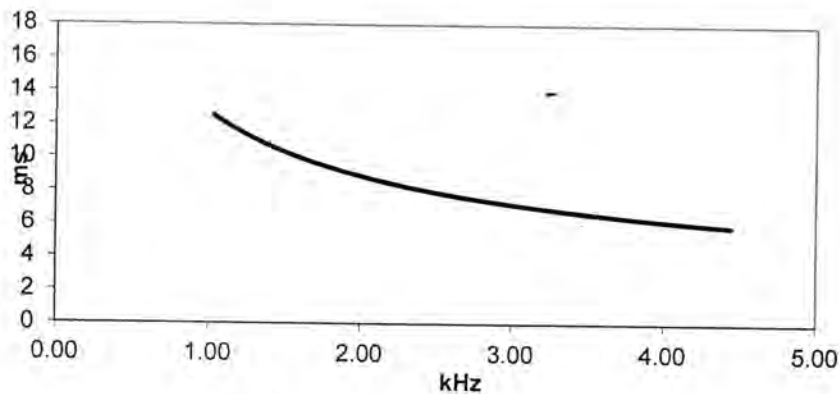


Figure -4: The fitting of the second case

Now the work is illustrated the comparison between the two cases (figure no.3 and figure no.4) by the figure no.5 which shows clearly the difference between the two cases (include the range less than 1 kHz and without this range), by applying the equation (A) the value of (b) is calculated, figure no. 5, shows the values as following:

For the case without frequency lower than (1 kHz) ($b = -0.5183$), for the case includes frequency lower than (1 kHz) ($b = -0.245$), the difference between the two cases (values) show the effect of this range because the standard value is $b = -0.4 (24)$, in vary studies the range of

(b) between -0.4 and -0.5 (23,24) (the value depends upon the level of the stimulus and the method of calculation), to compare the two values of (b) with another studies, we find that the value ($b = -0.5183$) in agreement but the value ($b = -0.245$) is not in agreement with the previous studies.

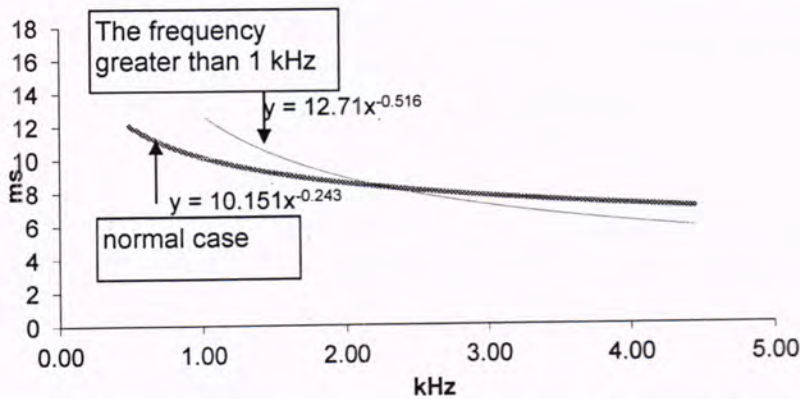


Figure-5: The comparison of the fitting between the two cases

The third step (the frequency less than 1 kHz)
Now the special case for the frequency lower than 1 kHz is illustrated, table (3) shows the latencies and there frequencies for four persons, figure (6) shows the TEOAEs of the frequency rang lower than 1 kHz.

Table -3: shows the frequencies and there latencies for the rang less than 1 KHz

First person		Second person		Third person		Fourth peron	
Freq.(kHz)	Latency(ms)	Freq.(kHz)	Latency(ms)	Freq.(kHz)	Latency(ms)	Freq.(kHz)	Latency(ms)
0.49	3.94	0.54	6.58	0.49	10.00	0.54	15.46
0.54	14.68	0.73	14.02	0.68	15.10	0.73	12.10
0.63	12.52	0.88	9.28	0.88	11.32	0.83	6.64
0.78	5.08	0.93	13.78				

Frequency less than 1 KHz

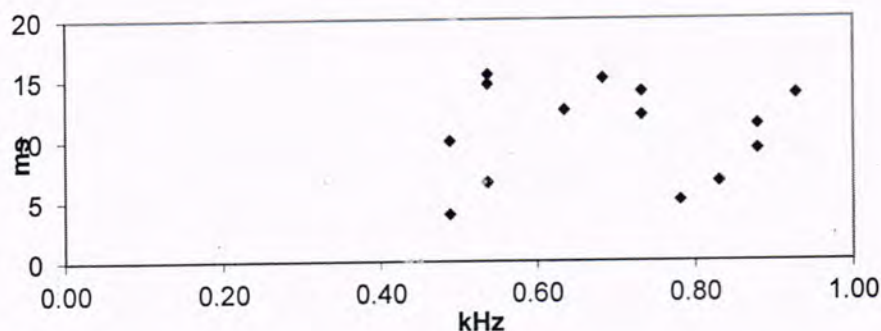


Figure- 6: TEOAE latency, as a function of frequency (frequency less than 1 kHz)

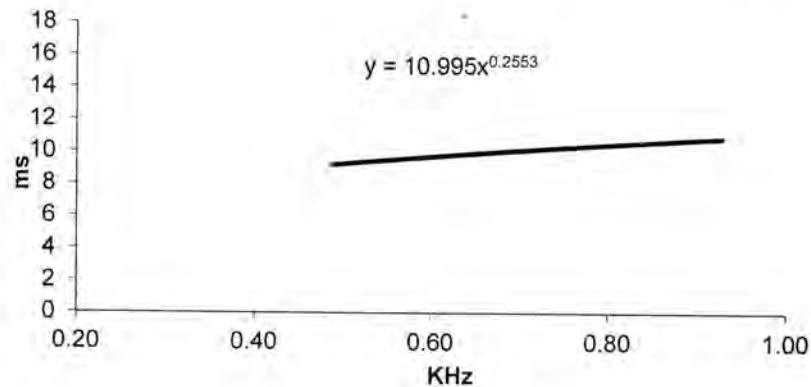


Figure-7: The fitting of the case (frequency less than 1 kHz)

Figure (7) illustrates the fitting of figure (6), from this figure we can conclude the following : The value of $b = 0.2553$ this value is not good because the standard value is $b = -0.4$, the shape of the curve also is not good and is not in agreement with the another parts of TEOAEs, this work improved by calculation and figures that the range of frequency less than 1 kHz is not in agreement with the TEOAEs latency, the short acquisition interval (20 ms) (for the latency) may cause a systematic underestimate of the average latency, we can consider this part (band) is deficient, for this reason we think that the TEOAEs latency it is better to present the band greater than 1kHz, this work is in agreement with the previous studies (25).

CONCLUSION

1. The distribution of latency-frequency of TEOAE which include all values is different of the distribution of latency-frequency of TEOAE without frequencies less than 1 kHz.
2. The band of frequency less than 1 kHz is not in agreement with another bands.
3. The curve of fitting without frequency less than 1 kHz better than with frequency less than 1 kHz.
4. The distribution of latency-frequency of TEOAE for the range less than 1 kHz is seemed distortion.
5. The curve fitting without the frequencies less than 1 kHz is better.
6. The TEOAEs latency is better to present the band greater than 1kHz.

REFERENCES

1. Adnan AL-Maamury "Analysis of transient evoked otoacoustic emissions" thesis, university of Rom, Italy(2006).
2. W. E. Brownell, C. R. Bder, D. Bertrand, and Y. de Ribaupierre, "Evoked mechanical responses of isolated cochlear outer hair cells," *Science* 227: 194-196, (1985).
3. D. C. Mountain, A. E. Hubbard, "Rapid force production in the cochlea," *Hear. Res.* 42:195-202, (1989).
4. T. Gold, *Hearing II: The physical basis of the action of the cochlea,* Proc. R. Soc. Lond. B. Biol. Sci. 135: 492-498 (1948).
5. D. T. Kemp, "Stimulated acoustic emissions from within the human auditory system," *J. Acoust. Soc. Am.* 64: 1386-1391 (1978).
6. L. H. Bannister, H. C. Dodson, A. F. Ashbury, and E. E. Douek, "The cortical lattice: A highly ordered system of subsurface filaments in guinea big cochlear outer hair cells," *Prog. Br. Res.* 74: 213-219, (1988).
7. A. Flock, A. Brestscher, and K. Weber, "Immunohistochemical localization of several cytoskeletal proteins in inner ear sensory and supporting cells," *Hear. Res.* 6: 75-89, (1982).
8. R. S. Kimura, "Hairs of the cochlear sensory cells and their attachment to the tectorial membrane," *Acta Otolaryngol.* 61: 55-72, (1966).
9. A. M. Brown, and D. T. Kemp, "Otoacoustic emissions: The iso-suppression tuning properties of the distortion product $2f_1-f_2$ in gerbil and man," *Br. j. Audiol.* 17: 123-124, (1983).
10. H. Spoendlin, "Neural connection of the outer hair cell system," *Acta Otolaryngol.* 87: 381-387, (1979).

11. D. T. Kemp, "The evoked cochlear mechanical responses and the auditory microstructure-evidence for a new element in cochlear mechanics," *Scand. Audiol. Suppl.* 9: 35-47, (1979b).
12. D. T. Kemp, "Developments in cochlear mechanics and techniques for noninvasive evaluation," *Adv. Audiol.* 5: 27-45, (1988).
13. R. Probst, B. L. Lonsbury-Martin, G. K. Martin, "A review of otoacoustic emissions," *J Acoust. Soc. Am.* 89: 2027-2067, (1991).
14. D. D. Greenwood, "A cochlear frequency position function for several species-29 years later," *J. Acoust. Soc. Am.* 87: 2592-2605, (1990).
15. A. Moleti, R. Sisto, and G. Tognola, "Otoacoustic emission latency, cochlear tuning, and hearing functionality in neonates," *J. Acoust. Soc. Am.* 118: 1-9, (2005).
16. S. J. Norton, and S. T. Neely, "Tone-burst-evoked otoacoustic emissions from normal-hearing subjects," *J. Acoust. Soc. Am.* 81: 1860-1872, (1987).
17. S. T. Neely, S. J. Norton, M. P. Gorga, and W. Jestead, "Latency of auditory brain-stem responses and otoacoustic emissions using tone-burst stimuli," *J. Acoust. Soc. Am.* 83: 652-656, (1988).
18. G. K. Martin, D. Jassir, B.B. Stagner, M. L. Whitehead, B. L. Lonsbury-Martin, "Locus of generation for the $2f_1 - f_2$ vs $2f_2 - f_1$ distortion-product otoacoustic emissions in normal-hearing humans revealed by suppression tuning, onset latencies, and amplitude correlations," *J. Acoust. Soc. Am.* 103: 1957-1971, (1998B).
19. M. L. Whitehead, B.B. Stagner, G. K. Martin, and B. L. Lonsbury-Martin, "Visualization of the onset of distortion-product otoacoustic emissions, and measurement of their latency," *J. Acoust. Soc. Am.* 100: 1663-1679, (1996).

20. S. G. Mallat, and Z. Zhang, "Matching pursuit with timefrequency dictionaies," IEEE Trans. Signal Process. 41: 3397-3415, (1993).
21. J. H. Friendman, and W. Stuetzle, "Projection pursuit regression," Journal of the American statistical Association, Vol. 76 : 817-823, (1981).
22. R. Coifman, and M. V. Wickerhauser, " Entropy-based algorithms for best basis selection," IEEE Trans. on Information Theory. 38(2) (1992).
23. G. Notaro "wavelet and matching pursuit estimates of the transient-evoked otoacoustic emission latency, " J. Acoust. Soc. Am.122(6): 3576-3585 (2007).
24. G. Tognola, P. Ravazzani, and F. Grandori, "Timefrequency distributions of click-evoked otoacoustic emissions," Hear. Res. 106:112-122, (1997).
25. R. Sisto " Transient evoked otoacoustic emission latency and cochlear tuning at different stimulus levels," J. Acoust. Soc. Am. 122(4): 2183 – 2190 (2007).

Speckle Noise Reduction in SAR Images Using Non-Adaptive Mode-Filter

Dunia F. Talab

Department of Physics, College of Science, Al-Mustansiriyah University

Received 8/9/2010 – Accepted 14/11/2010

الخلاصة

تمثل الضوضاء الترقيفية (البقع) المشكلة الرئيسية التي تعاني منها الصور التشاكية. هذه المشكلة تجعل معالجة الصور الرادارية صعبة جداً. لذا فإن الهدف من هذا البحث هو تحقيق الترابط بين الطبيعة التشاكية للأمواج الكهرومغناطيسية والضوضاء الترقيفية التشاكية. في هذا البحث تم التركيز على دراسة الضوضاء المشوهة للصور وقد تم اعتماد النموذج الضري للضوضاء التشاكية.

المرشحات غير المحسنة واحدة من التقنيات المستخدمة في تطبيقات معالجة الصور الرقمية، وفي بحثنا هذا استخدمنا مرشح المنوال التقليدي غير المحسن لإزالة الضوضاء التشاكية في الصور الرادارية. وتم تقييم كفاءة هذا المرشح باستخدام نافذة متحركة (5×5) والمقارنة فيما بينه وبين نتائج الصورة الرادارية الأصلية، وكان للمرشح قابلية في حفظ الحافات وإعطائه تنعيم عالي في المناطق المتجانسة.

ABSTRACT

Speckle noise is main problem in coherent images. This problem makes the processing of synthetic aperture radar (SAR) images is very difficult. Therefore, this paper proved the conjugation between the coherent nature for electromagnetic wave and the coherent speckle noise.

In this research efforts detected to study the degradation noise for images, this is performed by adopting the multiplicative noise model.

Non-adaptive filters are typically used for noise removal or to performing some type of image enhancement, in this work adopt traditional non-adaptive Mode filter, where these filter applied with window size (5×5) to remove speckle noise from SAR image. The result shows the best result to preserve the edges and produce high smoothing in homogeneous image regions.

INTRODUCTION

Images have a very special role for humans in interpreting our world. Developments in image acquisition technology are enabling us to extend our visual faculties beyond the limitations of our physical presence and the resolving power of eyes. It aims to introduce two of the most rapidly developing and exciting areas in this field Synthetic Aperture Radar (SAR) imaging and Laser imaging of which has the capacity to provide significant, but widely differing benefits to mankind.

Laser and SAR signals have a statistical nature because they are formed by coherent superposition of signals from randomly backscattering sites located randomly inside the medium being imaged. The coherent summation of signals gives rise to an interference pattern commonly known as speckle. This speckle has a random nature as it is formed

from signals from randomly located scatters. The analysis of this speckle has been a major subject of investigation [1].

Various methods had been suggested to reduce the speckle effects, these methods can be divided into two categories; the first category is concerned with the methods which improve the appearance of the speckle in SAR images by either averaging non-correlated images obtained from non-overlapping spectra, or by averaging the non-correlated images for different signal polarization, while in the second category speckle is smoothed after the image has been recorded [1,2]. The technique to be used in this work is the second category mentioned above.

MATERIALS AND METHODS

The smoothing methods can, also, be classified into two classes of filters, the first class is the *adaptive filters* that are dependant on image model and local image statistics (Mean, Variance and Coefficient of variation). The second class is the conventional (*non-adaptive*) filters that are independent on image model [2,3].

Some of the filters are implemented in the frequency domain, while other are performed in the spatial domain [1]. Filters that utilized the spatial domain are practically preferable than those utilize the frequency domain, because they are; easier, simpler and faster [2,4].

SAR IMAGES

Primary Radar (Radio Detection and Ranging) is an active system, it used for aircraft involves a similar pulse-echo technique except that it uses electromagnetic wave (EMW) which, like light, travel with a speed of 3×10^8 m/s [1,5], which, in its simplest form, relies upon the time of-flight of microwave echoes to reveal the presence and range of remote radio-opaque objects. Although it has many non-imaging applications (e.g. collision avoidance for cars), there has always been a strong desire to use this sensing strategy to acquire images of remote objects. Such images are commonly achieved by using a rotating antenna to scan the emitted microwave energy across the field-of view to be imaged [6]. Imaging radar data are being used in a variety of applications, including geologic mapping, ocean surface observation, polar ice tracking, and vegetation monitoring. Most of these applications are still in a developmental stage because our knowledge is still limited on how to extract information for radar image data and how to use the normal combination of radar parameter. Qualitatively, SAR images can be interpreted using the same photo interpretation techniques used with visible and near infrared imaging [2].

In a SAR image the brightness of the pixels is proportional to the intensity of the energy of the return echo, or backscatter, from that point

in the scene. Just as in optical images, the intensity of SAR image depends on the surface inclination and roughness (relative to the incident wavelength) of the target [7].

SAR processing requires that the microwave pulses must be coherent, this brings with it the inherent problem of 'speckle' which is highly descriptive term for the effect that this type of noise has on the image. The amount of speckle is inversely proportional to the square root of the number of looks whilst the increase in size of the resolution cell is directly proportion [2].

SAR images invariably contain a high level of image noise or speckle and this complicates the segmentation process. This speckle, associated with a homogeneous distributed target area, is due to the coherent nature of the SAR system. The presence of speckle, which can be modeled as a strong, multiplicative noise, makes the usual different edge detectors inefficient [3].

Generally, SAR image, is consider as a very important tools that can be used to image the earth surface with high spatial resolution, and this system can be used in various weather conditions and in all day time. Three types of SAR image format, these are: amplitude images format, intensity images format, and square root of intensity images format [1,4]. In fact in both: the square-root-method, and the amplitude method, a similar results has been obtained, because of the fact that $I = A^2$ [8,9], where the amplitude SAR images can be presented by [4].

$$A_{ij} = \frac{1}{L} \sum_{K=1}^N [I_{ijk}]^{\frac{1}{2}} \quad \dots\dots(1)$$

In some digital SAR imaging techniques, the dynamic range of the SAR intensity is compressed, using the square-rooted values of the averaged intensity values, given by the form [5];

$$S_i = \sqrt{\frac{1}{N} \sum_{K=1}^N I_{ik}} \quad \dots\dots(2)$$

Where: I = intensity, L = number of looks, and the distribution function of N looks intensity SAR image is represented by convoluting N negative exponential distribution functions.

The multiplicative model is given by:

$$I(x, y) = R(x, y).F(x, y) \quad \dots\dots (3)$$

where $I(x, y)$ and $R(x, y)$ represent respectively, the observed signal, real signal, and $F(x, y)$ represent the multiplicative noise. This kind of noise makes visual and automatic interpretation very difficult task. Images corrupted by multiplicative noise have the characteristic that the brighter the area the noisier it is. For more information see [5,10].

MODE FILTER

Mode-filter is an example of the non-adaptive filters in which the window's central pixel value is replaced by the point's value of the greatest repeated in the sliding mask. The Mode-filter is defined by take the value of highest repetition in the sliding mask. A definite disadvantage of the mode is that it need not be unique, as is illustrated by the following data [11]:

5 8 3 6 3 4 9 8 5 8 3

Here 3 and 8 both occur with the highest frequency of three. (The fact that there is more than one mode is sometimes an indication that the data are not homogeneous, that is, they constitute a combination of several sets of data). Another disadvantage of the mode is that if no two values are alike, the mode does not exist [11].

STATISTICAL ANALYSIS ESTIMATORS

a- Mean, Variance and Standard Deviation

The estimates of the *average* or *mean value* of a random variable x_i can be written as [12]:

$$\mu = \bar{x}_i = \sum_{i=0}^{L-1} x_i p(x_i) \quad \dots (4)$$

While the estimates of the *variance* of such random variable is given by [12]:

$$\sigma_i = (STD)_i = \sqrt{\sum_{i=0}^{L-1} (x_i - \bar{x}_i)^2 p(x_i)} \quad \dots (5)$$

L is the total number of a variables and $p(x_i)$ is the probability of (x_i) in the system of variables.

b- Estimated Signal-To-Noise Ratio, Equivalent Number of Looks

Calculation of the *Signal-To-Noise Ratio* (SNR) defined as the mean over the standard deviation [5]:

$$SNR = \frac{\mu}{\sigma} \quad \dots (6)$$

The number of looks used to generate the image is usually, known as " N "; otherwise, the number of looks of each simulated image can be estimated as follow[11]:

$$ENL = (SNR)^2 \quad \dots (7)$$

RESULTS AND DISCUSSION

The current implementation is done by using Microsoft Visual Basic program, which can be described by the next block diagram:

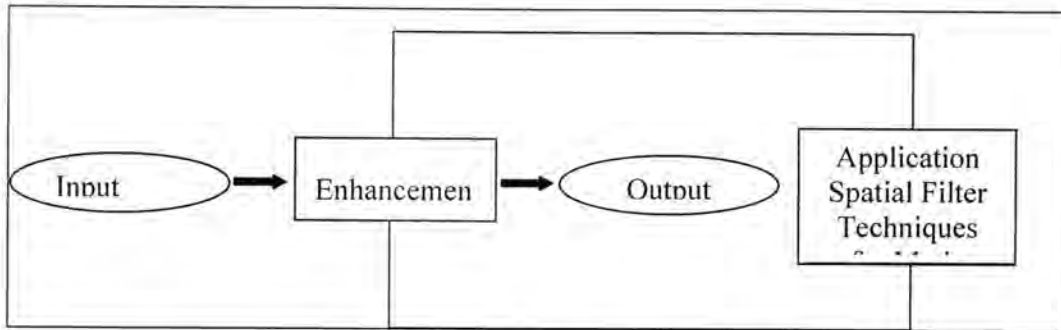


Fig.1:- Block Diagram Represents the Traditional Filtering Techniques

We can illustrate the figure as follows:

- 1- Input image.
- 2- Define spatial mask.
- 3- Determine block size (we use 5×5).
- 4- Calculate central pixel value.
- 5- Replace the mask windows central pixel value by the: point's value of the greatest repeated (for Mode filter).
- 6- The output is the smoothing image.
- 7- End algorithm.

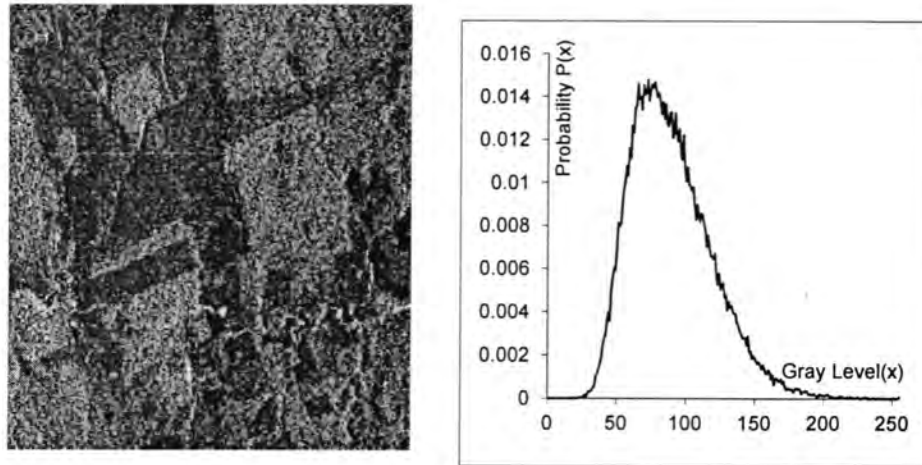
It should be noted that; the traditional smoothing filter adopted in this research, have been performed by utilizing a smoothing window of size 5×5 . The results are demonstrated in figure (2), where these represent the smoothing results for SAR image by using with window size 5×5 , with the histograms of this smoothing SAR images.

The original image used is a (Amplitude SAR)(ASAR), image, polarization, amplitude data, three nominal look and resolution of approx., obtained on 9/26/96. The grays ranged between 0 to 255. It is presented in figure (2-a). The image is from the surrounding of the Tapajo's National Forest/Para', Brazil. In this site, several forest areas have been cleared and converted into pasture and agricultural fields or abandoned. The equivalent number of looks was estimated as 4.76, using samples selected from homogeneous areas [12].

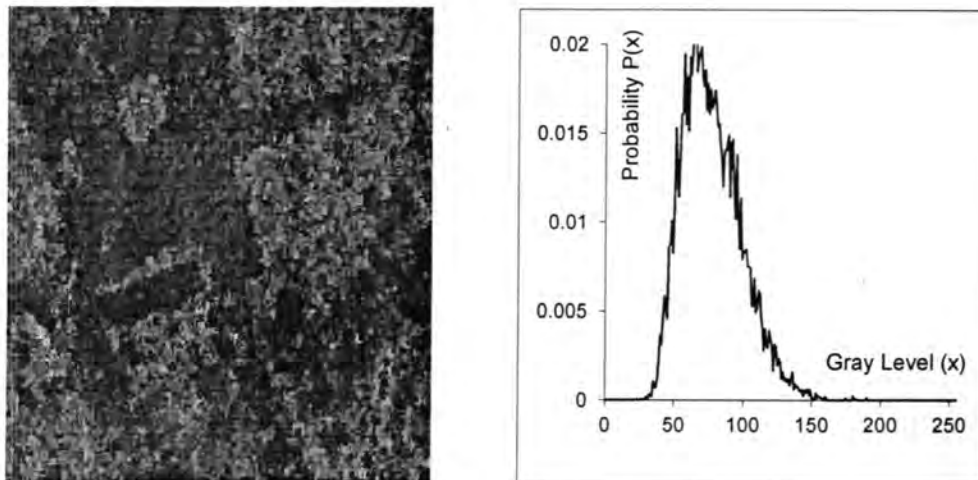
Also figure (3) show the relationship between (ENL and SNR) from: (a)- Original SAR image. (b)- Smothing image with window size 5×5 .

Tables (1) show the statistical analysis estimators: Mean, Variance, Equivalent Number of Look (ENL), and the Signal to Noise Ratio (SNR) Values for Original Image and Smoothing Images Obtained by Mode Filter.

- From the results obtained it can be prove that the speckle noise represents a multiplicative noise.



A

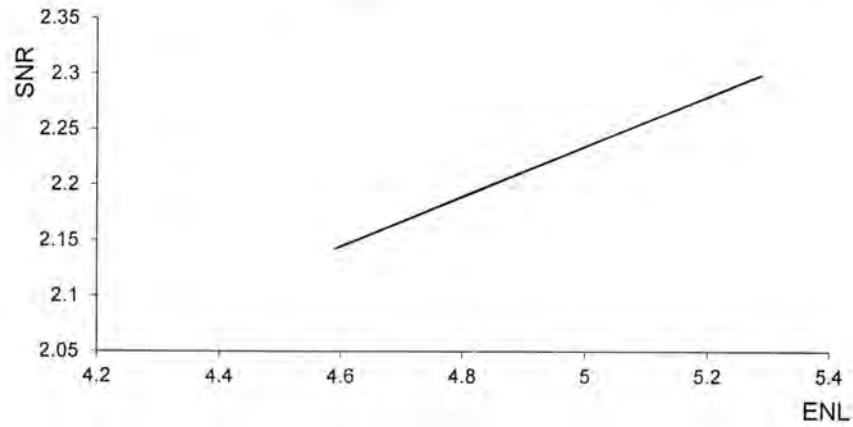


b

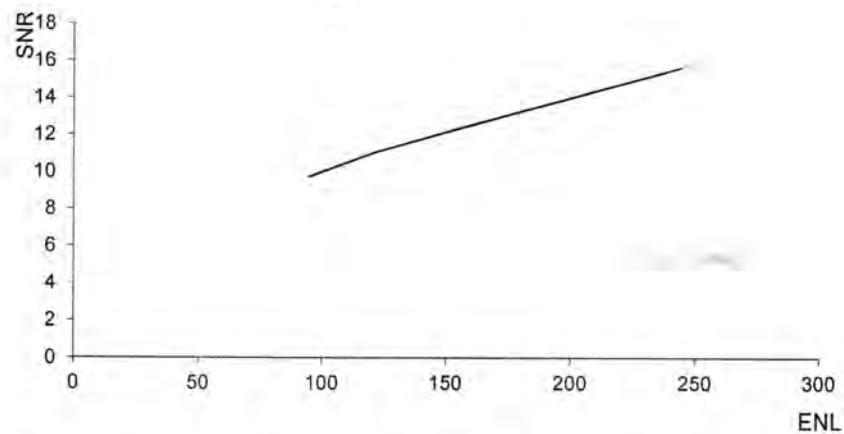
Figs-2: The smoothing result of the SAR image

(a)- The original image.

(b)-The smooth image by use Mode filter with window size (5×5).



a



B

Figs-3: The relationship between (ENL and SNR) from: (a)- Original SAR image. (b)- Smothing image with window size (5x5).

- After adopting these filters we can see: If the filter performance is compared with the histogram of the original image, shown in figs.(2-a), the better smoothing performance is achieved when the filter is implemented on SAR image.

Table -1:

Original Synthetic Aperture Radar Image				
Block No	Block color = Bright Block		Block Size = 20	
	Mean	Variance	ENL	SNR
1	115.405	820.491	4.431	2.105
2	114.500	707.264	5.060	2.249
3	113.145	757.844	4.611	2.147
4	112.000	745.355	4.594	2.143
5	106.580	586.448	5.287	2.299
6	103.795	618.268	4.757	2.181

Original Synthetic Aperture Radar Image				
Block No	Block color = Dark Block		Block Size = 20	
	Mean	Variance	ENL	SNR
1	75.360	241.505	6.419	2.533
2	70.597	274.684	4.953	2.225
3	71.300	279.974	4.957	2.226
4	71.207	272.304	5.083	2.254
5	71.107	242.971	5.681	2.383
6	63.482	179.220	6.138	2.477

Smoothing Simulation (5-Look) Intensity Blood Image By Use Mode Filter				
Block Size = 20		Window size = (5×5)		
Block No	Block color = Bright Block			
	<u>Mean</u>	Variance	ENL	SNR
1	176.937	4733.320	6.614	2.571
2	167.665	4369.380	6.433	2.536
3	165.785	4081.797	6.733	2.594
4	152.797	4173.191	5.594	2.365
5	146.360	3700.436	5.788	2.406
6	139.087	3554.101	5.443	2.333

Smoothing Simulation (5-Look) Intensity Blood Image By Use Mode Filter				
Block Size = 20		Window size = (5×5)		
Block No	Block color = Bright Block			
	<u>Mean</u>	Variance	ENL	SNR
1	54.910	671.921	4.487	2.118
2	48.920	208.853	11.458	3.385
3	48.920	208.853	11.458	3.385
4	47.730	969.177	2.350	1.533
5	45.050	462.927	4.384	2.093
6	38.320	1127.458	1.302	1.141

REFERENCES

- 1- Gonzales R., and Woods R., "Digital Image Processing", Pearson Education International Prentice Hall, Inc. 3rd Edition, (2008).
- 2- Jason L. M., Marwan Y. A. and Evan H., "Advanced Image Processing With DirectX®9 Pixel Shaders"; 3D Application Research Group ATI Research, From ShaderX² –Shader Programming Tips and Tricks with DirectX9, edited by Wolfgang Engel, (2003).
- 3- Awcock G. J., "Technology and Applications of Radar, and Tomographic Medical Image Acquisition Systems", Electronics and Communication Engineering Journal, June (1998).
- 4- FjØrtoft R., Lopês, A. J. B., and Marthon P., "Optimal Edge Detection and Edge Localization In Complex SAR Images With Correlated Speckle", IEEE Transactions on Geoscience and Remote Sensing, 73, (5), pp. 3-5, September, (1999).
- 5- Al-Zuky A. A. D., "Quantitative Analysis of Synthetic Aperture Radar Images", Ph.D Thesis Physics Dept., College of Science, Baghdad Univ., (1998).
- 6- Al-Amrri S. J. K., "Maximum A Posteriori Filter For Restoration Speckle Images", MSC. Thesis, Physics Dept., College of science, Baghdad Univ. (2000).
- 7- Umbaugh S. E., "Computer Vision and Image Processing: A Practical Approach Using CVIP Tools", Prentice Hall PTR, Upper Saddle River, NJO7458,(1998).
- 8- Sloan A., "Image Recognition With Poor Quality Imagery ", Advanced Imaging, Vol. 18, pp. 8-9, and 37, March (2008).
- 9- Goodman J. W.; "Speckle Phenomena in Optics: Theory and Applications", J. Opt. Soc. Am., (2007).
- 10- Baraldi A. and Parmiggiani F.; "A Refined Gamma MAP SAR Speckle Filter With Improved Geometrical Adaptivity", IEEE Transaction on Geoscience and Remote Sensing, 33, (5),pp. 1-5, September (1995).
- 11- Mohammad E. J.; "Digital Filters For Speckle Noise Reduction", M. SC. Thesis Submitted to The College of Science, Al-Mustansiriyah University, (2001).

- 12- Frery A. C., Yanasse C. F., Vieira P. R., Sidnei J. S., and Renno C. D.; "A User-Friendly System for Synthetic Aperture Radar Image Classification Based on Grayscale Distributional Properties and Context", Anais do X SIBGRAPI, p.p. 1-8, (1997).

Determination of the Energy Spectrum and Mass Composition Based on Cherenkov Light Lateral Distribution Function

Sarah Hussein Ali and Ahmed A. Al-Rubaiee

Al-Mustansiriyah University, College of Science, Department of Physics

Received 23/11/2019– Accepted 14/11/2010

الخلاصة

في هذا العمل تم استخدام دالة مقترحة لتقريب دالة التوزيع الفراغي لضوء جيرينكوف للبروتون و نوى الحديد ضمن مدى الطاقة 10^{16} - 10^{13} إلكترون فولت و لثلاث زوايا 0 و 10 و 20 و مقارنه النتائج النظرية لاشعاع جيرينكوف مع النتائج العملية في منظومه Tunka-25 لنفس الجسيمات و مدى الطاقة وأظهرت المقارنة توافقاً جيداً ضمن مدى الطاقة المذكور.

ABSTRACT

In this work we used a proposed function for parameterization of Cherenkov light LDF for primary proton and iron nuclei in the energy range 10^{16} - 10^{13} eV for three zenith angles 0° , 10° and 20° and we compare the approximated results for Cherenkov light with measured of Tunka-25 array for same particles and rang energy and this comparison papered a good agreement in this energy range.

INTRODUCTION

The nature of Galactic sources of high energy cosmic rays is not clear, despite of essential progress in the theory of their acceleration and propagation [1]. Extensive Air Shower was first detected by measuring the number of electrons in the EAS reaching the surface of the earth. The most reliable method of cosmic rays energy measurement in the specified energy range is the method of EAS Cherenkov light observation. A series of such experiments are carried out in Tunka Valley (50km from Lake Baikal) since more than 10 years like: Tunka-4 [2], Tunka-13 [3] and Tunka-25 [4].

In this work we will preformed the approximated LDF of Cherenkov light and the results of the experimental data of Tunka-25 array for (p and Fe) for zenith angles 0° , 10° and 20° at energy range 10^{13} - 10^{16} eV

Approximate Calculations for Lateral Distribution Function:

The lateral distribution function (LDF) is the function that describes the lateral variation of Cherenkov flux with the core distance. The lateral distribution function is widely used in event reconstruction, aiming to obtain information about primary particle. Integration over the total range of core distance of LDF results in the shower size, i.e., the total number of particles [5].

For Approximation of simulated Cherenkov light LDF, we used the proposed function [5] as a function of the distance R from the shower axis and the energy E_0 of the initial primary particle, which depends on four parameters a, b, σ, r_0 :

$$Q(E_o, R) = \frac{C \exp[a - (R/b + (R-r_o)/b + (R/b)^2 + (R-r_o)^2/b^2)]}{b[(R/b)^2 + (R-r_o)^2/b^2 + R\sigma^2/b]} [\text{m}^{-2}], \quad (1)$$

where $C = 10^3 \text{ m}^{-1}$; R is the distance from the shower axis; a, b, σ, r_o are parameters of Cherenkov light LDF.

The calculations for Cherenkov light LDF are performed for primary proton and iron nuclei in the energy rang 10^{16} - 10^{13} eV. We found an energy dependence of the parameters a, b, σ, r_o that allows us to calculate the Cherenkov light LDF for any primary energy. This energy dependence of LDF parameters is approximated as:

$$k(E_o) = c_o + c_1 \log(E_o/1\text{eV}) + c_2 \log^2(E_o/1\text{eV}) + c_3 \log^3(E_o/1\text{eV}), \quad (2)$$

where $k(E_o) = a, \log(\gamma/1\text{km}), \log \sigma, \log(r_o/(1\text{km}))$, and c_o, c_1, c_2, c_3 are coefficients, were obtained by using the procedure of approximation for LDF parameters depending on the type of the primary particles (p, Fe) at $\theta = 0, 10$ and 20 .

TUNKA-25 ARRAY OF EAS REGISTRATION

The Tunka EAS Cherenkov array is located in Tunka Valley in Russia, 25 detectors arranged in the square of $340 \times 340 \text{ m}^2$, 85m in distance between each detector, at 675 m above sea level (see figure (1)) [3].

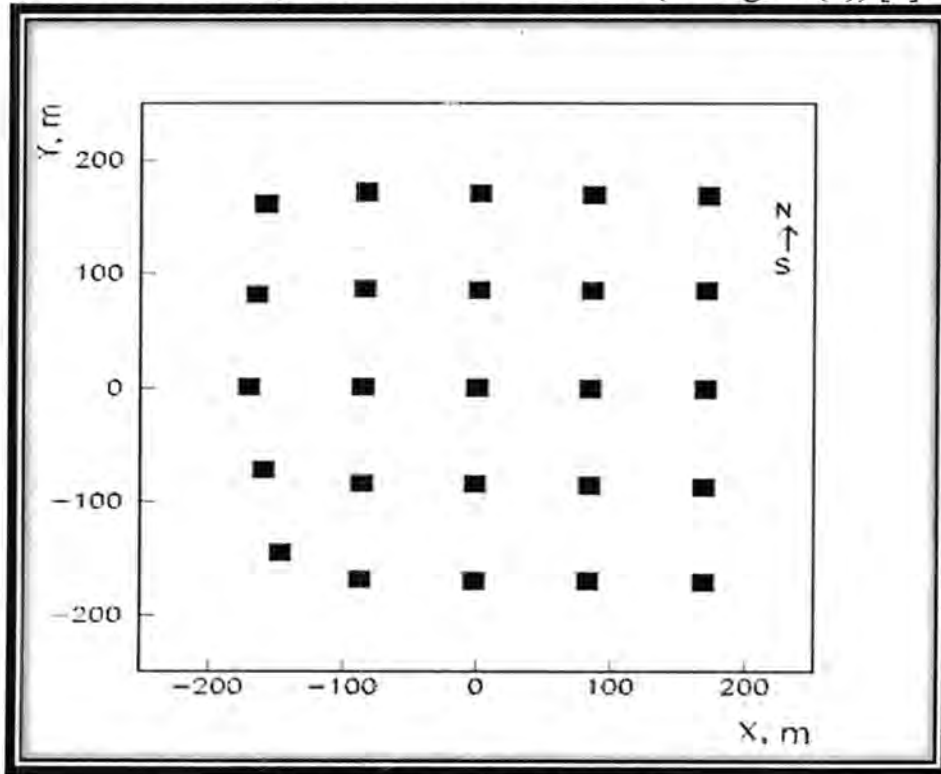


Figure -1: TheTunka-25 array [3]

The wide-angle Tunka-25 Cherenkov array designed for studying the CR spectrum and the mass composition near the "knee". Tunka-25 consists of 25 detectors which consist of an electro-optical preamplifier with a hemispherical photocathode, and 4 detectors with pulse shape [6].

COMPARISON OF CHERENKOV LIGHT WITH EXPERIMENTAL DATA

The method of EAS core location reconstruction is based on fitting of the Q_i data by LDF function with light density at core distance 175 m [7] when:

$$Q_{(R)} = Q_{kn} f(R), \quad (3)$$

Q_{kn} is the light flux at the distance R_{kn} [7], which is given as:

$$Q_{kn} = Q_{175} \left(\frac{R_{kn}}{175} \right)^{-2.2}, \quad (4)$$

and:

$$f(R) = \begin{cases} \exp\left(\frac{(R_{kn}-R)}{R_0}\left(1 + \frac{3}{R+3}\right)\right), & R < R_{kn} \\ \left(\frac{R_{kn}}{R}\right)^{2.2} & 200 \geq R \geq R_{kn} \\ \left(\frac{R_{kn}}{200}\right)^{2.2} \left(\left(\frac{R}{200} + 1\right)/2\right)^{-b}, & R > 200 \end{cases}, \quad (5)$$

where R is the core distance (in meters), R_0 is a parameter of the first branch of LDF and R_{kn} is the distance of the first change of LDF, R_0 and R_{kn} are given by [7]:

$$R_0 = \exp(6.79 - 0.56P), \quad (6)$$

$$R_{kn} = 207 - 24.5P \quad (7)$$

where the steepness P is given by [8] :

$$P = 7.3 - (0.008 \times \Delta X), \quad (8)$$

and

$$\Delta X = X_0 - X_{max}, \quad (9)$$

where $X_0 = 955 \text{ g.cm}^{-2}$ (The total vertical depth of the atmosphere); and X_{max} is the depth of the shower maximum development which is given by [5]:

$$X_{max} = 560 + 65 \log\left(\frac{E_0}{10^{16} \text{eV}}\right) \quad (10)$$

The parameter b in eq. (5) can be defined as [7]:

$$b = \begin{cases} 4.48 - 12.3 \ln(6.5P), & P < 6 \\ 3.43, & P \geq 6 \end{cases} \quad (11)$$

The comparison of the approximated LDF of Cherenkov light with the measured LDF with Tunka-25, have been successfully performed for primary proton and iron nuclei with the energy range 10^{13} - 10^{16} eV and for three zenith angles 0° , 10° and 20° .

RESULTS AND DISCUSSION

In figure (2) the comparison between the approximated Cherenkov light LDF with that measured with Tunka-25 array was presented for primary showers for iron nuclei at energies 10^{14} , 2.10^{14} and 5.10^{14} eV.

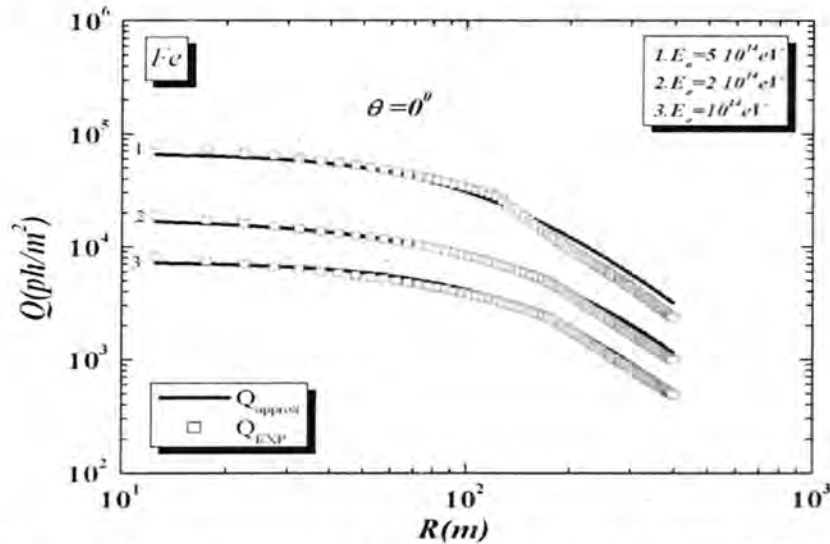


Figure -2: Comparison of the approximated Cherenkov light LDF (solid line) with the data obtained for the Tunka-25 (square line) for iron nuclei at ($\theta = 0^\circ$), at energies 10^{14} , 2.10^{14} [6] and 5.10^{14} [7]eV.

The figure (3) shows the comparison between the approximation LDF (solid line) and measured LDF (square line) of Tunka-25 for primary proton at energy range 10^{13} - 10^{16} eV.

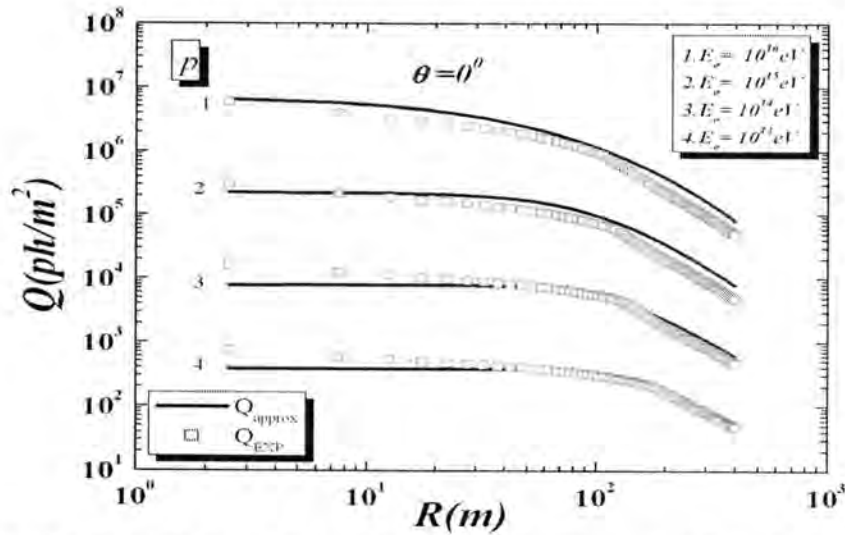


Figure -3: Comparison of the obtained LDF approximation (solid line) and measured LDF (square line) of Tunka-25 for vertical angle for (a) proton at energies 10^{13} [6], 10^{14} , 10^{15} and 10^{16} eV [7].

The figures (4-6) describe the obtained LDF (solid line) and measured LDF (square line) of Tunka-25 for different energies at zenith angle 10° and 20° for primary proton and iron nuclei.

In figure (4) one can see the result of the approximated LDF of Cherenkov light (solid line) and measured LDF (square line) of Tunka-25 for primary proton at zenith angle 10° in energy range 10^{13} - 10^{16} eV.

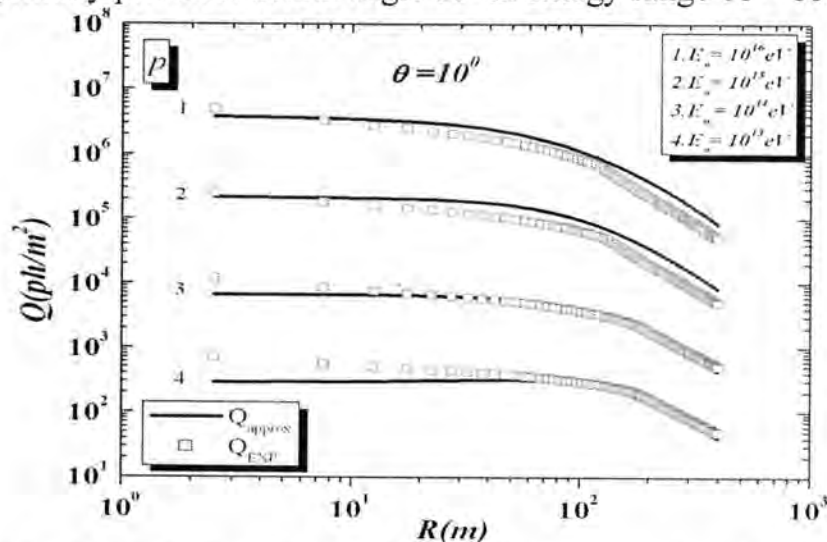


Figure -4: The approximated LDF of Cherenkov light (solid line) and measured LDF (square line) of Tunka-25 for proton at zenith angle 10° for energies 10^{13} , 10^{14} [8], 10^{15} and 10^{16} eV [7].

The comparison between the approximated LDF of Cherenkov light (solid line) and measured LDF (square line) of Tunka-25 is preformed in

figure (5) for iron nuclei at zenith angle 10° in energies 5.10^{13} , 5.10^{14} and 5.10^{16} eV.

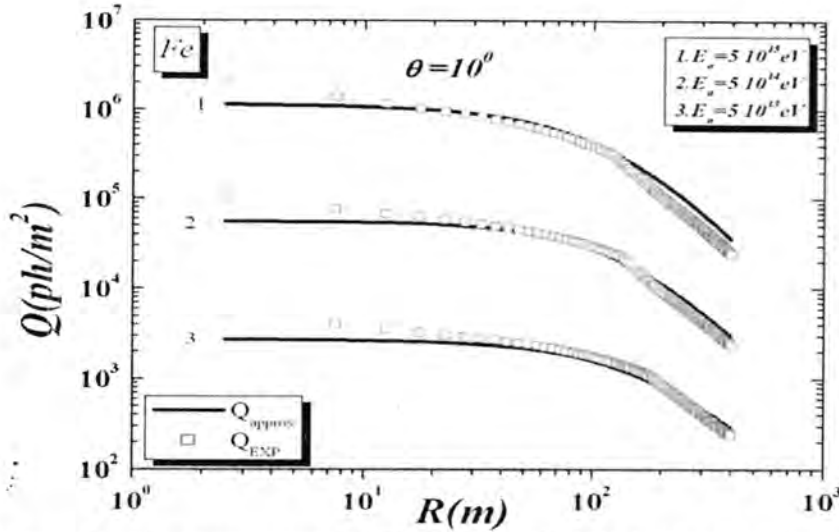


Figure -5: The approximated LDF of Cherenkov light (solid line) and measured LDF (square line) of Tunka-25 for iron nuclei at zenith angle 10° for energy 5.10^{13} [6], 5.10^{14} and 5.10^{15} eV [7].

The figure (6) displays the difference between the primary proton and the iron nuclei initiated EAS (solid line) in comparison with the Tunka-25 (square line) at the energy range 10^{14} - 10^{16} eV for $\theta = 20^\circ$.

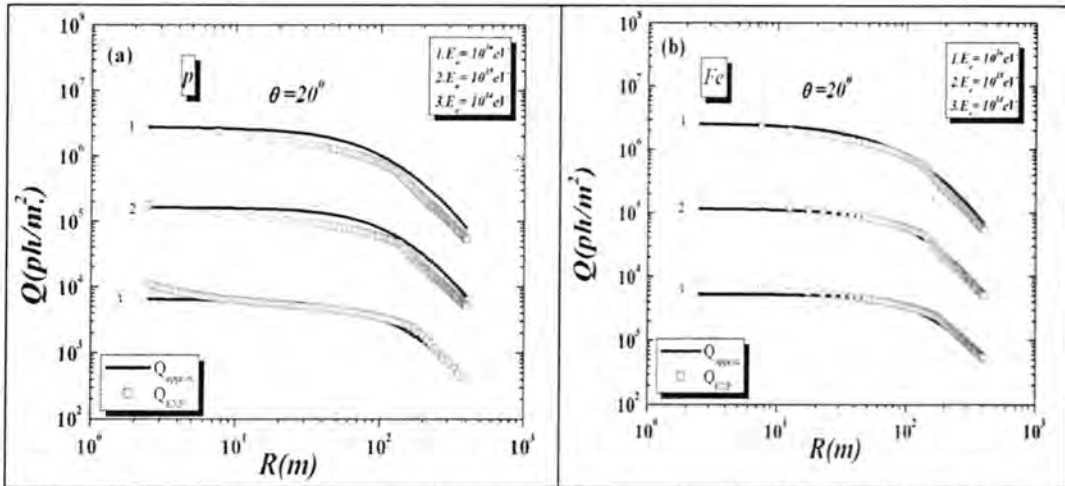


Figure -6: Comparison of the obtained approximation (solid line) of LDF and measured LDF (square line) of Tunka-25 for zenith angle 20° (a) proton at energies 10^{14} [8], 10^{15} and 10^{16} eV [7], (b) Iron nuclei at energies 10^{14} [8], 10^{15} and 10^{16} eV [7].

From Figs. (2-6) one can see that the lateral distribution function of Cherenkov light is directly proportional with energy of the particles as a result of the ionization of energy loss of these particles and we observed that the Cherenkov radiation is decreased depending on the distant (R) from the shower axis as a result of the energy loss of particles. Also we observed a fluctuation in the end of the curves, especially at the lowest energy 10^{13} eV because of the straggling of the charge particles

We conclude that the main advantage of the given approach consists of the possibility to make a library of lateral distribution function samples which could be utilized for analysis of real events which detected with the Extensive Air Shower array and reconstruction of the primary cosmic rays energy spectrum and mass composition.

REFERENCES

1. Anatoly Erlykin, Romen Martirosov and Wolfendale A.W. The Origin of Cosmic Rays// CERN Cour. 51, 1. 21-23 (2011).
2. Bryanski S.V., Vasilchenko Y.V., Gress O.A. et al. The Energy Spectrum of Primary Cosmic Rays by the Data of Tunka Cherenkov Array // Proc. 24th ICRC, Roma, 2,724 (1995)
3. Budnev N., Chernov D., Galkin V. et al.: Tunka EAS Cherenkov array, Hamburg, 7-15 Aug. 581-584 (2001).
4. Budnev N.M., Chernov D.V., Gress O.A. et al. Cosmic ray energy spectrum and mass composition from 10^{15} to 10^{17} eV by data of the Tunka EAS Cherenkov array // Proc. 29 ICRC, Pune, India (Aug. 03-10, 2005). Tata Institute of Fundamental Research, Mumbai, 6., 257-260 (2005).
5. Matthews, J.: A Heitler model of extensive air showers. Astro. Phys. 22. 387-397 (2005).
6. Budnev N.M., Chernov D.V., Gress O.A. et. al., The Tunka experiment: towards a 1-km² EAS Cerenkov light array in the Tunka valley. Int. J. Mod. Phys. A. 20, 6796-6798 (2005).
7. Prosin V.V., Budnev N.M., Chvalaiev O.A. et. al., The Cosmic Ray Mass Composition in the Energy Range 10^{15} - 10^{18} eV measured with the Tunka Array: Results and Perspectives// Nucl. Phys. Proc. Suppl., 190, 247-252 (2009).

8. Chernov D., Kalmykov N., Korosteleva E. The Tunka Experiment:
Towards a 1-km² Cherenkov EAS Array in the Tunka Valley // Int. J.
Mod. Phys. A., 1, 1-3, (2004).

Study the Effect of Thermal Annealing on Structural Properties of PbSe Thin Films Prepared by Thermal Evaporation in Vacuum

Usama A. A. Dakhel, Hanan A. Naif, and Hala F. Dagher
Al-Mustansiriyah University, College of Science, Physics Department

Received 20/6/2010 – Accepted 2/3/2011

الخلاصة

في هذا البحث تم دراسة تأثير التلدين الحراري على الخصائص التركيبية لأغشية PbSe الرقيقة المحضرة على قواعد زجاجية بدرجة حرارة الغرفة بواسطة طريقة التبخير في الفراغ تحت ضغط 10^{-5} Torr بعد ذلك تم تلدينها بدرجات حرارة مختلفة لمدة ساعة لكل عينة. تم دراسة الخصائص التركيبية للنماذج المحضرة بواسطة جهاز حيود الاشعة السينية، حيث استعملت نماذج الحيود لتحديد حجم الحبيبة وحسب معادلة شيرر تم حساب العوامل التركيبية مثل المطاوعة (ϵ)، كثافة الانخلاعات (ρ) وذلك حسب العلاقات الرياضية التي تربطها بالحجم الحبيبي.

ABSTRACT

In this paper the effect of thermal annealing on the structural characterization of PbSe thin films were studied. The thin films were deposited on glass substrates at room temperature using thermal technique under the pressure of 10^{-5} Torr, later they were annealed at different temperatures for one hour.

The structural characteristics of the prepared samples were investigated by using X-ray diffraction (XRD) technique, it is used to determine the crystalline structure. The grain size of the films (D) were determined from the XRD pattern of the prepared films according to Sherrer's equation. Other structural parameters were calculated such as microstrain (ϵ), and dislocation density (ρ) using a mathematical relations related each parameter with the grain size.

INTRODUCTION

Lead selenide (PbSe) can be classified as a semiconductor material, as an important material for applications such as IR detectors, photographic plates, and photoresistors(1), thermoelectric cooling materials and solar cells (2,3,4). Among the group (IV-VI) compounds, lead selenide (PbSe) thin film is used as a target material in infrared sensor, grating(2,5). It has a cubic crystal structure (and a direct narrow band gap of (0.27eV) in room temperature(1,6,7). The energy level spacing can be even larger than the bulk band gap. The similar and small effective masses of both the electrons and the holes imply that this strong confinement effect is split equally between electrons and holes so that the electronic structure is simple.(8)

There are several methods for the preparation of selenides including solid state reaction(9), electrochemical methods(10), microwave assisted preparation(11), chemical path deposition(12), high temperature pyrolysis of single source precursors(13), vacuum deposition(14), H₂Se methods(15), and photochemical methods(16).

Vacuum deposition has several advantages, it may be used on a large area and the physical properties of the films can easily be controlled by the deposition condition (e.g. deposition rate, temperature and thickness)(17).

Most semiconductor crystals share a common basic structure. The crystal structure begins with a cubic arrangement of 8 atoms. This cubic lattice extended to a face-centered cubic (fcc) lattice, by adding an atom to the center of each face of the cube (leading to a lattice with 14 atoms).

The full lattice structure combines two of these fcc lattices, one lattice interpenetrating the other(18).

Crystallographic directions and planes are important in both the characteristics and the applications of semiconductor materials since different crystallographic planes can exhibit significantly different physical properties.

Standardized rotation of Miller indices is used to define the crystallographic planes and directions normal to those planes. The general crystal lattice defines by a set of unit vectors (a,b, and c) so that an entire crystal can be developed by copying the unit cell of the crystal and duplicating it at integer offsets along the unit vectors(19).

The planes are defined relative to the crystal axes by a set of three integers (hkl) where corresponds to the plane's intercept with the x,y, and z-axis respectively. The direction normal to the (hkl) plane is designated by (hkl)(19).

THEORETICAL PART

X-ray diffraction of PbSe thin films taken from diffractometer is used to analyze various crystalline aspects. According to the Bragg's law:

$$n\lambda = 2d \sin \theta \quad \dots(1)$$

The direction of propagation of scattered beam (θ) is related to the inter planer distance (d) in the lattice (hkl) which represents the property of the material and related with the lattice constant and miller indices(20).

The predominant growth of crystallites perpendicular to (111) plane, gives rise to the rock salt cubic structure of PbSe as indicated in the ASTM(21), these results are agreed with other studies (1,22).

This fact indicates that the degree of crystallinity is found to be more pronouncing in films, the lattice parameter (a) is calculated in this case by means of the plane-spacing equation for cubic crystal, which is given by(1):

$$\frac{1}{d^2} = \frac{h^2 + k^2 + l^2}{a^2} \quad \dots(2)$$

and the grain size is calculated by using the Scherer's formula, (23)

$$D = \frac{K\lambda}{\beta \cos \theta} \quad \dots(3)$$

Where:

K: is the shape factor

λ : is the wavelength of the X-ray

θ : is the Bragg's angle

β : is the corrected FWHM for instrumental broadening

A dislocation is an imperfection in a crystal associated with the misregistry of the lattice in one part of the crystal with that in another part. Unlike vacancies and interstitial atoms, dislocations are not equilibrium imperfections, i.e. thermodynamic considerations are insufficient to account for their existence in the observed densities.

In fact, the growth mechanism involving dislocation is a matter of importance.

In the present study, the dislocation density estimated from Williamson and Smallman method using the relation (24).

$$\rho = 15\varepsilon / aD \quad \dots(4)$$

The origin of the strain is also related to the lattice misfit which in turn depend upon the deposition conditions. The microstrain (ε) developed in the PbSe film is calculated from the relation(25):

$$\varepsilon = (\beta \cos \theta) / 4 \quad \dots(5)$$

EXPERIMENTAL PART

The experimental arrangement is permitted to prepare thin film samples by thermal vacuum evaporation technique on a glass substrate using a molybdenum boat, at vacuum of 10⁻⁵ Torr(Edward) . Lead selenide powder is used with the parity of 99.90% and the melting point is equal (1078 °C) produced from Koch Light Lab. UK. The thickness of the films measured by use weight method, some films were annealed (at 100,200)°C because the best crystalline structure obtained in this temperatures.

The structural analysis is performed by X-ray diffraction, using graphite-monochromatized Philips (pw1710) with filtered CuK α radiation ($\lambda=1.5418\text{\AA}$) as X-ray source at 40Kv and 20mA in the scanning angle (2θ) at R.T .

RESULTS AND DISCUSSION

The grain size was determined according to XRD pattern and due to eq.(3). The (XRD) pattern for PbSe thin films of thickness (600Å) as shown in Fig.(1).

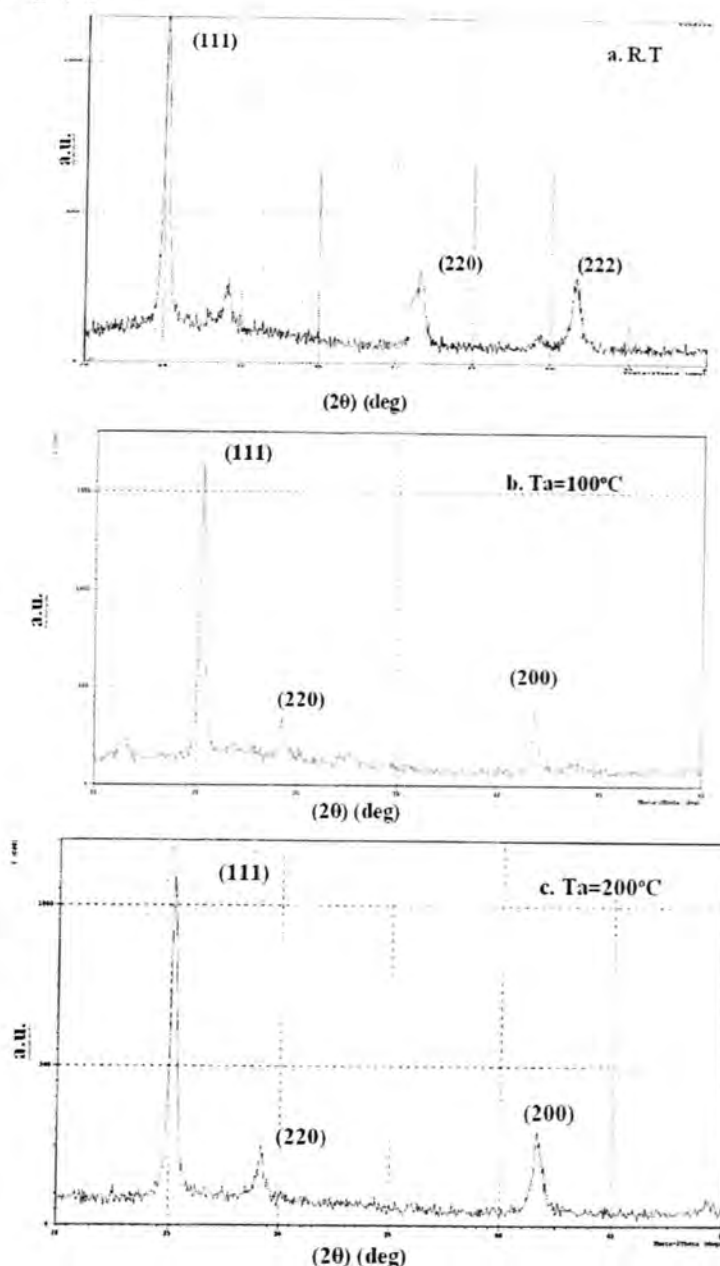


Figure -1: X-ray diffraction of vacuum evaporated PbSe thin film of thickness (600Å) at (a) R.T. before annealing (b) after annealing at 100°C, (c) after annealing at 200°C

From this figure it is observed that the featureless spectra of the films deposited at substrate temperature reveal that the films process polycrystalline structure whereas the presence of peak in the (111). Also, observed from this figure, PbSe films were found to exhibit two diffraction peaks associate with (111), at room temperature (220) (222)

and (220) (200) in annealing temperatures (100, 200) $^{\circ}$ C. This peaks reflections of which the intensity of the (111) orientation is predominant.

The presence of large number of peaks indicates that the film is polycrystalline in nature.

Table (1) shows the comparison between the theoretical results according to the ASTM with the experimental results obtained from this study.

Table -1: Comparison between the theoretical and experimental results for PbSe thin films

hkl	2 θ Exp.	2 θ ASTM	d (Å) Exp.	d(Å) ASTM
R.T	25.143	25.164	3.539	3.536
100 $^{\circ}$ C	25.191		3.532	
200 $^{\circ}$ C	25.296		3.517	

The lattice parameter (a), grain size (D), dislocation density (ρ) and microstrain (ϵ) for the orientation peak (111) are given in the table (2).

Table -2: Structural parameters of PbSe thin films

T($^{\circ}$ C)	hkl	d (Å)	2 θ	Lattice constant(a) (nm)	FWHM (β)(rad)	Grain size (D)(nm)	Dislocation density (ρ) (lines/cm) $\times 10^{-5}$	Microstrain (ϵ)
R.T	111	3.539	25.143	6.129	0.404	21.008	0.226	0.00172
	220	2.168	41.621	6.132	0.594	14.931	0.448	0.00242
	222	1.769	51.599	6.131	0.589	15.631	0.409	0.00231
100 $^{\circ}$ C	111	3.517	25.296	6.093	0.2782	30.5789	0.118	0.00106
	220	2.157	41.846	6.101	0.2868	30.9853	0.116	0.00104
	200	3.052	29.236	6.104	0.2965	28.9317	0.125	0.00119
200 $^{\circ}$ C	111	3.532	25.191	6.118	0.3298	25.789	0.140	0.00150
	220	2.163	41.707	6.120	0.4199	21.153	0.171	0.00223
	200	3.058	29.172	6.117	0.2819	30.426	0.118	0.00108

From this table, it is observed that increase in grain size with increasing the annealing temperature (T_a =R.T and 100 $^{\circ}$ C), thus, there is a decrease in the density of nucleation centers, and under these circumstances, a smaller number of centers start to grow this is due to crystallization of the structure while the decreasing in the grain size at (T_a =200 $^{\circ}$ C) happened due to the defect such as the dislocation.

Also, it can be noticed that the lattice constant (a) is approximately equal the theoretical value (a =6.124) which was obtained from ASTM.

It is observed that FWHM decrease with increasing the inter planer distance (d). This decrease in the value of FWHM indicates increase in grain size or decrease in the dislocation density and microstrain. This results agree with study⁽¹⁾.

Figure (2) shows the effect of annealing temperature on the grain size, dislocation density and microstrain.

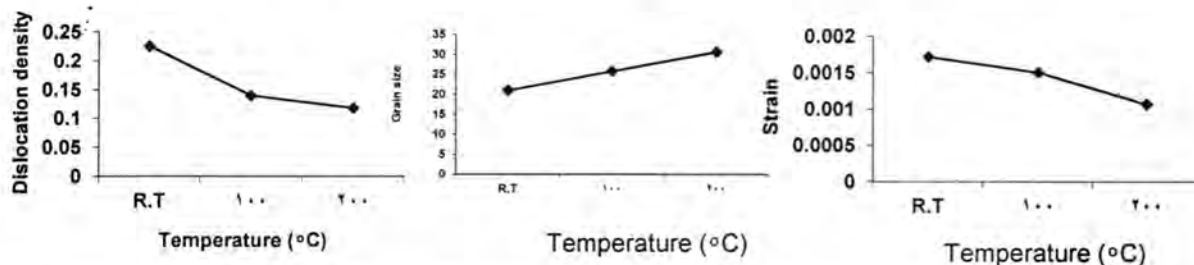


Figure -2: The effect of annealing temperature on the grain size, dislocation density and microstrain.

After annealing, all the samples showed better directional ordering. When the annealing temperature was over (200)°C, the particles showed contact to each other and formed nanoarrays. The duration of the thermal annealing (1 hour)

From the present study, it can be concluded that the PbSe thin film is uniform and having good adherence with the substrate surface. XRD analysis confirms the cubic structure of the substance with predominant (111) orientation and addition to other two prominent planes in annealing temperatures (R.T., 100, 200)°C.

The grain size increase with the annealing process, and the FWHM decrease with increasing the inter planer distance (d), and this decreasing of FWHM indicates decrease in the dislocation density and microstrain.

REFERENCES

1. Prabahar, S.; Suryanarayanan, N.; Rajasekar, N.; Srikanth, S. "Lead selenide thin films from vacuum evaporation method – structural and optical properties" *Chalcogenide letters*, 6, 5, May: 203-211(2009).
2. Badr, X.; Maahmoud M.A. "Size-dependent spectroscopic, optical, and electrical properties of PbSe nanoparticles", *Egypt, cryst. Res. Technol.* 41, 7: 658-663 /DOI 10.1002/crat.200510645(2006).
3. Das, D.V., Bhat, K.S., *J.Mater.Sci.* "Materials in Electronics I", 169 (1990).
4. Law, M.; Luther, J. M.; Song, Q.; Hughes, B.K.; Perkins, C.L.; Nozik, A. J. "Structural, optical, and electrical properties of PbSe nanocrystal solids treated thermally or with simple amines". *National Renewable energy laboratory, Golden, Colorado 80401, J.Am.Chem.Soc.*, 130 : 5974-5985(2008).
5. Ali, M.S.; Khan, K.A.; Khan, M.S.R.; "Temperature effect on the electrical properties of Pb" *Phys. Status. Solidi. (a)* 149, 611 (1995).

6. Gautier, C.; Breton, G.; Averous, M.; "Study of PbSe layer oxidation and oxide dissolution" J. Electrochem. Soc. 145, 512 (1998).
7. Wise, F.W. "Lead-salt quantum dots: the limit of strong quantum confinement" Acc. Chem. Res. 33, 773 (2000).
8. Cui, Y. "Lead chalcogenide Nanowires and hyperbranches for multiexciton generation solar cells" MRS spring meeting, Symposium D.D, San Francisco, California, Apr. 12, (2007).
9. Coustal, R.; J. Chem. Phys. 38, 277 (1958).
10. Xu, D.S.; Shi, X.S.; Guo, G.L.; Gui, L.; Tang, X.Q. "Electrochemical preparation of CdSe nanowire arrays" J. Phys. Chem. B 104, 5061 (2000).
11. Wang, X.; Tang, Z.; Correa-Duerre, M. A.; Pastorize-Santo, I.; Giersig, M.; Kotov, N.A.; Liz-Marzan, L.M. "Mechanism of strong luminescence photoactivation of citrate-stabilized water-soluble nanoparticles with CdSe cores" J. Phys. Chem. B 108, 15461 (2004).
12. Lokhande, C.D.; Patil, P.S.; Tributsch, H.; Ennaoui, A. "ZnSe thin films by chemical bath deposition method". En. Mater. Sol. Cell. 55, 379 (1998).
13. Ptatschek, V.; Schreder, B.; Herz, K. "Sol-Gel Synthesis and Spectroscopic Properties of Nanocrystalline CdSe-Films" J. Phys. Chem. B 101, 8898 (1997).
14. Prabahara, S.; Suryanarayanan, N.; Balasubramanian V.; Srikanth, S.; Kathirvel, D. "Photoluminescence studies on lead selenide thin films from thermal evaporation" Arch. Appl. Sci. Res., 2 (5): 292-297 Coimbatore, India (2010).
15. Metcalf, H.C. ; Williams, J.E.; Caskta, J.F. "Modern Chemistry"; Holt, Reinhart, Winston, New York, P.54 (1982).
16. Zaho, W.; Zhu, J.; Chen, H.; "Photochemical preparation of rectangular PbSe and CdSe nanoparticles" J. Cryst. Growth 252, 587 (2003).
17. Ibrahim, A.A.; El-Sayed, N.Z.; Kaid, M.A.; Shour, A.A. "Structural and electrical properties of evaporated ZnTe thin films" Physics Department, Faculty of Science, Miniauniversity, Minia, Egypt. 75: 189-194 (2004).
18. Tyagi, M.S. "Introduction to semiconductor materials", John Wiley & Sons, New York, (1991).
19. Kuroyanagi, A.A. "Properties of polycrystalline ZnSe thin films grown by ion beam deposition" Appl. Phys 68. 5567, (1990).
20. Zishan, S.; Khan, H.; Majeed, M.A. Khan, Husain, "Studies on thin films of lead chalcogenides". M. Current Appl. Phys. 5, 561, (2005).
21. Molin, A.N.; Dikumar, A.I.; "Thin Solid Films" 265, 3 (1995).

22. Zhou, W.L.; Jibao, H.; Fang, J.; Huyuh, T.; Kennedy, T.J.; Stokes, K.L.; Oconnon, C.J. "Self-assembly PbSe nanoparticles into nanorings". Advanced Materials Research Institute, University of New Orleans, New Orleans, LA 70148, Mat. Res. Soc. Symp. Proc. Vol.775, P. 10.5.1-5.
23. Klug H.P.; Alexander L.E.; "X-ray diffraction procedures for polycrystalline and amor phous materials", 2nd ed. New York: Wiley; (1974).
24. De C.K.; Mishra N.K. Indian, J. Phys. A71, 530, (1997).
25. Hearman R.F.S. "Physics of solid state" (eds) S. Balakrishna M. Krishnamurthi and B Ramachandra Rao (New York: Academic Press), P. 408, (1969).

A Study of the Deposition Angle Effect on the Structural Properties of (CdS) Thin Films

Raad S. Al – Rawie and Hussein Ridha Ahmed

Al- Mustansiriyah University/ College of Science / Department of Physics.

Received 7/11/2010 – Accepted 2/3/2011

الخلاصة

في هذا البحث تم دراسة الخصائص التركيبية لاغشية (CdS) الرقيقة المرسبة على قواعد زجاجية بسلك اغشية وبزاويا ترسيب مختلفة بطريقة التبخير الحراري الفراغي . تم استخدام تقنية حيود الاشعة السينية لدراسة الخصائص التركيبية لاغشية CdS المرسبة بزوايا مختلفة وقد تبين ان الاغشية متعددة التبلور وتظهر قمة ذات شدة انعكاسية عالية عن المستوى (111) . ان زيادة زاوية الترسيب تؤدي الى زيادة شدة الانعكاس عن المستوى (111) وتنقص من الحجم الحبيبي، بينما يؤدي زيادة سمك الاغشية الى زيادة شدة الانعكاس عن المستوى (111) وتنقص الحجم الحبيبي. ان تأثير زيادة زاوية الترسيب اعظم من تأثير زيادة سمك الاغشية على الخصائص المدروسة.

ABSTRACT

In this research, A study of structural properties for (CdS) thin films prepared by thermal vacuum deposition method on glass substrates at different angles and different film thicknesses. The X-ray diffraction technique (XRD) has been used to study the structural properties of (CdS) films deposited at oblique angles and it appeared that the films are polycrystalline, and there is a high intensity peak (111). The increase of deposition angle will increase the reflection intensity of (111) plane and decrease the grain size, while the increasing of film thickness will also increase the reflection intensity of (111) plane but decrease the grain size.

The influence of increasing deposition angle is greater than the influence of increasing films thicknesses on the studying properties.

INTRODUCTION

Cadmium sulfide is member of (II-VI) group of semiconductors CdS has a (yellow – orange) colour, and two – crystal structures, cubic and hexagonal closed Packed (wurtzite) phases. The direct band gap of about 2.4 eV (1) . It exists near the photon energy of maximum solar radiation spectrum, it causes absorption in the short wavelength side, and has a high absorption coefficient within the solar radiation to generate carriers across the band gap with wavelength less than (0.520 μ m) (2). CdS is used as low – cost photovoltaic devices and usually used as a very suitable window layers which are prepared as thin as possible to avoid optical transition losses (2). There are many previous studies on the structural properties of (CdS) thin films as, Rami et.al (2), A.Ashour (3), N.Gaewdang and T.Gaewdang (4), and Korkmaz Sibal (5).

There are many important changes in structural properties in obliquely deposited of many materials as Ag_2S (6), As_2Se_3 (7), Al (8), Cr (9), NiCo (10), Au (11), As_2S_3 (12) and AgCl (13). This changes the keen interest in this field and many workers began intensive studies of the changes occurring in various metal, semimetal and

semi conducting materials in bulk or thin film form. So far, there have been no reports of such studies on (CdS) films.

In this research a studying of structural properties for obliquely deposited (CdS) thin films.

MATERIALS AND METHODS

The Deposition Angle Effect on the Growth and Structure Properties:

The films were coated at angles (θ°) as measured between the line from the sample center to the deposition boat and the line normal to the surface on which deposition occurs Figure (1) (14). In the state of obliquely deposited thin films, a rod or needles form like of high density, separated by low density voids (15,16) then the film density less than the material density in its bulk and the film density decreases with increasing deposition angle (θ°) because the voids between the needle like forms increases when deposition angle increases (17,18). It is postulated that in the initial stages of film formation a random distribution of small crystallites is created on the substrate and each crystallite acts as a nucleus for further growth, thus the region behind the crystallite is prevented from receiving metal vapor because this region is in the shadow of the crystallite.

Therefore, as the crystallite grows into a column, the area behind it is left vacant as far as its shadow extends. The size of the crystallites, the spacing between them and their inclination to the substrate vary for different materials and evaporation conditions (8).

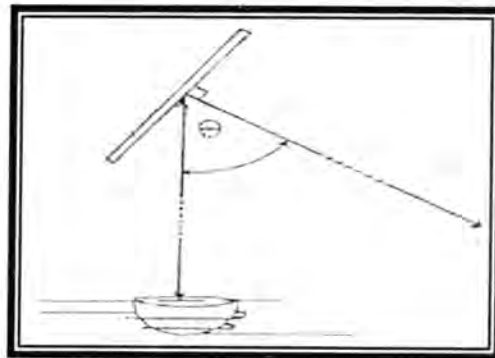


Figure -1: show vapor beam direction on obliquely base with angle (θ°). (14)

The columnar growth occurs depending on geometric shadow phenomenon which is resulted from covering the falling atoms by the atoms precede it because of the inclination of the base towards the vapor ray during the process of film growth, and this leads to the appearance of voids and self shadowing phenomenon on which the columnar growth attributed to (16,19). This self shadowing model of

columnar growth in oblique angle-vapor deposited films was confirmed (1960) (14). The columnar microstructures mainly observed in crystalline and amorphous thin films possess many morphological features in common. The structure consists of a low density or void network that surrounds an array of parallel (uniform – sized) rods of higher density. The column orientation in films deposited at oblique incidence is always more nearly perpendicular to the substrate than the vapor beam direction (16).

In this research, a vacuum thermal evaporation system type (Edward Speedvac Unit) has been used, the material placed inside a resistive heater in a form of a boat made of tungsten connected to electric source. The substrates and boat are (10.95 cm) apart. The glass substrates made from slide microscopes manufactured in Germany in "Objekttrager Factory" which dimensions of (1.25x1cm). They cleaned gently, then the slides will be ready to be used.

Films thickness (t) measured by the weight method.

(XRD) instrument type (Shimad Zu 6000) was used which made in Japan, have (Cu) target gives (1.5406 \AA) wavelength using (30 mA) current and (40 Kv) voltage.

RESULTS AND DISCUSSION

The X-ray diffraction of the (CdS) powder has been studied to know the material structure. The X-ray diffraction spectrum exhibits that the material is pure, polycrystalline with high orientation and strong reflections from some (h k l) planes as shown in figure (2).

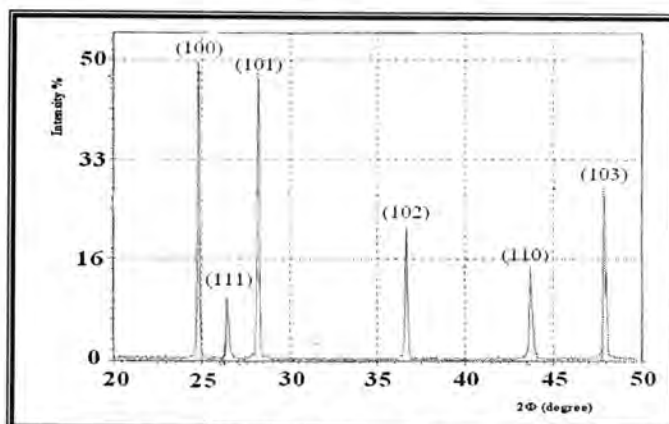


Figure -2: diffraction spectrum of (CdS) powder.

Figure (3) shows X-ray diffraction patterns for (CdS) films with deposition angles $\Theta = (0^\circ, 30^\circ, 50^\circ, 70^\circ)$ respectively and fixed thickness ($t=350$) nm. The films exhibit a polycrystalline nature having (111), (101), (102), (103), (100), planes. The peak intensities of (111) increase with increasing deposition angle, while the other planes have weak intensities. The diffraction peak existed at $2\Phi = (26.56^\circ)$ corresponding

to (111) cubic planes, this agree with the reference (20). Films of the same thickness ($t=350$ nm) and deposition angles $\Theta=(0^\circ, 30^\circ, 50^\circ, 70^\circ)$ have (111) plane of reflection intensity about (36.5%, 45%, 59%, 80%) respectively. Obviously, the deposition angle has great influence on the crystal structure and the columnar growth which have needle like structure. When the angle increases the columnar growth and the voids between columns increase (16).

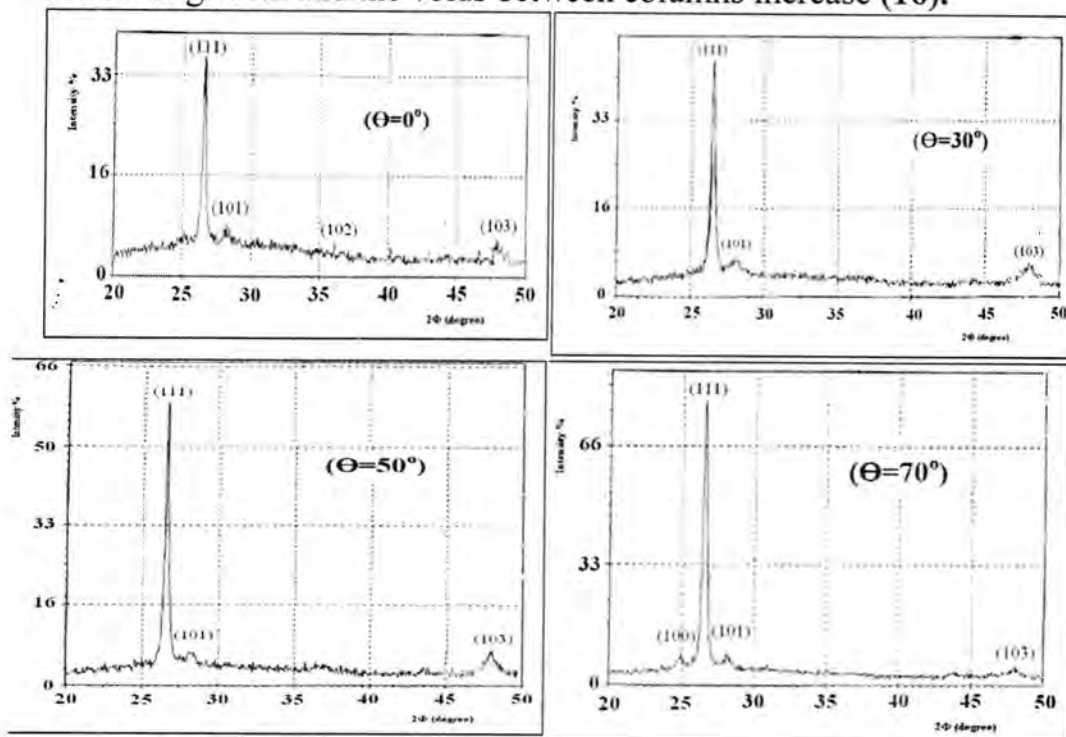


Figure :3- diffraction spectrum of (CdS) films deposited with thickness ($t=350$ nm).

Figure (4) shows the diffraction spectrum of (CdS) films deposited at angle ($\Theta=70^\circ$) with films thicknesses $t=(350, 300, 250)$ nm respectively, we observe that the thickness increasing of the same deposition angle increase reflection intensity of the plane (111) because of the crystal growth become stronger and more oriented with film thickness (20,21).

Then the reflection intensity of the plane increasing (111) when deposition angle ($\Theta=70^\circ$) are about (36%, 60%, and 80%), for film thicknesses $t=(250, 300, 350)$ nm respectively.

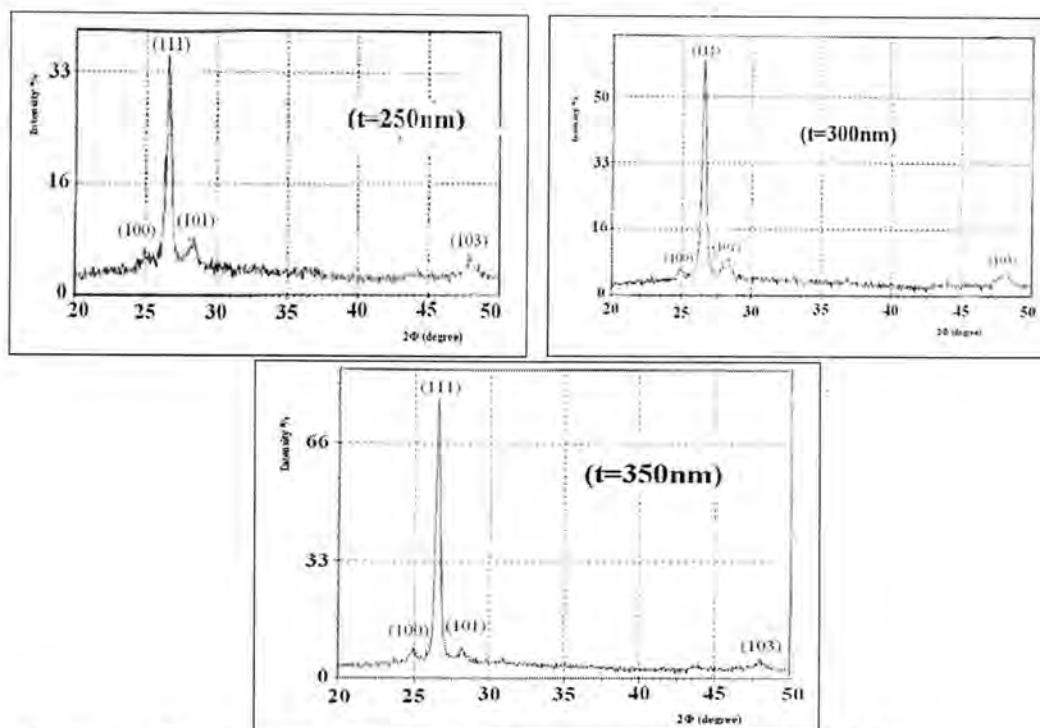


Figure-4:diffraction spectrum of (CdS) films deposited at angle ($\Theta=70^\circ$).

Table (1) shows the X-ray diffraction results for deposited (CdS) films at different angles on glass substrates at room temperature in which the values of Bragg angles ($2\theta^\circ$) and spaces (d) between planes ($h\ k\ l$) are fixed and there is a comparison between the ratio of (I/I_1) of the results that we found in this research with (ASTM) tables.

(I) represents the reflection intensity in diffraction patterns.

(I_1) represents the highest intensity in (XRD) patterns of (CdS) films deposited at different angles and thickness.

There is an obvious difference between the results that we found in this research and the values fixed in (ASTM) because of the intensity change in main peak of the reflection from (111) as a result of the deposition angle change.

It is clear that the deposition method and preparation conditions had a great effect on films structure prepared in this research closer to a single crystal.

It is obvious that the varying of the deposition angle has a great effect on the structural properties of these films.

Table-1: shows (hkl) planes and comparison between ((I/I₁) of (XRD) in this research with (ASTM) of the (CdS) films deposited at different angles and varying thickness

Film Thickness t (nm)	α°	$2\theta^\circ$	d (Å)	(hkl)	I/I ₁ (XRD)	I/I ₁ (ASTM)
350	0	26.5615	3.35317	111	42.5	100
		28.4454	3.13523	101	4.8	100
		36.1025	2.48590	102	3.5	29
		48.2830	1.88341	103	6.7	80
	30	26.551	3.35446	111	54.7	100
		28.2332	3.15831	101	4.29	100
		47.9542	1.89556	103	6.33	40
	50	26.5951	3.34901	111	74.7	100
		28.2768	3.15354	101	2.7	100
		47.9521	1.89563	103	7.2	40
	70	24.8929	3.57403	100	8.1	75
		26.5753	3.35146	111	100	100
		28.2020	3.16174	101	4.5	100
		48.0220	1.89304	103	4.5	80
300	70	24.9387	3.56757	100	4.07	75
		26.5801	3.35087	111	74.2	100
		28.2920	3.15188	101	4.7	100
		47.9820	1.89452	103	6.7	40
250	70	24.9224	3.56987	100	4.5	75
		26.5962	3.34888	111	42.9	100
		28.2872	3.15241	101	4.9	100
		47.9927	1.89413	103	4.2	40

Table (2) shows the grain size (D_g), dislocation density (δ) and micro strain (ϵ) results of (CdS) films deposited at different angles and varying thickness by using Scherrers formula (22).

$$D_g = \frac{K \lambda}{\beta \cos \phi} \text{ (nm)} \quad \dots\dots\dots (1)$$

Where:

$K=0.94$ is const.

λ : is the wavelength of incident X-ray radiation = (1.5404Å for CuK_α).

β : is the intrinsic full width at half maximum of the peak.

ϕ : is the Bragg's diffraction angle of the respective XRD peak.

$$\delta = \frac{1}{D^2} \quad \text{(lines/cm}^2\text{)} \quad \dots\dots\dots (2)$$

$$\epsilon = \left(\frac{\lambda}{D \sin \phi} \right) - \left(\frac{\beta}{\tan \phi} \right) \quad \dots\dots\dots (3)$$

Then we notice that (D_g) decrease with increasing deposition angle of fixed film thickness ($t=350$ nm) also the grain size increases with

thickness increasing for a fixed deposition angle ($\Theta=70^\circ$). This agrees with the references (20) and (21). On the other hand, the dislocation density (δ) results which influenced by varying deposition angle for fixed thickness ($t=350$ nm), (δ) increases with increasing of deposition angle from $\Theta=(0^\circ-70^\circ)$ and the dislocation density (δ) decreases with increasing of film thickness from ($t=250-350$ nm) for a fixed deposition angle ($\Theta=70^\circ$).

The results of dislocation density (δ) and micro strain (ϵ) depend on the grain size results (D_g) (22), as shown in table (2).

Table-2: grain size (D_g), dislocation density (δ) and micro strain (ϵ) of CdS films (deposited at different angles and thickness).

Film Thickness t (nm)	Deposition angle θ°	Miller indices (hkl)	Grain size D_g (nm)	Dislocation density $\delta \times 10^{11}$ (lines/cm ²)	Micro strain $\epsilon \times 10^{-3}$
350	0	111	28.47	1.23	1.44
	30	111	28.17	1.26	1.42
	50	111	25.81	1.50	1.55
	70	111	24.17	1.71	1.63
300	70	111	22.695	1.94	1.78
250	70	111	20.11	2.47	2

1- From (X-ray diffraction) investigation, it is observed that the CdS films exhibit a polycrystalline nature having (111), (101), (102), (103), (100) planes, the peak intensities of (111), dislocation density (δ) (crystalline defects), micro strain (ϵ) increases and grain size decreases with increasing deposition angle. The variation of deposition angle has a great influence on the structural properties of these films which has a great effect on other properties. The increasing of film thickness when the deposition angle is constant has an influence on increasing reflectance intensity from plane (111), increasing the grain size and decreasing dislocation density and micro strain.

2- The influence of increasing deposition angle is greater than the influence of increasing films thicknesses on the structural properties.

REFERENCES

1. S.J.Fonash " Solar Cell Device Phys.", Academic Press, New York, (1981).
2. M.Rami, E.Benamar, M.Fahoume, F.Charabi and A.Ennaoui , (Effect of Heat Treatment With CdCl_2 on The Electrodeposited (CdTe / CdS) Hetero junction), " M.J.Condensed Matter ", 3 (1) P.66 (2000).
3. A. ASHOUR, (Physical Properties of Spray Pyrolysed CdS Thin Films), " Turk. J. Phys ", 27 P.551 (2003).
4. Ngamnit Gaewdang and Thitinai Gaewdang, (Thickness Dependence of Structural, Optical and Electrical Properties of CdS and CdS:In Films Prepared by Thermal Evaporation), " Technical digest of internationalPVSEC-14 ", P.581 (2004).
5. Korkmaz, Sibel " Characterization of CdS Thin Films and Schottky Barrier Diodes ", College of Science, department of physics, Middle East, Technical University, Turk., (2005).
6. D.Karashanova, K. Starbova, N. Starbov, (Microstructure Correlated Properties of Obliquely Vacuum Deposited (Ag_2S) Thin Films), " Journal of Optoelectronics and Advanced Materials ", 5 (4) P.903 (2003).
7. Frank. Jansen , (The Columnar Microstructure And Nodular Growth of $\alpha\text{-As}_2\text{Se}_3$ Films) " Thin solid films ", 78 P.15 (1981).
8. R. T. Kivaisi , (Optical Properties of Obliquely Evaporated Aluminum Films) " Thin solid films ", 97 P.153 (1982).
9. R. T. Kivaisi, (Optical Properties of Selectively Absorbing Chromium Films Deposited at Oblique Angle of Incidence), " Solar energy materials ", 5 P.115 (1981).

- 10.H.Aitlamine, L.Abelmann, and I. B. Puchalska , (Induced Anisotropies in NiCo Obliquely Deposited Films and Their Effect on Magnetic Domains), “ J.Appl.Phys ”, 71 (1) P.353 (1992).
- 11.David L. Everitt, William J. W. Miller, N. L. Abbott, and X. D. Zhu1, (Evolution of a preferred orientation of polycrystalline grains in obliquely deposited gold films on an amorphous substrate), “ Physical Review B ”, 62 (8) P. 4833 (2000).
- 12.[12] M.V.Sopinsky, V.I.Mynko, I.Z.Indutnyi, O.S.Lytvyn, P.E Shepeli , (Surface Self – Ordering in Obliquely Deposited As_2S_3 Films) “Chalcogenide Letters ”, 5 (11) P.239 (2008).
- 13.R. Georgieva, N.Starbov, D.Karashanova, K.Starbova, (Microstructure and Related Properties of Obliquely Deposited AgCl Thin Films)“ Journal Of Optoelectronics And Advanced Materials ”, 11 (10) P.1521 (2009).
- 14.M.J.Peterson,F.H., Cocks, (The Preparation of Textured (Te) Thin Films With Pronounced A circular Morphology and Concomitant High Absorptivity), “ J.Mater.Sci. ”, 14 P.2709 (1979).
- 15.N.G.Nakhodkin, A.I.Shalderr and A.F.Bardamid, (Structural Peculiarities of Amorphous Germanium Films), “ Thin solid films ”, 34 P.21 (1976).
- 16.A. G. Dirks and H. J. Leamy, (Columnar Microstructure in Vapor-Deposited Thin Films), “ Thin solid films ”, 47 P.219 (1977).
- 17.J. K. Cho,T.Yamazaki,E.Kita and A.Tasaki, JPN. , (Magnetic Anisotropy of Co Thin Films Prepared by Obliquely Incidence), “ J.Appl.Phys. ”, 27 (2) P.240 (1988).
- 18.W. F. Weston, T.C. Baker,C,J.Smith, A.L.Chavez V.K. Grotzky and J.F.Capes, (Physical Vapor Deposition of Chromium and Iron), “ J.Vac.Sci. Tech. ”, 15 (1) P.54 (1978).

19. J. W. Patten, (The Influences of Surface Topography and Angle of Adatom Incidence on Growth Structure in Sputtered Chromium), " Thin solid films ", 63 P.121 (1979).
20. Abdullah Serhan. Al-Shammari, " Preparation and characterization of chlorine doped Cadmium Sulfide (CdS:Cl) thin films and there applications in solar cells ", College of Science, department of Physics and astronomy, King Saud University, (2005).
21. Shadia J. Ikhmayies, Riyadh N. Ahmad-Bitar, (Effect of Film Thickness on The Electrical and Structural Properties of CdS:In Thin Films), " American Journal of Applied Sciences " 5 (9) P.1141 (2008).
22. A. Moses Ezhil Raj, L.C. Nehru, M. Jayachandran, and C. Sanjeeviraja, (Spray Pyrolysis Deposition and Characterization of Highly (100) Oriented Magnesium Oxide Thin Films), " Cryst. Res. Technol. ", 42 (9) P.867 (2007).

Empirical Models for Solar Radiation Estimation by Some Weather Data for Baghdad City

Enas A. Habbib

Department of Atmospheric Sciences, College of Sciences, Al-Mustansiriyah University

Received 6/10/2010 – Accepted 2/3/2011

الخلاصة

يهدف هذا البحث الى تطوير التنبؤ العلاقة بين الاشعاع الشمسي الكلي مع واحد او اكثر من مجموعة من العوامل الجوية: معامل الشفافية والمعدل اليومي لدرجة الحرارة و نسبة درجة الحرارة العظمى والصغرى اليومية و الرطوبة النسبية وفترة سطوع الشمس النسبية لمدينة بغداد ولفترة 22 سنة (1986-2005). تم الحصول على بيانات الاشعاع الشمسي والعناصر الانوائية السطحية من قبل موقع ناسا الالكتروني. تم استحداث معادلات احصائية وذلك من خلال تطوير انموذج انكستروم. تم حساب كل من قيم معامل الارتباط (r) ومعدل خطأ الجذر التربيعي (RMSE) ومعدل خطأ الانحياز (MABE) ومعدل الخطأ المنوي ومعدل الخطأ المنوي (MAPE) ولكل معادلة.

ABSTRACT

The aim of this research is to developing equations to predict the relationship between global solar radiations with one or more combinations of the following weather parameters: clearness index, mean of daily temperature, ratio of maximum and minimum daily temperature, relative humidity and relative sunshine duration for Baghdad city for 22 years (1984- 2005). data of solar radiation and surface parameters were obtained from Meteorology NASA website. Using Angstrom model as a base, other equations regression were developed by modifying Angstrom formula. The correlation coefficient (r) and Root Mean Square Error (RMSE), Mean Bias Error (MBE) and Mean Absolute Bias Error (MABE) and Mean Percentage Error (MPE) Mean Absolute Percentage Error (MAPE) values were determined for each equation.

INTRODUCTION

The design of a solar energy conversion system requires precise knowledge regarding the availability of global solar radiation and its components at the location of interest. Since the solar radiation reaching the earth's surface depends upon climatic conditions of the place, a study of solar radiation under local climatic conditions is essential. [1] Several researchers have determined the applicability of the Angstrom type regression model for estimating global solar irradiance. The best way of knowing the amount of global solar radiation at a site is to install pyranometers at many locations in the given region and look after their day-today maintenance and recording, which is a very costly exercise. The alternative approach is to correlate the global solar radiation with the meteorological parameters at the place where the data is collected. The resultant correlation may then be used for locations of similar meteorological and geographical characteristics at which solar data are not available. [2]

The extraterrestrial solar radiation on a horizontal surface G_0 is a function only of Latitude and independent of other location parameters. As the solar radiation passes through the earth's atmosphere, it is further modified by processes of scattering and absorption due to the presence

of cloud and atmospheric particles. Hence, the daily global solar irradiation incident on a horizontal surface G is very much location-specific and less than the extraterrestrial irradiation [3]. There are several correlations available for such estimation in developing countries [4-9]. The objective leading to this paper is to continue in the effort to develop predictive

METHOD OF ANALYSIS

The monthly means daily solar radiations, sunshine duration, temperature, relative humidity, were for period of 22 years (1983-2005) were obtained from solar radiation and surface Meteorology NASA for four selected locations in Iraq [10].

The data obtained to cover a period of 22 years (1984 - 2005) for Baghdad located at latitude 33.02N and longitude 46.14E. The monthly averages data processed in preparation for the correlations are presented in table 1.

Table-1. Meteorology data and global solar radiation for Baghdad.

Months	G/Go	S/S _{max}	T	θ	RH
January	0.550186	0.4526	9.6348	0.2069	37
February	0.596154	0.4929	11.4261	0.2008	38
March	0.584507	0.4812	16.1048	0.2795	29.9
April	0.533136	0.5362	22.9761	0.3705	22.3
May	0.581688	0.5678	29.1265	0.435	17.1
June	0.65625	0.7028	33.3874	0.4823	16.2
July	0.620567	0.7477	36.1696	0.4923	17.1
August	0.643954	0.7764	35.7817	0.4799	19.4
September	0.614618	0.733	31.9739	0.4558	27.2
October	0.545953	0.578	26.1961	0.4429	42.3
November	0.520979	0.439	17.8178	0.394	55.7
December	0.529293	0.429	11.6291	0.2857	32.4

The simplest model used to estimate monthly average daily solar radiation on horizontal surface is the well-known Angstrom equation is given: [11]

$$G = G_o \left(a + b \left(\frac{S}{S_{max}} \right) \right) \quad (1)$$

Where,

G is the monthly mean horizontal daily total terrestrial solar radiation.

G_o is the monthly mean horizontal daily total extraterrestrial solar:

$$G_o = \frac{24 \times 3600}{\pi} G_{sc} \left(1 + 0.033 \cos \frac{360n}{365} \right) \left(\cos \phi \cos \delta \sin w + \frac{2\pi W_s}{360} \sin \phi \sin \delta \right) \quad (2)$$

Where

G_o : monthly mean daily extraterrestrial radiation MJ/m²

G_{sc} : solar constant = 1367 W/m²

δ : Declination angle

ϕ : Latitude of the station

W_s = sunset hour angle for the typical day n of each month in degrees
 $= \cos^{-1} (-\tan \phi \tan \delta)$

n : mean day of each months.

S : is the monthly mean of daily hours sunshine duration was divided by the number of hours of insolation (S_{\max}). The values of S_{\max} were computed from the following equations:

$$S_{\max} = \frac{2}{15} \cos^{-1} (-\tan \phi \tan \delta) \quad (3)$$

S_{\max} is the number of hour of insolation, δ is the declination angle and is ϕ the latitude of the station. Then the monthly average of daily global radiation G was normalized by dividing with the monthly average of daily extraterrestrial radiation G_0 . Therefore, Clearness index K_T is defined as the ratio of the observed/measured horizontal terrestrial solar radiation (G), to the calculated/predicted horizontal extraterrestrial solar radiation (G_0).

DATA ANALYSIS

To estimate prediction of global solar radiation using meteorological parameters ,multiple linear regression analysis were used ($K=G/G_0, S/S_{\max}, RH, \theta$, and T) where K is the clearness index, S/S_{\max} is the relative sunshine duration, RH is the relative humidity, θ is the ratio of minimum to maximum daily temperature and T is the monthly average daily temperature (Table 1 and 2).The performance of the models were evaluated on the basis of the statistical measured like the RMSE (Root Mean square Error), MBE (Mean Bias Error),MABE (Mean Absolute Bias Error), MPE (Mean Percentage Error) and MAPE (Mean Absolute Percentage Error)[12].

$$RMSE = \left\{ \sum \left[(G_{pre} - G_{obs})^2 \right] / n \right\}^{1/2} \quad (4)$$

$$MBE = \sum \left[(G_{pre} - G_{obs}) \right] / n \quad (5)$$

$$MABE = \sum \left[\left| (G_{pre} - G_{obs}) \right| \right] / n \quad (6)$$

$$MPE = \left[\sum \left(\frac{G_{obs} - G_{pre}}{G_{obs}} \times 100 \right) \right] / n \quad (7)$$

$$MAPE = \left[\sum \left(\left| \frac{G_{obs} - G_{pre}}{G_{obs}} \right| \times 100 \right) \right] / n \quad (8)$$

The regression and correlation coefficients values are illustrated on Table 2. Figure 1 shows the comparison between measured and predicted values of the correlation equation.

RESULTS AND DISCUSSION

Monthly averaged data for the clearness index, the relative sunshine duration, the relative humidity, the ratio of minimum to maximum daily temperature and the monthly average daily temperature are analyzed for Baghdad city in Iraq. We have been get linear regression analysis from using equation (1) to four variables showed in Table 2. It is seen that the correlation coefficient r , correlation of determination R^2 , MBE (w/m^2), MABE (w/m^2), RMSE (w/m^2), MAPE (w/m^2) and MPE (%) varies from one variable to another variable. correlation coefficients (0.827- 0.895) are high for all the variables. These results illustrate that, there are statistically significant relationships between the clearness index, relative sunshine duration, the relative humidity, the ratio of minimum to maximum daily temperature and the monthly average daily temperature. This is further clear by high values of coefficient of determination R^2 (0.684- 0.801) across the variables.

Table- 2: Shows equation with regression and statistical indicators

Equations	R	R^2	RMSE	MBE	MABE	MPE	MAPE
Equation 9	0.827	0.684	0.042502	0.012269	0.62864	-0.13008	3.53660
Equation 10	0.678	0.406	0.078307	0.022605	0.83083	-0.23967	4.82835
Equation 11	0.468	0.219	0.227327	-0.15509	1.04646	-0.53883	5.861642
Equation 12	0.470	0.221	1.194443	-0.1547	1.0332	-0.34092	5.9485
Equation 13	0.840	0.706	4.130543	-3.86027	3.86026	23.49758	23.49758
Equation 14	0.886	0.785	0.740682	-0.05519	0.56641	-0.04532	2.925225
Equation 15	0.864	0.747	0.772309	-0.0607	0.62091	-0.12099	3.28811
Equation 16	0.886	0.785	0.746375	0.176237	0.61839	-1.29515	3.208317
Equation 17	0.869	0.756	0.744486	-17.5177	17.5177	-0.05337	3.207967
Equation 18	0.894	0.799	0.724523	-0.01409	0.51933	-0.13275	2.626675
Equation 19	0.895	0.801	0.73375	-0.02691	0.50191	-0.0572	2.536842

The correlation coefficient of 0.827 exists between the clearness index and relative sunshine duration also coefficient of determination of 0.8746 implies 87.46% of clearness index can be accounted using relative sunshine duration.

$$\frac{G}{G_o} = 0.411 + \left(0.295 * \frac{S}{S_{max}} \right) \quad (9)$$

The correlation coefficient of 0.678 exists between the clearness index and monthly average daily temperature also coefficient of determination of 0.406 implies 40.6 % of clearness index can be accounted using monthly average daily temperature.

$$\frac{G}{G_o} = 0.508 * (0.00314 * T) \quad (10)$$

$$\frac{G}{G_o} = 0.625 - (0.00159 * RH) \quad (11)$$

The correlation coefficient of 0.470 exists between the clearness index and relative humidity also coefficient of determination of 0.221 implies

22.1% of clearness index can be accounted using ratio of minimum to maximum daily temperature.

$$G/G_0 = 0.505 - (0.201 * \theta) \quad (12)$$

The correlation coefficient of 0.468 exists between the clearness index and relative humidity also coefficient determination of 0.219 implies 21.9% of clearness index can be accounted using relative humidity.

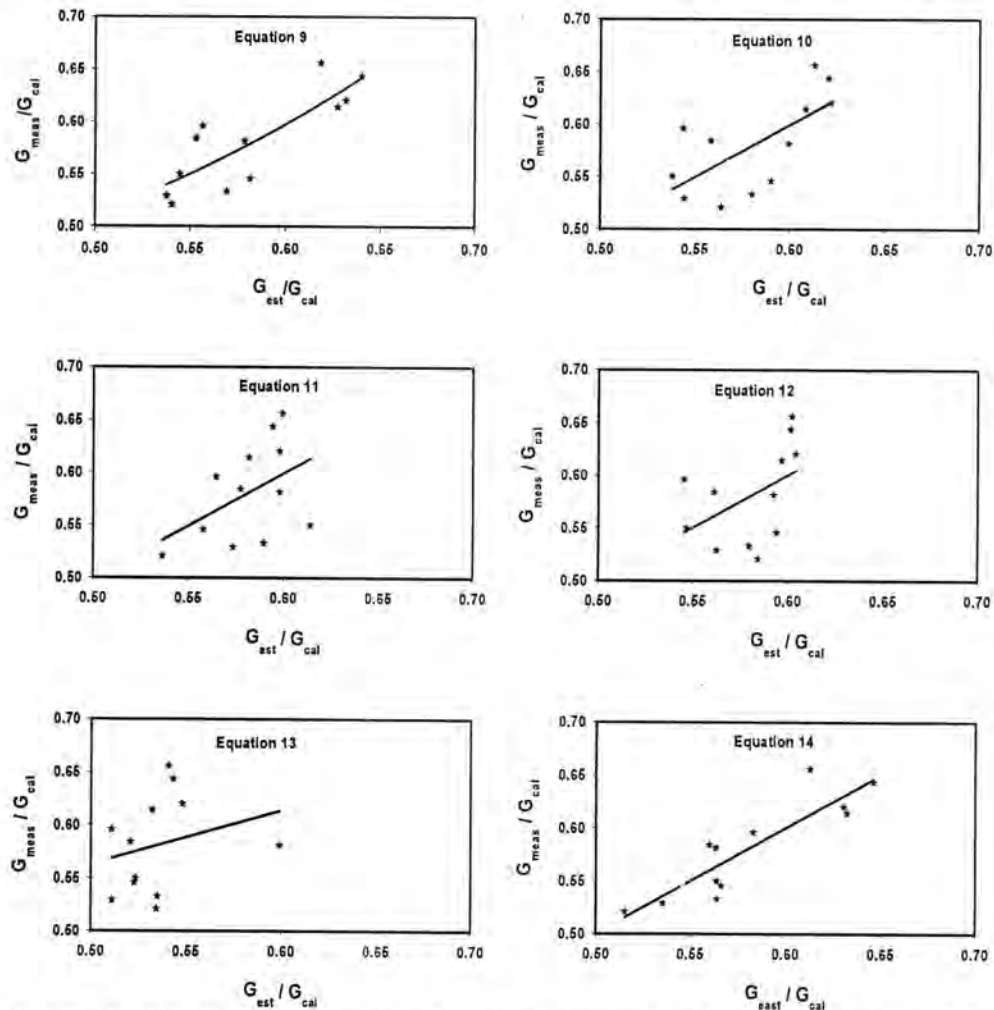


Figure-1: (Eq. 7-12). Comparison between measured and predicted values of the correlation equation.

The correlation coefficient of 0.840 exists between the clearness index, relative sunshine duration and relative humidity, also coefficient of determination of 0.706 implies 70.6% of clearness index can be accounted using relative sunshine duration and relative humidity.

$$G/G_0 = 0.439 - \left(0.272 * \frac{S}{S_{max}} \right) - (0.000552 * RH) \quad (13)$$

The correlation coefficient of 0.886 exists between the clearness index, relative sunshine duration and ratio of minimum to maximum daily

temperature, the coefficient of determination of 0.785 implies 78.5% of clearness index can be accounted by relative sunshine duration and ratio of minimum to maximum daily temperature.

$$\frac{G}{G_0} = 0.409 - \left(0.445 * \frac{S}{S_{\max}} \right) - (0.226 * \theta) \quad (14)$$

The correlation coefficient of 0.869 exists between the clearness index, relative sunshine duration and monthly average daily temperature, the coefficient of determination of 0.747 implies 74.7% of clearness index can be accounted by relative sunshine duration and monthly average daily temperature.

$$\frac{G}{G_0} = 0.354 + \left(0.523 * \frac{S}{S_{\max}} \right) - (0.00319 * T) \quad (15)$$

The equation (5) and (6) can be modified by incorporating extra parameters to the set of correlation equations for two variables.

The correlation coefficient of 0.886 exists between the clearness index, relative sunshine duration, ratio of minimum to maximum daily temperature and relative humidity, the coefficient of determination of 0.785 implies 78.5% of clearness index can be accounted by relative sunshine duration, ratio of minimum to maximum daily temperature and relative humidity.

$$\frac{G}{G_0} = 0.413 + \left(0.439 * \frac{S}{S_{\max}} \right) - (0.221 * \theta) - (0.000636 * RH) \quad (16)$$

The correlation coefficient of 0.9718 exists between the clearness index, relative sunshine duration, relative humidity and the monthly average daily temperature, the coefficient of determination of 0.756 implies 75.6% of clearness index can be accounted by relative sunshine duration, monthly average of daily temperature and relative humidity.

$$\frac{G}{G_0} = 0.413 + \left(0.377 * \frac{S}{S_{\max}} \right) - (0.00291 * T) - (0.000359 * RH) \quad (17)$$

The correlation coefficient of 0.894 exists between the clearness index, relative sunshine duration, the monthly average daily temperature and ratio of minimum to maximum daily temperature. The coefficient of determination of 0.799 implies 79.9% of clearness index can be accounted by relative sunshine duration, ratio of minimum to maximum daily temperature and monthly average of daily temperature.

$$\frac{G}{G_0} = 0.480 + \left(0.297 * \frac{S}{S_{\max}} \right) - (0.436 * \theta) + (0.00401 * T) \quad (18)$$

The correlation coefficient of 0.946 exists between the clearness index, relative humidity, ratio of minimum to maximum daily temperature and the monthly average daily temperature. The coefficient of determination of 0.8957 implies 89.57% of clearness index can be accounted by relative sunshine duration, ratio of minimum to maximum daily temperature and monthly average of daily temperature.

The correlation coefficient of 0.895 exists between the clearness index, relative sunshine duration, ratio of minimum to maximum daily temperature, relative humidity, and the monthly average daily temperature. The coefficient of determination of 0.801 implies 80.1% of clearness index can be accounted by relative sunshine duration, ratio of minimum to maximum daily temperature, relative humidity and monthly average of daily temperature.

$$\frac{G}{G_0} = 0.484 + \left(0.284 * \frac{S}{S_{\max}} \right) - (0.505 * \theta) + (0.0002433 * RH) + (0.498 * T) \quad (19)$$

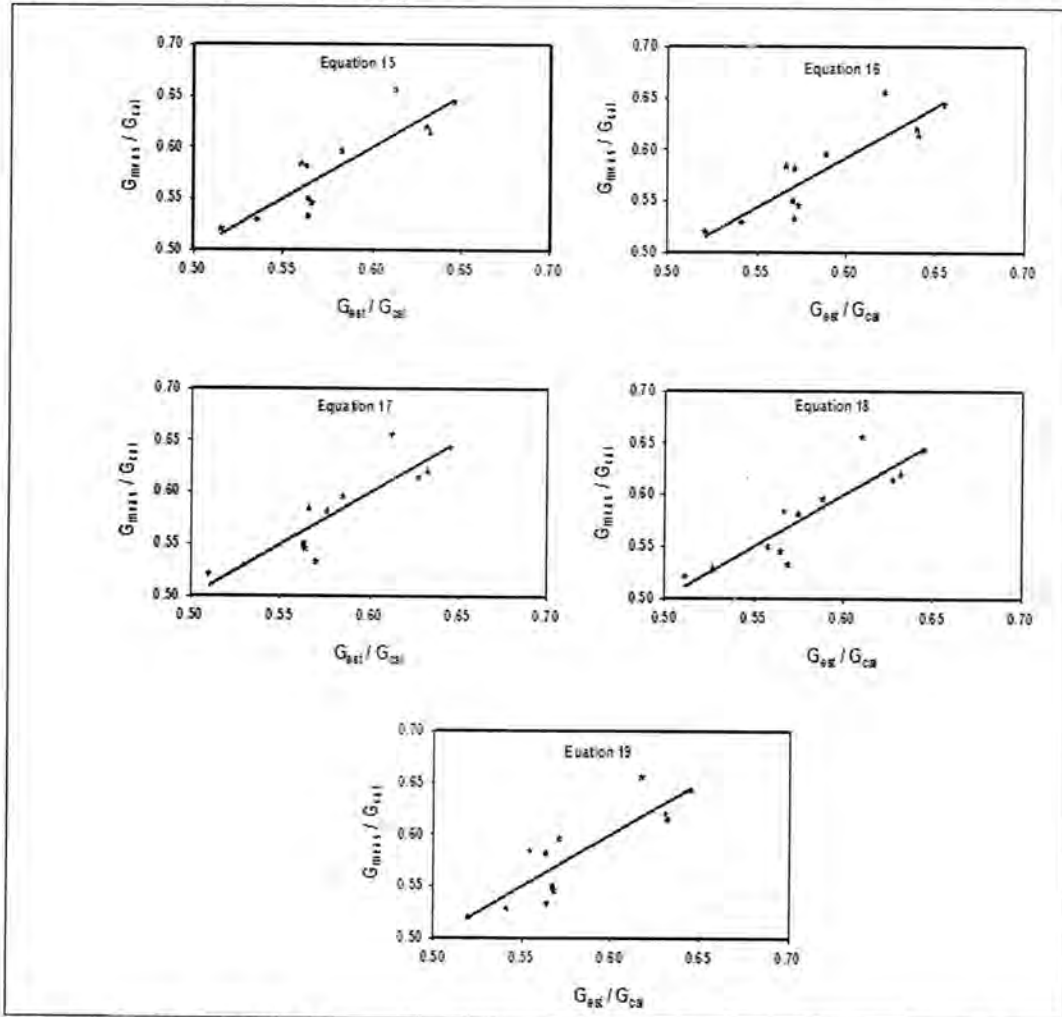


Figure -2: (Eq. 13-17). Comparison between measured and predicted values of the correlation equation.

The monthly global solar radiation, relative sunshine duration, means temperature, ratio of minimum to maximum temperature and relative humidity have been employed in this study to develop several correlation equations. Four variables have been developed with different types of equations obtained. It was illustrated that equation (19) has the highest value of correlation coefficient and correlation of determination, which gives good results when considering statistical indicators that is, RMSE, MBE, MABE, MPE and MAPE. The equation could be

employed in estimation of global solar radiation of location that has the same geographical location information as Baghdad.

REFERENCE

1. Firoz Ahmed, Intikhab ULFAT, Empirical Models for the Correlation of Monthly Average Daily Global Solar Radiation with Hours of Sunshine on a Horizontal Surface at Karachi, Pakistan, Turk J Phys, 28(3): 301 – 307. (2004).
2. A. A. El-Sebailland A. A. Trabea, Estimation of Global Solar Radiation on Horizontal Surface over Egypt, Egypt. J. Solids, 28 (1). (2005).
3. Louis E. Akpabior, Sunday E. ETUK, The Relationship Between Global Solar Radiation and Sunshine Duration for Onne, Nigeria, Turk J Phys, 161 - 167. (2003).
4. Louis E. AKPABIO1, Sunday O. UDO2, Sunday E. ETUK, Modeling Global Solar Radiation for a Tropical Location: Onne, Nigeria, Turk J Phys, 29(2): 63 – 68. (2005).
5. A. AL-SALAYMEH, Modeling of Global Daily Solar Radiation on Horizontal Surface for Amman city, Emirates Journal for Engineering Research, 11 (1): 49-56. (2006).
6. A. Sabziparvar, General Formula for Estimation of Monthly Mean Global Solar Radiation in Different Climates on the South and North Coasts of Iran, International Journal of Photoenergy. (2007).
7. Falayi E. O, Adepitan J. O.2, Rabiou A. B, Empirical models for the correlation of global solar radiation with meteorological data for Iseyin, Nigeria, International Journal of Physical Sciences. 3 (9): 210-216. (2008).
8. A.M.AL-Salihi, K.J.AL-Jumaily, O.T, Al-Tai, Estimation Global Solar Radiation on Horizontal Surface using Different Correlation Formula for Baghdad city, proceeding in 6th scientific conference of college of Science-AL-Mustansiriyah University, 21(6), Baghdad, Iraq. 2010.
9. A.M.AL-Salihi, M.M.Kadum. A.J, Mohammed, Estimation of Global Solar Radiation on Horizontal Surface using Routine Meteorological Measurements for Different cities in Iraq, Asian journal of Scientific research, 3(4), 240-248. (2010).
10. NASA: edmall.gsfc.nasa.gov/html/science-briefs/ed-stickler/edirradiance.
11. Angstrom AS, Solar and terrestrial radiation meteorological society 50, 121-126. (1924).
12. Javier A., Marta B., Chiquinqira H., Estimation of Global Solar Radiation in Venezuela, ISSN, 33, 280-283. (2008).

Wind Power Potential and Characteristic Analysis of the "Bakrajo Region" Sulaimani /Iraq

Salahaddin Abdul Qader Ahmed¹, Meeran Akram Omer², and Awni Adwar Abdulahad³

^{1,2} University of Sulaimani, College of Science, Dept. of physics

³ Al Mustansariyah University, College of Science, Dept. of Atmospheric Science

Received 14/2/2010 – Accepted 14/11/2010

الخلاصة

تم في هذا البحث دراسة أحصائية للطاقة الكامنة للرياح من خلال المعدلات الشهرية المقاسة لسرعة الرياح في منطقة بكرجو/السليمانية. اربعة سنوات (2004-2007) من السلاسل الزمنية لسرعة الرياح المقاسة في المنطقة قد استخدمت حسب توزيعات ويبل لدراسة طاقة الرياح. ووجد بان منطقة بكرجو (قرب مطار سليمانية) ذات مصدر ضعيف لطاقة الرياح، فقد كانت اكبر قيمة لسرعة الرياح على ارتفاع 50 متر (2.4 م/ثا)، حيث كان توزيع ويبل مناسباً لتقدير كثافة الطاقة حيث ان قيم الشكل والمقياس لمعاملات ويبل تراوحت بين (4.76-5.59) و (2.43-2.74) م/ثا على ارتفاع 50م على التوالي.

ABSTRACT

Wind power potential of the Bakrajo region has been statistically analyzed based on the monthly measured wind speed data, four years (2004-2007) hourly mean wind speed have been employed. The annual and monthly wind speeds and wind density are estimated. The Weibull distribution function has been derived from the available data with its two parameters identified. The wind power of this region has been studied based on the Weibull function. It has been found that the region has a poor wind power resource, where the maximum wind speed was 2.4 m/sec at 50 m height. Weibull distribution shows a good approximation for estimation of power density where the values of the shape and scale Weibull parameters range between (4.76-5.59) and (2.43-2.74) m/sec at 50 m height respectively.

Key words: Mean wind speed, Weibull distribution function, wind power density.

INTRODUCTION

The region concerned in this study is situated in west of Sulaimani North of Iraq, 35° 32' N Latitude 45° 56' E Longitude and 752 m above sea level which contain of automatic Agro meteorological station. The region is a village where there are an airport, college and near Sulaimani city about 5 km apart.

No investigations of the wind power potential were done for this region since a few studies of wind power potential have been carried out at Sulaimani center. Ahmed and Amin study the feasibility of wind power potential at Sulaimani region by using yearly long term data, they have investigated wind power potential at some locations by analyzing the local weather data and wind turbine characteristics, more work needs to be done about wind power potential analysis in this region [1,2].

The objective of this paper is to statistically analyze wind power potential based on hourly measured wind data. The analysis of wind potential energy requires careful statistical assessment of wind characteristic such as mean wind speed and its frequency distribution. In

order to accurately predict the potential wind energy at higher altitude, the statistical based distribution,

Weibull function has been used as an acceptable distribution function that accurately fit the wind speed frequency along its duration course [3, 4].

Mathematical Analysis and Formulation

There are several continuous mathematical functions, or called the probability density function that can be used to model the wind speed frequency curve by fitting time-series measured data. [3, 4, 5]

In recent years much effort has been made to construct an adequate statistical model for describing the wind speed frequency distribution which can be used as a tool in predicting the energy out put of wind energy conversion systems. [6, 7]

Vertical Extrapolation of Wind Speed

Wind speed near the ground changes with height, this requires an equation that predicts wind speed at any height in terms of the measured speed at another height. The most common expression for the variation of wind speed with height is the power law having the following form [8,9]

$$\frac{v_2}{v_1} = \left(\frac{h_2}{h_1} \right)^\alpha \text{------(2-1)}$$

Where v_1 (m/sec) is the actual wind speed recorded at height h_1 (m), and v_2 (m/sec) is the wind speed at the required or extrapolated height h_2 (m). The exponent α depends on the surface roughness and a wind speed, a value 1/7 is used for low surface roughness using this method, wind speed were extrapolated to 50 m height, where most modern wind turbines are usually operated [3].

Weibull Distribution of Wind Speed

The variation in wind speeds are best described by the Weibull probability distribution function $f(v)$ with two parameters, the shape parameter k and the scale parameter a (m/sec), the probability of wind speed being v during any time interval is given by its probability density function, as following [10]

$$f(v) = \left(\frac{k}{a} \right) \left(\frac{v}{a} \right)^{k-1} e^{-\left(\frac{v}{a} \right)^k} \text{------(2-2)}$$

And cumulative distribution function $F(v)$ as

$$F(v) = 1 - e^{-\left(\frac{v}{a} \right)^k} \text{------(2-3)}$$

The shape and scale parameters can be estimated by using the Maximum Likelihood Method (MLH) as [1,4]

$$k = \left(\frac{\sum_{i=1}^n v_i^k \ln(v_i)}{\sum_{i=1}^n v_i^k} - \frac{\sum_{i=1}^n \ln(v_i)}{n} \right)^{-1} \text{-----} (2-4)$$

$$a = \left(\frac{1}{2} \sum_{i=1}^n v_i^k \right)^{\frac{1}{2}} \text{-----} (2-5)$$

Where v_i is the wind speed in time stage i and n is the number of non zero wind data points.

Relative Error of the Annual Mean Wind Speed

The annual mean wind speed is analyzed with the relative error ξ of each year as follows [11]

$$\xi = \frac{\bar{v}_i - \bar{v}}{\bar{v}} \times 100\% \text{-----} (2-6)$$

Where \bar{v}_i is the annual mean wind speed of the year concerned, \bar{v} is the average (monthly mean) wind speed of all the years.

Average Wind Power Density Analysis

The mean power density per unit area can be calculated directly from the following equation, if the mean value of V^3 , which is $\left(\bar{v}\right)^3$ is already known in (m/s)³ [7,11]

$$P_w = \frac{1}{2} \rho \bar{V}^3 \text{-----} (2-7)$$

Where ρ is air density and if the probability density function that represents the wind data is known, the mean wind speed can be determined from:

$$\bar{v} = \int_0^{\infty} v f(v) dv \text{-----} (2-8)$$

Then the mean value of V^3 can be determined as:

$$\left(\bar{v}\right)^3 = \int_0^{\infty} v^3 f(v) dv \text{-----} (2-9)$$

Wind power density per unit area of a site P_w based on a Weibull probability

density function (Weibull PDF) can be expressed, from equation (2-7) and integrating equation (2-9) as follows[7,11]

$$P_w = \frac{1}{2} \rho a^3 \Gamma\left(1 + \frac{3}{k}\right) \text{-----} (2-10)$$

where

$$a^3 = \frac{\bar{v}}{\Gamma(1 + \frac{3}{k})}, \quad \bar{v} \text{ is mean wind speed and } \Gamma \text{ is gamma}$$

function, given by $\Gamma(z) = \int_0^{\infty} t^{z-1} e^{-t} dt$

RESULTS AND DISCUSSION

Wind Speed Analysis

Data for wind speed used in this present work were obtained during the period 2004-2007, the wind speeds were analyzed using different statistical softwares, the main results obtained from the present study can be summarized as follows, the mean monthly wind speed values and the two Weibull parameters scale and shape calculated using Maximum Likelihood Method (MLM) Equations (2-5 and 6), from the available data for the overall and individual four years are presented in Table (1), as indicated for the overall four years the monthly mean wind speeds were found and the values are between maximum 2.74 m/sec corresponding to year 2004 to a minimum 1.31 m/sec corresponding to year 2005, at 10 m height and at 50 m height the maximum value 3.45 m/sec corresponding to year 2004 and the minimum 1.64 m/sec corresponding to year 2005, which arises in July and November for both years respectively.

Figures (1 and 2) show the monthly variation of the mean wind speeds at both 10 and 50 meters heights for the studied area respectively.

Table -1: Mean wind speeds (m/sec) and the two Weibull parameters at both (10 and 50) meters height for all the years (2004-2007).

	Mean Wind Speed at 10 m				Calculated Wind Speed at 50 m			
	2004	2005	2006	2007	2004	2005	2006	2007
Jan	1.66	1.65	1.24	1.51	2.07	2.06	1.77	1.89
Feb	2	1.82	2	1.47	2.5	2.28	2.5	1.84
Mar	1.45	2	1.99	1.7	1.81	2.5	2.49	2.12
Apr	1.96	2.26	1.87	1.75	2.45	2.83	2.34	2.19
May	1.95	2.25	1.77	1.51	2.44	2.81	2.21	1.89
Jun	2.54	2.48	2.28	2.12	3.18	3.1	2.85	2.65
Jul	2.76	2.58	2.69	2.63	3.45	3.23	3.36	3.29
Aug	2.44	2.63	2.3	2.34	3.05	3.29	2.88	2.93
Sep	2.34	2.2	1.59	1.95	2.95	2.75	1.99	2.44
Oct	1.84	1.65	1.52	1.72	2.3	2.06	1.89	2.15
Nov	1.64	1.31	1.42	1.4	2.05	1.64	1.77	1.75
Dec	1.62	1.47	1.37	1.79	2.02	1.84	1.71	1.74
Mean	2.02	2.03	1.85	1.79	2.52	2.53	2.31	2.24
Shape	5.44	5.6	4.85	4.77	5.43	5.59	4.85	4.76
Scale	2.18	2.19	2.01	1.94	2.72	2.74	2.51	2.43

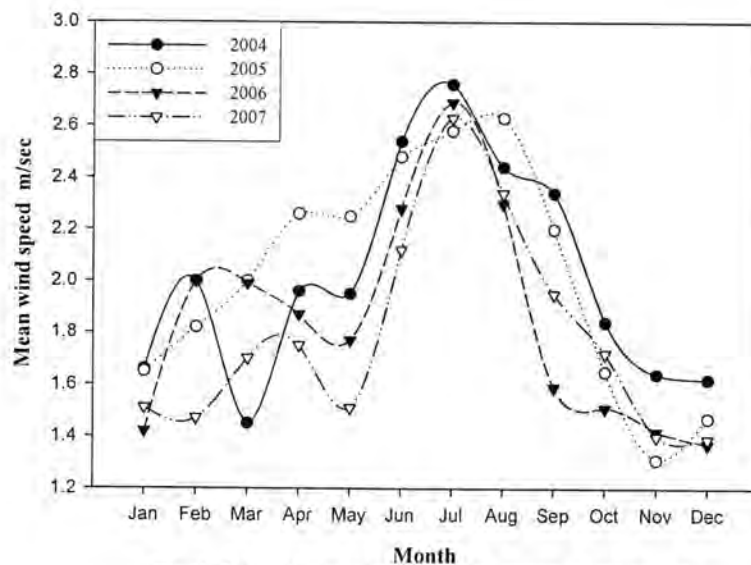


Fig-1: Monthly variation of the mean wind speed at 10m height for the studied area

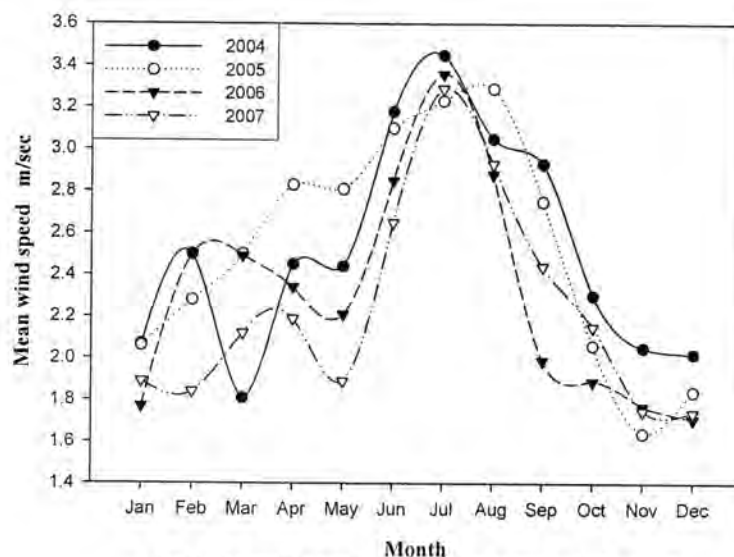


Fig-2: Monthly variation of the mean wind speed at 50m height for the studied area

The Wind Speed Probability Distribution

The wind speed probability distribution predominantly determines the performance of wind power systems. Once the wind speed distribution is known, the wind power potential could be easily obtained. The Weibull distribution function, expressed by Equation (2-2), is one of the normally used functions to illustrate the wind speed distribution [12,13,14].

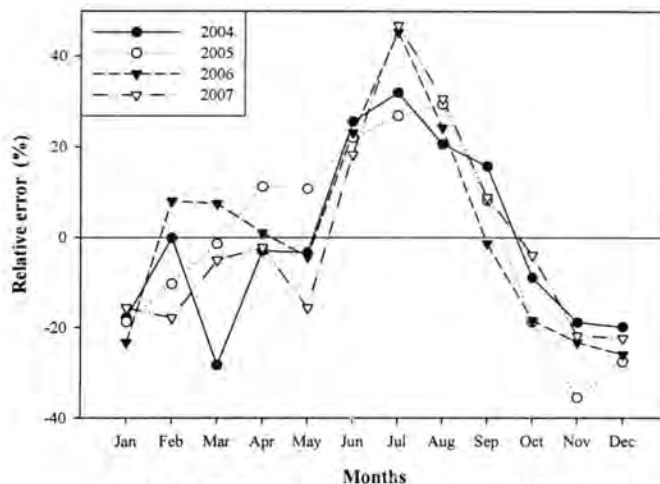


Fig-6: relative error of monthly mean wind speed for each year from 2004 to 2007 for the studied area

Mean Wind Power Density Variation

The monthly variation of the mean wind power density estimated at 50 m height using Equation (2-7), with considering the air density of the studied area to be 1.135 kg/m^3 .

The variation in the values of wind power density matches with the variation of the monthly mean wind speed values as illustrated in Figure (7). The lowest value of wind power density of 2.79 w/m^2 in November 2005 corresponds to the lowest wind speed in the same year, and the highest value of 26.23 w/m^2 in July 2004 corresponds to the highest wind speed in the same year as shown in Table (2), and the remaining months lie between the lowest and highest power density values previously mentioned.

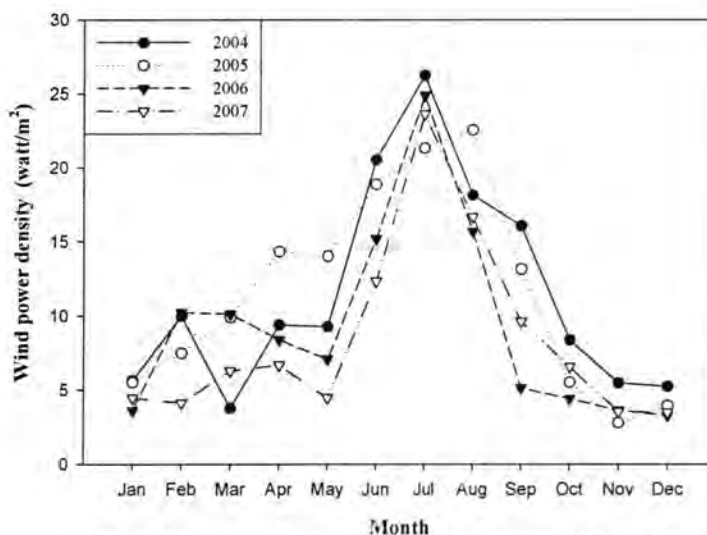


Fig-7: Monthly variation of the wind power densities for each year from 2004 to 2007 for the studied area

Table -2: Monthly mean wind power density at 50 m height for all the years (2004-2007).

	Power Density (w/m^2) at 50 m height			
	2004	2005	2006	2007
Jan	5.66	5.53	3.63	4.47
Feb	9.98	7.5	10.25	4.13
Mar	3.78	9.89	10.12	6.31
Apr	9.39	14.34	8.4	6.69
May	9.28	14.04	7.08	4.47
Jun	20.54	18.85	15.18	12.33
Jul	26.23	21.33	24.88	23.61
Aug	18.13	22.54	15.67	16.67
Sep	16.07	13.16	5.16	9.63
Oct	8.4	5.53	4.42	6.58
Nov	5.5	2.79	3.63	3.55
Dec	5.26	3.94	3.28	3.49
Mean	11.52	11.62	9.31	8.49

- 1) The wind power resource is poor in the studied area , where the data of annual mean wind speed of (2.02, 2.03, 1.86 and 1.79) m/sec at 10 m height and (2.52, 2.53, 2.31 and 2.24) m/sec at 50 m height are derived from the monthly measured time series wind speed data for years 2004-2007 respectively.
- 2) The values of shape and scale Weibull parameters range between (4.76–5.59) and (2.43–2.74) m/sec at 50 m height respectively.
- 3) The estimated relative errors of the monthly mean wind speed for each year of the studied area indicated that the monthly mean wind speeds were higher than the annual mean wind speed at months May till September while its lower for the rest months of the year meanly.
- 4) The Weibull distribution provide better power density estimation and the lowest value of the power density of $2.79 w/m^2$ in November 2005, and the highest value of $26.23 w/m^2$ in July 2004 are found which indicates to a poor sit for installing a wind energy conversion system.

REFERENCES

1. Salahaddin A.K.Ahmed "Wind Analysis and Distribution of Wind Energy Potential over Iraqi Kurdistan Region" , Ph.D Thesis Uni. of Sulaimani Coll. of Science (2009)
2. Amin S.H "Geographic Analysis of the Wind Characteristics in the Iraqi Kurdistan Region and its Potential Exploitation" M.Sc Thesis, Uni. of Sulaimani, Coll. of Human Science(2007).
3. W.Al-Nassar, S.Al-Hjraf, A.Al-Enizi, L.Al-Awadhi,"Potential Wind Power Generation in the State of Kuwait" Renewable Energy 3,2149-2161(2005).
4. [4] Tsang – Tung Chang, Yu-Ting Wu, Hua – Hsu, Chia – Ren Chu, Chun Min Lio. "Assessment of Wind Characteristic and Wind

- Turbine Characteristics in Taiwan" Renewable Energy, 28, 851-871(2003).
5. Ali Naci Cilik " On the Distribution Parameters used in Assessment of the Suitability of Wind Speed Probability Density Functions" Energy Conversion and Management 45, 1735-1747(2004).
6. Dray L. Johnson : Wind Energy System" Electronic Edition(2006).
7. M.J.M. Stevens and P.T.Smulders. "The Estimation of the Parameters of the Weibull Wind Speed Distribution for Wind Energy Utilization Purpose" Wind Engineering. 3, 2, 132-145(1979).
8. Mahyoub H. Al-Buhairi "A statistical Analysis of Wind Speed Data and an Assessment of Wind Energy Potential in Taiz-Yemen" Ass.Univ.Bill.Envir.Res. 9, 2, 21-33(2006).
9. M. Akhlaque Ahmed, Firoz Ahmed and M. Wasim Akhtar "Assessment of Wind Power Potential for Coastal Areas of Pakistan," Turk.J.Phys. 30, 127-135(2006).
10. Mukund A. Patel, "Wind and Solar Power Systems" CRC Press LLC-USA Chap. (4 and 5)(1999).
11. Wei Zhon , Hongxing Yang , Zhaohrug Fang, "Wind Power Potential and Characteristics Analysis of the Pearl River Delta Region /China. Renewable Energy 31, 739-753(2006).
12. A. I. Al-Temimi, "Wind Power Assessment in Iraq" Ph.D Thesis Al mustansiriyah Univ. Coll. of Science(2007).
13. S. Rahman, I.M.EL.Amin, F Ahmed, S.M. Shaahid, A.M. Al-Shehri, J.M Bakhawain. Wind power Resource Assessment for Rafha, Saudi Arabia. Renewable and Sustainable Energy Reviews, 11, 937-950(2007).
14. A.S.K. Darwesh and A.A.M. Sayigh , "Wind Energy Potential in Iraq" Solar and Wind Technology, 5, 3, 215-222(1988).

بسم الله الرحمن الرحيم

تعليمات النشر لمجلة علوم المستنصرية

1. تقوم المجلة بنشر البحوث الرصينة التي لم يسبق نشرها في مكان آخر بعد إخضاعها للتقويم العلمي من قبل مختصين وبأي من اللغتين العربية أو الانكليزية .
2. يقدم الباحث طلبا تحريريا لنشر البحث في المجلة على أن يكون مرفقا بأربع نسخ من البحث مطبوعة على الحاسوب ومسحوب بطابعة ليزيرية وعلى ورق ابيض قياس (A4) مع قرص (CD) محمل بأصل البحث على ان لا يزيد عدد صفحات البحث 10 صفحات وبضمنها الاشكال والجداول على ان لا يكون الحرف اصغر من قياس 12 .
3. يطبع عنوان البحث واسماء الباحثين (كاملة) وعناوينهم باللغتين العربية والانكليزية على ورقة منفصلة شرط ان لا تكتب اسماء الباحثين وعناوينهم في أي مكان اخر من البحث ، وتعاد كتابة عنوان البحث فقط على الصفحة الاولى من البحث .
4. تكتب اسماء الباحثين كاملة بحروف كبيرة وفي حالة استخدام اللغة الانكليزية وكذلك الحروف الاولى فقط من الكلمات (عدا حروف الجر والاضافة) المكونة لعنوان البحث ، وتكتب عناوين الباحثين بحروف اعتيادية صغيرة .
5. تقدم خلاصتان وافيتان لكل بحث ، احدهما بالعربية والاخرى بالانكليزية وتطبع على ورقتين منفصلتين بما لا يزيد على (250) كلمة لكل خلاصة.
6. يشار الى المصدر برقم يوضع بين قوسين بمستوى السطر نفسه بعد الجملة مباشرة وتطبع المصادر على ورقة منفصلة ، ويستخدم الاسلوب الدولي المتعارف عليه عند ذكر مختصرات اسماء المجالات.
7. يفضل قدر الامكان تسلسل البحث ليتضمن العناوين الرئيسية الاتية : المقدمة ، طرائق العمل ، النتائج والمناقشة ، المصادر ، وتوضع هذه العناوين دون ترقيم في وسط الصفحة ولا يوضع تحتها خط وتكتب بحروف كبيرة عندما تكون بالانكليزية .
8. يتبع الاسلوب الاتي عند كتابة المصادر على الصفحة الخاصة بالمصادر: ترقيم المصادر حسب تسلسل ورودها في البحث ، يكتب الاسم الاخير (للقب) للباحث او الباحثين ثم مختصر الاسمين الاولين فعنوان البحث ، مختصر اسم المجلة ، المجلد او الحجم ، العدد ، الصفحات ، (السنة) . وفي حالة كون المصدر كتابا يكتب بعد اسم المؤلف او المؤلفين عنوان الكتاب ، الطبعة ، الصفحات ، (السنة) الشركة الناشرة ، مكان الطبع .
9. بخصوص اجور النشر يتم دفع مبلغ (25000) عشرون الف دينار عند تقديم البحث للنشر وهو غير قابل للرد ومن ثم يدفع الباحث (25000) عشرون الف دينار اخرى عند قبول البحث للنشر وبهذا يصبح المبلغ الكلي للنشر خمسون الف دينار .

مجلة علوم المستنصرية

تصدر عن كلية العلوم الجامعة المستنصرية

رئيس التحرير
أ. د. رضا ابراهيم البياتي

مدير التحرير
د. صلاح مهدي الشكري

هيئة التحرير

- | | |
|------|------------------------------------|
| عضوا | أ. د. ايمان طارق محمد العلوي |
| عضوا | أ. د. انعام عبد الرحمن حسن |
| عضوا | أ. م. د. عوني ادوار عبد الاحد |
| عضوا | أ. م. د. ماجد محمد محمود |
| عضوا | أ. م. د. رمزي رشيد علي العاني |
| عضوا | أ. م. د. حسين كريم سليمان الوندائي |
| عضوا | أ. م. د. سعد نجم باشخ |

الهيئة الاستشارية

- | | |
|-------|--------------------------------|
| رئيسا | أ. م. د. يوسف كاظم عبد الامير |
| عضوا | أ. د. طارق صالح عبد الرزاق |
| عضوا | أ. د. مهدي صادق عباس |
| عضوا | أ. م. د. عبد الله احمد رشيد |
| عضوا | أ. م. د. حسين اسماعيل عبد الله |
| عضوا | أ. م. د. مهند محمد نوري |
| عضوا | أ. م. د. منعم حكيم خلف |
| عضوا | أ. م. د. عامر صديق الملاح |
| عضوا | أ. م. د. طارق سهيل نجم |